University of Plymouth

PEARL **https://pearl.plymouth.ac.uk**

04 University of Plymouth Research Theses 01 Research Theses Main Collection

1982

THE EVALUATION OF WAVE FORCES ON SEAWALLS

BLACKMORE, PAUL

http://hdl.handle.net/10026.1/1068

---

http://dx.doi.org/10.24382/3207
University of Plymouth

All content in PEARL is protected by copyright law. Author manuscripts are made available in accordance with publisher policies. Please cite only the published version using the details provided on the item record or document. In the absence of an open licence (e.g. Creative Commons), permissions for further reuse of content should be sought from the publisher or author.

store

THE EVALUATION OF WAVE FORCES ON SEA WALLS

P. BLACKMORE

Ph. D. 1982

LIBRARY STORE

LIBRARY STORE

THE EVALUATION OF WAVE FORCES ON SEAWALLS

by

PAUL BLACKMORE, B.Sc. (Hons)

This thesis is submitted in partial
fulfilment of the requirements for
the degree of Doctor of Philosophy
to
The Council for National Academic Awards

August 1982

Sponsoring Establishment
Department of Civil Engineering,
Faculty of Technology,
Plymouth Polytechnic.

Collaborating Establishments
SWWA Exeter
CIRIA London.

PLYMO[illegible] POLYTECHNIC

Accn No	7055000955
Class No.	Thesis 627.24 BLA
Contl No	X700276814

CONTENTS

Page No.

Acknowledgements i

Declaration ii

Synopsis iii

Nomenclature and abbreviations iv

Definitions vii

Part A

Introduction to Part A 1

Chapter One – Historical Review

- 1.0 Introduction 5
- 1.1 Full scale testing 5
- 1.2 Model studies 12
- 1.3 Development of wave theories 17
  - 1.3.1 Long and small amplitude waves 17
  - 1.3.2 Breaking and standing waves 19

Chapter Two – Instrumentation and monitoring of some seawalls

- 2.1 Introduction 34
- 2.2 Seawalls (location and instrumentation) 36
  - 2.2.1 Teignmouth seawall 36
  - 2.2.2 Brunel seawall 38
  - 2.2.3 Ilfracombe seawall 40
  - 2.2.4 Seaford seawall 41
- 2.3 Instrumentation 43
  - 2.3.1 Pressure transducers and amplifiers 44
  - 2.3.2 Accelerometers 49
  - 2.3.3 Ancillary equipment 50

2.4 Strain gauge installation and protection 51

2.5 Wave and foreshore characteristics 53

2.5.1 Wave height 53

2.5.2 Wave celerity 56

2.5.3 Wave period 58

2.5.4 Beach characteristics 59

2.6 Wind speed and direction 60

2.7 Damage to instrumentation at Seaford 61

Chapter Three - Data analysis and results

3.1 Introduction 96

3.2 Description of data 96

3.2.1 Establishing a sample length for statistical analysis 99

3.3 Data analysis techniques 104

3.3.1 Probability density function 105

3.3.2 Spectral density analysis 107

3.3.3 Auto-correlation analysis 113

3.3.4 Cross-correlation analysis 115

3.4 Current empirical equations for predicting wave impact pressures 117

3.4.1 Equating breaking wave pressures to the stagnation pressure 118

3.4.2 Bagnold's wave impact pressure model 120

3.4.3 Impact pressure as a function of wave height 123

3.5 The impulse momentum equation 124

3.6 Proposed equations for estimating wave impact pressure 134

3.7 The limiting case of impact pressure 139

3.8 The level of confidence in wave parameter measurement 141

3.9 Spatial and temporal distribution of impact pressures on the seawalls 142

  3.9.1 Spatial distribution of impact pressures on the Ilfracombe seawall 144

  3.9.2 Temporal distribution of impact pressures on the Ilfracombe seawall 146

3.10 Extreme wave statistics 148

  3.10.1 Distribution of extreme hydrostatic wave pressures 149

  3.10.2 Distribution of wave impact pressures 150

  3.10.3 Extreme value distribution of wave impact pressures 152

3.11 The effects of seawall shape on wave pressures 154

3.12 Relationship between impact and hydrostatic pressures for breaking waves 155

Chapter Four - Discussion 215

Chapter Five - Conclusions and suggestions for further research 228

Part B

Introduction to Part B 232

Chapter Six - Dynamic seawall analysis

6.1 Introduction 234

6.2 Single degree of freedom systems 235

6.3 Structural damping 238

6.4 Multi-degree of freedom systems 241

  6.4.1 The transfer function (receptance) method 245

6.5 Response to impact loading 247

6.6 Response to random wave loading 250

Chapter Seven - Seawall modelling by finite elements

7.1 Introduction 257

7.2 The need for a finite element analysis 258
7.3 Modelling techniques 259
7.3.1 Model constraints 260
7.4 Modelling seawall response 261
7.4.1 Static modelling considerations 262
7.4.2 Dynamic modelling considerations 265
7.5 Seawalls subjected to transient excitation 270
7.5.1 Transient response analysis by PAFEC 271
7.5.2 Response to wave impact pressures 274
7.6 The effects of damping on structural response 275
7.7 The effects of rise time on structural response 277
7.7.1 The effects of multiple impacts on structural response 280
7.7.2 Resonant amplification 282
7.8 The transfer function between wave pressure and seawall response 283
7.9 The effects of erosion at Seaford 285
7.10 Finite element analysis of a pressure transducer diaphragm 287

Chapter Eight - Discussion 314

Chapter Nine - Conclusions and suggestions for further research 320

References 322

Appendix A A1
Calculation of the parameters of the Weibull distribution A1
Estimating the parameters of a Type I extreme value distribution via Liebleins BLUE A5
Calculation of Return period A7

LIST OF FIGURES, TABLES AND PLATES

			Page No.
Figure	1.1	Stevensons spring dynamometer	27
	1.2	Luiggi pressure diagram	27
	1.3	Full scale sea waves; Pressure impulses	28
	1.4	Frequency of shock impulses	28
	1.5	Variation of shock pressure with wave height for similar waves.	28
	1.6	Experimental Data of Delmonte compared with the formula of Homma and Horikawa.	29
	1.7	Some common wave profiles	30
	1.8	Minikin wave pressure diagram	30
Table	1.1	Results from all known investigations to measure wave pressures on seawalls and breakwaters.	31
	1.2	Classification of Wave Theories	33
Figure	2.1	Map of Teignmouth showing location of seawalls.	63
	2.2	Section through Teignmouth seawall at central recording station.	64
	2.3	Transducer array on the Teignmouth seawall	65
	2.4	Section through Brunel seawall	66
	2.5	Transducer array on the Brunel seawall	67
	2.6	Map of Ilfracombe showing location of seawall.	68
	2.7	Section through Ilfracombe seawall at vertical transducer array.	69
	2.8	Transducer array at Ilfracombe seawall	70
	2.9	Map of Seaford showing location of seawall	71
	2.10	Typical cross section of Seaford seawall	72

			Page No
Figure	2.11	Transducer array on Seaford seawall	73
	2.12	Type 1 transducer and housing	74
	2.13	Strain distribution in type 2 pressure transducer.	75
	2.14	Type 2 transducer and housing	76
	2.15	Technimeasure FDPF - 24 - 17 strain gauge as used in the type 2 transducer.	77
	2.16	'Noise level' after amplification, from type 2 pressure transducer, at zero load and 100 KN/m^2.	78
	2.17	Response of a type 2 pressure transducer subjected to a transient caused by the impact of a steel ball.	79
	2.18	Method of sealing type 2 transducer	80
	2.19	Attenuation of wave pressure head with depth	81
	2.20	The location of the beach transducers and wave staff in relation to the pressure transducers on the seawall	82
	2.21	Cross section of the beach at Ilfracombe at the position of the beach transducers.	83
	2.22	Sieve analysis results	84
	2.23	Wind speed and direction measured at Ilfracombe on 6th April 1981.	85
Plate	2.1	Teignmouth seawall before the beach level rose by more than 3m in places.	86
	2.2	Installing pressure transducers in the Brunel seawall.	86
	2.3	Brunel seawall before reconstruction	87
	2.4	(a) Original Ilfracombe seawall	87
	2.4	(b) New Ilfracombe seawall under construction	88
	2.5	View from the window of the Ilfracombe recording station.	88

Page No.

Plate 2.6 Waves breaking on the Ilfracombe seawall 89

2.7 Erosion of the Seaford seawall 90

2.8 Pressure transducers after; machining, 6 months on the Ilfracombe seawall and 3 weeks on the Seaford seawall. 90

2.9 (a) 'Bolt-on' pressure measuring system in place on Seaford seawall. 91

2.9 (b) Close up of transducer mounting block 91

2.10 Ramps used to protect the cables laid across the promenade at Seaford. 92

2.11 Type 1 pressure transducer 92

2.12 Type 2 pressure transducer and strain gauge 93

2.13 Second generation measuring system in place on Ilfracombe seawall. 93

2.14 Fixing point for beach transducer at Ilfracombe. 94

2.15 Wave staff and one beach transducer at Ilfracombe. 94

2.16 Typical damage to pressure transducer after service on the Seaford seawall. 95

2.17 Grills with 6mm and 4mm diameter holes, as used at Seaford to protect the pressure transducers. 95

Figure 3.1 Typical condensed pressure/time history showing non-linear tidal effects. 159

3.2 Probability measurement 160

3.3 Amplitude probability density function plot showing the effect of a trend (due to tidal changes) on the pressure distribution. 161

3.4 Gaussion distribution with a non-zero mean 162

3.5 Spectral density plot of swell pressure on Ilfracombe seawall. 163

Page No.

Figure 3.6 Spectral density plot of wave forces on Seaford seawall. 164

3.7 Sample pressure/time history for Ilfracombe seawall. 165

3.8 (a) Sample acceleration/time history for Seaford seawall synchronised with (b) pressure/time history. 166

3.9 Spectral density plot background acceleration of Seaford seawall. 167

3.10 Spectral density plots of peak and average accelerations of Seaford seawall. 168

3.11 Seaford seawall response at fundamental mode of vibration. 169

3.12 Ilfracombe seawall response at fundamental mode of vibration. 170

3.13 (a) Correlogram of pressure measured at transducer No.1 171

3.13 (b) Correlogram of transducer No.1 illustrating data is non-stationary over long time periods. 171

3.14 (a) Cross-correlogram between transducers No.1 and No.3, in a vertical plane. 172

3.14 (b) Cross-correlogram between transducers No.1 and No.4, showing expanded τ scale 172

3.15 (a) Cross-correlogram between transducers No.3 and No.4, in a horizontal plane. 173

3.15 (b) Cross-correlogram between transducers No.3 and No.4, showing expanded τ scale. 173

3.16 The approximate slope of the wave front as it strikes the seawall. 174

3.17 The angle of incidence of a wave crest to the seawall. 174

3.18 Relationship between maximum dynamic pressure and wave celerity. 175

Page No.

Figure 3.19 Histograms of wave celerity measured during the periods when wave impacts occurred 176

3.20 Dynamic pressure versus $\rho C^2 H$ 177

3.21 Dynamic pressure P versus wave height H 178

3.22 Full scale data fitted to momentum/impulse relationship based on solitary wave theory 179

3.23 Impact pressure versus rise time (Ilfracombe data) 180

3.24 Relationship between impulse and $\rho C_b^2 T$ showing dependence on H_b/L_b 181

3.25 K' versus H_b/L_b 182

3.26 K" versus $1/L_b$ 182

3.27 Relationship between impulse and momentum showing the dependence upon $1/L_b$ 183

3.28 Hyperbolic relationship between rise time and impact pressure 184

3.29 Velocity of sound in water with entrained air 185

3.30 The dependence of impact pressure on the 'smoothness coefficient' (λ) 186

3.31 Typical pressure/time history of standing waves 187

3.32 Typical pressure/time history of breaking waves 188

3.33 Vertical distribution of impact pressure on Ilfracombe seawall 189

3.34 Proposed vertical pressure distribution for dynamic and static pressures 190

3.35 Horizontal impact pressure distribution on Ilfracombe seawall 191

3.36 Synchronised pressure/time histories for impact on four transducers simultaneously 192

3.37 Observed and theoretical c.d.f.'s 193

Page No.

Figure 3.38 Type 1 extreme value distribution for wave impact pressures at Ilfracombe. 194

3.39 Typical pressure/time history of wave impact on Ilfracombe seawall. 195

3.40 Typical pressure/time history of wave impact on Seaford seawall. 196

3.41 Frequency histogram of the ratio of impact pressure/hydrostatic pressure. 197

Table 3.1 Summary of data recording sessions at Ilfracombe and Seaford. 198

3.2 Summary of field data. 200

3.3 Impact pressure data, Tape No.11 201

3.4 Impact pressure data, Tape No.14 202

3.5 Impact pressure data, Tape No.15 204

3.6 Impact pressure data, Tape No.16 205

3.7 Impact pressure data, Tape No.16 207

3.8 Impact pressure data, Tape No.17 208

3.9 Impact pressure data, Tape No. 5 209

3.10 Impact pressure data, Tape No.13 210

3.11 Impact pressure data, Tape No. 3 211

3.12 Comparison between visual measurements of wave period and those obtained from spectral density and correlation analysis. 213

3.13 Maximum impact pressures estimated by assuming a Rayleigh Distribution. 214

Figure 6.1 Input-output spectral relationship for a linear system. 256

Figure 7.1 Finite element model of the Seaford seawall without erosion. 289

Page No.

Figure 7.2 Finite element model of the Seaford seawall with erosion 290

7.3 Finite element model of the Ilfracombe seawall 291

7.4 Finite element model of the Seaford seawall (without erosion) showing the material properties of the foundation and backfill necessary to ensure a model response similar to the real wall response. 292

7.5 Finite element model of the Seaford seawall (with erosion) showing the material properties of the foundation and backfill necessary to ensure a model response similar to the real wall response. 293

7.6 Finite element model of the Ilfracombe seawall showing the material properties of the foundation and backfill necessary to ensure a model response similar to the actual wall response. 294

7.7 Hydrostatic wave pressure for fully reflected waves 295

7.8 Stress contours on the Seaford seawall (no erosion) due to the pressure in figure 5.7 being applied at a S.W.L of 2.0m A.O.D. 296

7.9 Stress contours on the Seaford seawall (with erosion) due to the pressure in figure 5.7 being applied at a S.W.L of 2.0m A.O.D 297

7.10 Stress contours due to the pressure in figure 5.7 being applied at a S.W.L of 2.5m A.O.D. on the Ilfracombe seawall 298

7.11 Relationship between structral response and frequency ratio 299

Page No.

Figure 7.12 The impact pressure history as actually measured on the Ilfracombe seawall and as applied to the finite element model of this seawall 300

7.13 Ilfracombe (model) seawall displacement at node 193 for the impact pressure history shown in figure 7.12 301

7.14 The effects of changes in damping ratio on structural response 302

7.15 The effect of rise time and impact pressure on seawall response (deflection) 303

7.16 Non-dimensionalized response of the Ilfracombe seawall model when subjected to impacts with varying rise times. 304

7.17 The displacement of the Ilfracombe seawall model at node 193 when subjected to a triangular impulse (Load case number 2) 305

7.18 The effects of multiple impacts on wall response 306

7.19 Transfer function between wave pressure and response for the Ilfracombe seawall 307

7.20 Excitation spectral density measured on the Ilfracombe seawall 308

7.21 Comparison between measured and estimated spectral density of response for the Ilfracombe seawall 309

7.22 Deflection of the Seaford seawall (without erosion) 310

7.23 Deflection of the Seaford seawall (with erosion) 311

Page No.

Figure 7.24 Finite element model of transducer diaphragm 312

7.25 Deflected shape of transducer due to a u.d.l. 313

7.26 Deflected shape of transducer due to a point load 313

ACKNOWLEDGEMENTS

This research was financed by the D.O.E., M.A.F.F. and S.W.W.A. through C.I.R.I.A. under the guidence of the Project Steering Committee listed below :-

O.T. Addyman (Chairman)	Thames Water Authority
P.C. Barber	Metropolitan Borough of Wirral
R.J.E. Braybrooks	D.O.E.
R. Bustle	D.O.E.
J.E. Clifford	Sir William Halcrow & Partners
G.M. Gray	C.I.R.I.A.
R. Green	S.W.W.A.
W.B. Harris	C.H. Dobbie & Partners
T.S. Hedges	University of Liverpool
P.J. Hewson	Plymouth Polytechnic
A.B. Hughes	M.A.F.F.
R. Maddrell	Sir William Halcrow & Partners
F.L. Oates	S.W.W.A.
A.F. Whillock	HRS

I would like to express my thanks to Mr P.J. Hewson of Plymouth Polytechnic (main supervisor) for his help and encouragement through out the period of this research, and I am also grateful to Dr G.N. Bullock of Salford University (2nd supervisor) for his contributions to this research. I would also like to acknowledge the help of the following people :-

Mr W.J. Clemence, The Quay, Ilfracombe.
Mr P. Moya, The Viking Hotel, Seaford.
District Engineer, British Rail, Plymouth Region.
Staff and Techncian support from the Department of Civil Engineering, Plymouth Polytechnic, and my wife Dianne for her help in typing and collating this thesis.

DECLARATION

I hereby certify that this work has not been accepted for any degree and is not being concurrently submitted in candidature for any degree other than the degree of Doctor of Philosophy of the Council for National Academic Awards.

Candidate: Paul Blackmore ....

Paul Blackmore

The Evaluation of Wave Forces on Seawalls - P.A. Blackmore

Synopsis

This Thesis is divided into two parts, Part A deals with the measurement and analysis of wave pressures on real seawalls and Part B deals with the resulting structural response of these seawalls.

There have been only thirteen previous investigations to measure full scale wave impact pressures on coastal structures, and of these only five were conducted with sensitive electronic measuring equipment. The infrequent occurrence of impact pressures in a real sea has meant very little impact pressure data has been collected by these previous investigations. This investigation is the first of its kind to be carried out in the U.K. using modern measuring and recording equipment, the volume of wave impact data obtained (over 150 impacts recorded) is significantly greater than the combined results of all previous full scale investigations.

The magnitude of the wave impacts measured during this investigation were generally lower than those measured by other investigations, the maximum impact pressure being of the order of seven times the hydrostatic pressure. The pressures measured were found not to fit any current equations. The data has also shown that impact pressures can occur simultaneously over large areas and are not just localised events as previously thought.

The most important parameter in the generation of wave impact pressures in a real sea was found to be the percentage of air entrained in the breaking wave. None of the equations currently in use for estimating wave impact pressures consider this parameter, which probably explains why these equations do not fit the measured data. An explicit equation for estimating the maximum impact pressure was not found but a method is given whereby the impact pressure is related to local wave parameters including a coefficient based on the percentage air entrainment.

Finite element modelling of the seawalls has shown that impact pressures can cause a significant dynamic response in the seawalls although short duration impacts (as measured in most model studies) have a negligible effect on response.

Nomenclature and abbreviations

A = Area

a = Amplitude

B_e = Bandwidth

B_r = Half power point bandwidth

C = Damping

= Wave celerity

C_b = Wave celerity at breaking

C.I.R.I.A. = Construction Industry Research and Information Association

D = Water depth at one wave length seaward of seawall

= Thickness of air cushion

d = Water depth at seawall

d_o = Deep water depth

E = Modulus of elasticity

F = Wave force

F' = Coefficient

f = Empirical coefficient

f = Frequency

f_n = Natural frequency

f_r = Resonant frequency

$G_x(f)$ = Spectral density function

g = Acceleration due to gravity

H = Wave height

H_b = Wave height at breaking

H_m = Mean wave height

H_{max} = Maximum wave height

H_o = Deep water wave height

H_s = Significant wave height

$H(jf)$ = Transfer function
h = Height
h' = The height over which wave impact occurs
K = Stiffness
K' = Coefficient (dimensionless) dependent upon H_b/L_b
K'' = Coefficient dependent upon $1/L_b$
K_n = Wave number = $2\pi/L$
k = Coefficient
L = Wave length
L_b = Wave length at breaking
l = length
la = Virtual length
M = Mass
m = Mean
MDOF = Multi-degree of freedom
n = Number of cycles
P = Pressure
P_h = Hydrostatic pressure
P_o = Atmospheric pressure
P_d = Dynamic pressure
P_s = Static pressure
P_i = Impact pressure
$P(x)$ = Probability density function
Q = Volume
Ro = Diaphragm radius
$R_x(\tau)$ = Auto-correlation function
$R_{x_1x_2}(\tau)$ = Cross-correlation function
$S_{FF}(f)$ = Excitation spectral density
$S_{XX}(f)$ = Response spectral density

S.W.L. = Still water level.
SDOF = Single degree of freedom
T = Time period
T' = Record length
t = Time or diaphragm thickness
U = water velocity
u = Parameter of the Gumbel distribution
V = Velocity of wave propagation or voltage
V_o = Wave particle velocity
V_s = Velocity of sound in water
x = displacement
$\dot{x}$ = velocity
$\ddot{x}$ = acceleration
$x(t)$ = A time history
y = Eigen vectors
α = Parameter of the Weibull distribution
β = Parameter of the Weibull distribution
Γ = Incomplete Gamma function
δ = Logrithmic decrement = $2\pi\xi$
ε = Mean square error
ε_b = Bias error
ε_r = Random error
λ = Smoothness coefficient or eigen values
μ_x = Mean
ν = Parameter of the Weibull distribution
ξ = Damping ratio
ρ = Density
σ^2 = Standard deviation
τ = Time period
φ = Angle
ω = Angular natural frequency

Definitions

Wave Height (H)	is the vertical distance from the wave crest level to the trough level, for real seas the height will vary for successive waves.
Wave Length (L)	is the horizontal distance between successive wave crests or troughs.
Wave Period (T)	is the time interval between successive wave crests (or troughs) passing a fixed point. The wave period is assumed to remain constant at all times, for all conditions of water depth etc.
Wave Celerity (C)	is the velocity at which individual waves travel across the water surface, and is a function of wave length and period, i.e. $C = L/T$.
Wave Steepness $(\frac{H}{L})$	is the ratio wave height/wave length. Wave steepness increases as a wave travels from deep to shallow water, the limiting value is about 1/7 in deep water and about 1/10 in shallow water.

INTRODUCTION TO PART A

The study of wave forces on seawalls has been a popular subject for full scale and laboratory studies dating back to before the start of this century. Like almost every activity in Civil Engineering there are limited data on the loads that act on real seawalls and the behaviour of the walls under these loads, due mainly to the difficulties involved with full scale measurements and the relatively few occurrences of high pressure wave impacts in a real sea state. This has meant that seawalls are still, even today, designed on an empirical basis with little attempt being made to correlate design assumptions with the reality of the service conditions. This, although appearing to be satisfactory, probably produces an over design for the majority of these structures and an unsafe design in some cases, as evidenced by the failure, both progressive and sudden, of some seawalls.

Information on the wave pressures that act on real seawalls was found to be very scarce in the literature, so a computer aided search of publications was initiated as part of a comprehensive literature review. This computer search was carried out under general headings such as ; wave forces, wave measurement, seawalls, etc. and produced over one thousand titles, although less than five percent were directly relevant to this investigation. As a result of this review thirteen full scale investigations and almost fifty model studies were discovered, spanning the last one hundred years.

The pressures exerted on a seawall by breaking waves can be grouped into two distinct types; (1) A slowly varying pressure of relatively long duration with a magnitude of the order of the standing wave pressure (i.e. hydrostatic) and (2) A short duration transient pressure lasting from only a few milli-seconds in the laboratory to about two hundred milli-seconds at full scale, but with a maximum pressure generally much greater than the hydrostatic pressure. This short duration impact pressure only occurs for certain conditions of wave breaking, whilst the hydrostatic wave pressure occurs for every wave that impinges on a seawall whether it breaks or not. The magnitude of the hydrostatic pressure is easily and accurately calculated from theory, whereas the magnitude of the impact pressure cannot yet be estimated entirely by theoretical analysis due to the highly complex (and as yet not fully understood) mechanism of wave breaking. For this reason the equations currently used to estimate the impact pressure are semi-empirical and often based only on experience or 'rule of thumb'.

The first attempts to physically measure the magnitude of wave impact pressures on real seawalls were made in the Nineteenth century by Thomas Stevenson, the data obtained were unreliable due to his crude measuring apparatus which at the time was the state of the art. It was not until the 1930's that wave impact pressures were measured with reliable and highly sensitive electronic equipment (by Rouville et al at Dieppe Harbour), since this time only four other such investigations have been attempted in the field. The volume of reliable full scale data amassed from these field investigations is very slight considering the number of man hours expended and is due mainly to the infrequent occurrence of impact pressures in a real sea, (usually less than two percent of all breaking waves produce any impact pressures).

The physical difficulties in measuring wave impact pressures on real structures led to a large number of model scale laboratory investigations. In the laboratory under controlled conditions, waves can be caused to break on the model walls in such a manner that impact pressures can regularly be produced, but these model scale pressures are generally far in excess of those measured in the field on real structures. This is because, real multidirectional shoaling seas cannot be modelled easily and parameters such as the percentage of entrained air cannot be scaled down to model size because of surface tension. Therefore whilst laboratory studies are useful for examining the phenomenon of wave impacts, suitable scaling laws are not available to allow model impacts to be related to full scale structures.

Thus there is evidently a strong need for further full scale wave pressure data to be collected to provide a basis for a rational approach to the estimation of wave impact pressures.

Part A of this thesis attempts to resolve some of the many difficulties posed by the measurement and analysis of wave impact pressures on real seawalls, with the following specific objectives being;

(a) To measure the wave impact pressures on the chosen seawalls along with the corresponding wave parameters such as; wave height, celerity and period

(b) To measure the structural response of the seawalls induced by the wave loading

(c) To correlate measured data with existing data and design methods and hence formulate a rational method for estimating wave impact pressures

(d) To measure temporal and spatial pressure distributions on the seawalls and correlate with design pressure distributions

CHAPTER ONE

HISTORICAL REVIEW

1.0 Introduction

The impact pressures exerted by waves breaking against real seawalls is a relatively unexplored subject area, to the authors knowledge only thirteen such investigations have taken place in the last 150 years, with only one in Britain, at Penzance, in the late 1890's by F. Latham.

When an advancing wave front strikes a fixed obstacle such as a seawall, impact pressures are generated if the conditions (as defined later) are favourable. A typical pressure history for a wave producing an impact pressure consists of a relatively large transient pressure lasting in the order of milli-seconds, superimposed upon a longer period lower intensity pressure. The transient pressure is due to the impinging of the wave front on the seawall, with the lower intensity pressure (of the order of the standing wave) being due to the uprush of the following body of the wave. Transient pressures greater than ten times the standing wave pressure have been measured by Goda (1).

1.1 Full Scale Testing

In the early days of field measurement (i.e. the late 19th century) the major stumbling block was how to capture on record the short term transient impact pressures associated with breaking waves. The first successful field measurements of wave pressure were made with a spring dynamometer by Thomas Stevenson (2) at Skerryvore Rocks in the Atlantic Ocean between 1842 and 1844. The dynamometers Stevenson used consisted of circular steel discs from 75 to 225 mm in diameter, attached to a spring system by measuring rods, as shown in Figure 1.1. These instruments could not respond to short duration transient pressures because of their large mass and slow mechanical response and they could not measure hydrostatic pressures because of pressure equalisation on either side of the disc. The other major disadvantage was that only a maximum pressure was recorded for each measuring session. One important factor that emerged from Stevenson's investigation was that by far the greatest pressures were exerted at, or near still water level.

An extensive series of wave pressure measurements were subsequently carried out by Capt. D.D. Gaillard (3) between 1890 and 1902 at various localities on the Great Lakes of North America, including a very detailed study on Lake Superior in 1901 using spring dynamometers similar to those used by Stevenson. Then in 1902 Gaillard developed the first diaphragm dynamometer, this instrument was capable of measuring both static and dynamic pressures which could be read directly for each wave. The pressures were transmitted hydraulically using water as the hydraulic medium and because of the long pipe lengths involved some attenuation was inevitable. These diaphragm dynamometers, which could respond to transients of less than one second duration, were the forerunner of modern strain gauge and electromagnetic pressure transducers.

Gaillard also presented some vertical pressure distributions measured on the South Pier of the Duluth Canal, although the individual pressure readings were made on the same day it was believed that they did not occur simultaneously. However it is interesting to note that the maximum pressure again occurred near still water level (S.W.L.). Gaillards main conclusions were;

(i) The impact of a wave does not at all resemble that of a solid body impact.

(ii) The limiting case for wave pressure is the pressure exerted by a jet of water of similar dimensions and velocity striking a plane surface at the same angle as the wave.

The results of three other wave pressure investigations, carried out by F. Latham, H.M. Robert and C.H. McKinstry are also briefly reported by Gaillard (3), see summary of results in Table 1.1 .

In 1905 to 1907 Hiroi (4) made some measurements of wave pressure at Otaru Harbour and Cape Taito (Japan), he used modified spring dynamometers which he described as a combination of diaphragm and spring dynamometers, mounted in such a way as to be able to respond to hydrostatic as well as dynamic pressures. He also developed a wave-dynamograph, a form of dynamometer capable of recording every impinging wave on a clock-work revolving cylinder. The maximum pressure Hiroi measured was 344.8 KN/m^2 (50 lbs/in^2), and he concluded that the maximum wave pressure occurs at S.W.L. and acts over a relatively small area.

In 1915 Molitor (5) made a detailed study of wave pressures on breakwaters at Lake Ontario using spring dynamometers, included in his comprehensive investigation are measurements of all additional parameters which he thought might influence wave pressure, such as beach slope, wind speed and direction etc. He later published a paper (5) combining his results with those of Gaillard, in which he proposed a method for evaluating vertical wave pressure distribution. Only one vertical pressure distribution is presented using his own data and it is not clear how much additional data he collected. The maximum pressure shown in his distribution is 30.3 KN/m^2 (4.4 lbs/in^2) and occurs at S.W.L. Molitors methods of analysis have been used in the design of breakwaters on Lake Ontario sucessfully, but it is doubtful whether they would be applicable to structures subjected to ocean waves, because in the ocean the wave pressures are potentially much larger than those possible in the Great Lakes. This is apparent by the very low maximum pressures measured by Molitor compared to those of other investigations in the ocean.

In 1921 Professor Luiggi (6) published a diagram showing the vertical wave pressure distribution on a breakwater due to a 7m high wave, and claimed the pressure distribution for a wave of any height breaking on a similar structure could be calculated by multiplying his pressure values by a factor of H/7 (where H = wave height). Luiggi devised his pressure diagram whilst engaged in the construction of a breakwater at the Port of Valparaiso. He placed piles of graded stones of known masses on the breakwater and observed their behaviour under various wave conditions (the stones weighed up to 28 tonnes), and hence was able to calculate the forces necessary to move them. Luiggi found that the maximum pressure necessary to move the stones was 322 KN/m^2 (46.7 lbs/in^2) and occurred at S.W.L., tailing off rapidly below and more slowly above S.W.L. (Figure 1.2). The pressures given by Luiggi must be treated with some suspicion as they are only estimates and were not actually measured.

The first major field investigation to measure wave pressures on a coastal structure with modern measuring and recording equipment was carried out by Rouville, Besson and Petry (7) in 1937 at Dieppe. Rouville et al had three piezo-electric pressure transducers installed in a vertical array on the face of Dieppe Harbour wall, in such a way as to give the pressure distribution over the height of the breaking wave. The maximum impact pressure measured by Rouville was 689 KN/m^2 (100 lbs/in^2) and it was found that only two percent of the observed wave impacts resulted in pressures greater than hydrostatic. A typical impact pressure history of a wave producing a pressure much greater than hydrostatic (as measured by Rouville) is shown in Figure 1.3. The investigation of Rouville lasted for three years but measurements were not made continuously during this period and little impact pressure data was obtained, so it was not possible to obtain conclusive evidence of anything other than the existence of high pressure wave impacts, (the wave pressures measured by Rouville are the largest ever measured on a real structure). An attempt was made to synchronise photographs of a wave breaking with the pressure record, but with little success. The few published results of vertical pressure distribution (thought to be instantaneous, although it is not made clear), can not be made use of because the position of S.W.L. is not given relative to the transducers at the time of the impacts.

Cot (8) between 1951 and 1953 carried out pressure measurements using five pressure cells mounted on the face of the Le Havre breakwater in a cruciform pattern. Like Rouville, Cot was able to measure and record transient wave impacts of the order of 10 milli-seconds duration, again very few transients were observed during the investigation. The maximum pressure measured by Cot was 98 KN/m^2 (14.2 lbs/in^2), and was measured at a point below S.W.L.

Kuribayashi, Udai and Muraki (9) made a study of wave pressures on Haboro Harbour breakwater (Japan), between 1957 and 1958 using strain gauge pressure transducers. Although their main considerations were the classification of wave pressures by wave shape and frequency of occurrence, they also gave the maximum measured pressure as 110 KN/m^2 (15.9 lbs/in^2) and estimated the maximum possible pressure for a 4.5m wave to be 150 KN/m^2 (21.7 lbs/in^2), no details of pressure distribution were given.

In 1966 Muraki (10) presented some results from a continuation of the above study, the only relevant new information he presented was a relationship between wave height and wave pressure, (see Section 1.3.2).

The most recent investigation to yield any data was carried out at Cape Cod, U.S.A. in 1974 by Millar, Leveratte, O'Sullivan, Tochko and Theriault (11). For this study five strain gauge mounted steel diaphragms were fixed, at 300mm centres, to a flat machined into one side of a 2m long aluminium cylinder. The cylinder was embedded in the sand and stabilized using three anchor cables. The data was fed back to the shore through a cable slung from the top of the cylinder. Millar found that the nature and magnitude of impact pressures was directly related to breaker shape. Hence the breakers were categorised according to the impact pressures they produced as follows;

(a) Bore - formed after the collapse of a plunging breaker, produced the maximum impact pressure.

(b) Plunging breaker

(c) Spilling breaker

(d) Near breaking wave - produced the smallest impact pressure

Millar correlated the wave shape with the resulting impact pressure by visually tracking the wave as it approached, and finally impinged on the transducers. The largest impact pressure measured by Millar was 41.4 KN/m^2 (6 lbs/in^2) produced by a bore, extreme shock pressures were absent. No information is given on the angle of incidence of the waves so it is not known whether the waves approached normal to the transducers. The average wave heights encountered by Millar were approximately 60% lower than those occurring at Dieppe (Rouville et al). This combined with the unusual method of mounting the transducers accounts for the large difference in the maximum pressures measured. i.e.

689.7 KN/m^2 produced by a 2.5m wave (Rouville)
41.4 KN/m^2 produced by a 0.9m wave (Millar)

The most recent published field study of wave pressures on coastal structures, at the time of writing, is that at Geno, Italy, carried out in 1975 by Marchi, Raiter, Scarse and Stura (12) of the University of Geno. Marchi et al used a vertical array of five pressure transducers to measure the wave impacts, in a manner similar to that adopted by Rouville et al.

Two types of pressure transducer were used during this investigation;

(1) Differential inductive type

and (2) strain gauge type

The first field measurements were made in early 1975 and although no storms producing impact pressures occurred before publication, two records of swell conditions recorded in March 1975 are included in the report. These records of swell indicate that the dynamic pressure occurring along the base of the cassions due to the waves, is everywhere uniform and not influenced by the wave motion.

This was the first investigation to employ an automatic data collection system. An automatic station for collecting and amplifing data from the transducers was located in a cassion of the breakwater, it was provided with a logical circuit to identify storm waves and automatically transmit the wave pressure data by telemetry to the receiving station at the Institute of Hydraulics in Geno. This system represents the state of the art of wave pressure data collection.

1.2 Model Studies

Whereas full-scale studies are notably lacking, there are numerous reports of model tests to measure wave impact pressures. These range from experiments on seawall models (Refs 1 and 13 to 50), to dropping plates onto the water surface (Refs 51, 52 and 53), to tests on model cassions, cells and sluice gates (Refs 54 to 58). As the literature is so extensive and this research is more concerned with full-scale studies then only a brief summary of some of the many model studies is included herein, for more details the reader is directed to the references mentioned above.

Bagnold (14) in 1937 to 1939 was probably the first to carry out extensive seawall model experiments using vertical concrete walls in a wave tank. These experiments were designed to complement the full scale study of Rouville et al. Like Rouville, Bagnold found shock pressures occurred randomly and varied greatly for similar waves. He found the timing of the wave was critical and had to be such that the wave front was parallel to the wall at the instant of impact before consistent shock pressures were produced. This compares with Millar (11) who measured the largest pressures for waves with near vertical front faces, (i.e. the bores). Bagnold surmised from his work that impact pressures resulting from breaking waves were due to the retardation of the water mass by the entrapment of a thin lens of air which becomes compressed (adiabatically) and 'explodes' causing the shock pressures. Bagnold observed peak pressures in excess of ten times the normal hydrostatic pressure, up to a maximum value of 552 KN/m^2 (80 lbs/in^2). He concluded that these model pressures when scaled up to full size sea waves 3m high would represent pressures in the order of 6900 KN/m^2 (1000 lbs/in^2). The reason given to account for this large difference between predicted and measured full-scale pressures was that, in the laboratory studies the fresh water waves tended to be smooth and regular and not provide a true representation of real sea waves. This conclusion is also borne out by Denny (13) who found pressure was heavily dependant upon the smoothness of the wave front. Denny states, "when the waves carried ripples only four per cent of the wave height the shock pressures were nearly halved". He also found, like Bagnold, that the product of pressure and duration (the impulse) for a train of waves was much more consistent than the pressures themselves, i.e. the greater the shock pressure the shorter the duration. As can be seen from Figure 1.4 the shock impulse tends to a finite maximum which corresponds closely to that for a solitary wave.

Denny later found from his model studies that although the shock pressures were variable for similar waves the highest recorded pressure for a given wave seemed to be substantially proportional to the wave height (Figure 1.5) and the maximum pressure exerted by a wave was dependent upon the smoothness of both the seawall and the front face of the wave.

Carr(39) (1951) considered it to be wasteful to design seawalls using the value of the impact pressure, he substantiated this from his results by showing that the impulse ($I = \int P\,dt$) of the impact pressure was no more than 10% of the impulse of the total wave pressure. In his conclusion Carr suggests that designs be based on what he calls the persistent force component (the relatively long duration low pressure part of the impact history), of a breaking wave. He also states that by inclining the seawall 30° shoreward from the vertical it halved the forces produced on the wall.

Ross(35) in 1954 drew the same general conclusions from his experimental work as did Bagnold(14). The wave pressures measured by Ross were extremely variable, ranging from zero to a maximum of 147.6 KN/m^2 (21.4 lbs/in^2) for a wave of 12.5cm.

Ross made the following additional conclusions;

(1) Impact pressures occur when a wave with a vertical front face strikes a wall also with a vertical face.

(2) Impact pressures occur from the top of the wave to some distance below S.W.L.

In 1958 Weggel (38) from his experimental work classified impact pressures into two groups, termed ordinary and significant pressures. This classification was based on the magnitude and area of application of the pressure, significant pressures were those which occurred most frequently and acted over relatively large areas and were therefore important in the design of the structure, whilst ordinary pressures were the localised high pressure impacts. These conclusions are similar to those made by Carr (39). The maximum pressure recorded by Weggel was 80.7 KN/m^2 (11.7 lbs/in^2) and had a time history very similar to that in Figure 1.3.

Delmont (47) in 1972 set out to find a formula for predicting the forces exerted on a seawall by breaking waves. To do this he examined six theories from independent authors which related directly to his investigation. He reviewed these theories and compared them with his own experimental data obtained by measuring the total force on model seawalls in a wave tank. Delmont concluded that 'the formula presented by Homma and Horikawa (16), is the most useful one for toe depths less than about three inches', for depths greater than three inches Delmont recommends further research to find a suitable formula because none of those tested was found to be valid in these conditions. Delmonts own data show considerable scatter with a maximum value of 205.5 KN/m^2 (29.8 lbs/in^2) this data is shown in Figure 1.6 along with the equation of Homma and Horikawa.

Nagai has carried out a large number of experimental investigations, mainly concerning wave impact pressures on composite breakwaters (Refs 25, 26, 27 and 30), although he also investigated the pressures due to standing and partially standing waves (Refs 28 and 29).

Some of his conclusions are;

(i) The pressures exerted by breaking waves will not reach the water hammer pressure, this observation was based on experimental data which was found to have a magnitude substantially lower than that predicted by the water hammer expression.

(ii) Impact pressures are not due to the compression of an air pocket as suggested by Bagnold.

(iii) The vertical pressure distribution is dependent upon the type of breakwater investigated, the maximum pressure was found to occur from S.W.L. to the base of the wall depending on the breakwater type.

Other notable experiments were carried out by Hayashi and Hattory(17), Mitsuyasu(22),(23), Larras(40) and Rungren(43).

In all of the full scale and many of the experimental investigations reviewed, the main objective has been the measurement of wave impact pressures, in many cases the equally important wave characteristics of height, celerity, period and length have been neglected. There is then no way in which these wave pressures can be related to the sea state which produced them.

The other major problem apparent in field investigations is that authors do not clearly define how or where the wave parameters were measured, so it is often not clear whether the wave heights and celerities were measured in deep or shoaling water. For these reasons

it is difficult to be sure, when comparing data from different investigations, that like is being compared with like.

1.3 Development of Wave Theories

1.3.1 Long and Small Amplitude Waves

The analysis of non-breaking water waves lends itself to mathematical solution and many such solutions have been derived for particular types of wave in deep and shoaling water, (Refs. 59 to 70). The following is intended as a brief introduction to the history of modern wave theories, with mention given only to some of the more important theories.

There are two main families of waves, Oscillatory and Translatory. The oscillatory wave is assumed to have zero mass transport, whereas the translatory wave (such as a tidal bore) will always have a net mass transport. The Cnoidal wave is considered oscillatory even though there is a very small net mass transport, but the limiting case for the Cnoidal wave, known as the Solitary wave, is wholly translatory.

The two general approaches to wave theory are from small amplitude and long wave theory. The small amplitude theory is essentially linear and the equations tend to become exact as the motion tends to zero, (providing the convective inertia terms are neglected). The water particle motion is usually considered as being irrotational and although theoretically based on small wave lengths in deep water it can also be applied to relatively large waves in shallow water quite successfully (Ref 79).

The foundations for small wave theory as we know it today were laid by F.V. Gerstner in 1802. In his approach Gerstner assumed the wave shape to be described by a trochoid, and the water particle orbits circular even for shallow water waves. In 1844 Airy developed the Gerstner theory to include elliptical water particle orbits in shallow water. Airy assumed that the still water level marked the mean point between wave crest and trough, as this is only true for small amplitude waves, then Airy's theory is only strictly applicable to small waves. In 1880 G. Stokes published a paper based on Airy's work but modified to produce a steeper and higher wave crest and a wave trough more shallow and flat. Stokes theory has now been expanded in H/L (wave height /wave length) power series to include fifth and even higher order terms. Modifed forms of the small amplitude theory have been produced to describe waves generated by tsunami's, underwater explosions and bodies dropping on to the free water surface.

The long wave theory is essentially treated by numerical methods, as opposed to the analytical methods used for small amplitude waves. The theory is applicable when the relative depth is very small, the equations are nonlinear so the solutions are limited to particular cases only, such as Cnoidal, Solitary and waves in tidal estuaries.

The classification of water waves is a difficult task because there are so many possible categories such as linear/nonlinear, shallow water/deep water, oscillatory/translatory, rotational/

irrotational, these categories are not clear cut and so some over lapping can be expected. In Table 1.2 the most relevant theories are classified under small amplitude and long wave theories, some of the wave profiles given by these theories are shown in Figure 1.7 .

1.3.2 Breaking and Standing Waves

The preceeding wave theories are mostly highly theoretical and model the wave profile and boundary conditions to a high degree of accuracy within their own limits of applicability. The water particle velocities and accelerations and hence the pressures and forces can be predicted using these theories so long as the wave stays reasonably regular and stable. This is generally the case for offshore applications in deep water, but the coastal engineer is faced with the problem of standing and breaking waves for which cases the preceeding theories fall down.

Standing waves can be dealt with by a simple adaptation of linear wave theory by superimposing an image train of waves of identical characteristics but travelling in the opposite direction to the incident wave, which results in;([illegible])

$$P = 2\rho g H \frac{\cosh K(2 + d)}{\cosh Kd} \qquad \dots\dots\dots\dots\dots\dots (1.1)$$

where P = pressure variation with depth at instant of maximum amplitude.

K = wave number = $\frac{2\pi}{L}$

L = wave length

d = water depth at wall

H = wave height

Or, the method most frequently used by coastal engineers is to employ one of the semi-empirical formulae due to Nagai (28),(29), Sainflou (71) and others,

e.g. from Sainflou

$$F = \frac{\rho g d}{\cosh 2\pi d/L + \rho g d} (H + \delta d + d) \quad \ldots\ldots\ldots \quad (1.2)$$

where F = total wave force per unit length of wall

H = wave height

d = water depth at wall

δd = rise in mean water level $= \frac{H^2}{L} \coth \frac{2\pi d}{L}$

Breaking waves are a much more complex problem, at present there is no theoretical solution for calculating breaking wave forces. Although there are theories available derived from empirical fitting to experimental data by; Bagnold (14), Hiroi (4), Denny (13), Hayashi(18), Molitor(5), Nagai(31), Minikin(72),(73) and many others.

Molitor (5) and Gaillard(3) derived solutions of the form

$$P_i = \frac{f\omega}{2g} (V + Vo)^2 \quad \ldots\ldots\ldots\ldots\ldots\ldots\ldots\ldots \quad (1.3)$$

where P_i = wave impact pressure at S.W.L.

ω = unit weight of water

V = velocity of wave propagation

Vo = water particle orbital velocity

f = empirical coefficient

Gaillard gave a limiting value for f of 2, whereas Molitor suggested f was proportional to the wind speed and gave a value of 1.8 for ocean waves.

Due to the problems of measuring the orbital velocity of equation 1.3 in a real sea, Hayashi et al$^{(17)}$ and later Millar et al$^{(11)}$ dropped the Vo term and changed f accordingly as shown below.

$$\frac{P_i}{\omega} = f \frac{C^2}{2g} \qquad \ldots\ldots\ldots\ldots\ldots\ldots\ldots\ldots\ldots \quad (1.4)$$

where P_i = impact pressure of breaking wave

C = wave celerity

f = 4 (Hayashi)

f = 1.6 to 2 (Millar)

These preceeding empirical equations do not include a wave height term directly (celerity is related to wave height by first order solitary wave theory, $C = \sqrt{gd(1 + \frac{H}{d})}$), some authors such as Hiroi$^{(4)}$ and Muraki$^{(10)}$ assumed that wave height had a direct bearing upon the wave impact pressure and so gave the following equations;

Hiroi :- $P_i = k\,H$ $\ldots\ldots\ldots\ldots\ldots\ldots\ldots\ldots$ (1.5)

where k is a constant = 1.5

Muraki :- $P_o = k\,H_o$ $\ldots\ldots\ldots\ldots\ldots\ldots\ldots\ldots$ (1.6)

where k is a coefficient which varies from 1 to 1.43

Homma and Horikawa(16) proposed the following equation for the total wave force exerted against a vertical seawall, based on data gained from their model studies;

$$F = 4.18\ d^2\omega \quad \ldots\ldots\ldots\ldots\ldots\ldots\ldots\ldots \quad (1.7)$$

where F = total wave force per unit width of wall (including the hydrostatic pressure)

d = height of S.W.L. at the wall

the following limitations apply to this equation

(a) $d > 0.2H$ (H = wave height at seawall)

(b) beach slope must be > 1 : 30

(c) waves must break in front of, and not right on the seawall.

Delmonte(47) found this equation to be quite accurate within the limits of application when applying it to his own experimental data, as shown in Figure 1.6 .

Nagai(28),(29) proposed the following equations; in S.I. units

for average impact pressure :-

$$P_{max(ave)} = 96\ (0.008 + d\ \frac{dH}{d_o L})^{1/3} \quad \ldots\ldots\ldots \quad (1.8)$$

and for maximum impact pressure:-

$$P_{max} = 103\ (0.01 + d\ \frac{dH}{d_o L})^{1/3} \quad \ldots\ldots\ldots \quad (1.9)$$

where H = unobstructed wave height at breakwater

L = wave length at breakwater

d = water depth at wall

d_o = water depth at toe of rubble mound

Equations 1.8 and 1.9 were developed for composite type breakwaters and as such might not be applicable to pressures on seawalls.

Bagnold(14) derived the basis for what is probably the most widely used formula for predicting the pressures of breaking waves. Bagnold produced a mathematical model of a wave impact by considering the wave as a 'piston' moving in a 'cup of air', as shown below.

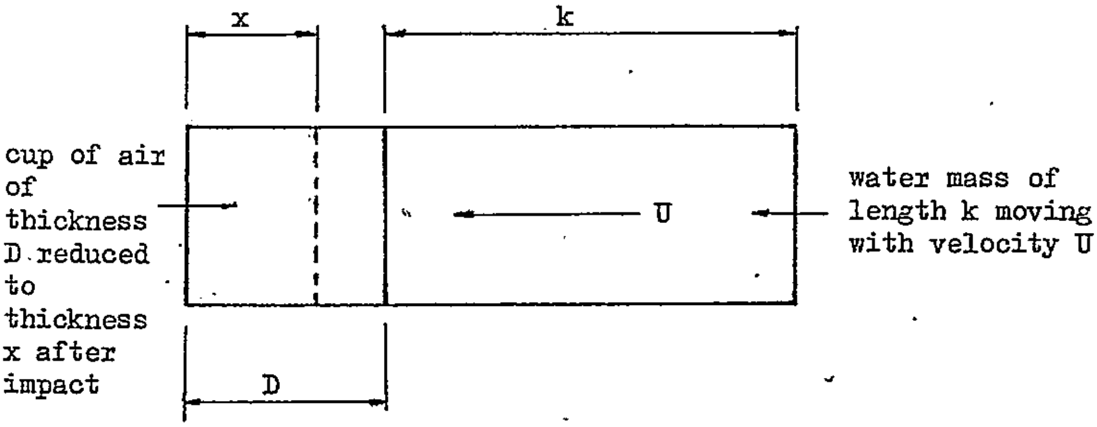
x
k
cup of air of thickness D reduced to thickness x after impact
U
water mass of length k moving with velocity U
D

The following expression resulted;

$$(P_{max} - P_o) = 2.7 \frac{U^2 k \rho}{D} \qquad \text{..............} \quad (1.10)$$

where $(P_{max} - P_o)$ = maximum impact pressure

As it stands equation 1.10 cannot be used because of the unknown dimensions of k and D.

Bagnold found that the area under the pressure time curve, (the impulse) from his experimental data approached but never exceeded a definite value, which equalled the momentum destroyed. In equation form written as;

$$k \cdot \rho U = P\,dt$$

or $$k = \frac{P\,dt}{\rho U} \quad \ldots\ldots\ldots\ldots\ldots\ldots\ldots\ldots\ldots\ldots\ldots\ldots \quad (1.11)$$

From his model tests Bagnold obtained a value for k of 0.2H, which when substituted into equation 1.10 gives;

$$P_i = 0.54 \ \rho U^2 \frac{H}{D} \quad \ldots\ldots\ldots\ldots\ldots\ldots\ldots\ldots\ldots\ldots\ldots \quad (1.12)$$

When Bagnold compared equation 1.12 with the full scale data of Rouville(7), he found that in 2 out of 7 cases the impulse measured from the pressure time curves exceeded his calculated value of $\rho U k$. This led him to suggest k might actually be slightly greater than 0.2H.

It is still not possible to use Bagnolds equation (1.12) for full scale waves because of the difficulty in evaluating the thickness of the air cushion (D). To overcome this problem Minikin(72) modified Bagnolds equation to the following ;

$$P_i = 2\pi d/LD_r \ \ \rho Hg \ (\frac{D_r + d}{2}) \ \ \text{lbs/ft}^2 \quad \ldots\ldots \quad (1.13)$$

this simplifies to the following (in S.I. units)

$$P_i = 101.1\omega \frac{H}{L} \, d(\frac{d}{D_r} + 1) \quad KN/m^2 \quad \text{..........} \ (1.14)$$

where P_i = impact pressure

H = wave height at the wall

L = wave length at toe of rubble mound

D_r = water depth at toe of rubble mound

d = water depth at seawall

The maximum dynamic pressure is assumed to act at S.W.L. with a parabolic distribution above and below this level as shown in Figure 1.8 . The total wave pressure is obtained by including the hydrostatic component, given by;

$$P_s = \omega \frac{H}{2} \quad \text{acting at S.W.L.} \quad \text{...........} \ (1.15)$$

and

$$P_d = \omega (\frac{H}{2} + d) \quad \text{acting at depth } d \quad \text{........} \ (1.16)$$

Minikins equation was originally derived for composite breakwaters founded upon rubble mounds, but has since been adapted in Ref. 74 for use on vertical seawalls. D_r now becomes the water depth at one wave length seaward from the seawall, and L now becomes the wave length at this depth. The bed slope limitation for this revised formula is of the order of 1 : 15 .

From this section it is evident that there is no consensus of opinion as to the location and value of the maximum impact pressure on seawalls subjected to breaking waves. Gaillard, Molitor and Hiroi all measured maximum impact pressures at S.W.L., Cot measured maximum pressures below S.W.L. and Millar found the location could vary depending upon the wave type. This is therefore an area which requires further investigation, and is discussed further in Chapter Three.

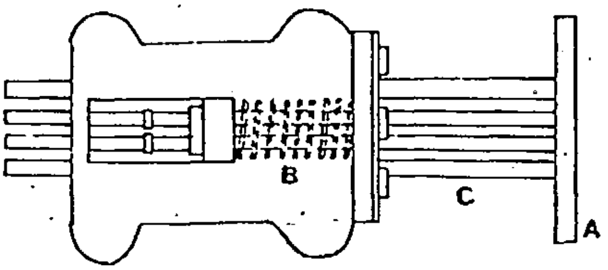

Figure 1.1 Stevenson's spring dynamometer (after Gaillard(3))

(A) Circular disc

(B) Spring

(C) Measuring rods coated with a paraffin/wax mixture; as the rods move inwards due to waves impinging on disc (A) the wax mixture is scraped off, maximum pressure during any period of measurement can be determined knowing the stiffness of spring (B) and the length of rod (C) scraped clean.

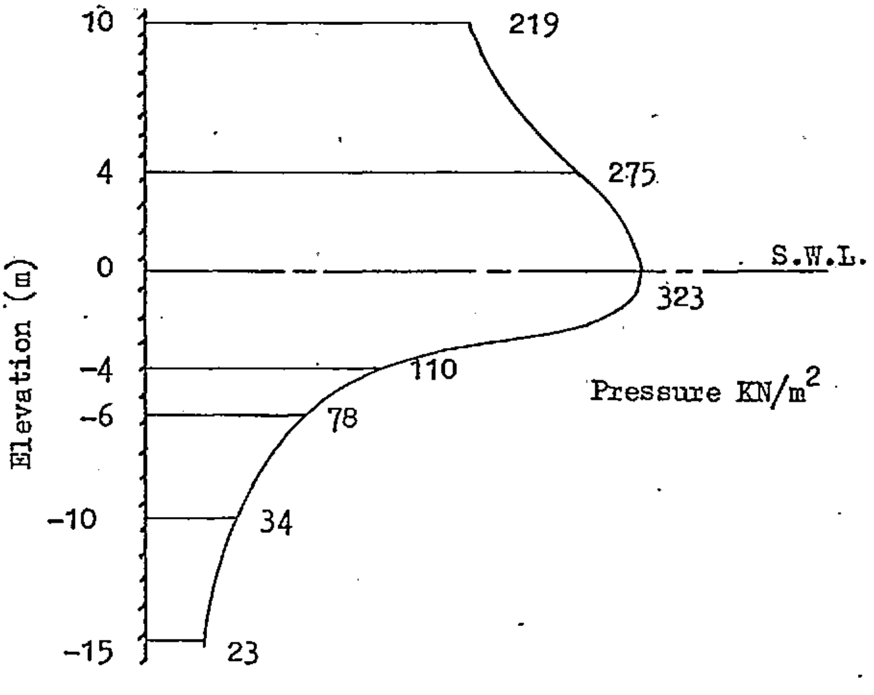

Figure 1.2 Luiggi pressure diagram

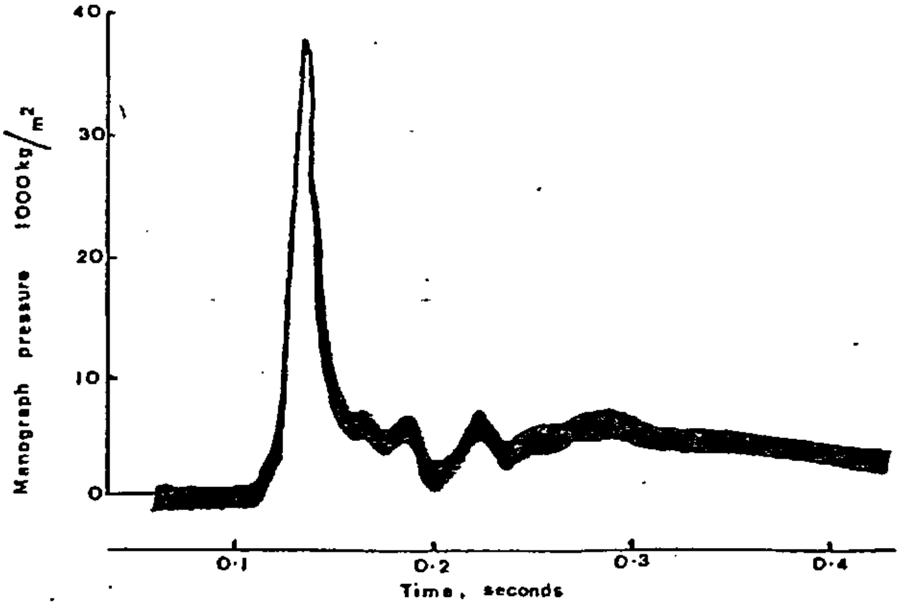

Figure 1.3 Full scale sea waves;Pressure impulses (after Rouville et al 1938)

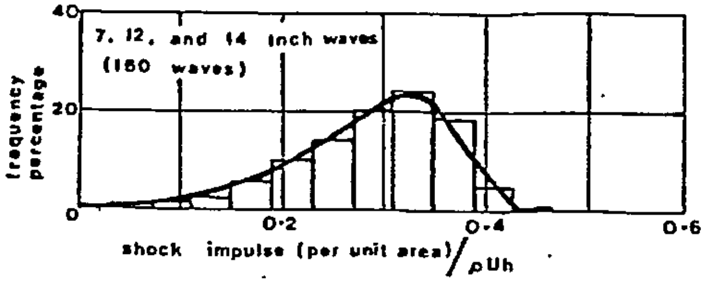

Figure 1.4 Frequency of shock impulses (after Denny 1951)

p - water density
U - wave velocity
h - wave height

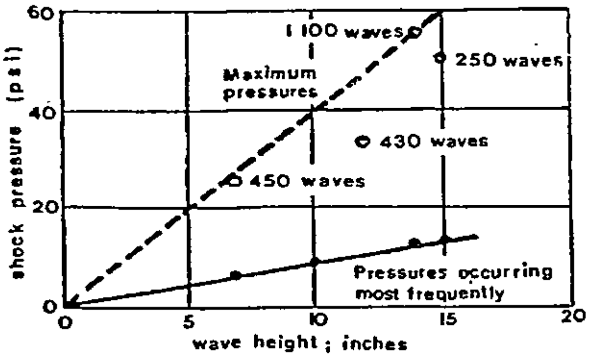

Figure 1.5 Variation of shock pressure with wave height for similar waves (after Denny, 1951)

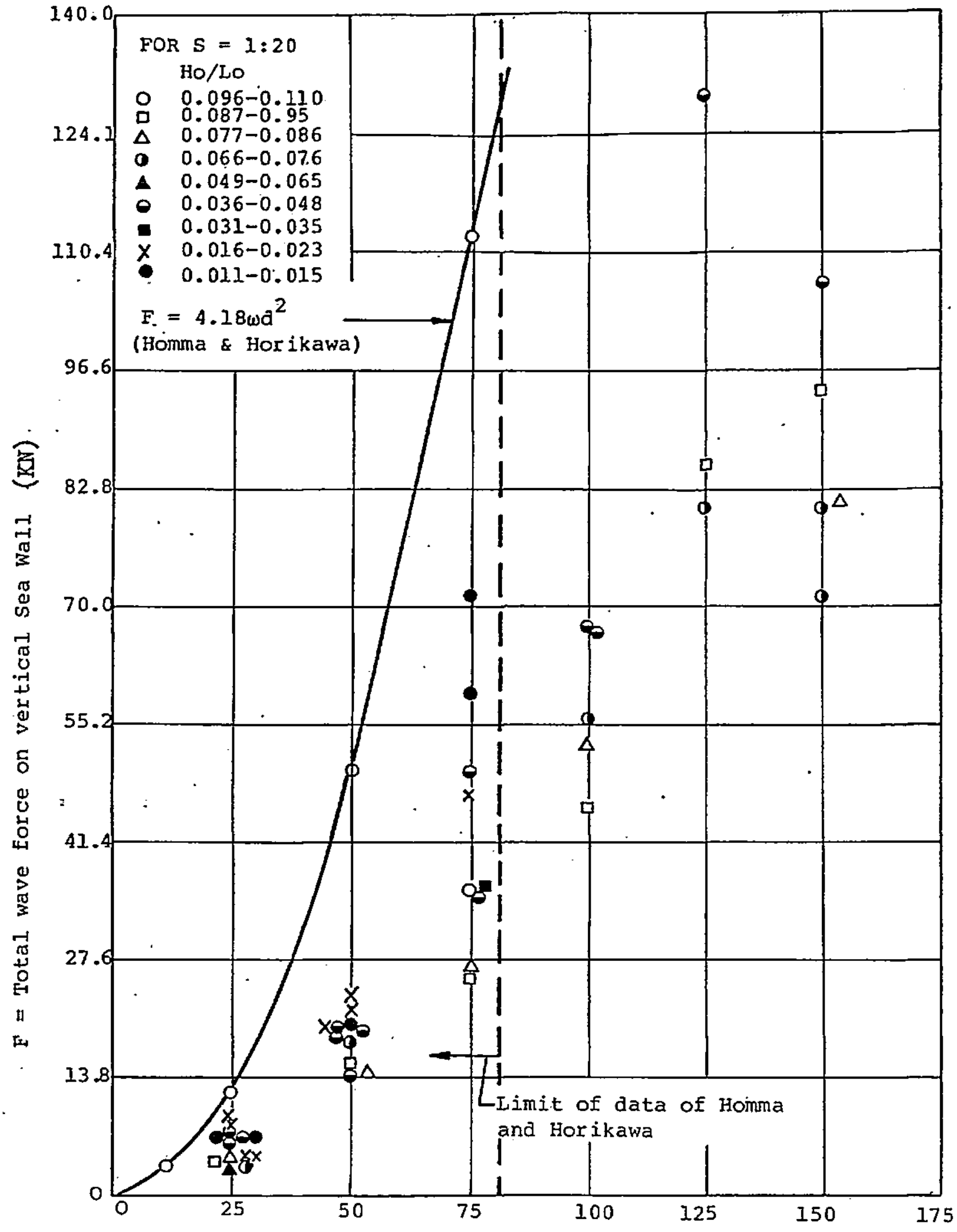

FIG. 1.6 Experimental Data of Delmonte Compared with the Formula of Homma and Horikawa (after Delmonte 1972).

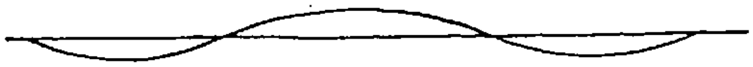

(a) Airy wave in deep water

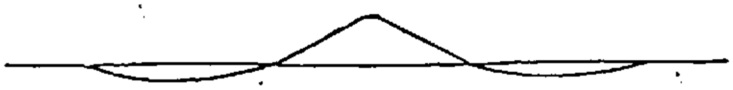

(b) Stoke's wave in deep water

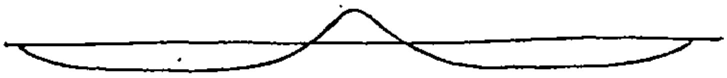

(c). Cnoidal wave

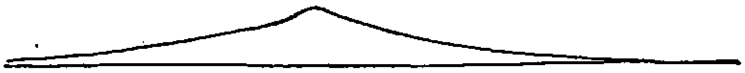

(d) Solitary wave

Figure 1.7 Some common wave profiles

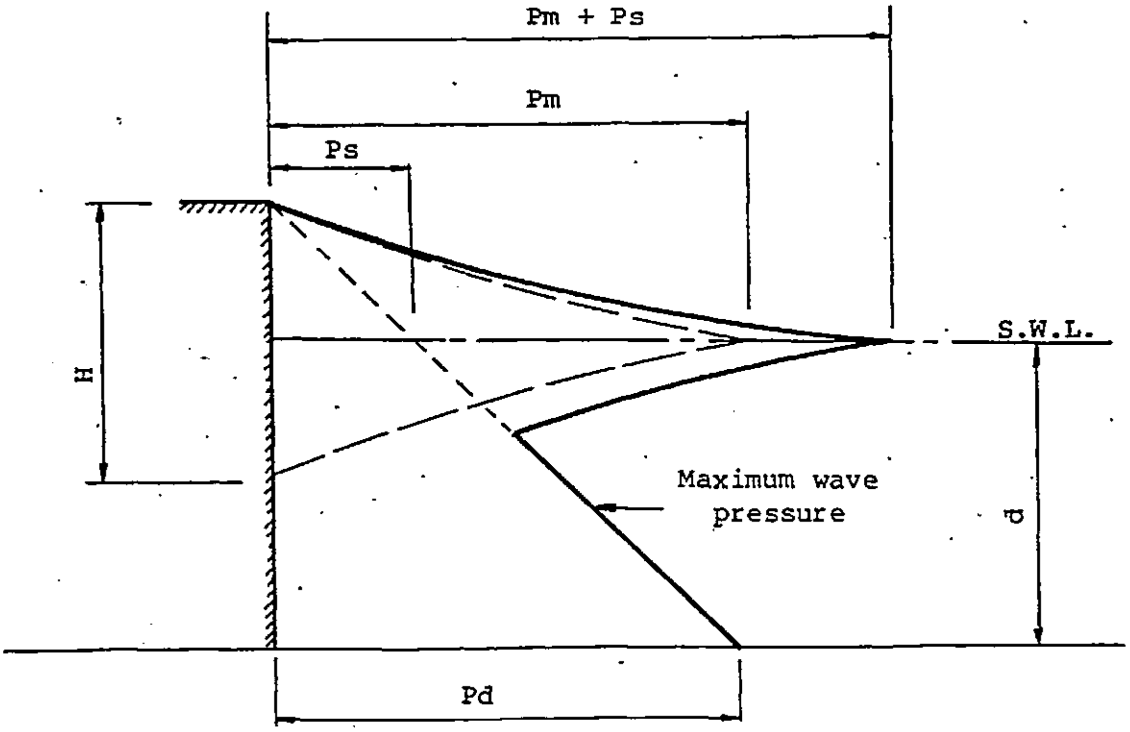
Pm + Ps
Pm
Ps
H
S.W.L.
Maximum wave
pressure
d
Pd

Figure 1.8 Minikin wave pressure diagram.

Table 1.1 Results from all known investigations to measure wave pressures on seawalls and breakwaters

Investigator	Location of Measurements	Maximum Pressure Measured		Average Pressure Measured		Wave Height	Pressure Measuring Apparatus
		KN/m^2	(lbs/in^2)	KN/m^2	(lbs/in^2)	m	
T. Stevenson	Skerryvore Rocks, 1843-44	291	(42.2)	Summer 29 Winter 100	(4.2) (14.5)	- -	Spring Dynamometer
	Bell Rock	145	(21.0)	-		-	" "
	Dunbar Harbour, 1858	375	(54.4)	-		6.1	" "
	Buckie	322	(46.7)	-		6.1	" "
F. Latham	Penzance Harbour, England	-		96	(13.9)	-	Spring Dynamometer
H.M. Robert	Oswego Harbour, N.York, 1884	45	(6.5)	24	(3.5)	4.3 - 5.5	Spring Dynamometer
C.H. McKinstry	Milwaukee Bay, 12-2-1894	68	(9.9)	-		-	Spring Dynamometer
	8-4-1894	165	(24.0)	-		4.0	
D.D. Gaillard	St. Augustine, Fla. 1890-91	32	(4.5)	-		1.8	Spring Dynamometer
	Lake Superior, S. Pier 1902	113	(16.4)	-		4.9	" "
	" S. Pier 1902	79	(11.4)	-		4.0	Diaphragm Dynamometer
	" E. B'water 1902	121	(17.5)	-		-	Spring Dynamometer
	Black Rock, 1902	99	(14.3)	-		-	" "
D.A. Molitor	Lake Ontario, Canada, 1915	30	(4.4)	-		2.8	Spring Dynamometer
I. Hiroi	Otaru Harbour, Japan, 1920	345	(50.0)	-		-	Spring Dynamometer

Table 1.1 (continued)

L. Luiggi	Port of Valparaiso, 1921	322 (46.7)	-	7	-
M.A. Rouville P. Besson R. Petry	Dieppe, France, 1937	690 (100)	-	2.5	Piezo-electric Pressure Transducer
P.D. Cot	Le Havre, France, 1954	98 (14.2)	-	2.5	Pressure Cells
T.Kuribayashi Y. Muraki G. Udai	Haboro Harbour, Japan 1957 to 59	110 (15.9)	-	4.5	Straingauge Pressure Transducer
R.L. Miller S. Leverette J. O'Sullivan	Cape Cod, America, 1974	41 (6.0)	19 (2.75)	0.9	Straingauge Pressure Transducer

TABLE 1.2 CALSSIFICATION OF WAVE THEORIES.

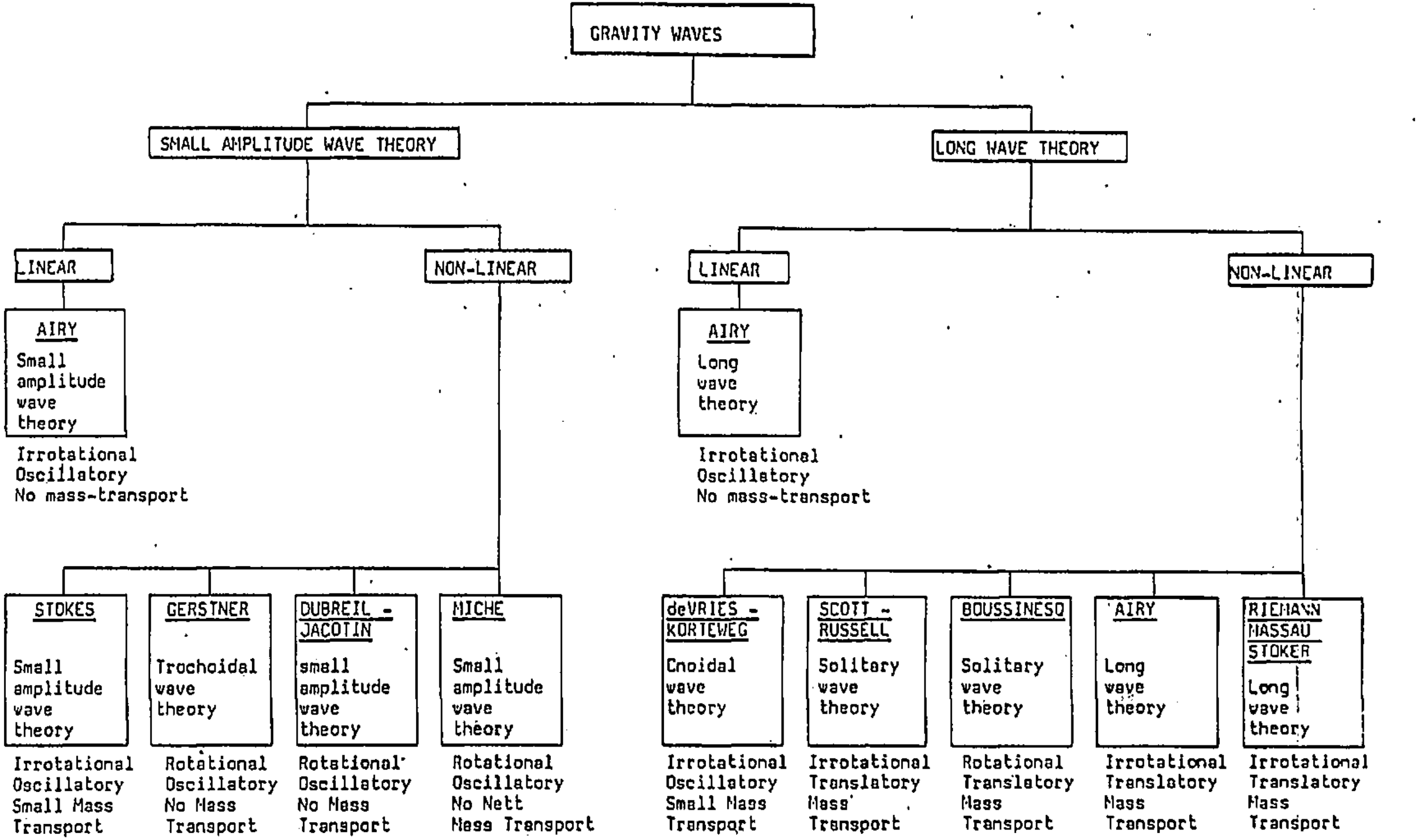
GRAVITY WAVES
SMALL AMPLITUDE WAVE THEORY
LONG WAVE THEORY
LINEAR
NON-LINEAR
AIRY
Small amplitude wave theory
Irrotational
Oscillatory
No mass-transport
LINEAR
NON-LINEAR
AIRY
Long wave theory
Irrotational
Oscillatory
No mass-transport
STOKES
Small amplitude wave theory
Irrotational
Oscillatory
Small Mass Transport
GERSTNER
Trochoidal wave theory
Rotational
Oscillatory
No Mass Transport
DUBREIL - JACOTIN
small amplitude wave theory
Rotational
Oscillatory
No Mass Transport
MICHE
Small amplitude wave theory
Rotational
Oscillatory
No Nett Mass Transport
deVRIES - KORTEWEG
Cnoidal wave theory
Irrotational
Oscillatory
Small Mass Transport
SCOTT - RUSSELL
Solitary wave theory
Irrotational
Translatory
Mass Transport
BOUSSINESQ
Solitary wave theory
Rotational
Translatory
Mass Transport
AIRY
Long wave theory
Irrotational
Translatory
Mass Transport
RIEMANN
MASSAU
STOKER
Long wave theory
Irrotational
Translatory
Mass Transport

CHAPTER TWO

INSTRUMENTATION AND MONITORING OF SOME SEAWALLS

2.1 Introduction

This investigation originally started with the instrumentation of a seawall at Teignmouth in South Devon, funded jointly by the S.W.W.A. and C.I.R.I.A. The first pressure measurements were made in late November 1978, but by the end of January 1979 after only two recording sessions, the beach level had risen in places by over 3m completely burying the pressure transducers and making further wave pressure measurements impossible. This prompted a search for additional seawalls with which to continue the investigation, the instrumentation was (originally) designed to be installed insitu in the seawalls so this limited the choice of wall to those either undergoing construction or major repair. The second wall to be instrumented (during the summer of 1979) was about three miles to the East of the Teignmouth seawall and formed part of the Brunel seawall owned by British Rail. Additional funding became available at this time, so two more seawalls at Ilfracombe (North Devon) and Seaford (East Sussex) were included.

The following is a brief description of the four chosen seawalls;

(1)	Teignmouth seawall	- a 5.5m insitu concrete wall with a curved re-entrant face with bull nose.
(2)	Brunel seawall	- a 3.5m slightly inclined flat faced block work wall
(3)	Ilfracombe seawall	- a 7.5m precast concrete block wall with a curved re-entrant face with bull nose

(4) Seaford seawall - a 5m insitu concrete wall with a combined stepped and curved face with bull nose.

The impact pressures were measured by means of strain gauge mounted stainless steel diaphragms, this measuring system was originally designed to be fixed insitu into the seawalls to afford the greatest degree of protection and for the convienience which would allow measurements to be made simply by plugging in the transducer outputs.

Seawall accelerations were also measured by means of accelerometers bolted to the walls. This data gives an insight into the behaviour of the seawalls under wave loading and also allows the seawall displacements to be calculated.

The layout of the pressure transducers on each seawall face was the subject of much discussion, the major problem was in deciding on the spacing in the horizontal and vertical planes. After consulting all available literature on full scale testing, the only investigation found to contain any reference to the measurement of horizontal pressure distributions was that of Cot(8), but even this paper gave little information on the reasons for his choice of layout. The transducer layout used by Cot at Le Havre is shown below

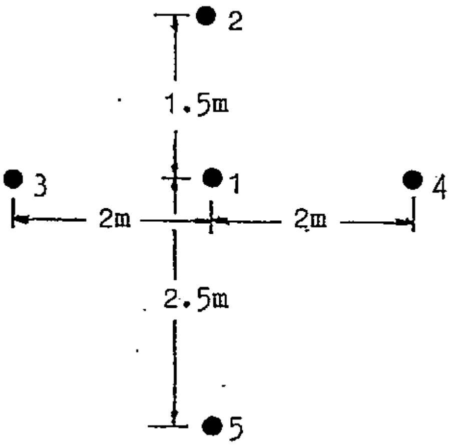

The maximum number of transducers that could be installed in any wall for continuous measurement was limited to seven. This was the number of data recording channels available at the time, additional recording facilities became available only after all installations were completed.

The vertical pressure distribution was considered the more important therefore the majority of transducers were concentrated in this plane near M.H.W.S. level, the actual vertical spacing being decided by the local features of each wall. Because data concerning the horizontal spacing of transducers was so scarce and the resources were not available for model testing, the ideal configuration of transducers could not be assertained. So where possible a horizontal group of closely spaced transducers with additional transducers at larger spacings were incorporated into the walls. This seemed the best compromise because the closely spaced group would provide data on the horizontal extent of any wave impacts, whilst the larger spacing would enable any change in pressure along a wave front to be measured. As four seawalls were instrumented a different horizontal spacing could be employed on each, ranging from 100m at Teignmouth to 0.75m at Ilfracombe.

2.2 Seawalls (Location and Instrumentation)

2.2.1 Teignmouth Seawall

Teignmouth is a small port on the South coast of Devon(75), about 15 miles from Exeter, Figure 2.1. A new seawall was built here to replace an existing masonary wall which fronted the town centre, the existing

wall was continually being breached during heavy seas leading to flooding of the town. The new wall is of mass concrete construction some 5.5m high with a curved re-entrant face, as shown in Figure 2.2 and Plate 2.1 .

Provision was made during construction for the installation of five pressure transducers in the wall face. To measure the vertical wave pressure distribution three transducers were grouped in a vertical array, the middle transducer was positioned on the vertical section of the wall at level 3.46m A.O.D., and the remaining two transducers were spaced at 0.75m centres above and below this point at levels 4.21m and 2.71m, (Figure 2.3). The horizontal transducer array consisted of two transducers at level 3.46m A.O.D., spaced 50m to the West and 100m to the East of the vertical array.

Three manholes, immediately behind the seawall, were built during construction of the wall, one was located behind the vertical transducer array and the other two behind the single transducers. The cables from each transducer were fed through ducts cast into the wall to the manholes behind, the transducer cables were then all fed back through ducts to the central manhole (behind the vertical transducer array), which was used as the data recording station. This manhole was about 2.5m x 2m x 2m high and had a mains electricity supply and provision for heating and lighting, access was through a manhole cover on the promenade 1.5m from the front of the wall, Figure 2.2. Because of this close proximity to the front of the wall, entry to the manhole was not possible during rough weather because of overtopping waves and spray. This also meant that if the manhole was occupied when waves were over topping then it had to be evacuated because the cover could not be made water tight due to the risk of suffocation. The manholes had no provision for drainage so consequently they needed to be pumped out periodically to prevent the transducer cables becoming waterlogged.

Two accelerometers were used to measure seawall acceleration and were fixed to brackets on the back of the seawall in the recording station at approximate levels of 3.5m and 1.9m A.O.D.

Construction of this seawall was finished in late 1977 at which time the beach level was near the base of the wall at level 1.5m, but during the severe winter storms of 1978-79 the beach level rose to about 4.5m completely covering all five pressure transducers making further wave pressure measurements impossible for the duration of this investigation.

2.2.2 Brunel Seawall

The instrumented section of the Brunel seawall is actually a short (40m long) breakwater running parallel and about 35m infront of the main seawall, Figure 2.1, Plate 2.2, its original purpose was to protect a lifeboat slipway, now obsolete.

The wall is about 3.5m high and 3.5m wide at the base tapering to 2m at the top (Figure 2.4) it is built of large granite blocks with a rubble and mass concrete heart. During the 1978-79 winter storms this wall was extensively damaged (Plate 2.3), this allowed the installation of pressure transducers during its reconstruction in the summer of 1979. Only three transducers were built into this wall because the type of construction allowed no more, two transducers were arranged in a vertical plane 800mm apart, with the third transducer 8m to the West at the same level as the upper transducer of the vertical array, Figure 2.5. Levels were not measured relative to O.D. because there were no bench marks within easy reach.

The transducers were mounted flush with the front face of the wall and the cables were passed through to the back face of the wall in ducts. Flexible armoured conduit was then fixed to the back face of the wall and led up to the recording station, the transducer cables were then fed through it. Fixing the armoured conduit to the wall proved a problem because of its granite construction, so the conduit had to follow the softer mortar joints. The conduit was eventually secured with galvanised saddles at 300mm centres attached to the wall by 50mm galvanised nails fired from a percussion gun.

The recording station at this site was the old lifeboat shed used for storage by its owners British Rail. There was no mains electricity available so all equipment (including lighting) was operated from a static inverter powered by lead acid batteries. Because of the exposed location of the wall and the problems with access at high water, no measurements of wall acceleration were made.

In November 1979 the project was expanded to include the seawalls at Ilfracombe and Seaford, because of the doubling of the work load Mr. A. Tsiaras was employed to take over the monitoring of the Brunel and Teignmouth (still non operational) seawalls to research into programming and digitisation of wave pressure records. Any wave pressure data collected was still made available to this research project.

2.2.3 Ilracombe Seawall

Ilfracombe is a small holiday and fishing port on the North Devon coast about 15 miles from Barnstaple, Figure 2.6 . The existing seawall was backed onto by a row of houses and shops (Plate 2.4) and had been standing for over a hundred years, with only localised repair and strengthening. The new seawall constructed from pre-cast concrete blocks, (Figure 2.7) runs approximately 20m seaward of the existing wall, it is up to 7.5m high with a curved reentrant face. The area between the existing and new walls was infilled to form a promenade and catchment area for over topping waves. This new wall was chosen for instrumentation because it is usually subjected to very severe seas during the winter months and as it was undergoing construction it allowed the insitu installation of the pressure transducers. Nine transducers were installed in this wall, five were positioned to measure the vertical pressure distribution at levels 1.61m, 3.21m 4.21m, 5.21m and 6.36m A.O.D. The remaining four transducers were installed at level 3.21m, spaced at 0.75m and 19.5m either side of the vertical array (Figure 2.8). Only seven of the nine transducers could be monitored at any one time (six if an accelerometer was used), until the end of 1980 by which time additional recording facilities were obtained, allowing recording on up to fourteen channels simultaneously.

Transducer blanks were cast into the blocks along with cable ducts at the casting yard, then on delivery to the site the blanks were removed and the transducers screwed on complete with ample lengths of 20mm diameter flexible armoured conduit. Seawall construction progressed layer by layer, each layer being backfilled with insitu mass concrete as it was laid. It was not possible to be on site at all times during backfilling so the armoured conduit was routed up the back face of the seawall by the contractors. This caused problems because the conduit was bent through sharp angles with the consequence that new transducer cables (needed for the reasons explained in Section 2.4) could not be pulled through.

The recording station was set up in a bedroom of No. 4, The Quay, Ilfracombe, overlooking and about 35m behind the new seawall. This was an ideal location as it gave good access under all sea conditions, had a mains electricity supply and provided a good view of the seawall (Plate 2.5).

To measure horizontal wall accelerations a plate was cast into the top of the wall, onto which an accelerometer could be bolted, a specially made bolt-on cover was made to protect the accelerometer from overtopping waves and spray. Plate 2.6 shows the wave conditions which frequently occur during the winter months.

2.2.4 Seaford Seawall

Seaford is a residential town on the East Sussex coast about 4 miles from Newhaven, Figure 2.9, the seawall here is about 5m high with a combined stepped and curved profile, Figure 2.10.

The deep water close inshore and the shingle beaches in the area produce an extremely abrasive environment, eroding the seawalls by up to 35mm a year resulting in regular wall failure on approximately a 15 year cycle (Plate 2.7). The last major failure at Seaford occurred in the mid-sixties after which it was extensively repaired, by the late seventies erosion had exposed considerable areas of reinforcing steelwork, so to prevent a possible failure the wall was refaced in late 1979. This wall was not an ideal choice but was selected for instrumentation by the project steering committee.

Five pressure transducers were built into the wall during the refacing, three in a vertical array at levels 2.95m, 3.5m and 4.1m with the remaining two transducers 1.5m either side of this array at level 2.95m. The transducer cables protected by armoured conduit were cast into the wall and routed through a drainage hole in the wall to a junction box at the back of the promenade. After only one month in the wall the transducers were so badly damaged by the shingle carried in the waves that they were rendered useless (Plate 2.8). By May 1980 two of the five transducers had been eroded from the wall, and the general condition of the wall in the vicinity of the transducers was poor. Therefore the whole section where the transducers had been cast-in was refaced resulting in the loss of the remaining transducers. Fortunately it was possible to install a second batch of transducers just 20m to the East of the original batch. This second batch whilst incorporating the same basic transducer, were designed so that they could be bolted into place on the face of the wall only when they were required thus they were not exposed unnecessarily (Plate 2.9). Ten transducer mounting points were cast into the seawall in June 1980, three at level 2.7m, three at level 2.95m, three at level 3.5m and one at level 4.1m, (all levels referred to O.D.). At levels 2.7m, 2.95m and 3.5m the horizontal spacing was 1m centre to centre as shown in Figure 2.11 .

These ten mounting points allowed various transducer configurations to be tried, although all ten mounting points could not be used simultaneously due to lack of data recording channels. By December 1980 all of the lower mounting points were eroded from the wall so this site was then abandoned.

Seawall accelerations were measured at Seaford by bolting the accelerometer to a heavy steel block and relying on its weight to keep it in continuous contact with the seawall whilst measurements were being made. No cover was available so the accelerometer had to be removed if there was a chance of wave overtopping.

The recording station at Seaford was a private underground carpark immediately behind and about 20m from the seawall. The transducer cables terminated in a junction box at the back of the promenade, so an additional length of cable was connected by means of a multiway plug and laid across the road into the underground carpark. The cable was protected by specially made wooden ramps, as shown in Plate 2.10. The underground carpark had a major disadvantage in that the seawall could not be seen when recording, therefore for all visual measurements of wave height, celerity and period it was necessary to go up to road level. This was impossible during bad weather because of the spray and shingle over topping the wall, so in these conditions no visual measurements were made.

2.3 Instrumentation

A main requirement of this investigation was the measurement of wave pressures, including any high pressure transients, and the

simultaneous measurement of wall accelerations in order to build up a complete picture of the structural behaviour of the walls. The pressure measurements were made using strain gauge mounted diaphragm pressure transducers and horizontal wall accelerations were measured using servo-drive accelerometers, all data was stored on magnetic tape using multichannel F.M. tape recorders.

2.3.1 Pressure Transducers and Amplifiers

When this investigation started there were no commercially available pressure transducers suitable for field use in seawalls, and capable of responding to the dynamic high frequency wave pressure transients expected. Due to financial constraints, suitable transducers could not be commissioned commercially, hence they were designed and manufactured at Plymouth Polytechnic.

The pressure transducers installed in the Teignmouth and Brunel seawalls, now referred to as type 1, consisted of four parallel wire strain gauges (Technimeasure PL10) bonded to a stainless steel disc 120mm diameter and 2mm thick (Figure 2.12, Plate 2.11). The disc was attached to its housing by means of a clamping ring as shown in figure 2.12. These transducers and associated amplifiers proved unreliable in use for two reasons, firstly the clamping ring tended to introduce additional strains into the diaphragm as it was tightened thereby altering the calibration, (on site calibration was not possible because the calibration equipment could not be attached to the transducers insitu). Secondly the strain gauges used were not well suited to this application because they were only capable of responding to changes in radial strain due to the orientation of the strain gauge wires, yet they were necessarily positioned near the region of zero radial strain, (Figure 2.13). This inevitably led to minimal signal output under normal operating pressures, hence the amplifiers had to operate at near maximum gain, resulting in signal instability drifting and noise of the order of 50 milli-volt/volt bridge supply, (where the calibration was 1 volt = 138 KN/m^2 (20 lbs/in^2)).

To overcome these problems the complete system of amplifiers and pressure transducers was redesigned. The new transducers (Figure 2.14, Plate 2.12), now referred to as type 2, were also manufactured at Plymouth Polytechnic. The type 2 transducer incorporates an integral diaphragm as part of a one piece construction, thereby eliminating the need for a clamping ring. The transducers were designed to accept a 25mm diameter circular foil strain gauge made especially for this type of application by Technimeasure (pattern No. FD PF - 24 - 17). This strain gauge employed both radial and tangential components (Figure 2.15) to give a maximum change in strain for a given pressure, its coefficient of thermal expansion matches as nearly as possible that of the stainless steel diaphragm to minimise any effects of differential thermal expansion.

The type 2 amplifiers were designed by C.I.L. (Creative Instrumentation Limited) specifically for strain gauge bridges, they were built at the Polytechnic from commercial kits. A circuit was incorporated to sense voltage drops in the power cables due to the long lead wires used and to compensate for any drop to maintain a constant bridge voltage. This improved transducer/amplifier system as used at Ilfracombe and Seaford performed very well giving excellent stability and reliability. Signal stability was checked by leaving the transducers and amplifiers running in the laboratory for twenty four hours, with the transducers both submerged in water and in the dry, drift was monitored on a chart recorder. Any drift occurring was almost entirely due to temperature effects which were measured by a thermal couple attached to the transducer diaphragm. One degree centigrade was found to cause a change in voltage output of less than 0.2 milli-volts.

After reviewing previous work and discussion with engineers involved in seawall design (who generally use a dynamic pressure of 100 KN/m^2 for seawalls in U.K. waters), the transducers were designed to measure pressures upto 300 KN/m^2 with a linear response, although the normal working pressure was expected to be about 20 KN/m^2. The calibration used for the type 2 transducers was 0.1 volts ≡ 100 KN/m^2 (1 mV ≡ 1 KN/m^2) for reasons of amplifier stability and ease of data analysis.

The transducer output at a pressure of 100 KN/m^2 was calculated from the following(76);

$$e_o = \frac{0.82\, P R_o^2\, (1 - \nu^2)}{t^2\, E} \times 10^3 \text{ mV/V} \qquad \ldots\ldots\ldots (2.1)$$

where e_o = voltage output mV

P = applied pressure N/mm^2

R_o = diaphragm radius mm

t = diaphragm thickness mm

E = Youngs Modulus N/mm^2

ν = Poissons ratio

thus

$$e_o = \frac{0.82 \cdot 0.1 \cdot 13^2 \cdot (1 - 0.285^2)}{1^2 \cdot 210 \cdot 10^3} \quad \mathrm{mV/V}$$

$$e_o = 0.061 \ \mathrm{mV/V}$$

Therefore to achieve the required calibration of 100 KN/m^2 = 100 mV an overall gain of approximately 1650 is required. This was obtained by using a bridge voltage of 5 volts and an amplifier gain of 330, this comparitively low amplifier gain was chosen because it gave the optimum compromise between the noise level, stability, drift and amplification. At this overall amplification the noise level was reduced to the order of 1 mV/V as shown in Figure 2.16 .

No two transducers were identical because they were all hand machined so there were always slight variations in the diaphragm thickness, slight variations also occurred between amplifiers and between strain gauges although to a lesser extent. Therefore the theoretical output voltage (e_o) was never acheived with a gain of 1650, but was generally within 10% of the required value. This meant a slightly different amplification was necessary for each transducer, so the transducers and amplifiers were numbered and calibrated in matched pairs. A shunt resistor was used to set the calibration correctly, by knowing the voltage output of the shunt when the transducers were correctly calibrated, it was simply a matter of switching in the shunt and adjusting the amplifier gain to give the same value as before. Thus the transducers could be calibrated on site before and after each recording session to ensure no malfunctions had occurred during the recording. Bridge voltage was also checked on site with a voltmeter.

Both types of transducer were calibrated statically using a pressure chamber, a separate pressure chamber was built for each type of transducer, and by immersion in a water tank using various 'heads' of water. Dynamic calibration was carried out by dropping a steel ball onto the transducer diaphragm from various heights, and viewing the response on an oscilloscope combined with a transient recorder. From these tests the system was found to be able to respond to transients of less than 1mS duration (Figure 2.17), this seems satisfactory as no previous full scale investigation has measured impacts with durations of this order.

The natural frequencies of the transducers were calculated from Ref. 77, as follows;

$$f_n = \frac{0.471\ t}{R_o^{\ 2}} \sqrt{\frac{g\ E}{\gamma(1 - \nu^2)}} \quad \text{Hz} \quad \ldots\ldots\ldots\ldots \ (2.2)$$

where f_n = natural frequency

γ = specific weight of diaphragm material

thus

$$f_n = \frac{0.471 \cdot 1}{13^2} \sqrt{\frac{9815 \cdot 210 \cdot 10^3}{8.28 \cdot 10^{-5} \cdot (1 - 0.285^2)}} \quad \text{Hz}$$

$$f_n = 15406 \text{ Hz} \qquad \text{(for type 2 transducer)}$$

So theoretically the type 2 transducer is capable of responding to transients of the order of $(15406)^{-1}$ seconds, which is 0.065 mS this is a shorter duration than even those transients measured in model studies, so the type 2 transducer should be capable of measuring any transient pressure that occurs in the field. The natural frequency of the type 1 transducer was also calculated from equation 2.2 and had a natural frequency of 4720 Hz.

2.3.2 Accelerometers

Because of the size and stiffness of the seawalls and the low frequency of the impinging waves (of the order of 0.2 Hz = 5 second period), the response frequencies of interest were expected to be quite low. Therefore to measure the horizontal wall accelerations at these low frequencies a linear drive servo accelerometer was used (Refs. 78, 79 and 80). The type chosen was model number A220-0001 (linear drive) supplied by Schaevitz em Ltd., with an operating range of ± 1g, where g is the acceleration due to gravity. The horizontal wall acceleration at any frequency, can be converted to the equivalent horizontal wall displacement by using the following expression;

$$\text{Displacement} = \frac{V\,g}{\text{amplifier gain}} \times \frac{1}{\omega^2} \qquad \ldots\ldots\ldots (2.3)$$

where V = accelerometer output in volts (r.m.s.) at the frequency considered

$\omega = 2\pi f$

f = the frequency under consideration

As displacement is inversely proportional to frequency squared, then frequencies above about 500 Hz produce negligible displacements of the seawall, of the order of 10^{-6}mm. For this reason the amplifiers had a cut off frequency of 600 Hz. This was considered justified because from preliminary analysis both by hand and computer (see Chapters Six and Seven), the first mode of vibration of the seawalls was of the order of 10 Hz with the second modes ranging from 60 to 100 Hz.

2.3.3 Ancillary Equipment

The output signals from the transducers and accelerometers were, after being suitably amplified, stored in analogue form on magnetic tape. Two tape decks were used, both were frequency modulated (F.M.) models with seven data channels, model numbers 7D and 7DS manufactured by Racal Thermionics Ltd.

The frequency response of the tape decks was dependent upon tape speed, at the fastest speed the response was d.c. to 20 KHz (at this speed the tape would only last for 7.5 minutes), at the slowest speed the response was d.c. to 200 Hz (the tape would last for 8 hours at this speed). The data was generally recorded at the slowest speed to allow the maximum data to be stored, a response of 200 Hz would allow transients of 5mS duration to be captured which from Chapter Three is seen to be more than adequate for full scale wave impacts.

The data in this format suited the analogue processing and analysis techniques, whilst also being the cheapest and most convenient method for storing the data, and also allowed repeated viewing.

The whole system of amplifiers, tape decks, oscilloscopes and

lighting were fully portable and could be operated at isolated sites using a static inverter supplying 240 V a.c. This gave approximately 8 hours continuous operation from a heavy duty 71 amp hour 12 volt lead acid battery at maximum output. Some problems were encountered with interference from the inverter in the form of voltage spikes which were originally confused with wave impacts, this problem was later eliminated by the use of suitable suppressors.

2.4 Strain Gauge Installation and Protection

The strain gauges in the type 1 transducers were simply bonded to the diaphragm and sealed along with the lead wire connections, by applying a quantity of epoxy potting compound, (Plate 2.11). This successfully sealed the installation but the added mass of the potting compound on the diaphragm altered its response characteristics to an indeterminable degree. To overcome this problem the type 2 transducers had the strain gauge bonded to the diaphragm and sealed with a very thin layer of epoxy resin, a perspex disc was then fitted 3mm clear of the diaphragm to allow the diaphragm to deflect. The soldered connections to the lead wires were made using solder tags attached to the perspex disc, the connections were then sealed with epoxy potting compound. The seal between transducer and housing was made by grinding a fine finish to both contact surfaces and applying a film of silicon rubber.

This method of protection worked successfully during trial recording sessions at Seaford and Ilfracombe but after about four weeks most of the transducer output signals became unstable, the cause was found to be the ingress of moisture into the transducers.

When the potting compound was broken out the strain gauges were seen to be badly corroded, this had the effect of changing the resistance of the gauge making it impossible to balance the bridge. The other problem this moisture caused was to short circuit the gauges allowing the signals to leak to earth.

Upon close examination it was found that the water was entering the transducers through the seal between the transducer and its housing this was happening because tiny particles of sand were being trapped between the faces during on-site assembly. Once inside of the transducer housing the water could seep through to the strain gauge by capillary action in the gaps between the lead wires and the potting compound. As a result, every transducer from both Seaford and Ilfracombe had to be replaced, even those units which appeared to be functioning correctly were replaced as a precaution with new units.

The revised method for sealing the transducers was to gently warm the units, after bonding and coating the strain gauges, to drive off any moisture present. The perspex disc was then fitted and sealed with silicon rubber and instead of the inflexible potting compound, a mineral wax was used because it was flexible and thus maintained a water tight seal even if some movement of the lead wires occurred. Silicon crystals were incorporated into the transducer to absorb any moisture remaining or subsequently entering, and as a final precaution the mineral wax was sealed with a film of epoxy resin. A rubber 'O' ring was fitted to the transducer to effect a good seal between transducer and housing and so eliminate the effects of sand between the mating surfaces. This revised method of sealing is shown in Figure 2.18 .

The cables built into the seawalls were seen to be corroded at the transducer end and possibly through out their length, although this could not be assertained because the sharp bends in the protective armoured conduit prevented the old cables from being pulled out and consequently prevented new cables from being inserted. Therefore a new self contained system of transducers and cables, complete with water proof conduit, was designed to be fixed to the face of the seawalls held in place by tensioned steel cables, (Plate 2.13). This system had the advantage of being detachable, so it could be removed after each recording session, thus allowing checks and calibration to be carried out in the laboratory. This system was also checked on site before and during recordings (to ensure water had not entered the transducers or cables) by using a Meggameter to measure the earthing resistance, i.e. the resistance between the strain gauge and housing.

2.5 Wave and Foreshore Characteristics

The most important of the wave characteristics (after the pressure) were judged to be wave height, wave celerity and wave period, hence these were the only parameters (other than pressure) which were measured at Ilfracombe and Seaford. These parameters were chosen because they generally feature in most equations for estimating the wave pressure (see Section 1.3.2). The only other parameter necessary is wave length which is difficult to measure but can be calculated by knowing the wave celerity and period.

2.5.1 Wave Height

At Seaford wave height was measured by a type 2 transducer fixed to groyne No. 36 about 50m seaward of the wall, the cable was routed back along the groyne and into the seawall through armoured ducting. This installation had to be abandoned when the wall was refaced, and instead a type 2 transducer (with a baffle fitted for protection) was fixed to groyne No. 36A, 20m seaward of the wall. This time the cable was tied to a stainless steel wire slung between the transducer and the top of the seawall.

At Ilfracombe no natural features existed on which to attach a wave height transducer, so a type 2 transducer was fixed to a threaded stainless steel rod cast into the rocky beach 14.4m in front of the wall (Plate 2.14). The cable was again tied to a stainless steel wire slung between wall and transducer.

As an additional visual check on wave height, graduated wave staffs were fixed to the beaches at Seaford and Ilfracombe (Plate 2.15). These wave staffs were erected before the beach transducers were installed, so all wave heights measured upto November 1980 (Seaford) and December 1980 (Ilfracombe) were from wave staffs only.

The visual wave height was measured generally for five minutes in every thirty minutes. It was difficult to obtain a comparison between transducer measured and visually measured wave heights because visually the smaller waves or waves with poorly defined crests tended to be ignored, whereas all waves were measured by the transducer, (attenuation was not a significant problem because water depths were generally less than 2m at the transducer when wave impacts occurred at the wall, see figure 2.19). Significant wave heights calculated from transducer records generally showed fair agreement with the average wave height measured visually, as shown below, and so allowed cross checking to identify any gross errors in the wave height measurement by either system.

Tape No.	Date	Site	Significant wave height from transducer record	Average wave height from visual observation
11	21-10-80	Seaford	-	0.90m
3	27-11-80	Seaford	-	1.20m
14	21-1-81 pm	Ilfracombe	0.78m	0.85m
14	22-1-81 am	Ilfracombe	0.69m	0.80m
15	22-1-81 pm	Ilfracombe	1.04m	1.00m
16	3-2-81	Ilfracombe	-	1.30m
16	4-2-81	Ilfracombe	-	1.10m
17	9-3-81	Ilfracombe	0.97m	0.90m

It has been found from the analysis of wave records that the height measured visually is often equal to the significant wave height as calculated from theory(82), (significant wave height is defined as the highest third of all waves present). The visual wave height measurement is used in calculations in Chapter Three for the above reason and for consistency because transducer measured heights were not available at the start of this investigation, also with visual measurements reflected waves (from the seawalls) can be ignored whereas these are automatically included in the transducer measurements.

Video filming of waves breaking on the Ilfracombe seawall was carried out on two occasions and was used as a qualitative check on wave height. No serious correlation between individual wave heights and impact pressure was possible because the video film was not synchronised with the transducer pressure record. This method has tremendous potential for detailed examination of wave action at the instant of impact with the seawall and should allow correlation between breaker type and impact pressure, providing the film can be synchronised with the pressure record. This method is only really viable at sites with regular waves where the breaker shapes can be clearly defined, thus there is little potential with the highly confused sea state at Ilfracombe.

2.5.2 Wave Celerity

Wave celerity was measured at both Ilfracombe and Seaford by timing a wave between two points a known distance apart. At Ilfracombe this was the distance between the wave staff and seawall and at Seaford two staffs were used originally and when the second batch of transducers was installed then the distance was taken between a wave staff and the wall. Measurements were taken for five minutes in every thirty, as for the wave height measurements. This method of measuring celerity was prone to errors due to the difficulty in locating the exact point of the wave crest as it passed the wave staff. For this reason two additional pressure transducers were fixed to the beach at Ilfracombe (Figure 2.20), from which it was hoped to be able to measure wave celerity.

The exact location of the beach transducers was governed by the local topograghical features of the beach, because of which they had to be sited close to rocky outcrops which generated turbulence and created numerous problems with the interpretation of the transducer records.

From the three beach transducers at Ilfracombe it is theoretically possible to obtain wave celerity and the angle of incidence of the wave crest, although in practise this was not possible because of the very confused sea state at Ilfracombe, which caused the waves to break and reform between transducers. Thus when viewing the outputs from the transducers on a chart recorder it was very difficult to follow a particular wave crest as it traversed between transducers because it would often just disappear.

An approximation of wave celerity was obtained from the shallow water relationship, taken as $C = (gd)^{\frac{1}{2}}$ to a first order of approximation, although for steep waves the Solitary wave theory ($C = (gd(1+ H/d))^{\frac{1}{2}}$) gives better results(83). Calculating wave celerity by this method relies heavily on an accurate estimate of the water depth d. At Ilfracombe the beach levels stayed almost constant because there was very little loose beach material here but an estimate of the average water depth could not easily be made because of the very rocky seabed, as shown in Figure 2.21. Whereas at Seaford the shingle beach could change level by over 1m in a single tide again making any estimate of water depth very approximate.

The visual measurement of wave celerity did not compare very well with the value calculated from $C = (gd)^{\frac{1}{2}}$, as shown in the table over the page. The reason for this is clear at Seaford with its variable beach level, and at Ilfracombe the probable reason is the rocky seabed which would theoretically mean the wave celerity would be changing rapidly with the change in seabed level, but in practise the wave cannot respond instantly to changes in depth and so it does not see the smaller peaks in the seabed and tends to assume the celerity for the average water depth, although large changes in depth over a small horizontal distance cause the wave to become unstable and it often breaks.

Therefore the average wave celerity measured visually was considered more reliable than the calculated value, so it is this visual value which is used in calculations in Chapter Three.

Tape No.	Date	Site	Wave celerity calculated from $C = (gd)^{\frac{1}{2}}$	Wave celerity measured visually
11	21-10-80	Seaford	-	3.64 m/S
3	27-11-80	Seaford	5.18 m/S	4.22 m/S
14	21-1-81	Ilfracombe	4.95 m/S	4.71 m/S
14	22-1-81$_{am}$	Ilfracombe	4.95 m/S	4.07 m/S
15	22-1-81$_{pm}$	Ilfracombe	5.19 m/S	4.16 m/S
16	3-2-81	Ilfracombe	4.43 m/S	4.67 m/S
16	4-2-81	Ilfracombe	-	4.29 m/S
17	9-3-81	Ilfracombe	3.96 m/S	3.56 m/S

2.5.3 Wave period

Wave period was measured visually by timing the interval between successive waves passing the wave staff. This method suffered from the same problem as the measurement of the wave celerity because of the difficulties in locating the wave crest in the confused sea. Wave period could not easily be measured from the beach transducer outputs for the same reasons as the celerity could not be measured from them. An indication of average period can be obtained from spectrum density plots and from correlograms as discussed in Sections 3.2.3 and 3.2.4. Wave period estimated from these methods was generally quite close to that measured visually so some confidence can be placed on the visual measurements and consequently the visual measurements are used in calculation in Chapter Three.

2.5.4 Beach Characteristics

The foreshore at Ilfracombe (Plate 2.4) is very rocky, the rock is mostly shale rising in places to seven or eight metres above beach level, the beach slope is difficult to determine but an average slope is probably between 1 : 15 and 1 : 40, although there is very little of what could be called a beach in the vicinity of the transducers.

Seaford foreshore has a steeply shelving beach mostly of shingle (including flint) in the size range 5 to 30 mm, a typical sieve analysis sheet is shown in Figure 2.22. The beach level and slope is constantly changing depending upon the tidal conditions, the slope is generally within the range 1 : 6 to 1 : 15. Measurements of beach slope were made at Seaford during most recording sessions and samples of beach material were also taken to monitor any changes in composition or size. No samples of beach material were taken from Ilfracombe because there was very little loose material available to sample.

2.6 Wind Speed and Direction

Advance meterological reports of wind speed and direction were regularly obtained during the winter months for the Ilfracombe and Seaford areas, this gave an indication of the likely sea conditions at each site and so allowed forward planning of recording sessions. The largest steepest waves occurred at Ilfracombe when the wind was North Westerly, wind from the South or East generally produced smaller seas due to Ilfracombe's sheltered position in the Bristol Channel. At Seaford, because of its relative exposure, winds from any direction other than Northerly produced good recording conditions. As Ilfracombe is on a North facing coast and Seaford on a South facing coast it was on only very few occasions that storm conditions occurred simultaneously at both sites.

A report on the general prevailing weather conditions was obtained from local Meteorological offices at R.A.F. Mountbatten (for the Ilfracombe site) and Brighton (for the Seaford site), copies of weather reports and synoptic charts were also received from the South West Water Authority Storm Report Station at Exeter. This information was useful for providing a general idea of the wind conditions at each site, but the actual wind conditions on site varied according to the local topography. So to check the general forecast a Vector Instruments rotating cup annemometer (model number D600) was erected on site on some occasions, a typical trace appears in Figure 2.23. The wind speed and direction measured with the annemometer was almost always different from the meterological office forecast, (the annemometer was regularly serviced), the forecast for the day on which Figure 2.23 was recorded was Westerly force 2 or 3.

2.7 Damage to Instrumentation at Seaford

Damage to instrumentation was confined to the transducers at Seaford due to the combination of rough weather, a steeply shelving beach (which allows large waves to approach close to the wall before breaking), and a loose shingle/pebble beach material. This combination of factors resulted in a very harsh abrasive environment, sufficient to deform stainless steel diaphragms after only three weeks exposure. The central deformation of the diaphragms was 3mm (the limit of travel) with a generally smooth parabolic deformed shape, although small indentations caused by individual pebbles could be seen, Plate 2.16. Every transducer was damaged in this way, the most severe damage occurring at, or below S.W.L. lessening further up the wall. To combat this problem grilles were used to deflect the shingle, these grilles were manufactured from 6mm aluminium plate with various diameter drilled holes. The size of the holes was a compromise between maintaining the strength of the grille, keeping most of the shingle out and allowing as much of the wave through as possible. The eventual configuration of holes is shown in Plate 2.17 and consists of 19 No. 6mm diameter holes arranged in a circular pattern.

The grilles provided the required level of protection but the wave impact no longer occurred over a single front, but acted as 19 separate jets of water. This made any analysis nearly impossible because of the difficulty in correlating the measured pressure with that of the unobstructed wave pressure, consequently grilles were no longer used. As the next step new transducers were manufactured with a diaphragm thickness increased from 1mm to 2mm, this led to a reduced output voltage (by a factor of 4 because voltage is inversely proportional

to thickness squared, Eq. 2.1). This increased thickness helped to reduce the level of damage in the short term although after a matter of weeks extensive damage still occurred. In a final attempt to reduce the damage, a new pressure measuring system was designed to be bolted into place on the wall when measurements were required and removed immediately afterwards thus reducing the risk of unnecessary damage. Transducer damage still occurred but was carefully monitored and replacement was effected as soon as they failed to behave with a linear response.

If, when recording, the transducer outputs showed any signs of behaviour out of the ordinary, the tape footage was noted and the tape treated with caution until the exact cause was determined.

A finite element analysis of the transducer diaphragm was carried out (Chapter Seven) to give an indication of the pressure necessary to cause the deformations found at Seaford.

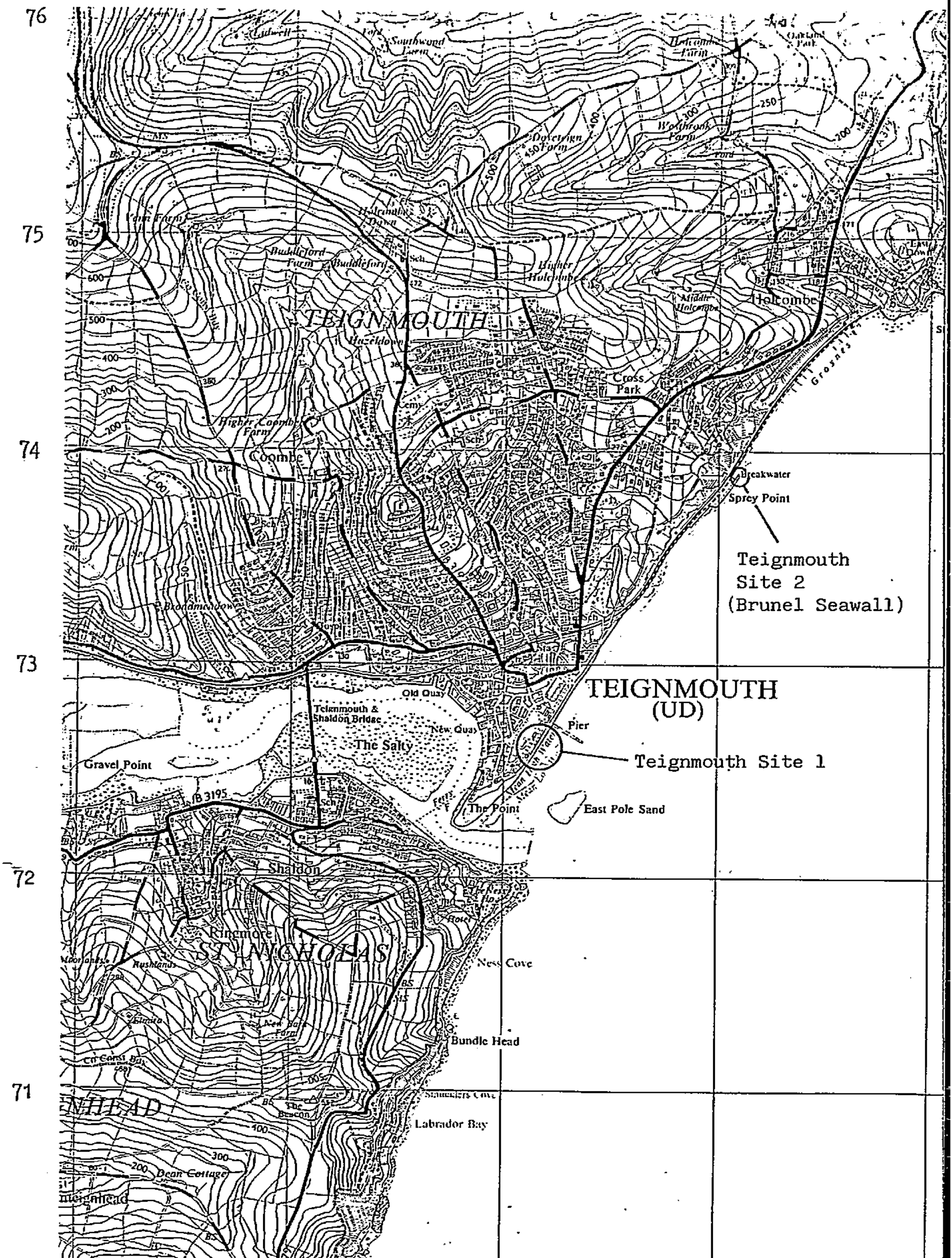
76
75
74
73
72
71
70
92
93
94
95
96
TEIGNMOUTH
Holcombe
Cross Park
Coombe
Breakwater
Sprey Point
Teignmouth
Site 2
(Brunel Seawall)
TEIGNMOUTH
(UD)
Old Quay
Teignmouth &
Shaldon Bridge
New Quay
The Salty
Pier
Teignmouth Site 1
Gravel Point
B 3195
The Point
East Pole Sand
Shaldon
Ringmore
ST NICHOLAS
Ness Cove
Bundle Head
Labrador Bay
Bean Cottage
A379

Figure 2.1 Map of Teignmouth showing location of seawalls

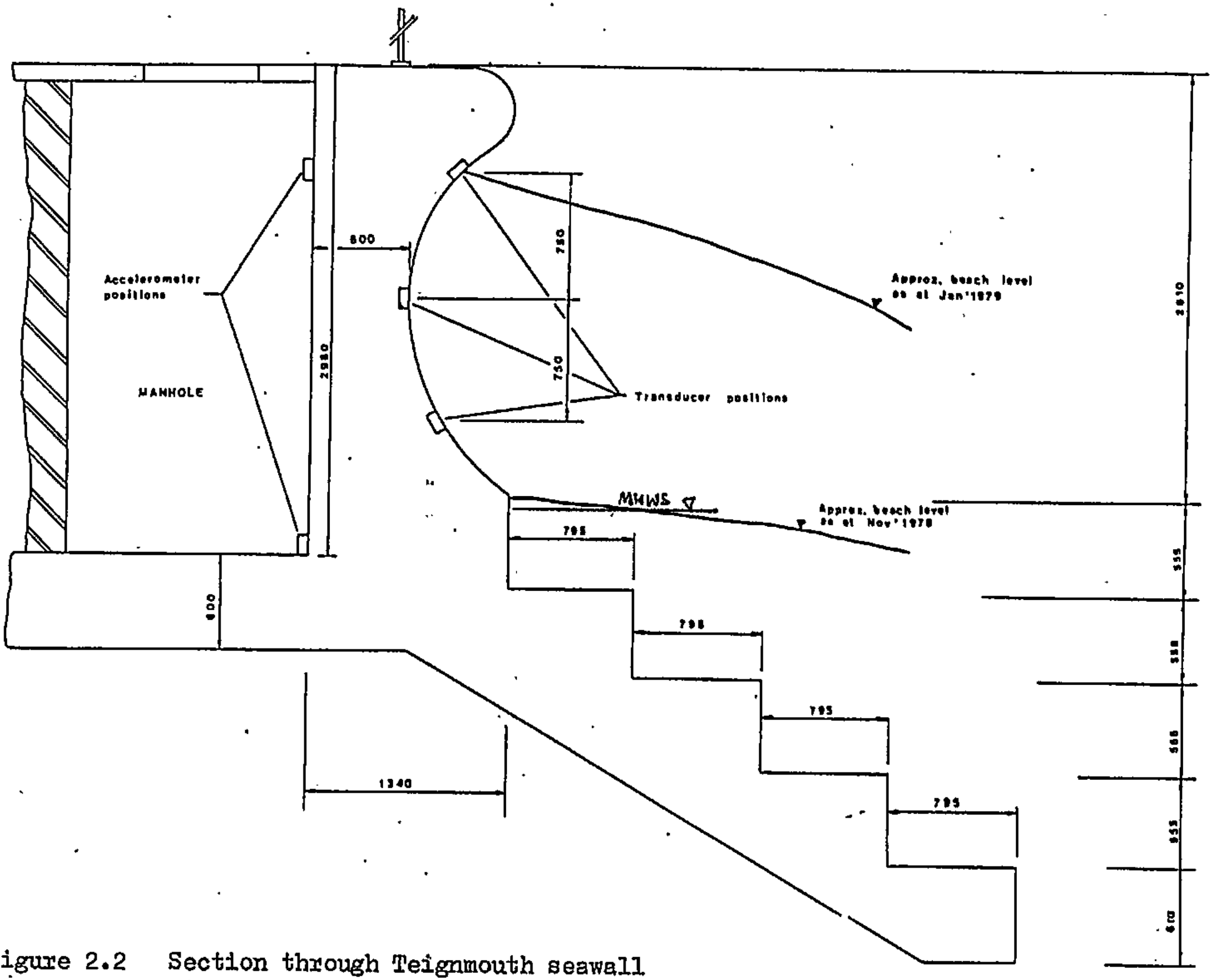
Accelerometer positions
MANHOLE
2980
800
600
1340
750
750
Transducer positions
Approx. beach level as at Jan'1979
MHWS
Approx. beach level as at Nov'1978
795
795
795
795
2810
555
558
565
555
610

Figure 2.2 Section through Teignmouth seawall at central recording station.

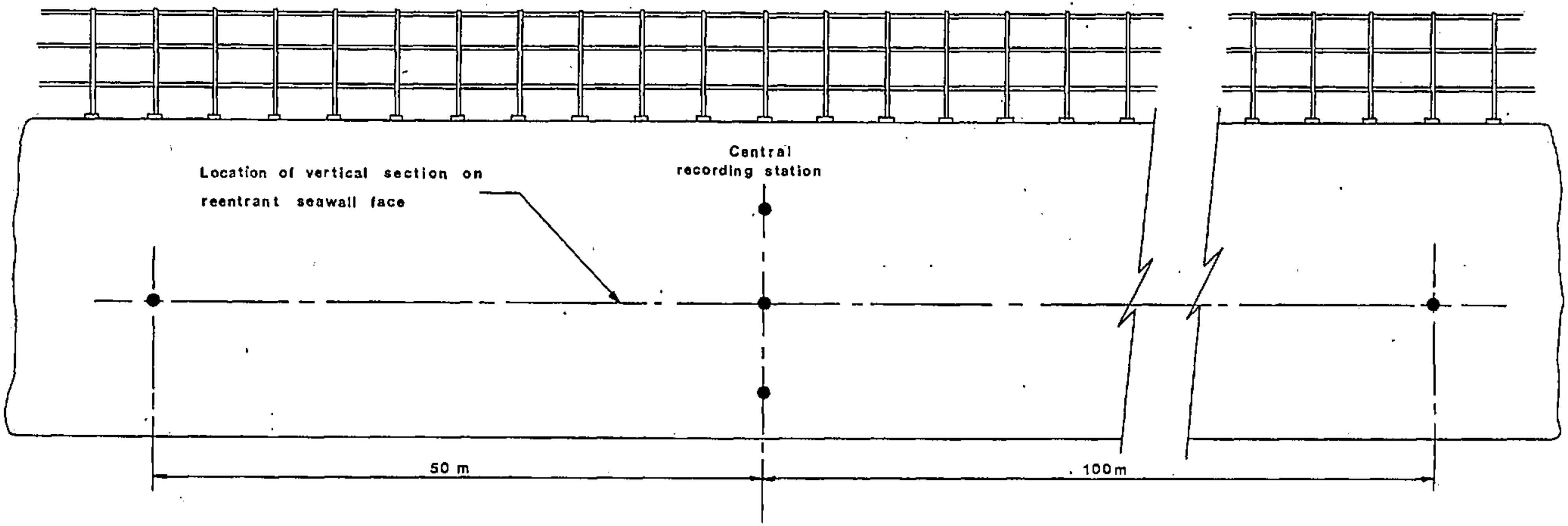
Central
recording station
Location of vertical section on
reentrant seawall face
50 m
100m

Figure 2.3 Transducer array on the Teignmouth seawall

Figure 2.4

SECTION THROUGH BRUNEL SEAWALL

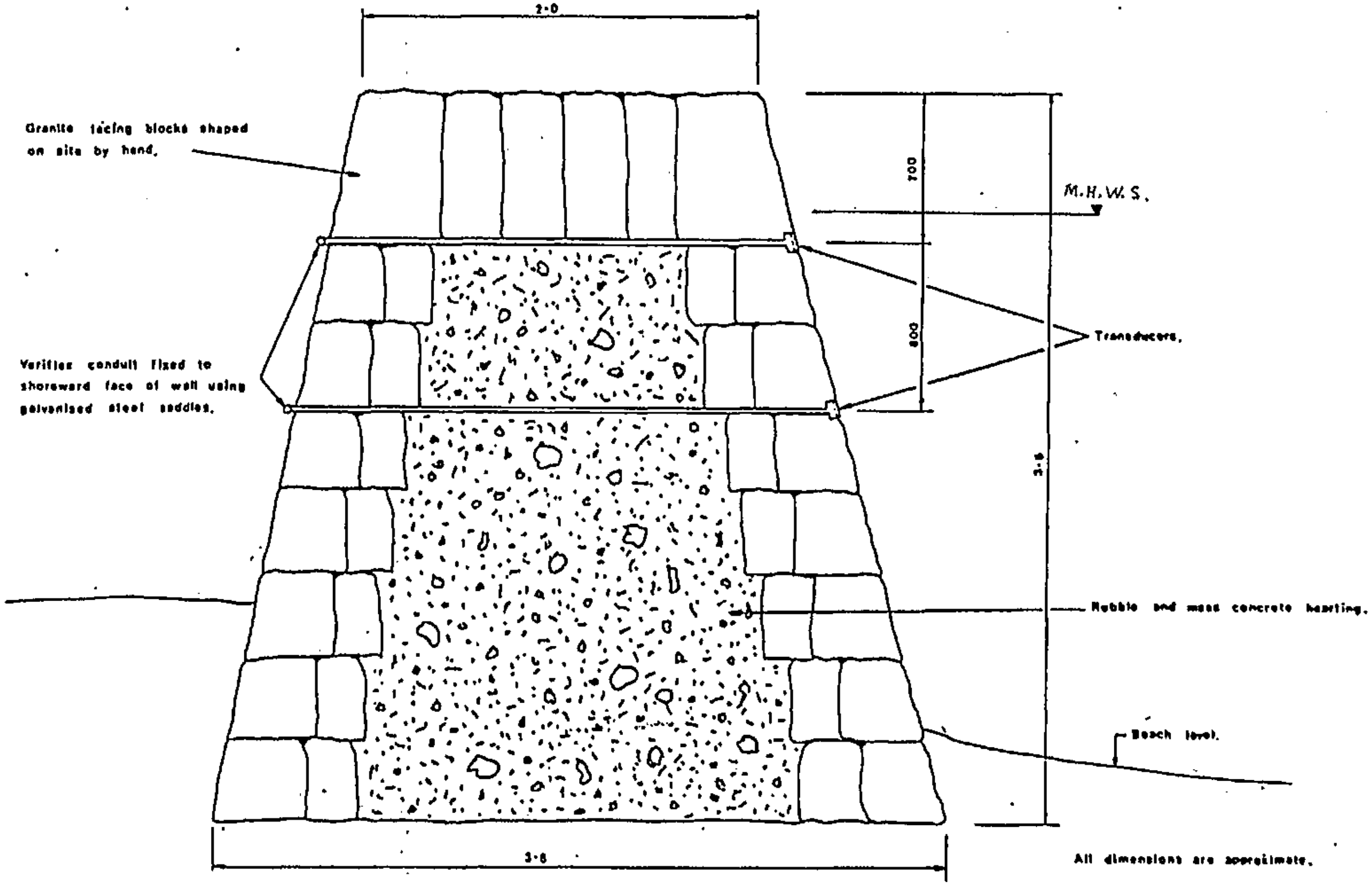
2·0
Granite facing blocks shaped on site by hand.
700
M.H.W.S.
800
Transducers.
Varitlex conduit fixed to shoreward face of wall using galvanised steel saddles.
3·6
Rubble and mass concrete hearting.
Beach level.
3·6
All dimensions are approximate.

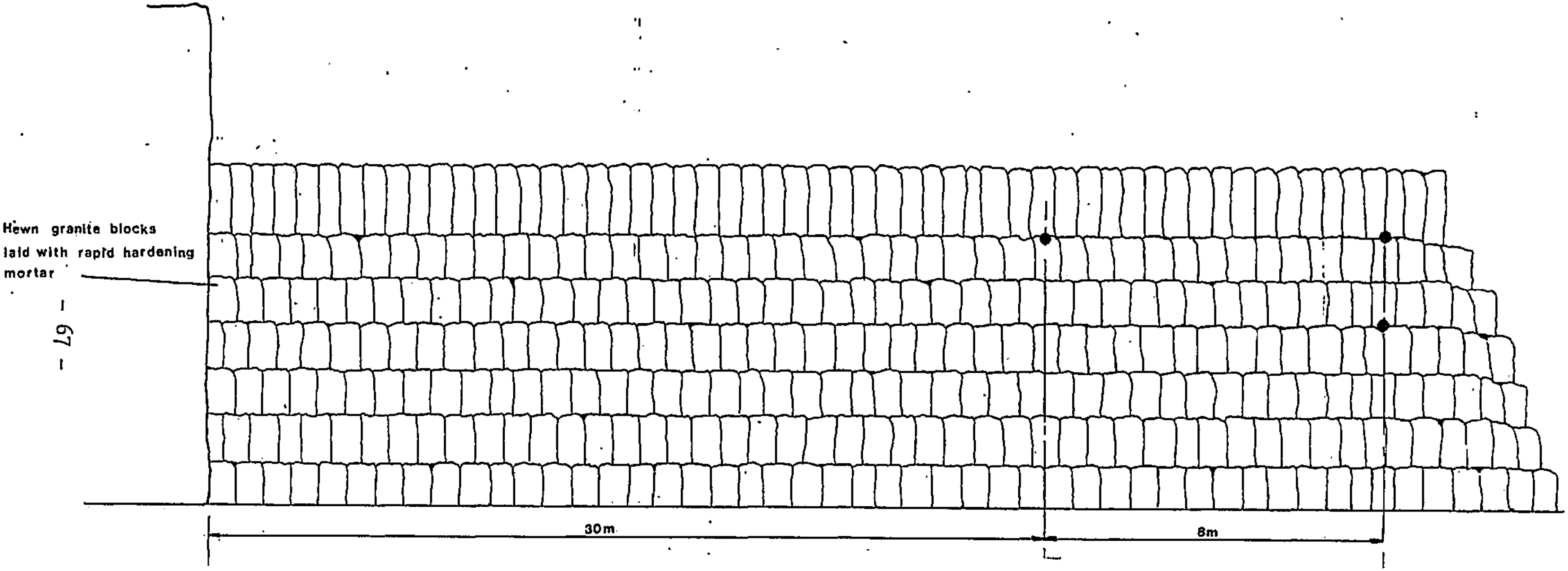
Hewn granite blocks laid with rapid hardening mortar
30m
8m

Figure 2.5 Transducer array on the Brunel seawall

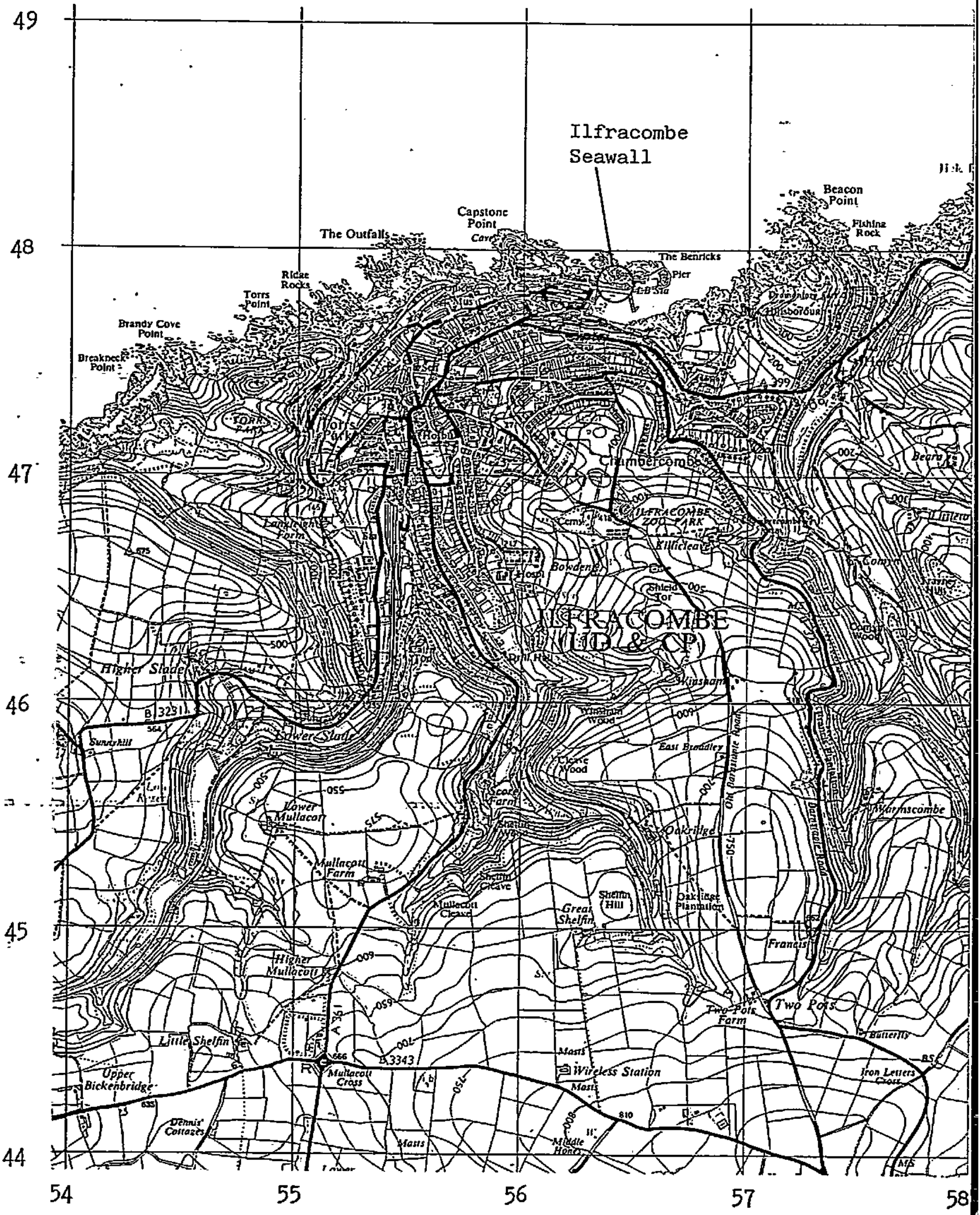
Ilfracombe
Seawall
49
48
47
46
45
44
54
55
56
57
58
Beacon Point
Fishing Rock
Capstone Point
Cave
The Outfalls
The Benricks
Pier
Ridge Rocks
Torrs Point
Brandy Cove Point
Breakneck Point
Hillsborough
Torrs Park
Chambercombe
ILFRACOMBE ZOO PARK
Killicleave
Langleigh Farm
Bowden
Shield Tor
ILFRACOMBE (U D & CP)
Higher Slade
Lower Slade
Sunnyhill
B 3231
Lower Mullacott
Mullacott Farm
Score Farm
Shelfin Cleave
Mullacott Cleave
Great Shelfin
Shelfin Hill
Oakridge
Oakridge Plantation
Winsham
East Bradley
Cleave Wood
Warmscombe
Francis
Two Pots
Two Pots Farm
Butterfly
Iron Letters Cross
Higher Mullacott
Little Shelfin
Upper Bickenbridge
Dennis' Cottages
A 361
B 3343
Mullacott Cross
Wireless Station
Masts
Middle Hone
A 399
Old Barnstaple Road
Beara
Comyn

Figure 2.6 Map of Ilfracombe showing location of seawall

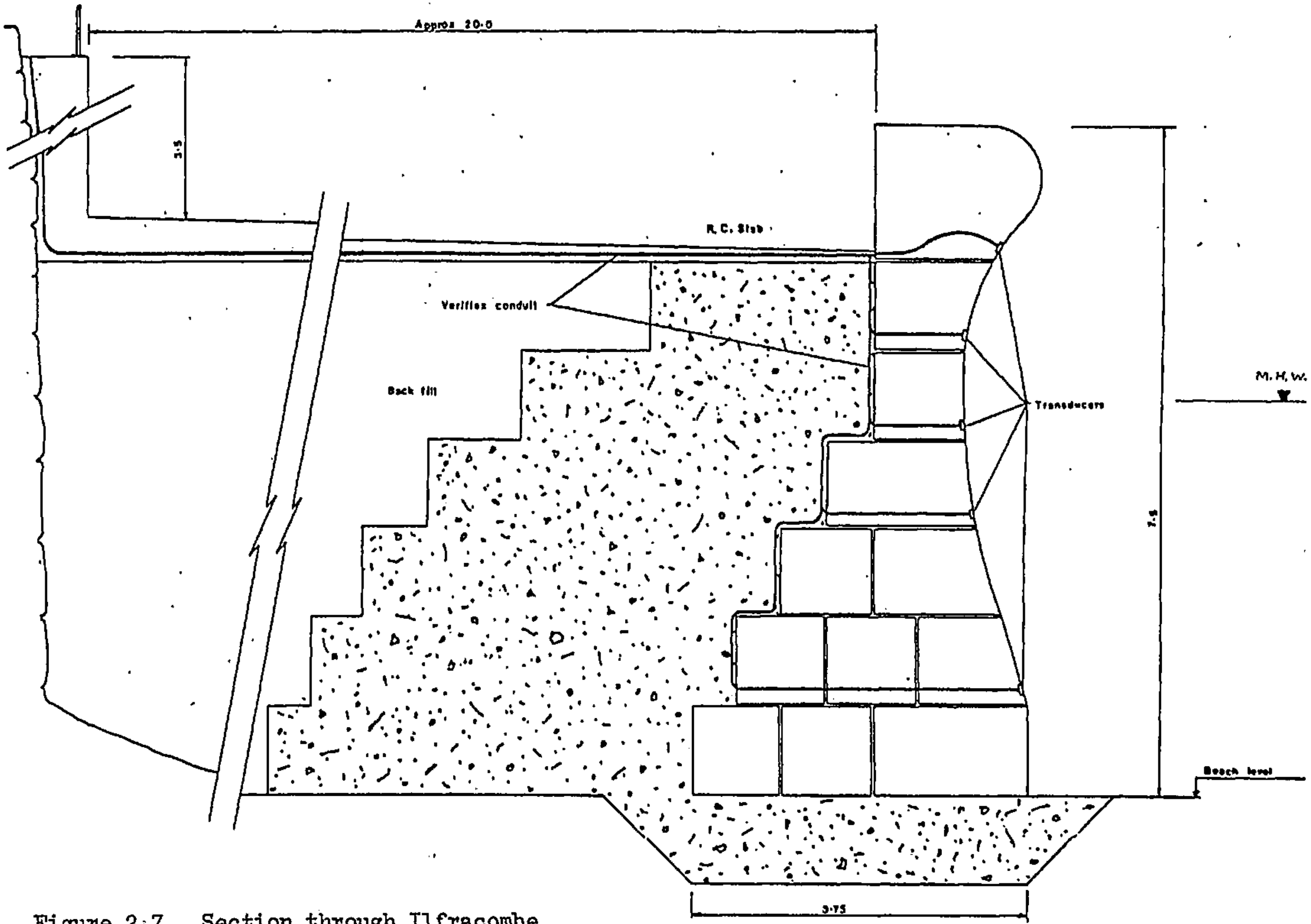
Approx 20.0
3.5
R.C. Slab
Veriflex conduit
Back fill
Transducers
M.H.W.S.
7.5
Beach level
3.75

Figure 2.7 Section through Ilfracombe seawall at vertical transducer array.

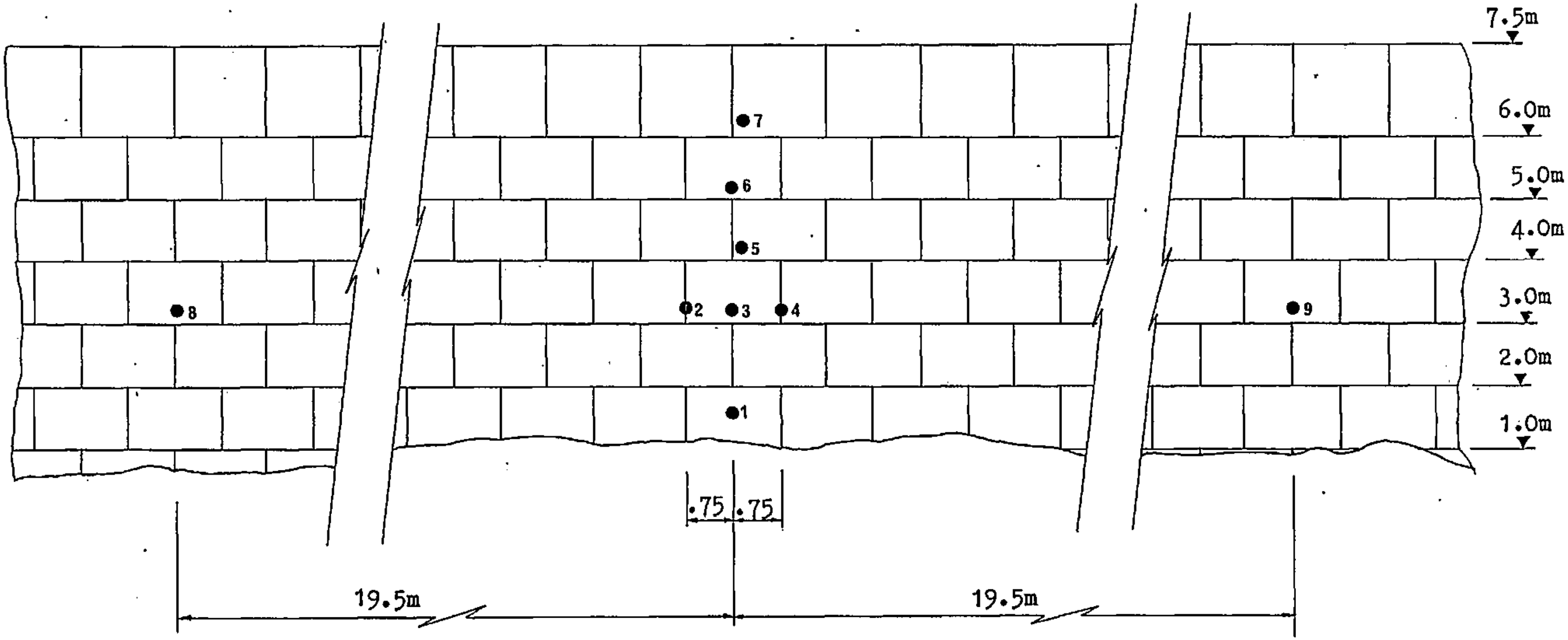
7.5m
6.0m
5.0m
4.0m
3.0m
2.0m
1.0m
7
6
5
2
3
4
8
9
1
.75
.75
19.5m
19.5m

Figure 2.8 Transducer array on Ilfracombe Seawall (scale 1 : 100)

All levels referred to O.D.

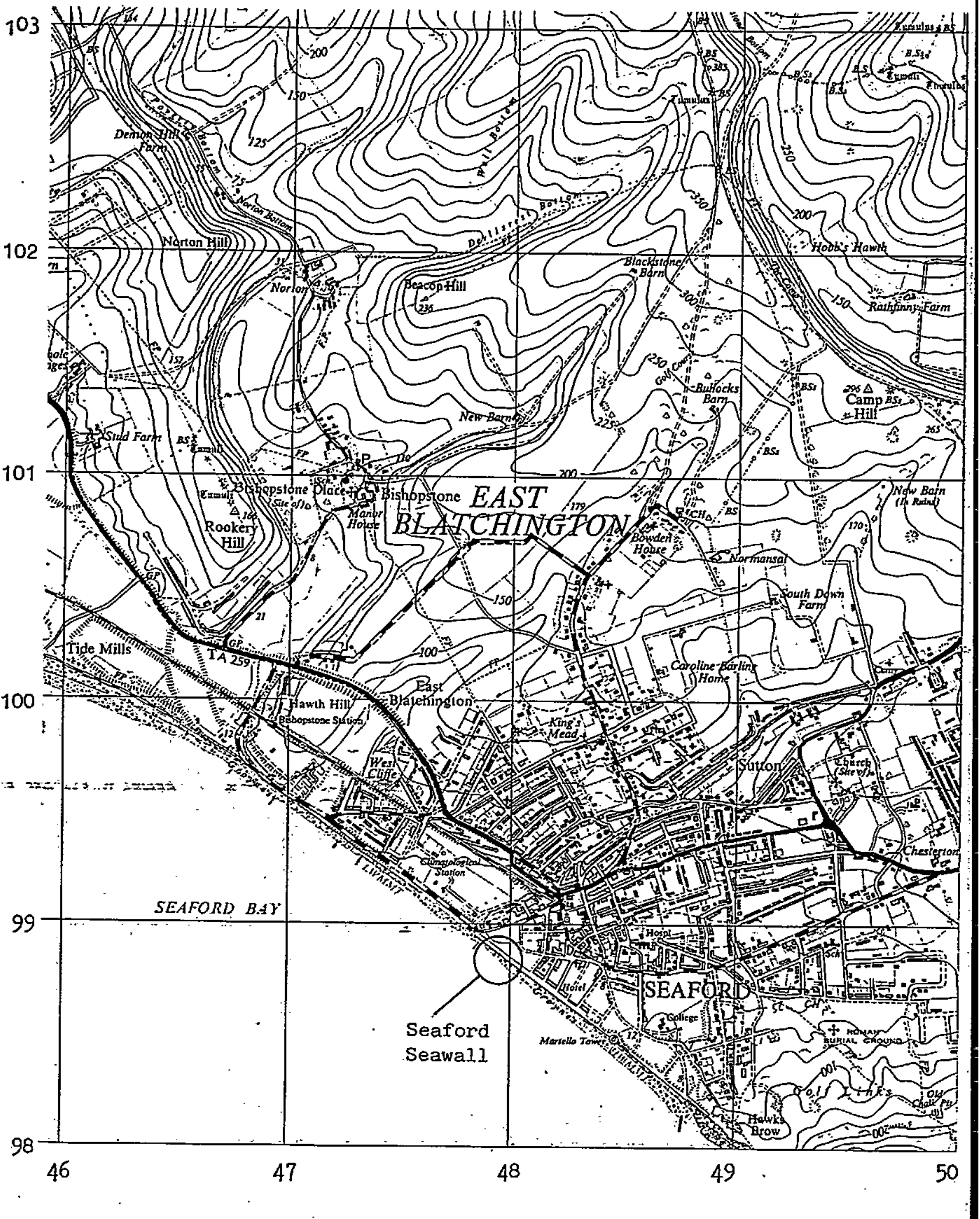
103
102
101
100
99
98
46
47
48
49
50
Denton Hill Farm
Norton Hill
Norton
Beacon Hill
Blackstone Barn
Hobb's Hawth
Rathfinny Farm
Bullocks Barn
Camp Hill
New Barn
Stud Farm
Bishopstone Place
Bishopstone
EAST BLATCHINGTON
Rookery Hill
Manor House
Bowden House
Normansal
South Down Farm
New Barn (In Ruins)
Tide Mills
TA 259
Hawth Hill
Bishopstone Station
East Blatchington
Caroline Barling Home
King's Mead
West Cliffe
Sutton
Church (Site of)
Chesterton
SEAFORD BAY
Climatological Station
Hospl
Hotel
SEAFORD
College
Martello Tower
ROMAN BURIAL GROUND
Golf Links
Old Chalk Pit
Hawks Brow
Seaford Seawall

Figure 2.9 Map of Seaford showing location of seawall

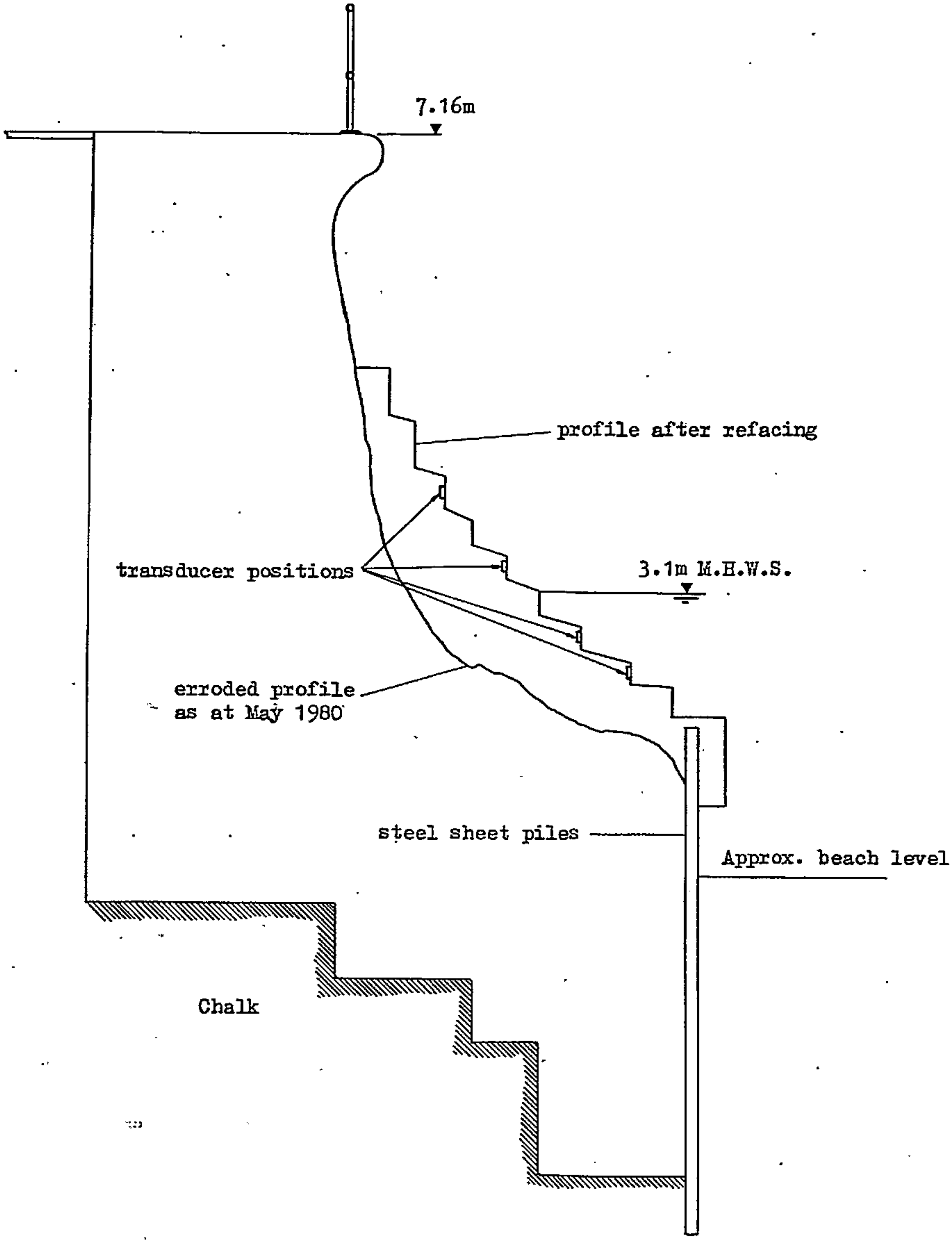
7.16m
profile after refacing
transducer positions
3.1m M.H.W.S.
erroded profile as at May 1980
steel sheet piles
Approx. beach level
Chalk

Figure 2.10 Typical cross section of Seaford seawall (scale 1 : 50)

All levels referred to O.D.

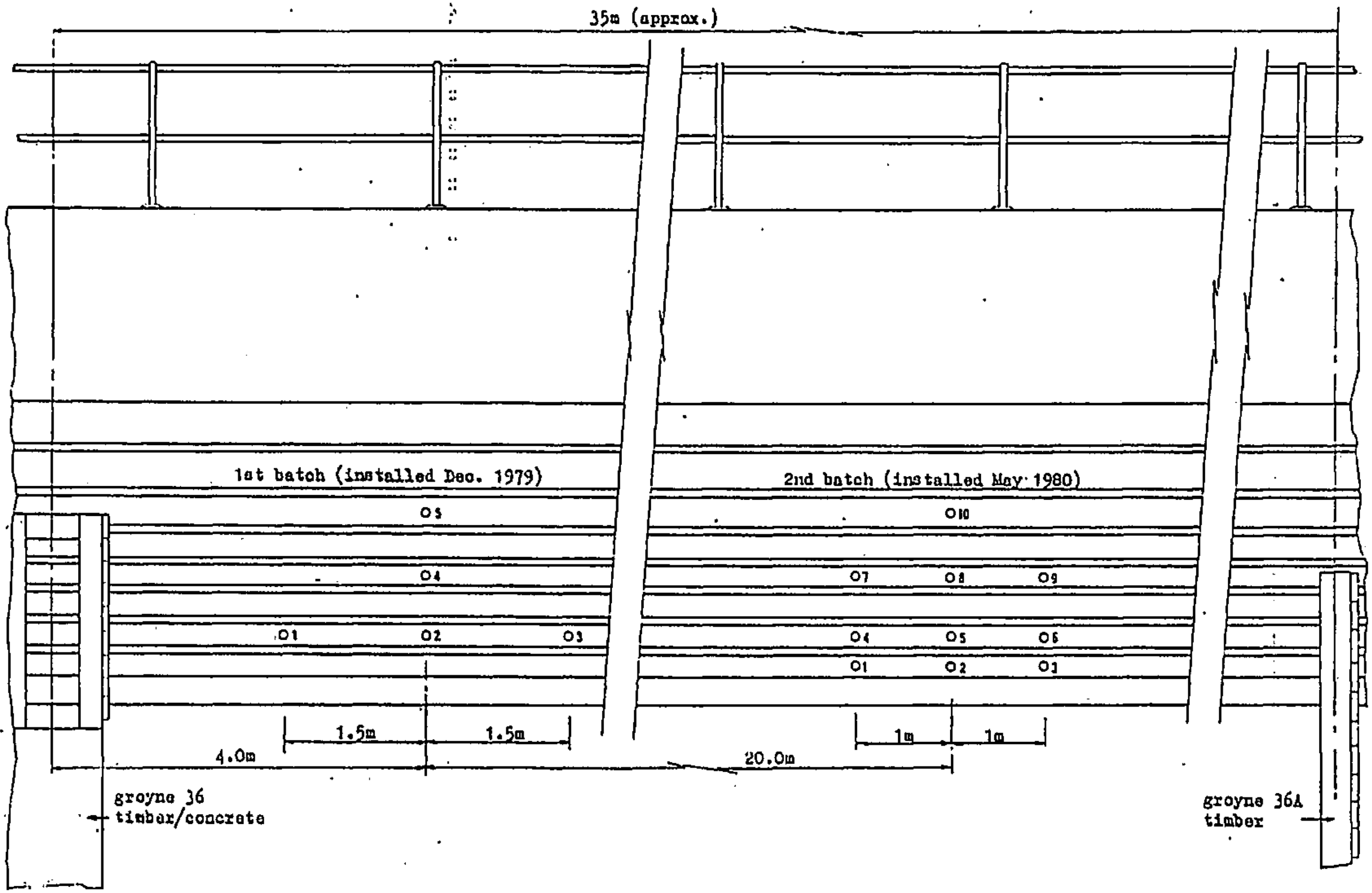
35m (approx.)
1st batch (installed Dec. 1979)
2nd batch (installed May 1980)
5
4
1
2
3
10
7
8
9
4
5
6
1
2
3
1.5m
1.5m
4.0m
20.0m
1m
1m
groyne 36
timber/concrete
groyne 36A
timber

Figure 2.11 Transducer array on Seaford seawall

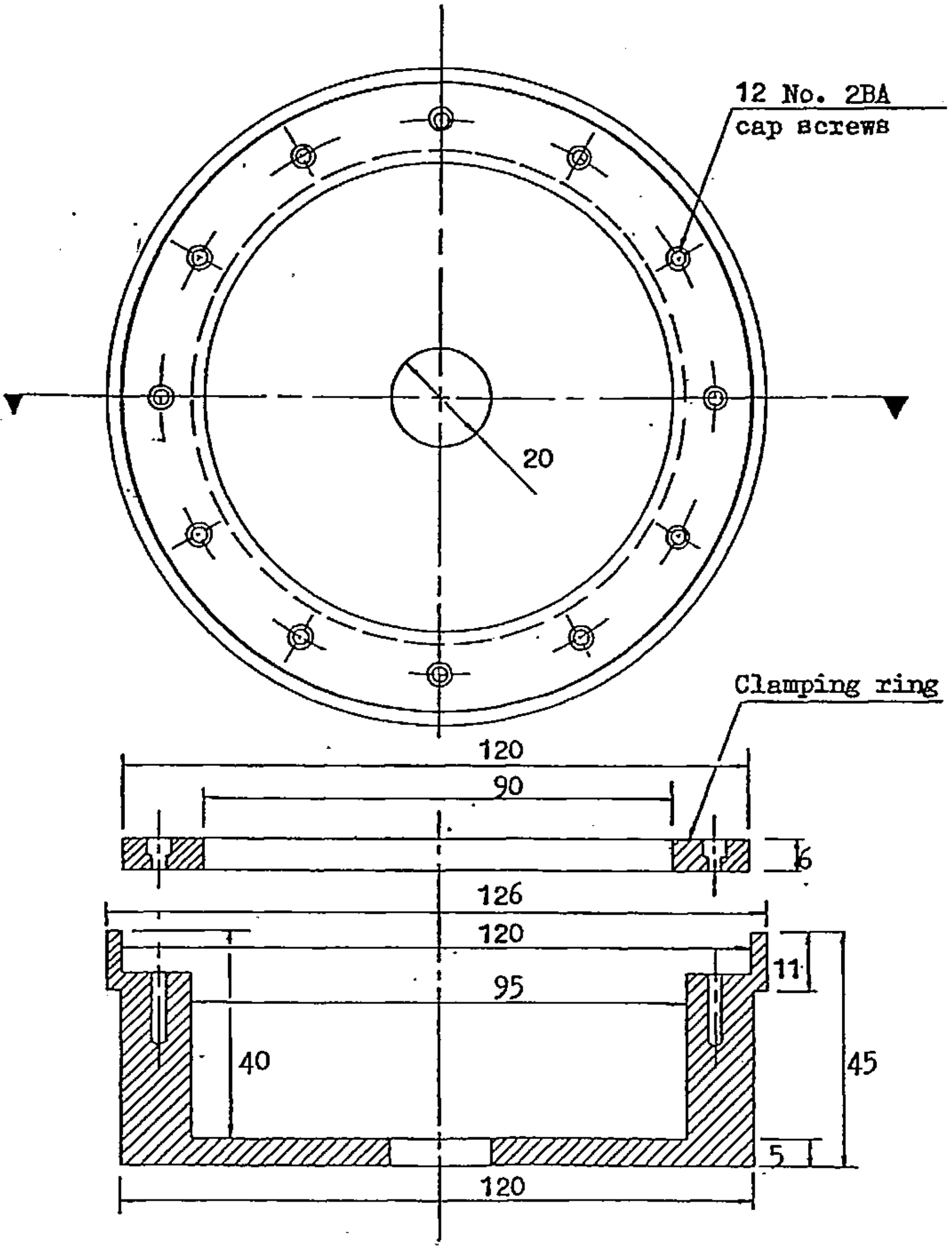
12 No. 2BA
cap screws
20
Clamping ring
120
90
6
126
120
95
11
40
45
5
120

Figure 2.12 Type 1 transducer and housing

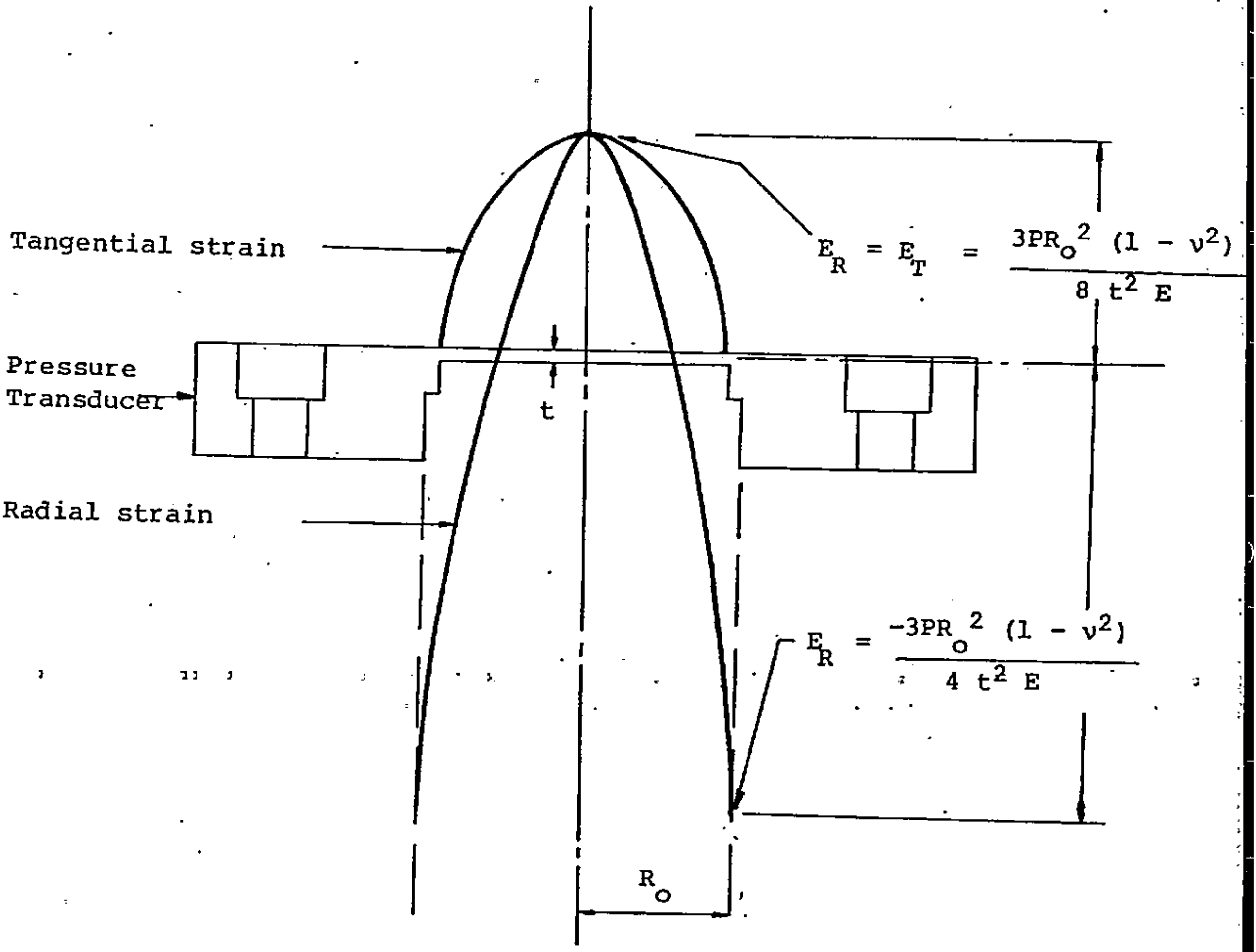
Tangential strain
Pressure Transducer
t
Radial strain
$E_R = E_T = \frac{3PR_o^2 (1 - \nu^2)}{8 t^2 E}$
$E_R = \frac{-3PR_o^2 (1 - \nu^2)}{4 t^2 E}$
R_o

Figure 2.13 Strain distribution in type 2 pressure transducer.

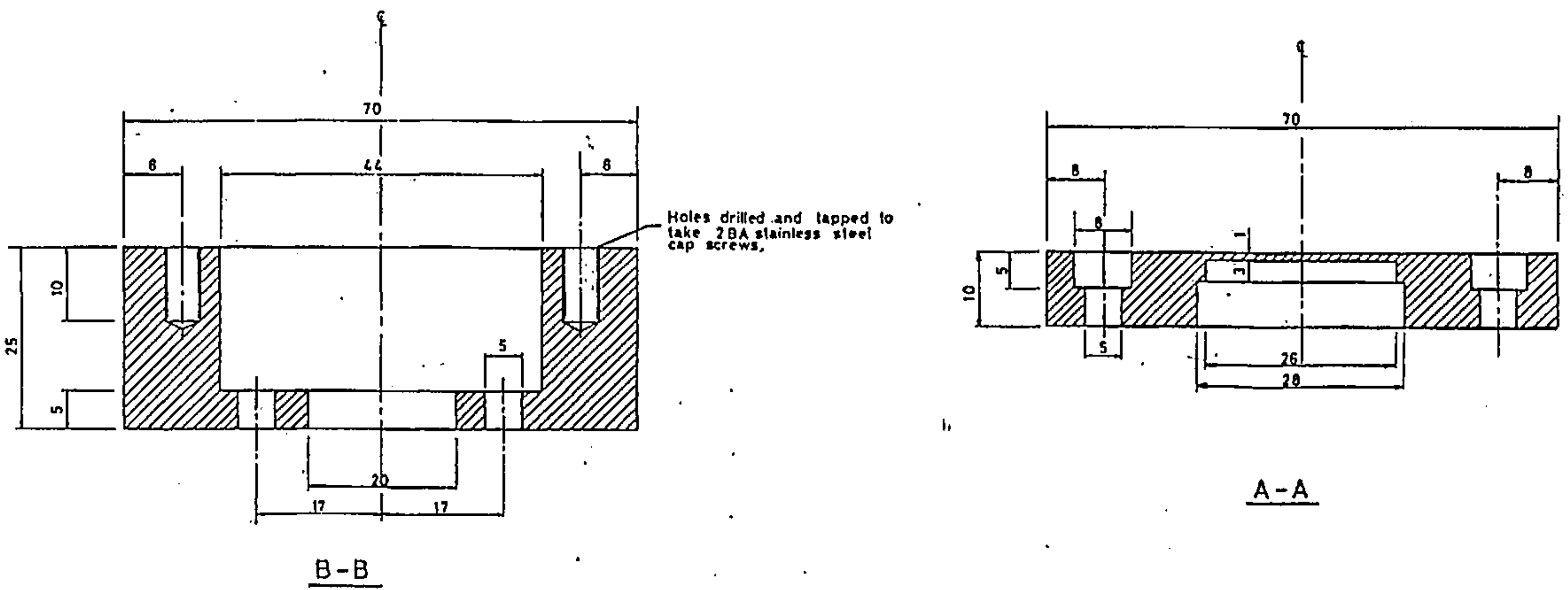

℄
70
8
44
8
Holes drilled and tapped to take 2BA stainless steel cap screws,
10
25
5
5
20
17
17
B-B
℄
70
8
8
8
1
5
3
10
5
26
28
A-A

Figure 2.14 Type 2 transducer and housing

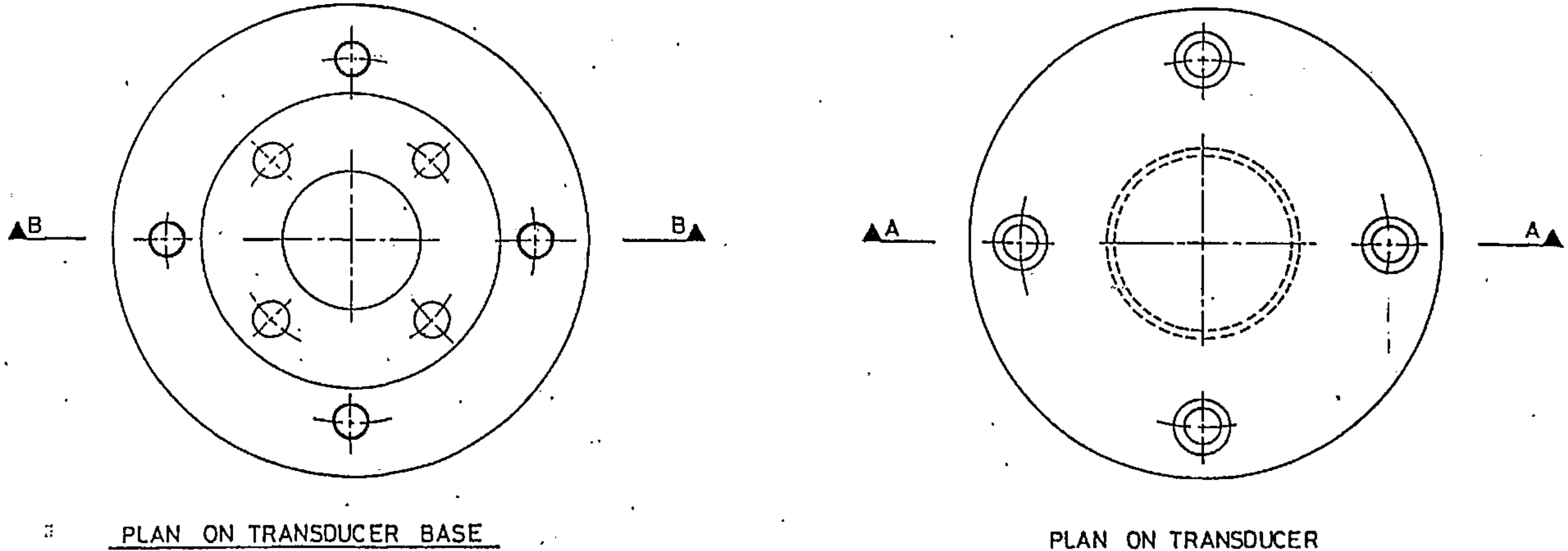

B
B
A
A
PLAN ON TRANSDUCER BASE
PLAN ON TRANSDUCER

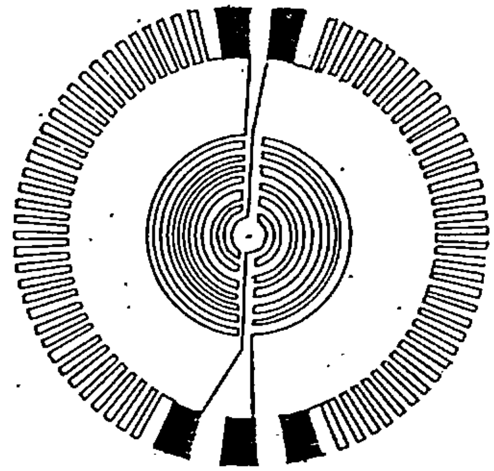

Figure 2.15 Technimeasure FDPF - 24 - 17 strain gauge as used in the type 2 transducer.

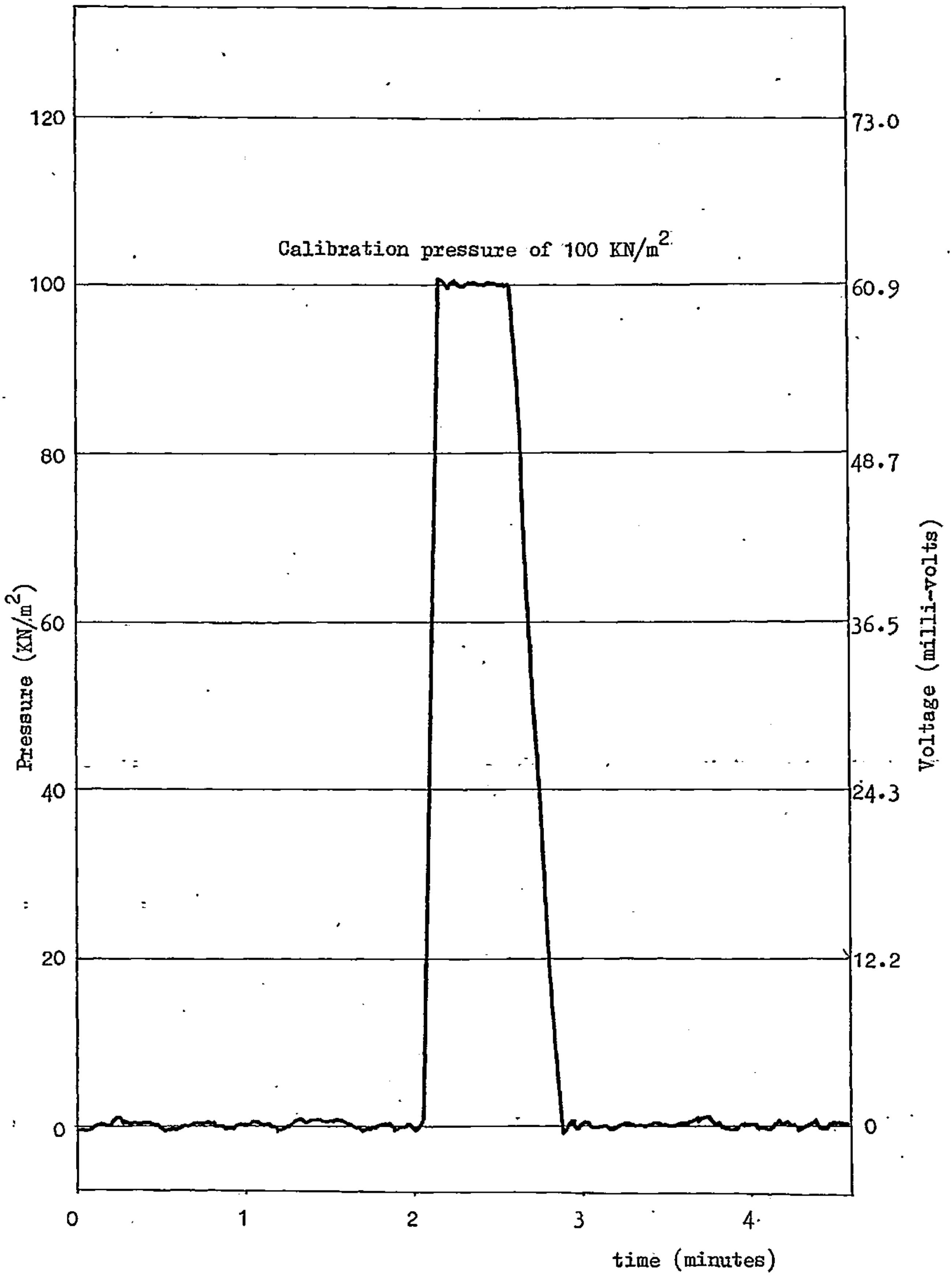

Figure 2.16 'Noise level' after amplification, from type 2 pressure transducer, at zero load and 100 KN/m^2.

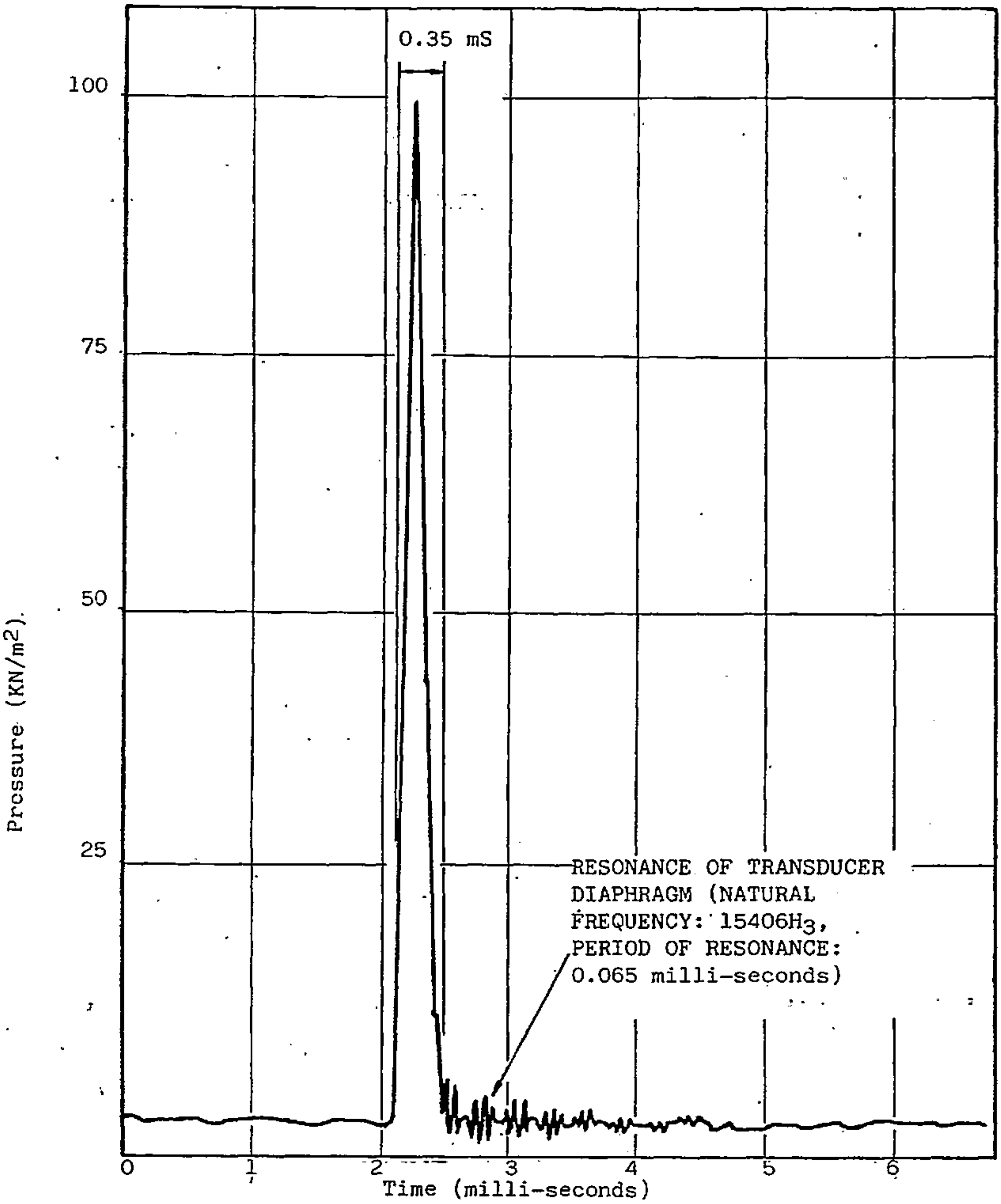

Figure 2.17 Response of a type 2 pressure transducer subjected to a transient pressure caused by the impact of a steel ball.

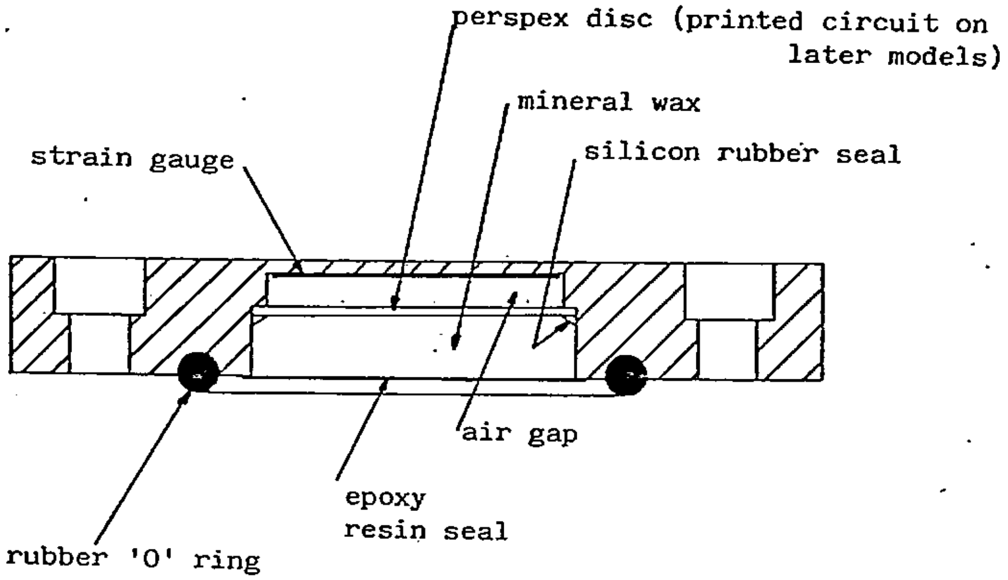
perspex disc (printed circuit on
later models)
mineral wax
strain gauge
silicon rubber seal
air gap
epoxy
resin seal
rubber 'O' ring

Figure 2.18 Method of sealing type 2 transducer

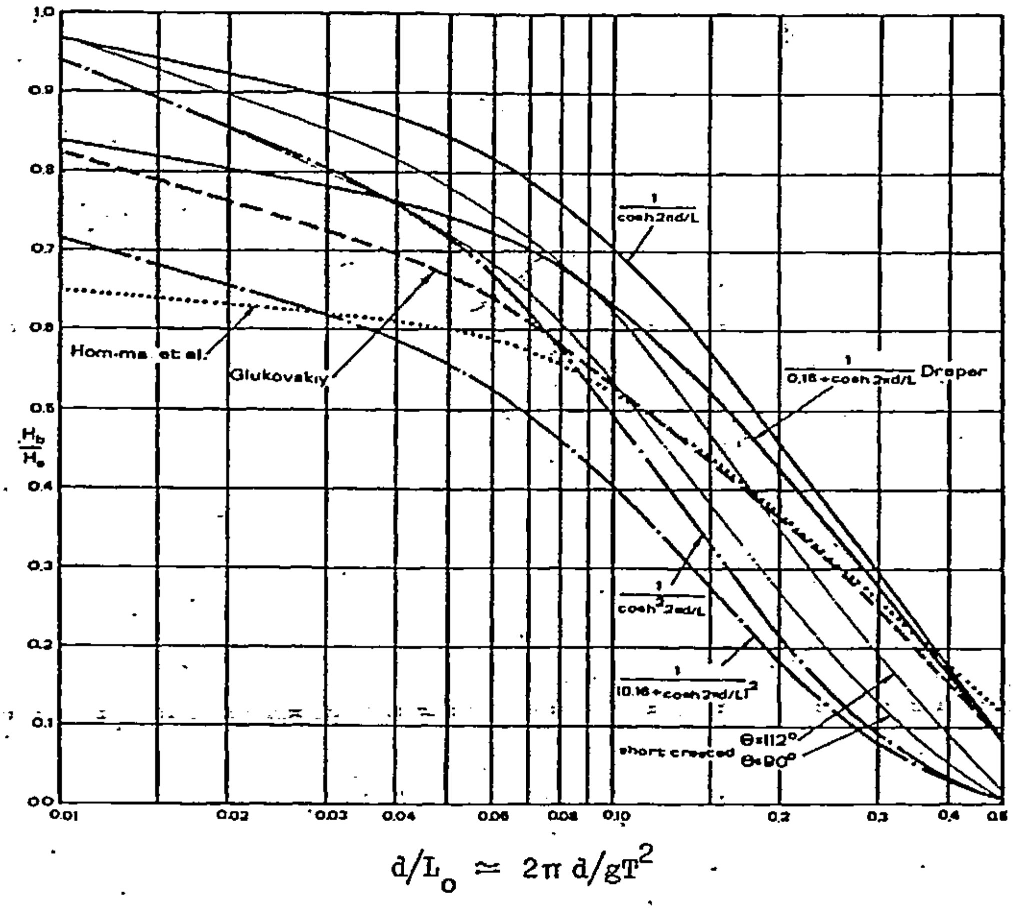

Figure 2.19 Attenuation of wave pressure head with depth (after Silvester (81))

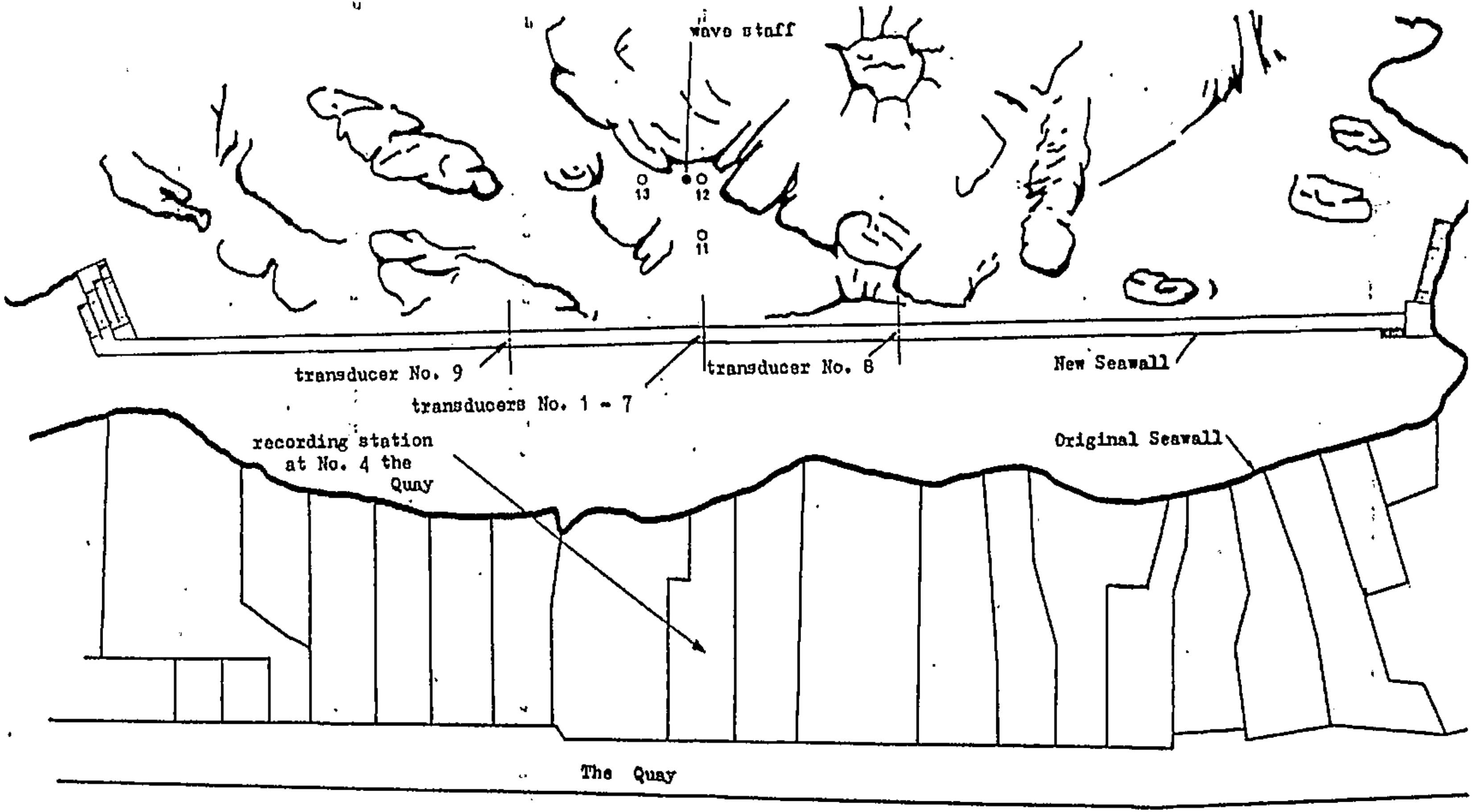
wave staff
13
12
11
transducer No. 9
transducers No. 1 - 7
transducer No. 8
New Seawall
recording station at No. 4 the Quay
Original Seawall
The Quay

Figure 2.20 The location of the beach transducers and wave staff in relation to the pressure transducers on the seawall.

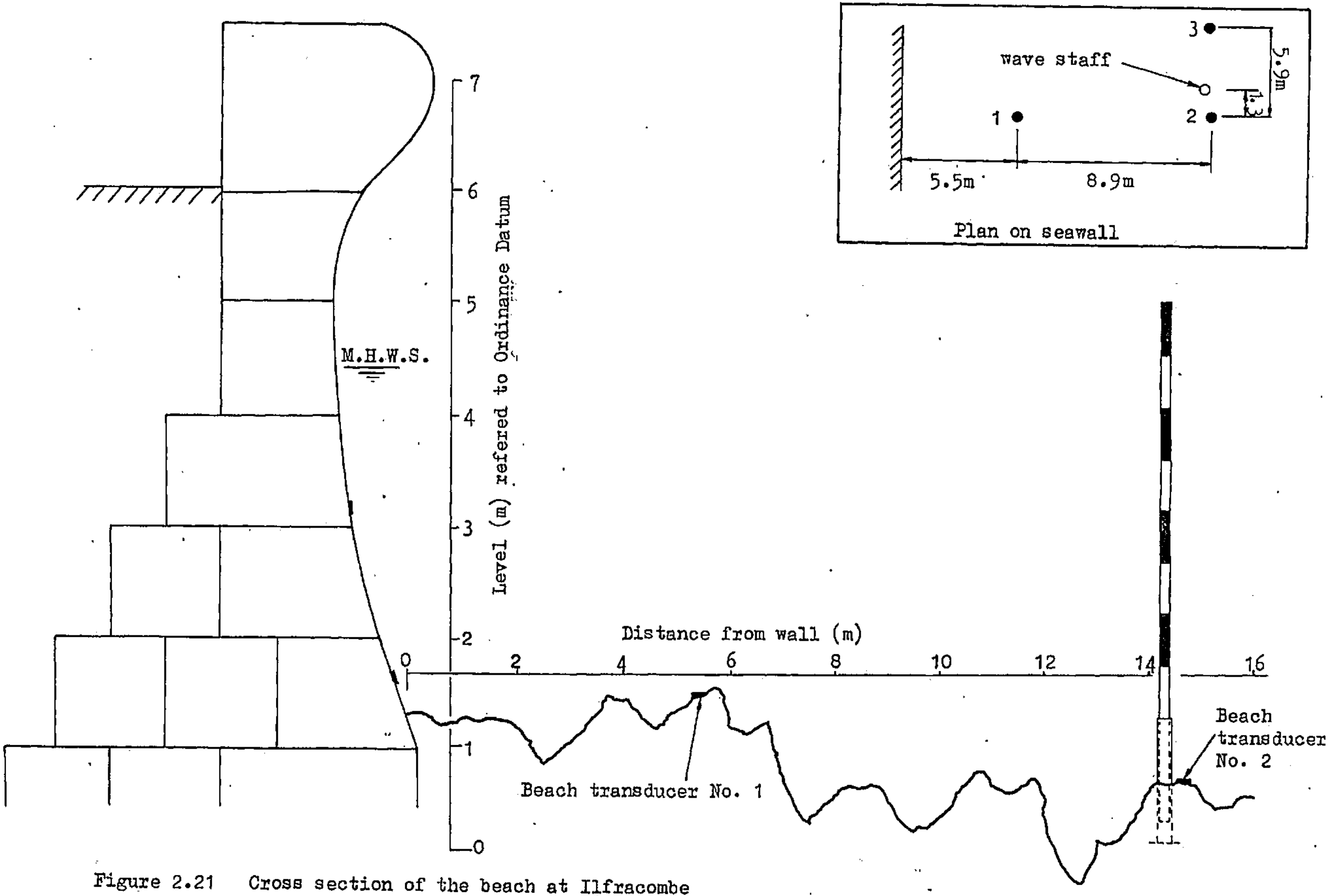
Plan on seawall
wave staff
1
2
3
5.5m
8.9m
5.9m
1.3
M.H.W.S.
Level (m) refered to Ordinance Datum
0
1
2
3
4
5
6
7
Distance from wall (m)
0
2
4
6
8
10
12
14
16
Beach transducer No. 1
Beach transducer No. 2

Figure 2.21 Cross section of the beach at Ilfracombe at the position of the beach transducers.

Figure 2.22

CIVIL ENGINEERING MATERIALS LABORATORY

SIEVE ANALYSIS RESULTS

AGGREGATE: SEAFORD SAMPLE 4

DATE: 12.5.80

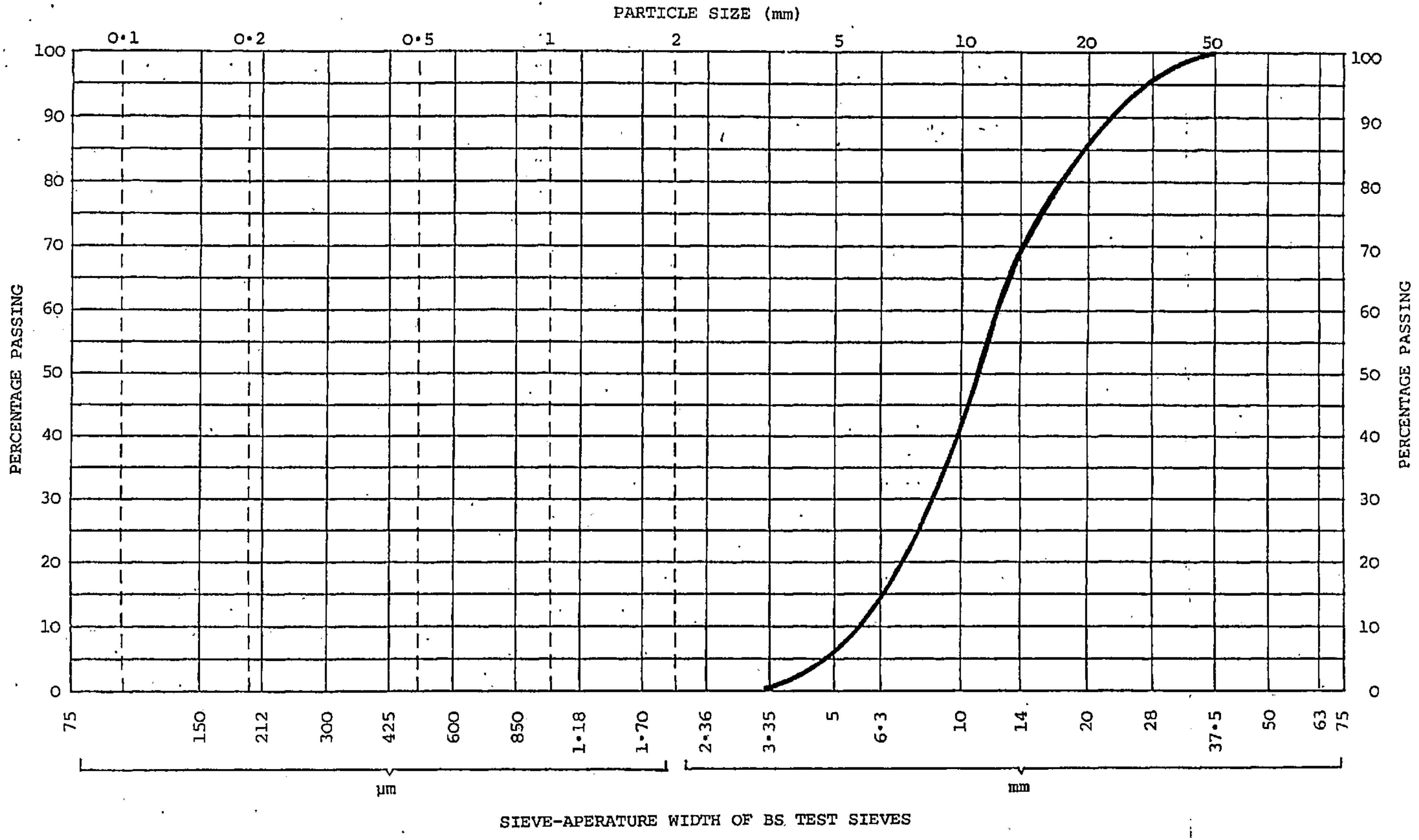

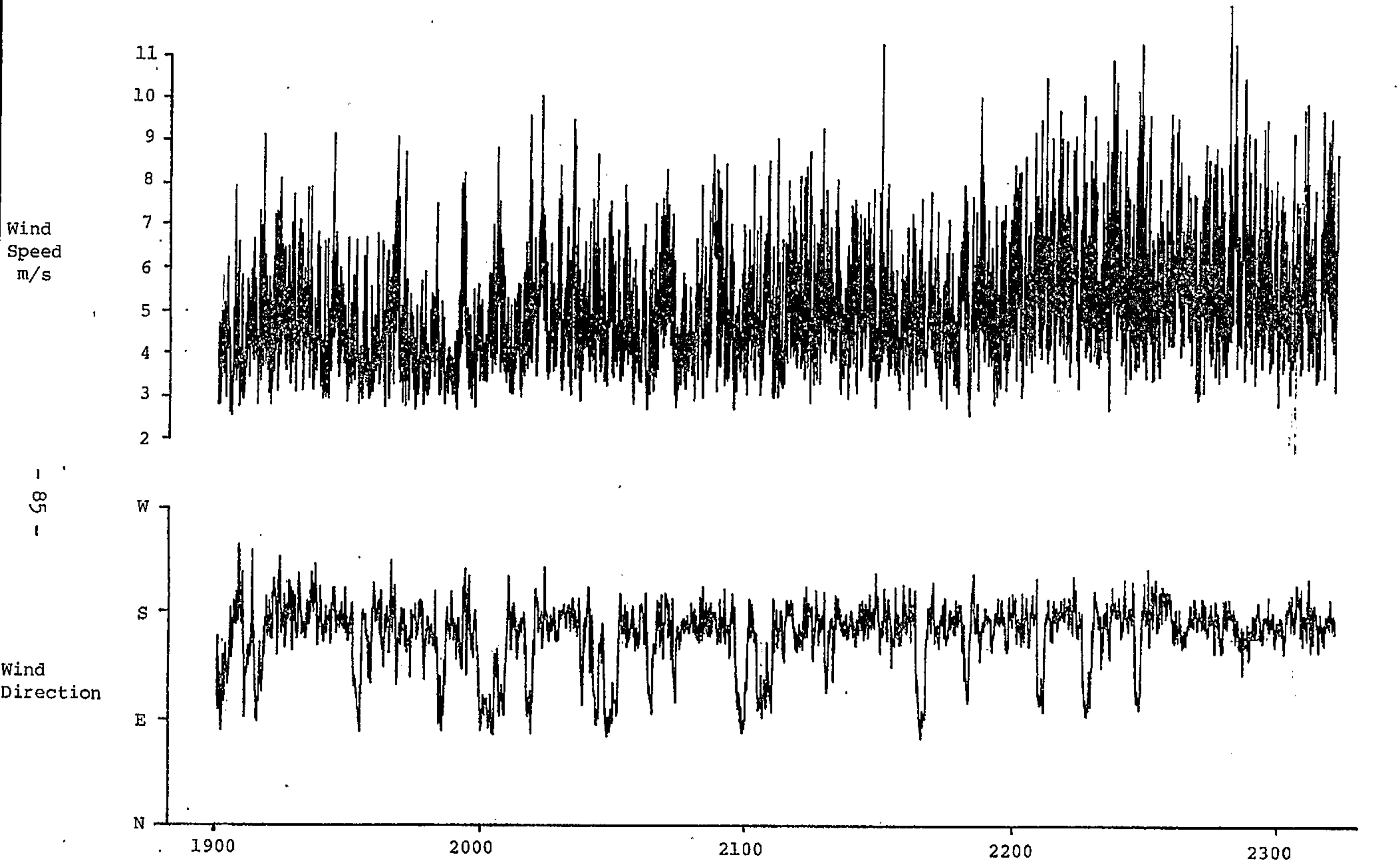

Figure 2.23 Wind speed and direction measured at Ilfracombe on 6th April 1981.

CHAPTER THREE

DATA ANALYSIS AND RESULTS

3.1 Introduction

Seawall design, even today, is still often based on 'rule of thumb' empirical methods for deriving design wave pressures, as evidenced by Water Authorities who generally use a design pressure for wave impact of 100 KN/m^2, this value being based on previous experience. It is true that these methods regularly produce adequate structures at most locations but the occasional failures, both progressive and sudden (such as the Brunel seawall) give cause for concern. What is needed is a unified , rational design method which will estimate a design wave pressure based on measured local wave parameters. This Chapter attempts to clarify the situation by combining previous and prototype data to produce a rational method for estimating wave impact pressures.

Probably the best known and most widely used semi-empirical equation for obtaining tha maximum wave impact pressure is that by Minikin(72) (equation 1.12), a modified version of which is recommended for use in seawall design by the U.S. Shore Protection Manual(74). Various equations for estimating wave impact pressure (including Minikin's) are investigated in this Chapter, and compared with the prototype impact pressure measurements made at Ilfracombe, Seaford and Teignmouth.

3.2 Description of Data

Ocean waves are irregular, being a combination of many wave components

with differing heights, celerities, periods, etc. and as these waves enter shoaling water transformation takes place at a different rate and a different depth for each of the various component waves. There are also the effects of reflection and refraction to be considered, both of which add to the irregularity of the seastate, especially at Ilfracombe with its rocky outcrops and irregular seabed.

The cumulative effects of the above factors is that by the time the waves reach the seawalls they are essentially random, hence the pressures on the walls are also random especially as pressure is also dependent on where the wave breaks in relation to the wall. Therefore the wave pressure data is of a non-deterministic nature so it is not possible to describe it using explicit mathematical relationships, thus the analysis methods are necessarily statistical.

As a first order of approximation and for ease of analysis, the data can be regarded as stationary and ergodic, on this assumption the data lends itself to specific types of analysis. The three basic types of statistical analysis used are, (power) spectral density, probability density and correlation analysis. These three functions furnish information in the frequency, amplitude and time domains respectively.

The wave pressure data can be divided into two distinct quantities; (i) the slowly varying long duration pressure of a hydrostatic nature, and (ii) the short duration transient pressure produced by breaking waves. The hydrostatic pressures are produced by every wave impinging on the wall, whilst the short duration transient pressures are produced by only about 2% of the waves striking the wall. The

occurrence of transient pressures depends upon the orientation of wave front at the moment of impact, as a general rule a vertical wave front will produce impact pressures but a non-vertical front will not(13),(35). The magnitude of the hydrostatic pressure measured by the pressure transducer is dependent upon the wave height and water depth above it. The magnitude of the transient pressures are much more difficult to determine, being dependent upon wave steepness, volume of air entrained in the wave, wave celerity, period, etc. From data collected so far, transient pressures of up to seven times the hydrostatic pressure have been measured, although under ideal conditions Von Karman(52) suggests that the theoretical maximum pressure could reach the water hammer pressure.

Wave pressure data was recorded on 37 separate occasions (totalling 450 hours of data, see Table 3.1), yet impact pressures were only measured on 8 of these occasions. This yielded a combined total of about 190 impacts from both Ilfracombe and Seaford although only about 160 were considered reliable, (summarised in Table 3.2 and given in full in Tables 3.3 to 3.11). Some early transients mainly from Seaford were not included because numerous 'spikes' were encountered on the data tapes, these spikes were due to mains interference and switching surges and could not easily be distinguished from wave impact transients, therefore the whole tapes were discarded. Later amplifiers contained mains filters which effectively solved the problem by eliminating this interference or reducing it to an insignificant level.

It is extremely difficult to carry out any useful statistical analysis with data containing both transient and hydrostatic pressure components because the transient pressures occur so infrequently that they become lost in the bulk of the data. Therefore the data is edited so that each type of data can be analysed separately.

The hydrostatic pressure component has a non-zero mean because of the rise and fall of the tide which introduces a positive d.c. component, this tidal component is generally much larger than the pressure exerted by the wave height, Figure 3.1. Therefore the hydrostatic pressure due to the tidal effects obscures the smaller fluctuations in pressure caused by the wave height. So ideally this d.c. tidal component should be filtered out, but because the tidal rise and fall is not linear (see Figure 3.1) this requires complex non-linear analogue filters which were not available. Therefore the analysis was carried out on the data in its raw state, this caused some problems as will be seen in Section 3.3.4. It is possible to remove all d.c. components from the data by using a.c. coupling which acts as a high pass filter with a cut off frequency set fractionally above zero Hz. There is some danger when using a.c. coupling of losing any wave components with very low frequencies, it was for this reason that a.c. coupling was not available for correlation analysis when the data of interest contained frequencies below 1 Hz.

3.2.1 Establishing a Sample Length for Statistical Analysis

In order to carry out any statistical analysis on the wave pressure data to a predetermined degree of accuracy, the length of the sample must be established.

Before the record length can be established some basic assumptions must be made as to the nature of the expected data. As already stated the data is of a random nature, and as a first approximation the data is assumed to be from a stationary ergodic process. This allows the properties of the data to be determined statistically, and further more, any time averaged properties computed from different samples of the same data should be the same, provided the random process is continuous and the factors initiating the process remain constant. In this particular case it means the average wave period, height and celerity remain constant, this was found to be the case over the relatively short recording periods of two to three hours, but not in the long term from day to day.

Having assumed the nature of the data it is now possible to estimate the sample length required from statistical error theory as given by Bendat and Piersol(85), Bevington(86) and Chatfield(87).

The sample length required to acheive a desired degree of accuracy can now be calculated, but however, the estimate includes factors which are unknown prior to the data collection. Therefore certain assumptions about the nature of the expected data must be made. The power spectral density will in most cases require a longer time record to acheive a specified degree of accuracy than will other statistical functions(88). Therefore the normalised mean square error (ε^2) of the spectral density estimate is used to estimate the length of record required.

ε^2 can be approximated by(85);

$$\varepsilon^2 = \frac{1}{B_e T'} + \frac{B_e^{\,4}}{576} \cdot \frac{G_x''(f)^2}{G_x(f)} \quad \ldots\ldots\ldots\ldots\ (3.1)$$

This equation can be resolved into a random error component (ε_r) and a bias error component (ε_b) as follows;

$$\varepsilon_r^{\ 2} = \frac{1}{B_e\ T'} \qquad \ldots\ldots\ldots\ldots\ldots\ldots\ldots\ldots\ (3.2)$$

$$\varepsilon_b^{\ 2} = \frac{B_e^{\ 4}}{576} \times \left(\frac{G_x''(f)^2}{G_x\ (f)} \right) \qquad \ldots\ldots\ldots\ldots\ldots\ (3.3)$$

where $\varepsilon = \sqrt{\varepsilon_r^{\ 2} + \varepsilon_b^{\ 2}}$ .... (3.4)

B_e = resolution band width

T' = record length

$G_x(f)$ = power spectral density function

$G_x''(f)$ = second derivative of $G_x(f)$ with respect to f

The random error ε_r is a measure of the variance of the estimate and is dependent upon the resolution bandwidth (B_e) and the record length (T') and so is a function primarily of the analysis parameters rather than unknown data parameters. The bias error ε_b is a measure of the systematic error inherent in the estimation procedure and includes the effects of non-linear system parameters and noise at the system input.

One way to estimate the bias error is to approximate the system to a simple second order model, the bias error is then a function of band width ratio B_e/B_r (where B_r is the half power point bandwidth of the system). This is shown in graphical form below(85).

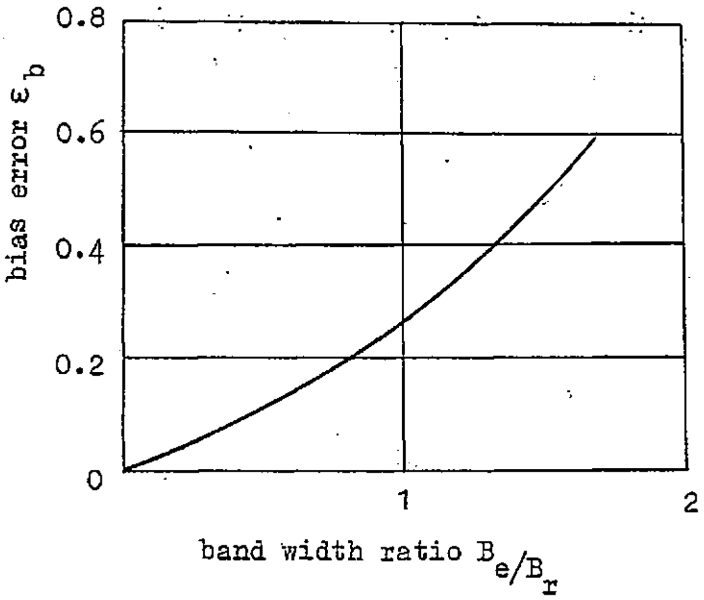

B_r cannot be measured until the data has been analysed but can be approximated by;

$$B_r = 2\,\xi\,f_r \quad \ldots\ldots\ldots\ldots\ldots\ldots\ldots\ldots \quad (3.5)$$

where ξ = damping ratio

f_r = resonant frequency

At this point some prior knowledge of the seawall response and wave characteristics is required to decide upon the lowest resonant frequency of interest. The degree of accuracy must now also be decided upon.

Assuming an average wave period of four seconds, (this is about the average wave period measured at Ilfracombe and Seaford), this is a wave frequency of 0.25 Hz which is taken as the lowest frequency of interest

(f_r). Assuming a maximum allowable bias error of 0.1 and a maximum allowable random error also of 0.1. This then only leaves the damping ratio to be estimated, from Ref. 82 a suitable value for a mass concrete structure would appear to be about 0.05.

Values of B_e and hence T' can now be found as follows;

From the figure on the previous page,

$$\text{for } \varepsilon_b = 0.1 \quad \frac{B_e}{B_r} = 0.5$$

$$\text{and as } B_r = 2\xi f_r$$

$$\text{then } B_e = \xi f_r = 0.0125 \text{ Hz}$$

T' can now be estimated from equation 3.2 rewritten as;

$$T' = \frac{1}{B_e \varepsilon_r^2} \text{ seconds} \quad \ldots\ldots\ldots\ldots\ldots \quad (3.6)$$

$$T' = \frac{1}{(0.0125)(0.1)^2} = 3555 \text{ S} = 59 \text{ minutes}$$

Therefore a minimum record length of approximately 59 minutes is required to achieve adequate resolution of frequencies down to 0.25 Hz. This value is arrived at through numerous approximations and assumptions and so is only taken to indicate the order of record length required.

From the accelerometer data the higher frequencies of the power spectrum are of interest because the first mode of vibration of the seawalls occurs at about 10 Hz (see Chapters Six and Seven), therefore frequencies below about 5 Hz are of no particular significance. To achieve adequate resolution at 5 Hz would require a record length of less than 3 minutes, with the sample length becoming proportionately less for higher frequencies.

3.3 Data Analysis Techniques

Because the impact pressures occur so infrequently (approximately one in every two thousand waves recorded produced any impact pressure), it is not possible to analyse them using spectral density, probability density or correlation techniques because each of these methods is statistical and requires a relatively long continuous sample to give adequate resolution. Therefore only the hydrostatic pressure component is analysed by these methods.

To locate the wave impact pressures was a very tedious process, because all impacts had to be located manually. This meant that all recorded data (450 hours of it) had to be viewed by the author to pick out the transients. The data tapes were played back on a chart recorder at eight times real time (wave impacts did not show up at speeds faster than this), transients and other points of interest were marked and viewed at real time using a transient recorder connected to an oscilloscope. The transient recorder was only single channel therefore simultaneous wave impacts at more than one pressure transducer could only be viewed, synchronised in time, on a multipen chart recorder fitted with a compensating device.

3.3.1 Probability Density Function (p.d.f.)

The principle reason for carrying out a probability density analysis is to establish a probablistic description for the instantaneous values of the data in the amplitude (pressure) domain. The probability density plots may be used to determine the type of data, i.e. sinusoidal or random, and also for distinguishing any non-linear effects.

A simple description of a first order probability distribution is to consider a random pressure history record, as in Figure 3.2. The probability of $x(t)$ lying between x_1 and x_2 at any instant in time may be found by summing the time intervals Δt_1, Δt_2, ... Δt_n during which time $x(t)$ falls inside the range x_1 to x_2 and dividing this value by the record length T. This ratio t_x/T approaches an exact probability description as T approaches infinity. The probability density function $p(x)$ is defined as;

$$p(x) = \frac{1}{\Delta x} P\left[x_1 < x < x_2 + \Delta x\right] = \frac{t_x}{T\,\Delta x} \quad \ldots\ldots\ldots (3.7)$$

assuming Δt and Δx tend to zero.

As probabilities of mutually exclusive events are additive the probability that $x(t)$ falls between x_1 and x_2 is;

$$P\left[x_1 < x < x_2\right] = \int_{x_1}^{x_2} p(x)\,dx \quad \ldots\ldots\ldots\ldots\ldots\ldots (3.8)$$

Furthermore, since the probability of $x(t)$ lying between ± infinity is unity, then the area under the probability distribution curve is also unity, that is;

$$P\left[-\infty < x < +\infty\right] = \int_{-\infty}^{+\infty} p(x)\, dx = 1 \quad \ldots\ldots\ (3.9)$$

To carry out this analysis manually would be extremely time consuming therefore the data is analysed using a Hewlett Packard Correlator (model No. 3721A) where the analogue data passes through an A-D converter and the above operation is then performed digitally.

As already mentioned the tidal effects are much larger than those due to the wave heights thus when the above analysis is carried out, the tidal effects completely obscure the true probability density distribution of the wave heights. To demonstrate this effect a two hour sample of pressure data was analysed using the Hewlett Packard Correlator, the same sample of data was then analysed in 20 minute records, Figure 3.3. The probability density plot of the whole pressure record has no recognisable distribution due to the influence of tidal effects. The tidal range is from 1 to 2 metres, which represents a pressure of about 10 to 20 KN/m^2, whereas the average wave height on this occasion was about $\frac{1}{2}$m which represents a pressure of about 5 KN/m^2. The individual 20 minute records all have probability density curves which quite closely approximate to a gaussian p.d.f., this is because in the short term the wave height is the dominating factor and tidal effects have little influence. Each 20 minute record has a similar probability density curve which suggests that the original assumptions that the data was stationary and ergodic are probably correct.

The distribution of wave heights is known to be gaussian (Wiegel$^{(38)}$), so the distribution of hydrostatic pressure due to wave height should also be gaussian because hydrostatic pressure is proportional to wave height. This is seen to be the case in Figure 3.3 where the individual 20 minute samples of data quite closely approximate to the theoretical gaussian curve (Figure 3.4). Thus the p.d.f. of the hydrostatic pressure can be assumed to be gaussian, given as;

$$p(x) = \frac{1}{(2\pi\sigma)^{\frac{1}{2}}} \; e^{-\frac{(x-m)^2}{2\sigma^2}} \qquad \ldots\ldots\ldots\ldots\ldots (3.10)$$

where m = mean

σ = standard deviation

3.3.2 Spectral Density Analysis

The (power) spectral density function gives the general frequency composition of the data in terms of the spectral density of its mean square value ($\overline{x^2(t)}$). The main use for such an analysis is to establish the frequency composition of the data, which in turn bears an important relationship to the basic characteristics of the physical system. For example, a spectral analysis of the wave forces on the wall measured by pressure transducers will provide data on the frequency composition of the waves producing those forces, i.e. the excitation spectral density $S_{FF}(f)$. Whilst a spectral analysis of accelerometer data will furnish the spectral density of seawall response $S_{XX}(f)$. It is shown in Chapter Six how the spectral density of wall response can be related to the spectral density of wall excitation by use of a transfer function.

Spectral density analysis is essentially an application of Fourier analysis, although modified for stochastic rather than deterministic processes, (Fourier analysis is covered in more detail in Chapter Six, Section 6.3.2). A general spectral density function can be defined as;

$$\overline{x^2(t)} = \int_0^\infty S_{FF}(f)\, df \quad \ldots\ldots\ldots\ldots\ldots\ldots\ldots (3.11)$$

where $S_{FF}(f)$ is the single sided spectral density function in terms of cycles per second (Hz) with typical units of V^2/Hz

$\overline{x^2(t)}$ is the mean squared time history

Spectral density analysis can be best understood by considering analogue data analysis techniques outlined by the following procedures,

(a) The pressure record is frequency filtered using a narrow band-pass filter of bandwidth B_e Hz.

(b) The instantaneous filtered signal is squared.

(c) The squared signal is averaged over the record length.

(d) The mean square output is divided by the bandwidth B_e

The square root of the area under the spectral density curve will give the r.m.s. value of the signal being analysed between the frequencies considered.

Spectral density estimates were obtained for pressure and acceleration data on the Ilfracombe and Seaford seawalls using a Hewlett Packard Spectrum Analyser (model No. 3582A). The 3582A accepts data in analogue format, digitises it and computes the spectral density function by means of the Fast Fourier Transform (FFT). The FFT is a modified version of the standard Fourier series procedure whereby the total number of computations is reduced by a factor of 10^2, (see Cooley and Tukey$^{(84)}$). The 3582A has a frequency range of 20 mHz to 25.5 KHz with a resolution bandwidth B_e down to 20 mHz, the bandwidth cannot be directly selected but is a result of selecting a span width and filter shape. Three different frequency domain filters are available; (i) flat top, (ii) Hanning and (iii) uniform, these filters represent a trade off between amplitude uncertainty and frequency resolution. The flat top filter is optimized for amplitude measurements, the uniform filter is best for frequency resolution and the Hanning offers a compromise between the two.

A sample of pressure data from Ilfracombe, due mainly to regular swell and standing waves, was analysed via the Spectrum Analyser. The spectral density plot is shown in Figure 3.5, most of the energy in this record is contained in the 0.1 to 0.3 Hz frequency band, this compares quite closely with the visual measurements of wave period obtained on this occasion, which were found to range between 3 and 7 seconds (0.33 to 0.143 Hz). For comparison, a sample of data taken from a pressure transducer at Seaford was analysed, this sample was recorded on a day with strong on-shore winds and a very confused seastate which made it difficult to distinguish and follow the progress of individual waves. The spectral density plot of this record is shown in Figure 3.6, from this figure it is seen that the energy level is almost uniform over the frequency range 0.1 to 1.0 Hz (10 to 1 second wave period) at a level of about -65 dbV. This shows that there were no predominant wave periods because similar energy is contained at all frequencies from 0.1 to 1 Hz, whereas for the standing wave data at Ilfracombe there is very little energy contained by waves outside of the predominant periods. A comparison between visual wave period measurements and those indicated by spectral density analysis is given in Table 3.12. Samples of the pressure histories used to produce Figures 3.5 and 3.6 are given in Figures 3.7 and 3.8 respectively.

In both Figures 3.5 and 3.6 a peak occurs at about 0.75 Hz, this peak has a very narrow bandwidth characteristic of a sinusoidal signal. The exact cause of this peak is not known, but it is definitely generated by the recording and amplifing system and is not a characteristic of the forcing function (i.e. the wave pressure). The cause of this spurious signal was isolated to the recording and amplifing equipment by running the pressure measuring system 'dry' in the laboratory, where this peak was still found to occur with the same order of magnitude. This signal was only generated with the tape deck and amplifiers both running, it was not produced by either tape deck or amplifiers running on their own. This indicates some form of cross excitation between the tape deck and amplifiers. Thus even though this signal could not be eliminated, (band pass filtering was not practical due to the very narrow band width of the signal) it can be disregarded as being a system parameter and not a characteristic of the forcing function.

Seawall accelerations measured by accelerometers was also analysed via the Hewlett Packard Spectrum Analyser. Figure 3.9 shows a spectral density plot of acceleration data measured at Seaford at low water

when the waves were approximately 20m from the wall. Thus this plot is not due to direct wall excitation by waves but is the result of general background excitation such as vehicles driving along the promenade, wind and the transmission of wave energy through the beach to the wall. The bulk of the energy in Figure 3.9 is contained between 100 and 400 Hz with a peak at 264 Hz, this spectrum can be regarded as the 'signature' of the Seaford seawall any additional wall excitation by direct wave action will be simply superimposed upon this signature spectrum:

Figure 3.10 shows a spectral density plot of the Seaford seawall response with direct wave action on the wall. If Figures 3.9 and 3.10 are compared, the spectral densities above about 100 Hz are almost the same and both have a peak at 264 Hz of almost the same magnitude. The majority of the energy in Figure 3.10 is concentrated at the lower frequencies with a peak at about 10 Hz. Therefore it seems that direct wave action on the seawall adds very little to the response at frequencies above about 100 Hz due to the low frequency content of the wave forces but it adds greatly to the wall response at frequencies below about 30 Hz, (the response at these low frequencies becomes the dominant feature in Figure 3.10). To examine the response at these low frequencies in more detail, Figure 3.10 is expanded over the range 0 to 50 Hz as shown in Figure 3.11. In this Figure it can be seen that the peak occurs at 10.3 Hz and is the wall response at its fundamental bending mode of vibration. A similar spectral density plot was produced for the Ilfracombe seawall (Figure 3.12), in this figure the fundamental mode of vibration occurs at 8.9 Hz. Peaks occurring in the spectral density plots at 50Hz and its harmonics (e.g. 100 Hz, 200 Hz, etc.) are due to the 50 Hz mains supply and so can be disregarded, the amplifiers were later modified to suppress this mains interference.

Spectral density plots produced for a wide frequency range, such as Figures 3.9 and 3.10, are likely to give poor estimates of the spectral density at specific frequencies, this is because the resolution bandwidth is necessarily large so the average energy within this bandwidth is plotted at a single point on the spectral density curve causing smoothing and a loss of localised peaks. In Figure 3.10 the energy level at a frequency of 10 Hz is -30 dbV (resolution bandwidth of 6 Hz), whereas for the expanded plot of Figure 3.10 (i.e. Figure 3.11) the energy level at a frequency of 10 Hz is -44.1 dbV (6.25 mV)(resolution bandwidth of 0.3 Hz).

The acceleration of a seawall at any given frequency can be converted to a displacement, by knowing the accelerometer scale factor, as shown below;

The displacement at a frequency of say 10.3 Hz (Figure 3.11) is found as follows;

the spectral density at 10.3 Hz is 6.25 mV
amplifier gain = 10
accelerometer scale factor = 5 V/g

$$\text{therefore acceleration} = \frac{6.25 \cdot 10^{-3} \cdot 9.81}{5 \cdot 10} = 1.23 \times 10^{-3} \text{ m/s}^2$$

$$\text{and displacement} = \frac{1.23 \cdot 10^{-3}}{(2\pi f)^2} = \frac{1.23 \cdot 10^{-3}}{(6.28 \cdot 10.3)^2} \text{ m}$$

$$= 0.29 \times 10^{-6} \text{ m}$$

A sample of the acceleration/time history from which Figures

3.10 and 3.11 were produced is shown in Figure 3.8 synchronised with a sample of the corresponding pressure/time history.

It is difficult to interpret conclusively, spectral density curves such as those in Figures 3.11 and 3.12 because the seawall response is generated by random forced vibrations caused by the random wave loading. So the small peaks in these figures could be due to the forcing function or the wall response, or they might be due to the analysis methods, (such as representing the spectral density by 1024 discrete points instead of by a continuous function).

3.3.3 Auto-Correlation Analysis

Auto-correlation is a useful aid in determining the nature of data, i.e. whether it is random or deterministic. A deterministic time series will have an auto-correlation function which persists over all time displacements, whilst random data will tend to zero for large time displacements. An auto-correlation estimate is made by sampling a discrete time series x(t) at time t and t + τ , taking the product of these two values and averaging over the observation time T. As T approaches infinity an exact auto-correlation function can be written as;

$$R_x(\tau) = \underset{T \to \infty}{\text{limit}} \frac{1}{T} \int_0^T x(t) \cdot x(t+\tau)\, dt \qquad \ldots\ldots\ldots (3.12)$$

Technically the auto-correlation function supplies no new information over the spectral density function, it just presents the data in the time instead of frequency domain and as such is more useful for certain applications. The auto-correlation function is related to the spectral density function via the Fourier transform pair (see Section 6.6) as given below ;

$$R_x(\tau) = \frac{1}{2} \int_{-\infty}^{+\infty} S_{FF}(f) \; e^{2j\pi f\tau} \, df$$

$$S_{FF}(f) = 2 \int_{-\infty}^{+\infty} R_x(\tau) \; e^{-2j\pi f\tau} \, d\tau$$

If an auto-correlation function is calculated for a time series with trend (such as the hydrostatic pressure measured on the seawalls where the trend is caused by tidal effects), even if the data is completely random the auto-correlation function will only diminish to zero for very large time displacements. Little useful information can be inferred from a correlogram of this type because the trend dominates all other features. To demonstrate this effect, a 90 minute record of hydrostatic pressure measured on the Ilfracombe seawall was analysed using the Hewlett Packard Correlator. The resulting correlogram is shown in Figure 3.13(b), as expected no useful information is displayed. To obtain a sample of data without trend the signal should ideally be filtered, or alternatively a sample can be taken at the turn of the tide when for a short time there is no trend. This second method was used to obtain a sample of data for analysis, the resulting correlogram is shown in Figure 3.13(a). Well defined peaks occur in this correlogram at about 2.6 second intervals, with succeeding peaks gradually reducing in amplitude and widening as the degree of correlation decreases with increasing τ . These peaks in the correlogram of hydrostatic pressure are caused by the wave period which is seen to be fairly consistent at about 2.6 seconds, the visual measurement of wave period was found to be 2.67 seconds during the recording of this pressure record. Auto-correlation of wave pressure on the seawalls can therefore provide an indication of the average wave period, although the goodness of fit to the visual measurement of wave period in the case above is the exception rather than the rule, as can be seen from Table 3.12.

3.3.4 Cross-Correlation Analysis

The cross-correlation function is an extension of the auto-correlation procedure, whereby the relationship between two sets of data is established. An estimate of the cross-correlation function is made by sampling $x_1(t)$ at time t and $x_2(t)$ at time $t + \tau$ and averaging the product over the observation time T, in equation form written as ;

$$R_{x_1,x_2}(\tau) = \lim_{T \to \infty} \frac{1}{T}\int_0^T x_1(t) \cdot x_2(t+\tau)\, dt \quad \ldots (3.13)$$

If the cross-correlation function equals zero then no correlation exists between the samples $x_1(t)$ and $x_2(t)$, but if $R_{x_1,x_2}(\tau)$ is finite then there is some dependence of $x_1(t)$ on $x_2(t)$.

The cross-correlation function is used to establish the correlation between hydrostatic wave pressures on adjacent transducers, this supplies information on the time taken by a wave front traversing between transducers. Cross-correlation between transducers in a horizontal plane will allow the angle of incidence of the wave front to

be estimated by knowing the distance between transducers and the wave celerity. Cross-correlation between transducers in the vertical plane will allow the angle of the wave front (to the vertical) to be estimated, if both transducers in the vertical plane are below the trough of the wave then hydrostatic pressure will always occur simultaneously giving the impression of perfect correlation.

Cross-correlation could only be carried out on the data from Ilfracombe because this was the only site at which simultaneous horizontal and vertical pressures were measured.

Figure 3.14(a) shows a typical cross-correlogram for transducers 1 and 3 in the vertical plane, the largest peak occurs at zero time lag and seems to indicate that impacts occurred simultaneously at transducers 1 and 3. Peaks also occur at about 2.6 second intervals as in the auto-correlogram for the same data (Figure 3.13), although for large values of τ the peaks become irregular indicating a lower degree of correlation. To investigate whether impacts actually do occur simultaneously at transducers 1 and 3, the τ scale of Figure 3.14(a) was expanded to show the time lag from zero to 1 second in greater detail, (Figure 3.14(b)). With the better resolution it seems that some correlation exists at zero time lag, although the greatest correlation occurs at a time lag of approximately 0.08 seconds. An estimate of the average angle (to the vertical) of the wave front can now be made, providing the wave celerity and distance between transducers is known.

e.g. wave celerity = 4.71 ms^{-2}
distance between transducers 1 and 3 = 1.6m
τ = 0.08 seconds

therefore angle of wave front $\theta_v = \left(\frac{4.71 \cdot 0.08}{1.6} \right) \tan^{-1}$

$$\theta_v = 13.25^\circ$$

This assumes a completely plane wave front and vertical seawall, when in a real sea the wave front will be curved and irregular therefore this angle can only be very approximate, as shown in Figure 3.16.

Figure 3.15(a) shows the cross-correlogram between transducers 3 and 4 (in the horizontal plane), again a peak occurs near zero time lag. The degree of horizontal correlation between pressures is less than the vertical correlation because at Ilfracombe the rocky beach sets up reflected wave trains which run parallel to the seawall thereby reducing the degree of horizontal correlation in the long term. The τ scale of Figure 3.15(a) is shown expanded in Figure 3.15(b), where it is seen that maximum correlation occurs at a time lag of 0.15 seconds, this represents an angle of incidence of approximately 25°, (Figure 3.17). Both Figures 3.14(b) and 3.15(b) contain numerous small peaks superimposed upon the main peaks, these secondary peaks are due to the correlation of high frequency noise in the system.

3.4 Current Empirical Equations for Predicting Wave Impact Pressures

Before a seawall can be designed a maximum wave pressure and vertical pressure distribution must be obtained, these are usually found, for coastal structures, by calculating a maximum (design) wave for a given return period (Shore Protection Manual(74), Wiegel(83), Kinsman(90)). The total pressure for this design wave is then calculated from one of the many available empirical equations such as Minikin(72), (or any of

the equations given in Section 1.3.2). Most books on coastal engineering also give a method for estimating breaking wave pressures (Refs. 83 and 90 to 96).

Thus the engineer is faced with a multitude of equations for estimating breaking wave pressures, most of which have not been proved against reliable full scale data. These current empirical equations are based mainly on one of three assumptions, (i) breaking wave pressures are similar to those produced by a jet of water striking a flat plate, or (ii) breaking wave pressures are caused by the compression of an air cushion, or (iii) breaking wave pressures are proportional to the wave height.

3.4.1 Equating Breaking Wave Pressures to the Stagnation Pressure

This is probably the most frequently used approach to explain breaking wave pressures and assumes that a breaking wave is similar to a jet of water of uniform cross-section with velocity V striking a flat plate. The maximum resulting pressure will be the stagnation pressure given by;

$$P_s = \tfrac{1}{2}\rho V^2 \quad \dots\dots\dots\dots\dots\dots\dots\dots\dots\dots \quad (3.14)$$

Obviously a breaking wave does not have a uniform velocity gradient or act over a constant area, therefore a coefficient f is added to equation 3.14 to take account of this. Rearranging Eq. 3.14 into a velocity and pressure head gives;

$$\frac{P_m}{\rho g} = f\,\frac{V^2}{2g} \quad \dots\dots\dots\dots\dots\dots\dots\dots\dots\dots \quad (3.15)$$

P_m is the maximum impact pressure from the breaking wave, and velocity V is often taken as the wave celerity C. The coefficient f ranges from 1.6 (Millar et al$^{(11)}$), to 80 (Salih-Kirkgoz$^{(36)}$).

Hayashi and Hattori$^{(17)}$ demonstrated how thirteen independent formulae could be reduced to the form of equation 3.15. They also attempted to find a value for the coefficient f using model seawalls, they concluded that impact pressures did not even fit equation 3.15, but the hydrostatic pressure closely followed the f = 4 line.

All known full scale data, including data from this investigation, plus some model scale data is plotted in Figure 3.18 as pressure head versus velocity head. Where authors have measured more than one value of impact pressure for the same wave celerity, only the maximum value given is plotted. In Figure 3.18, wave celerity is the critical parameter because it is squared, therefore the value needs to be accurately measured. During this investigation celerity was measured visually and from beach transducers as described in Section 2.4, the visual measurements were used in producing Figure 3.18 and are presented in the form of histograms in Figure 3.19. The wave celerity tended to be fairly consistent over the relatively short measurement periods of two to three hours, with a mean value generally 15 to 20% less than estimated by first order theory, (see Section 2.5, Table 2.2). Wave celerity and impact pressure (if any) were not measured for each individual wave, so the average wave celerity during each period of measurement was plotted in Figure 3.18 against the maximum impact pressure for that session. Maximum impact pressure was used instead of the average because the other data in Figure 3.18 is also in terms of maximum impact pressure for a given velocity head.

Most of the early full scale data in Figure 3.18 tends to follow the f = 2 line whilst the recent full scale data is more scattered. This is probably because the early investigators used transducers incapable of measuring impact pressures, so their results represent hydrostatic pressures, whereas the more recent investigations (including this one) measured true impact pressures. The model scale data is extremely variable both between different investigations and within each investigation, the coefficient f ranges from 4 (Hayashi(17)) to 80 (Salih-Kirkgoz(36)). Thus it seems that equation 3.15 does not adequately fit either full scale or model scale wave impact pressure data.

3.4.2 Bagnold's Wave Impact Pressure Model

Bagnold assumed that wave impact pressures were generated by the compression of an air cushion trapped between the wave front and the seawall, (this assumption was later taken up and developed even further by Mitsuyasu(23)). Bagnolds original equation (see Section 1.3.2) is given below;

$$(P_{max} - P_o) = 2.7\frac{\rho V^2 L}{D}$$

D is the thickness of the enclosed air cushion and L is the length of the hypothetical piston. Bagnold found L was proportional to wave height (H), and assumed L = H/5, thus Bagnolds original equation can be written as;

$$P_i = A\rho C^2 \frac{H}{D} \qquad \ldots\ldots\ldots\ldots\ldots\ldots\ldots\ldots\ldots \quad (3.16)$$

where $P_i = (P_{max} - P_o)$ = impact pressure

C = wave celerity

A = unknown coefficient

The impact pressure (P_i) is seen to vary inversely with the thickness of the enclosed air cushion (D), which in turn is dependent upon the surface roughness of the seawall. Equation 3.16 suggests that if the air cushion were absent then infinite pressures would result. However, Bagnold found from his research that this was not the case, and infact negligible pressures were produced when the air cushion was absent. Therefore for each seawall there must be a minimum air cushion thickness for which a maximum impact pressure results. The air cushion thickness is governed by the physical properties of the seawall such as surface roughness, profile etc., and on the smoothness of the wave front. Thus for similar seawalls in similar environments the value of D_{min} (minimum air cushion thickness) will probably be of the same magnitude, therefore when considering the maximum wave impact pressure on real seawalls it should be possible to assume D_{min} is a constant.

therefore equation 3.16 will become;

$$P_{i_{max}} = B \rho C^2 H \quad \ldots\ldots\ldots\ldots\ldots\ldots\ldots\ldots \quad (3.17)$$

Where $B = \frac{A}{D_{min}}$

Equation 3.17 is displayed graphically in Figure 3.20, there is a fairly large degree of scatter in the data with no correlation between full scale and model-scale data. The early full scale data along with most of the data from this investigation displays a reasonable fit to the following quadratic curve;

$$P_{i_{max}} = -5.78 \times 10^{-3}(\rho C^2H)^2 + 5.95(\rho C^2H) + 0.4 \quad \ldots. (3.18)$$

although the data from Rouville$^{(7)}$ does not fit this curve, neither does the model scale data.

There is a definite separation between model and full scale data along the line $P_i = 6\rho C^2H$. The model scale data generally has a larger value of the coefficient B than does the full scale data, this is to be expected because B is proportional to $1/D_{min}$, and as D_{min} for models is obviously smaller than D_{min} for full scale structures then the value of B will be correspondingly higher for the model data. Figure 3.20 indicates that impact pressures might be related to ρC^2H but the relationship does not seem to apply to all data probably because the value of D_{min} is not the same for all data. It seems therefore that regarding D_{min} as a constant is unsatisfactory and would be difficult to evaluate for real structures.

The major disadvantage with Bagnold's equation is that it includes the parameter D (the thickness of the air cushion), to overcome this problem Minikin$^{(72)}$ modified Bagnolds equation in an unclear manner to produce the following equation, (equation 1.12 from Section 1.3.2),

$$P_i = \frac{101.1\ H\rho g}{L}\ d\left(1 + \frac{d}{D}\right)\ \ KN/m^2$$

But this equation is still not generally applicable to full scale data (as seen later in Section 3.6).

3.4.3 Impact Pressure as a Function of Wave Height

A linear relationship between impact pressure and wave height was first proposed by Hiroi(4) in 1920, his equation is shown below; (Eq. 1.5 from Section 1.3.2).

$$P_{i_{max}} = F \rho g H$$

where F is a constant = 1.5

An equation of this type was proposed as recently as 1966 by Muraki(10), as shown below; (Eq. 1.6 from Section 1.3.2)

$$P_i = F' H_o$$

where F' = an empirical coefficient ranging from 1 to 1.43
H_o = initial wave height

To test the validity of these equations a plot of impact pressure versus wave height was produced using all known full scale data (Figure 3.21). The early full scale data exhibits a linear relationship between impact pressure and wave height represented by the line F = 16. The model scale and later full scale data (considered more reliable than early full scale data) do not appear to fit these simple linear equations as proposed by Hiroi and Muraki.

After investigating the validity of the current empirical equations used at present to estimate wave impact pressures, it can be said that no equation applies to the general case of both model and full scale data, although some equations appear to fit particular cases of full scale data. Therefore a more fundamental approach is called for, as adopted in Section 3.5 .

3.5 The Impulse Momentum Equation

The equations so far considered result from the assumption that a wave can be approximated to a steady uniform jet of water, or can be related to the wave height, or that impact pressures are the direct result of rapid compression of a thin lens of air, (as suggested by Bagnold). It was found that these equations did not adequately fit the measured data, but as Bagnold's equation forms the basis for many of the equations currently used in seawall design (Refs. 72 and 74) it was decided to investigate his basic assumption. To do this the first type 2 pressure transducers were mounted flush in the seawalls whilst the second generation (type 2) transducers were mounted proud of the seawalls on 100 x 150 x 25mm thick stainless steel blocks (Plate 2.9(b)). If Bagnold's air cushion hypothesis applied to real sea waves then the block mounted transducers would measure only hydrostatic pressures, because any air cushion present would leak to the sides of the block under the action of the advancing wave front. For waves of similar characteristics both the flush mounted and block mounted transducers measured impact pressures of the same order. This was observed on three different seawalls so it seems likely that impact pressures in a real sea are not dependent upon compression of an air cushion, but are the direct result of the wave front impacting against the seawall, a view also held by Hayashi(18), Nagai(30) and Ross(35).

If this is the case then the gross kinematics of the wave impact problem can be defined by Newton's second law,

$$F = Ma = \frac{d(Mv)}{dt} \qquad \dots\dots\dots\dots\dots\dots\dots\dots \quad (3.19)$$

rewriting Eq. 3.19 as;

$$F\,dt = M\,dv \qquad \dots\dots\dots\dots\dots\dots\dots\dots \quad (3.20)$$

and integrating both sides,

$$\int_{t=0}^{t=t_i} F\,dt = \int_{v=v_b}^{v=0} M\,dv \qquad \dots\dots\dots\dots \quad (3.21)$$

This is the momentum impulse relationship, where M is the mass of fluid moving at velocity v resulting in a force F on the wall, the limit $0 \leqslant t \leqslant t_i$ is the time interval over which the fluid velocity is reduced from a value v_b before impact to zero, (see definition sketch below). Equation 3.21 assumes the total wave momentum is destroyed at impact with no losses due to turbulence etc.

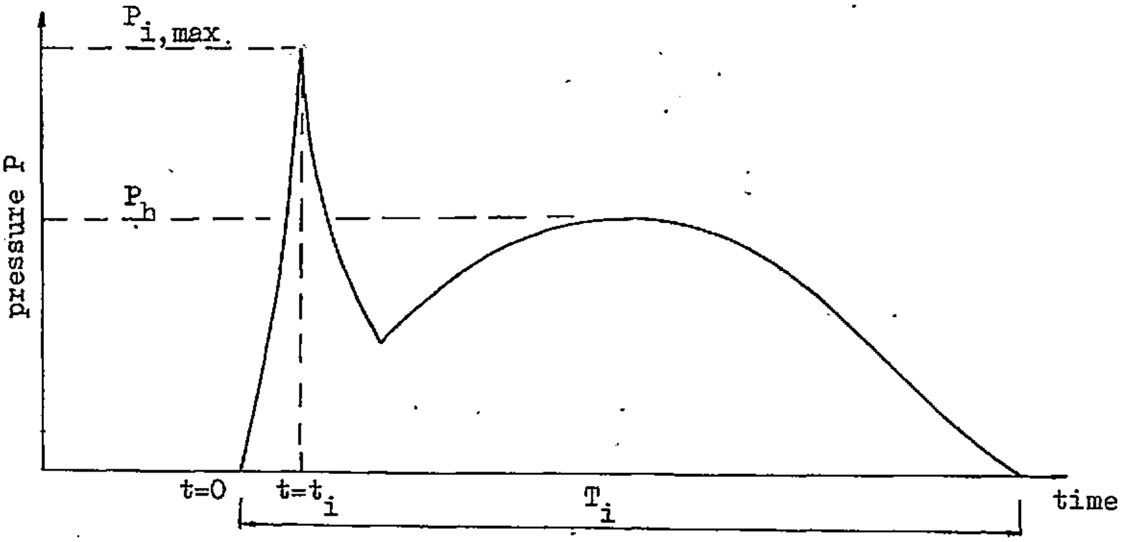

As an oscillatory wave travels through shoaling water it becomes steeper until at breaking each wave of the train can be assumed to be a mutually exclusive event and hence may be described, approximately, by solitary wave theory. This approach was used by Carr(37), Denny(13) and Ross(35), who approximated the R.H.S. of equation 3.21 to ;

$$\text{Impulse} = \rho\, Q\, C_b \quad \ldots\ldots\ldots\ldots\ldots\ldots\ldots\ldots \quad (3.22)$$

where Q = volume of solitary wave = $4d^2\left(\frac{H}{3d}\right)^{\frac{1}{2}}$

C_b = celerity of solitary wave = $\left(gd\left(1 + \frac{H}{d}\right)\right)^{\frac{1}{2}}$

H = wave height at breaking

d = water depth at wall

Using the limiting case when $H_b/d = 0.78$, which is the maximum ratio of wave height to water depth in shoaling water before breaking occurs(35), equation 3.22 reduces to;

$$\text{Impulse} = 55.5\, H_b^{5/2} \quad \ldots\ldots\ldots\ldots\ldots\ldots\ldots \quad (3.23)$$

Equation 3.23 is in imperial units (lb.sec/ft), in S.I. units equation 3.23 becomes;

$$\text{Impulse} = 15.8\, H_b^{5/2} \quad \ldots\ldots\ldots\ldots\ldots\ldots\ldots \quad (3.24)$$

When the data from this investigation is fitted to equation 3.24 (Figure 3.22), the scatter is considerable with no data near the line $I = 15.8\, H_b^{5/2}$. This suggests that impulse cannot be reduced solely to a function of wave height for the general case of random wave impact. The waves encountered during this investigation had troughs below S.W.L. and so were not truly solitary waves, so it is not surprising that they do not fit equation 3.24.

Therefore returning to equation 3.21 and rewriting the R.H.S. for the general case in terms of easily measurable parameters. Assuming the horizontal water particle velocity at impact can be replaced by the wave celerity at impact (C_b), and assuming the fluid is incompressible, (Salih-Kirkoz(36) found the effects of fluid compressibility were negligible during wave impact).

Integrating the R.H.S. of equation 3.21;

$$\text{gives} \quad -M\,C_b \qquad \ldots\ldots \qquad (3.25)$$

dropping the -ve sign because the pressure on the wall is of interest and assuming the mass M remains constant throughout the impact, then equation 3.25 can be written as;

$$\text{Vol}\,\rho\,C_b \qquad \ldots\ldots \qquad (3.26)$$

where ρ and Vol are density and volume respectively

Considering only unit width of wave crest, Vol can be replaced by the equivalent height and length of the water mass involved in the impact. The height of the impinging mass of water cannot be greater than H_b, but the length of the impinging water mass is not a measurable quantity hence it is often referred to as the virtual length(14), an idealistic representation of virtual length is shown below;

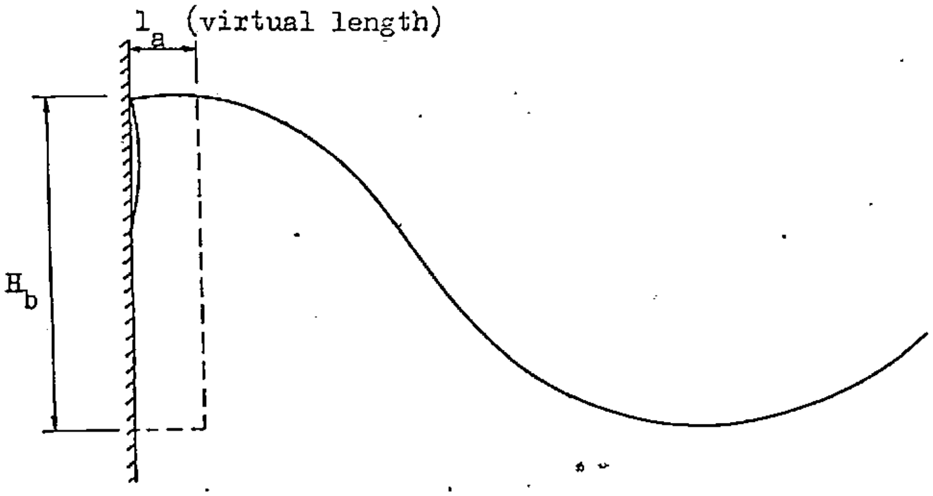

Salih-Kirkgoz(36) found the virtual length to be $0.2H_b$ at S.W.L. although different at other levels. If the virtual length is assumed to have an average length l_a over the height of the wave, then equation 3.26 becomes;

$$\rho H_b l_a C_b \qquad \ldots\ldots\ldots\ldots\ldots\ldots\ldots \quad (3.27)$$

The average virtual length is some fraction of the total wave length at breaking (L_b) dependent to a large extent on the local wave steepness H_b/L_b. Weggel et al(44) found l_a varied between $0.02H_b$ and $0.1H_b$ depending on the wave steepness at breaking.

Thus l_a may be replaced by $K' L_b$, where K' is a dimensionless coefficient dependent upon wave steepness, equation 3.27 now becomes;

$$K' \rho H_b L_b C_b \qquad \ldots\ldots\ldots\ldots\ldots\ldots\ldots \quad (3.28)$$

Wave period T is generally easier to measure than wave length, so rewriting equation 3.28 in terms of wave period gives;

$$K' \rho H_b \; T \; C_b^{\,2} \qquad \text{KN.s/m} \qquad \ldots\ldots\ldots\ldots\ldots\ldots\ldots \quad (3.29)$$

Equation 3.29 gives the momentum per unit width of wave crest at impact.

The L.H.S. of equation 3.21 is now considered,

$$\text{i.e.} \qquad \int_{t=0}^{t=t_i} F \; dt$$

This is the time integral of force on the wall, or impulse. From observation of numerous impact pressure histories on the Ilfracombe and Seaford seawalls, a linear (or very nearly linear) relationship has been found to exist between rise time and pressure over the time interval $0 \leqslant t \leqslant t_i$, during which time the pressure on the wall rises from zero to a maximum $(P_{i,max})$ as shown in the sketch on page 125.

Therefore the relationship between P and t can be written as;

$$\frac{P}{t} = \frac{P_{i,max}}{t_i} \qquad \ldots\ldots\ldots\ldots\ldots\ldots\ldots\ldots\ldots\ldots \quad (3.30a)$$

$$\text{or} \qquad P = \frac{P_{i,max}}{t_i} \cdot t \qquad \ldots\ldots\ldots\ldots\ldots\ldots\ldots\ldots \quad (3.30b)$$

If F (the force on the wall) is replaced by a pressure P acting over a constant area A, and equation 3.30b is combined with the L.H.S. of equation 3.21, the following equation term results;

$$\int_{t=0}^{t=t_i} \frac{P_{i,max}}{t_i} \cdot A \cdot t \; dt \qquad \ldots\ldots\ldots\ldots\ldots\ldots\ldots \quad (3.31)$$

Again only considering unit width of wave crest, the area A may be replaced by h_i, the height over which the impact occurs.

Equation 3.31 becomes;

$$\frac{P_{i,max}}{t_i} \; h_i \int_{t=0}^{t=t_i} t \, dt \qquad \ldots\ldots\ldots\ldots\ldots\ldots \; (3.32)$$

which when integrated becomes;

$$\frac{P_{i,max} \; t_i}{2} \; h_i \quad \text{KN.s/m} \qquad \ldots\ldots\ldots\ldots\ldots\ldots\ldots \; (3.33)$$

This is the impulse per metre width of wave crest at impact.

Equation 3.33 predicts a hyperbolic relationship between $P_{i,max}$ and t_i (as the impact pressure increases the rise time decreases), this is seen to be the case in Figure 3.23 where pressure versus rise time is plotted for the Ilfracombe data. This relationship seems intuitively correct because as previously shown, maximum impact pressure occurs for maximum wave steepness and as one would expect a steep wave will be brought to rest quicker than a less steep wave because the transfer of momentum occurs proportionately quicker.

If equations 3.33 and 3.29 are equated a revised form of the momentum impulse equation results;

$$\frac{P_{i,max} \; t_i}{2} \, . \, h_i = K' \rho \, H_b \, T \, C_b^{\,2} \qquad \ldots\ldots\ldots\ldots\ldots\ldots \; (3.34)$$

h_i (the height over which impact occurs) is the only parameter in equation 3.34 which can not be easily measured, so if h_i is assumed to equal the breaking wave height (H_b), the validity of this assumption is tested in the following pages, then equation 3.34 is in a usable form and becomes;

$$\tfrac{1}{2} P_{i,\max} t_i = K' \rho T C_b^2 \quad \ldots\ldots\ldots\ldots\ldots\ldots \quad (3.35)$$

The L.H.S. of equation 3.35 can be obtained directly from impact pressure histories on the seawalls, (Tables 3.3 to 3.11). A value for the coefficient K' can be obtained by plotting values of $P_{i,\max}\ t_i/2$ against values of $\rho T C_b^2$, as in Figure 3.24.

It has not been possible to measure wave parameters for each individual wave impact, therefore average values of T and C_b are plotted in Figure 3.24, the figures in parenthesis indicate the number of individual wave impacts averaged to produce each point. Figure 3.24 also contains additional data from Ross$^{(35)}$ and Rouville$^{(7)}$, these were the only papers to give values of the impulse on the wall, the values from Rouville were scaled from impact pressure histories given in his paper.

It has been assumed that the coefficient K' is a function of wave steepness (H_b/L_b), so to test this assumption values of K' calculated from equation 3.29 were plotted against corresponding values of H_b/L_b, (Figure 3.25). There is some scatter in Figure 3.25 but a definite relationship between wave steepness and K' is apparent, the best fit being the line $K' = 0.31\ H_b/L_b$. Therefore this value of K' has been used to calculate the lines of varying wave steepness shown on Figure 3.24 .

In equation 3.29 it was assumed that $h_i = H_b$, thus equation 3.29 can be written as;

$$\tfrac{1}{2} P_{i,max}\, t_i = K'' \rho H_b\, T\, C_b^{\,2} \qquad \ldots\ldots\ldots\ldots (3.36)$$

$$\text{where} \quad K'' = \frac{K'}{h_i} \qquad \ldots\ldots\ldots\ldots\ldots\ldots\ldots\ldots (3.37)$$

As K' is a function of wave steepness, and h_i is proportional to H_b, then K" is simply a function of $1/L_b$, where L_b is the wave length at breaking. When values of K" (calculated from equation 3.36) are plotted against corresponding values of $1/L_b$ (Figure 3.26), the full scale data displays a good fit to the line $K'' = 0.3/L_b$; scatter in Figure 3.26 is mainly confined to the model data of Ross. So the assumption that K" is a function of $1/L_b$ seems to be satisfactory.

If the expressions for K' and K" are substituted back into equation 3.37, the result is;

$$\frac{0.3}{L_b} = \frac{0.31\, H_b}{L_b\, h_i} \qquad \ldots\ldots\ldots\ldots\ldots\ldots (3.38)$$

$$\text{or} \quad H_b = 0.97\, h_i$$

this indicates that the impact pressure occurs over approximately the entire wave height, (as is also found from the measured data in Section 3.9).

Equation 3.36 is presented graphically in Figure 3.27, where it can be seen that as the wave length increases, the resulting value of the impulse decreases.

Figures 3.27 and 3.24 are both rather short of data to be conclusive but one encouraging point is that both model and full scale data appear to fit these equations quite closely. Equation 3.35 (Figure 3.24) can be further substantiated by adding the K' values obtained by Carr (0.11), Denny (0.07) and Bagnold (0.018) from their model studies. In these cases K' was taken to be a constant calculated from solitary wave theory (Eq. 3.26) which equalled the percentage of wave momentum translated into impulse energy. Carr and Denny found that K' approached a definite maximum value from their model studies and so assumed this maximum value to be a constant which could be applied to any size wave. From Figure 3.25 it is apparent that K' is not a constant but dependent upon the local wave steepness H_b/L_b. The maximum value of K' from Figure 3.24 is 0.043, which corresponds to the limiting value of wave steepness of 1/7 H_b/L_b. Carr and Denny obtained maximum values slightly greater than this (0.07 and 0.11 respectively) but the solitary wave theory used by these authors would tend to over estimate the value of K'. This is because they took the wave height to be the depth limited value (H = 0.78d), which when substituted into the equation for the volume of a solitary wave;

$$Q = 4d^2 \sqrt{H/3d}$$

gives;

$$Q = 4(1.28H)^2 \sqrt{H/3(1.28H)}$$

or $$Q = 3.34\ H^2$$

so when waves smaller than this limiting value occur (for the same depth of water), then H/d will be reduced to a lower value. Therefore taking H to be say 0.6d

then;

$$Q = 4(1.67H)^2 \sqrt{H/3(1.67H)}$$

or $$Q = 4.98\ H^2$$

Thus as H/d reduces, the volume of the solitary wave (Q) decreases with the effect that waves of less than the limiting depth (H/d = 0.78) will have smaller values of K'.

Bagnold gave an average value of K' as 0.018, which corresponds quite closely to the full scale data measured during this investigation.

3.6 Proposed Equations for Estimating Wave Impact Pressure

A method of relating impact pressure to easily measurable wave parameters is now required, in Figure 3.18 it was seen that when the stagnation pressure of a jet impinging on a flat plate ($P = \frac{1}{2}\rho V^2$) was taken to represent the wave impact pressure then considerable scatter occurred. This made it very difficult to select a suitable value of the coefficient f, and indicated that some other parameter might be influencing the wave impact pressure generation.

Returning to Figure 3.24, there is good correlation between impulse ($P_i t_i/2$) and momentum ($\rho C_b^2\ T$), yet the only additional parameters between Figures 3.18 and 3.24 are wave period (T) and rise time (t). Wave period does not change sufficiently between model and full scale waves to cause the degree of scatter in Figure 3.18, but rise time does (as shown in Figure 3.28). Thus rise time seems to be the important parameter missing from current equations for estimating the wave impact pressure.

Therefore although wave impulse can be estimated with a reasonable degree of accuracy (from equation 3.35), wave impact pressure cannot because for a given impulse the pressure can vary enormously depending upon the rise time. The rise time is the time taken for the transformation of wave momentum into impulse energy, which in turn is dependent on the percentage of air entrained in the wave. Figure 3.29, after Lundgren(21), shows how, for just 1% air entrainment, V_s falls from 1450 m/s to 100 m/s.

In Figure 3.24, model scale wave impulse is about an order of magnitude less than wave impulse from this investigation, yet model rise times are approximately two orders of magnitude less than rise times measured during this investigation, (Figure 3.28). These proportionately quicker model rise times indicate a faster transformation of momentum. This occurs because model waves are generally smooth, regular and unidirectional, whilst real sea waves are often random and influenced by numerous factors which contribute to cause 'white water' and so increase air entrainment. This demonstrates a major inconsistency between model and full scale wave impacts, and indicates that linear scaling of impact pressures between model and full scale studies, as suggested by Bagnold(14), Denny(13), Ross(35) and others, is invalid and could lead to gross over estimations of the impact pressure. Although it appears that linear scaling of the wave impulse is possible.

So returning to equation 3.35;

$$P_{i,max}\, t_i/2 \;=\; K'\rho C_b^{\,2}\, T$$

This relationship between impulse and momentum was shown in Figure 3.24 to be satisfied by both model and full scale data, being dependent only on the dimensionless parameter of local wave steepness. Hence to examine the effect of rise time, P_i was plotted against $\rho C_b^{\,2}T$, these two quantities are related by a coefficient (λ) with units of sec^{-1} which depends upon rise time and wave steepness, e.g.

$$P_i = \lambda\rho C_b^{\,2}\, T \qquad \ldots\ldots\ldots\ldots\ldots\ldots\ldots\ldots\ldots\ldots \; (3.39)$$

Equation 3.39 is shown graphically in Figure 3.30, as expected there is a definite separation between model and full scale data, although some full scale data from Rouville has a λ value similar to model data. Other full scale data from Gaillard(3), Cot(8), Kuribayashi et al(9) and Molitor(5), and model scale data from Hayashi et al(17) and Mitsuyaso(74) are also included in Figure 3.30.

Most full scale data in Figure 3.30 is enveloped between the $\lambda = 0.1$ and 0.5 lines, whilst the model scale data generally lies between the $\lambda = 1$ and 10 lines. As already mentioned, rise time is proportional to the volume of air entrained in the breaking wave, which in turn is related to the beach slope, type of seabed, degree of wave reflection and other factors which cause white water and so increase air entrainment. The degree of air entrainment in a real sea is due to the culmination of the above factors and can not be measured, but would seem to be indicated

by the smoothness of the wave front. The smoother the wave front then generally the less entrained air, thus λ can be regarded as a wave front 'smoothness coefficient'. Model waves generally have a smooth front face resulting in λ values between 1 and 10 (Figure 3.30) whilst the irregular and partially broken waves at Ilfracombe have λ values between 0.1 and 0.2. The Teignmouth and Seaford data generally had λ values greater than those at Ilfracombe (0.2 to 0.5), this was as expected because at these two sites the sand and shingle beaches caused less wave disturbance (and hence air entrainment) than the rocky Ilfracombe beach. Rouvilles data has λ values between 0.7 and 2.5, the reason for these relatively high full scale values is probably because this investigation was carried out on a harbour wall in relatively deep water so the incident waves would tend to be more stable than those in shoaling water, consequently there would be less cause of air entrainment.

Thus values of λ can be tentatively assigned to seawalls depending on the smoothness of the prevailing incident waves as follows; for seawalls in shoaling water with unobstructed sandy foreshores a λ value of 0.5 might be adequate, whilst for walls with very rocky beaches or subjected to broken waves $\lambda = 0.1$ might be suitable, and for walls in deep water $\lambda = 1.0$ is suggested.

It should be possible to use equation 3.39 for both breaking and broken waves by the judicious selection of the coefficient λ. The pressures estimated by equation 3.39 are compared with the widely used equations given in the Shore Protection Manual$^{(74)}$

e.g. The Shore Protection Manual equation for breaking waves is;

$$P_i = 101\,\rho g \frac{H_b}{L} \frac{d_s}{D}(D + d_s) \quad \mathrm{KN/m^2}$$

and the Shore Protection Manual equation for broken waves is;

$$P_i = \tfrac{1}{2}\rho C_b^2$$

(see Section 1.3.2 for explanation of terms in the above equations)

Three hypothetical waves with the following parameters were chosen for comparison (waves encountered during this investigation generally lie between waves number 1 and 2).

	C_b	T	L_b	d_s	D	H
Wave No. 1	3 m/s	4 sec	12 m	1 m	1.6 m	0.78 m
Wave No. 2	5 m/s	6 sec	30 m	2.6 m	4.1 m	2.03 m
Wave No. 3	7 m/s	8 sec	54 m	5 m	7.7 m	3.9 m

the bed slope is taken to be 1 : 20

The results are as follows;

	Figure 3.30 ($\lambda = 0.5$)	S.P.M. (breaking waves)	Figure 3.30 ($\lambda = 0.1$)	S.P.M. (broken waves)
Wave No. 1	18 KN/m^2	104 KN/m^2	3.6 KN/m^2	4.5 KN/m^2
Wave No. 2	75 KN/m^2	285 KN/m^2	15 KN/m^2	12.5 KN/m^2
Wave No. 3	196 KN/m^2	590 KN/m^2	39 KN/m^2	24.5 KN/m^2

The Shore Protection Manual equation for breaking waves (based on

Minikin's equation(72)) over estimates the wave impact throughout the range of waves considered, by over five times for wave No. 1, decreasing to three times for wave No. 3. Minikins equation is based on Bagnold's air cushion hypothesis, which has been shown in earlier sections to be unsatisfactory, therefore this large difference in impact pressures is understandable.

The Shore Protection Manual equation for broken wave pressures (i.e. the stagnation pressure) is in fair agreement with the pressures estimated from equation 3.39 (with $\lambda = 0.1$), so it seems likely that equation 3.39 can be used to estimate breaking or broken wave pressures depending on the selection of λ.

3.7 The Limiting Case of Impact Pressure

The limiting value of wave impact pressure was suggested by Von Karman(52) to be the water hammer pressure given by;

$$P_{lim} = \rho_m V_s U_i \qquad \ldots\ldots\ldots\ldots\ldots\ldots\ldots\ldots\ldots\ldots (3.40)$$

where V_s is the velocity of sound through the wave
ρ_m is the density of the air/water mixture
U_i is the water particle velocity at impact

There has been considerable disagreement as to whether the water hammer pressure can occur during wave breaking, Bagnold(14) and Nagai(30) both concluded it was unlikely that water hammer pressures would occur, whilst Mitsuyaso(23) and Ross(35) thought that under certain circumstances the water hammer pressure might be developed. These conclusions were all based on the results of model studies.

In equation 3.40, V_s is the critical parameter, as already seen from Figure 3.29, where 1% of entrained air will reduce V_s from 1450 ms^{-1} to 100 ms^{-1}. In Figure 3.29, V_s falls to a minimum value at about 50% air entrainment ($V_s \simeq 20$ ms^{-1}) then rises again as the percentage of entrained air increases. Hence from equation 3.40, the minimum water hammer pressure will occur for 50% air entrainment and can be found as follows, assuming the water particle velocity can be replaced by wave celerity.

e.g. taking $V_s = 20$ ms^{-1}, $C_b = 4$ ms^{-1} and $\rho_m = 1025/2$ kgm^{-3}

$$\text{then } P_{lim,\ min} = \frac{1025}{2} \cdot 20 \cdot 4$$

$$P_{lim,min} = 41 \text{ KNm}^{-2}$$

the maximum water hammer pressure occurs at zero air entrainment, therefore taking $V_s = 1450$ ms^{-1}, $C_b = 4$ ms^{-1} and $\rho_m = 1025$ kgm^{-3}

$$\text{then } P_{lim,max} = 1025 \cdot 1450 \cdot 4$$

$$P_{lim,max} = 5945 \text{ KNm}^{-2}$$

Thus if the water hammer pressure is developed during wave breaking, then the impact pressure data from this investigation would be expected to fall between the limits above. But on only one occasion in over 150 impacts did the pressure even reach the lower limit, (Tables 3.3 to 3.11) and in the majority of cases the pressure was of the order of 10 to 15 KNm^{-2}.

It is physically impossible for pressures as low as this to exist from equation 3.40 given the wave celerity measured during this investigation. Therefore it seems unlikely that water hammer pressures are developed during wave breaking in a real sea.

3.8 Level of Confidence in Wave Parameter Measurement

The wave impact pressures were measured for each individual impact to an accuracy of 0.1 KNm^{-2}, the instrumentation was calibrated and checked before and after each recording session, thus a high degree of confidence may be attributed to the wave impact pressure measurements.

The other wave parameters of celerity, height and period were all measured by at least two independent methods. The degree of correlation between these various methods was generally poor with as much as 25% difference in the values obtained, (see Chapter Two for full details). Thus more confidence may be placed on the accuracy of the wave pressure measurements than on the measurement of the other wave parameters.

Values of wave celerity, height and period were not obtained for each individual wave, therefore it was not possible to correlate impact pressure to the exact parameters of the wave producing that impact. Instead, some statistical measure of celerity, height and period had to be used. Wave height was presented in terms of significant height (H_s) and celerity and period were expressed in terms of their arithmetic means ($\overline{C}_b$ and $\overline{T}$ respectively). This was not a very satisfactory way of presenting this data because it was found that on average only one wave in every 2000 produced an impact pressure, therefore the parameters H_s, $\overline{C}_b$ and $\overline{T}$ were obtained mainly from waves which did not produce impact pressures yet these parameters were used as estimates of waves which did generate impact pressures.

Thus when the average impact pressure ($\overline{P_i}$) is plotted, as in say Figure 3.30, the upper and lower limits are known exactly because P_i is a deterministic quantity actually measured for every wave impact. Whereas when terms containing H_s, $\overline{C_b}$ or $\overline{T}$ are plotted, again as in say Figure 3.30, the upper and lower limits are not known exactly, and even if these limits are estimated the values obtained are likely to be misleading because so few waves in the sample actually produced an impact pressure that it is highly improbable that these few waves would lie at the upper and lower extremes of the sample.

3.9 Spatial and Temporal Distribution of Impact Pressures on the Seawalls

A seawall will generally be subjected to both breaking and reflected (standing) waves during its lifetime. The vertical pressure distribution for a standing wave is easily calculated from the theory of Sainflou(71), but the vertical pressure distribution for a breaking wave is less well documented although potentially more important to the designer due to the larger pressures exerted.

The pressure/time history of a standing or non-breaking wave can be identified by its slow rise time and relatively low intensity, (Figure 3.31), its vertical pressure distribution will be largely hydrostatic having its greatest pressure intensity at the seabed. The pressure/time history of a breaking wave is characterised by a fast rise time and often a high intensity transient pressure followed by a longer duration pressure of the order of the standing wave pressure (Figure 3.32). There has been much speculation as to the vertical pressure distribution of a breaking wave, the Shore Protection Manual recommends that the maximum pressure be taken at S.W.L., decreasing parabolically above and below this level (Figure 1.8). Millar et al(11) suggest the location of the maximum pressure is dependent on the type of breaking wave, with a plunging breaker exerting its maximum pressure above S.W.L. and a bore exerting its maximum pressure below S.W.L.

Impact pressures can only occur over the height of the breaking wave so as the S.W.L. rises and falls, so too will the location of the impact pressure on the seawall. Therefore impact pressures can only be measured when the pressure transducers are within the region of the breaking wave. At Ilfracombe M.H.W.S. is 4.4m A.O.D. and beach level at the toe of the wall is about 1m A.O.D., therefore the largest potential wave (depth limited) which can reach the wall without breaking is about 3m. With this in mind the pressure transducers were concentrated about M.H.W.S. at levels 3.2m, 4.2m, 5.2m and 6.3m with one transducer near the base of the wall at level 1.6m. But due to a mild winter the average wave height at Ilfracombe was only of the order of 1m and no-where near limiting steepness, therefore impacts occurred mainly at the lower transducer when the water depth at the wall approximately equalled the wave height, (depth limited breaking). So simultaneous impacts occurring at two or more transducers in a vertical plane were only measured on 17 occasions, (13 times on 3.2.81 - Table 3.5 and 4 times on 22.1.81 - Table 3.7), 90% of impacts occurred on the flood tide and 10% on the ebb. This lack of simultaneous vertical impacts at Ilfracombe is due, in part, to the large spacing between the two lower transducers (1.6m), and the lower than average wave height. No simultaneous impacts in a vertical plane were measured at Seaford.

At Ilfracombe the horizontal transducer array was located at level 3.2m, so again very few simultaneous impacts occurred (a total of 19) because the waves generally broke at a lower elevation on the wall. At Seaford simultaneous impacts occurred at two transducers in the horizontal plane on only 4 occasions, so no representative pressure distributions can be inferred from this limited data.

3.9.1 Spatial Distribution of Impact Pressures on the Ilfracombe Seawall

Various authors (Hayashi et al(17) and Carr(39)) have found impact pressures to be very localised in extent and hence have allowed these pressures no structural significance. During this investigation impact pressures have been measured simultaneously on four pressure transducers covering an area of 1.6m x 1.5m, as shown below;

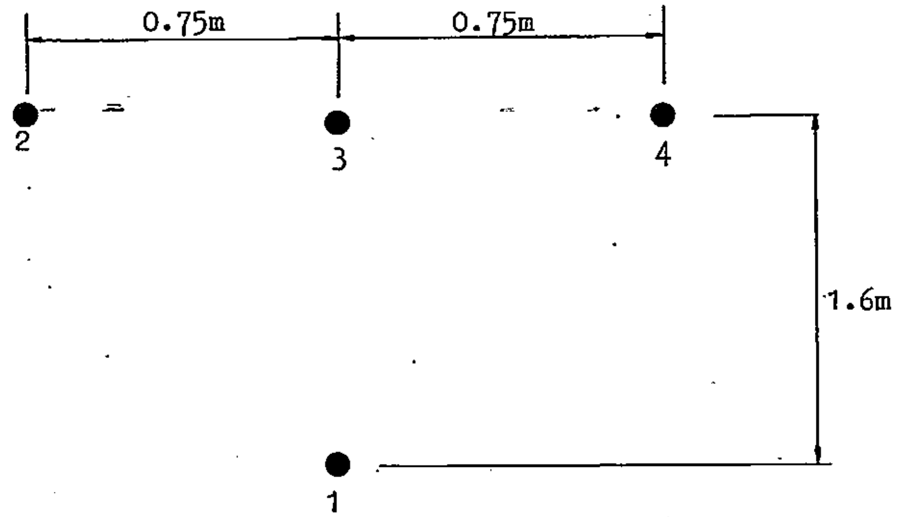

This data indicates that impact pressures are not as localised as previously thought, and can occasionally occur over large areas of the breaking wave front. The implications are that impact pressures occur over a large enough area to be credited with some structural significance in the design of seawalls, (this is investigated further in Chapter Seven).

The vertical pressure distribution measured on the Ilfracombe seawall is only defined by two points (transducers 1 and 3) which are 1.6m apart, as the largest significant wave height measured at Ilfracombe was only 1.3m then it is likely that these two transducers measured pressures near the top and bottom extremes of the breaking waves. These two points alone are not sufficient for any conclusive predictions about the vertical pressure distribution, ideally at least another three points would be required for a better description of the distribution.

If the simultaneous impact pressures at transducers No. 1 and 3 are examined (given in tables 3.5, 3.7 and 3.8), they are found to have similar magnitudes at each transducer for each impact. Out of the 17 simultaneous impacts measured, the maximum occurred at transducer No. 1 on 9 occasions, (i.e. approximately 50% of the time). All 17 simultaneous impacts at transducers 1 and 3 are shown in Figure 3.33, the average pressures at these two transducers are 12.38 KN/m^2 and 12.92 KN/m^2 at No. 1 and 3 respectively, which suggests an almost vertical pressure distribution over the height of the breaking wave. The impact pressures at transducers 1 and 3 are not identical for every wave because impact pressure depends on the percentage of air entrained in the wave and it is unlikely that the entrained air will be evenly distributed throughout the height of the wave.

On the basis of the very limited data available, the best vertical impact pressure distribution would seem to be a uniform distribution

over the height of the breaking wave with the magnitude calculated from equation 3.39. This pressure must now be located with respect to S.W.L., this will vary for different types of incident waves. For oscillatory waves S.W.L. occurs at a distance H/2 down from the wave crest, and for solitary waves S.W.L. occurs at a distance H down from the wave crest, for real seawaves S.W.L. will lie between these two extremes. The worst case from the point of view of over turning is the solitary wave, but for the general case it is proposed that S.W.L. be taken at mid wave height untill further data becomes available. This proposed impact pressure distribution is shown in Figure 3.34 combined with the hydrostatic pressure distribution.

The average horizontal impact pressure distribution was expected to be uniform across transducers 2, 3 and 4 at level 3.2m, but from Figure 3.35 it is seen that this is not the case, transducer No. 2 consistently measures lower pressures than Nos. 3 or 4. This could be due to some feature in the rocky beach which sets up some consistent irregularity in the incident wave; or more likely by a faulty transducer, although checks show the transducer to be functioning correctly. Ignoring transducer No. 2, the average pressure measured at transducers 1, 3 and 4 are 12.38 KN/m^2, 12.92 KN/m^2 and 12.72 KN/m^2 respectively, this suggests a uniform impact pressure distribution over the height and breadth of the wave front.

3.9.2 Temporal Distribution of Wave Impact Pressures on the Ilfracombe Seawall

The time lag (τ) between pressures arriving at adjacent transducers is dependent on the wave front steepness (to the vertical) and on the angle of incidence of the wave crest in the horizontal plane

Therefore a normal incident wave with a vertical face should result in a simultaneous impact at all points on the wall.

The 17 simultaneous impacts were replayed on a six channel Watanabe Multicorder (Model No. MC 6721) with compensator to allow synchronization of all six channels, although only four channels were required. Two samples of simultaneous impacts are shown in Figure 3.36, sample (a) was recorded on 3.2.81 and shows the largest measured impact at Ilfracombe (26.7 KN/m^2 on transducer No. 4), sample (b) was recorded on 22.1.81 and shows almost identical impact pressures at transducers 2, 3 and 4. In both samples the hydrostatic pressure (second peak) is very much larger at transducer No. 1 because this transducer is 1.6m below the level of transducers 2, 3 and 4. The time lag between the occurrence of the maximum pressures at transducers 2, 3 and 4 appeared to be zero ± 0.005 seconds, this was the greatest accuracy that could be achieved with the multicorder. In order to obtain a more accurate estimate of the time lag the signal would need to be digitised at a high sampling rate (say 1000 samples per second).

The time lag between the occurrence of maximum pressures at transducers 1 and 3 (in the vertical plane) varied according to the magnitude of the pressure measured at the upper transducer (No. 3). When the pressure at the upper transducer was of the same order, or greater than the pressure at the lower transducer (sample (a) in Figure 3.36) then the time lag was found to be zero ± 0.005 seconds, but when the pressure on the upper transducer was lower than that on the lower transducer (sample (b) in Figure 3.36) then a finite value of τ was observed. This value of τ was in all cases found to be less than the rise time, and usually of the order of 0.05 seconds, the impact pressure always occurred at the bottom transducer first.

These temporal impact pressure distributions demonstrate that a near vertical wave front imparts a greater force on a seawall than a non-vertical wave front, for a wave of similar characteristics.

3.10 Extreme Wave Statistics

A knowledge of the long term statistics of wave impact pressures on coastal structures, particularly the distribution of peak pressures, would be of immense use to designers as it would allow the direct selection of a design pressure without first selecting a design wave. This type of information can only be reliably predicted from wave pressure records spanning several years. The impact data collected to date is only considered reliable from the end of 1980 (due to problems with the instrumentation already discussed in Chapter Two), therefore only one winters data is available on which to base any predictions. Furthermore, as the winter 1980/81 was particularly mild it cannot be assumed typical of an average winter, so ideally this data should be adjusted to the data from a typical winter before it is used.

Success or failure of a seawall rests solely on its ability to withstand the maximum wave loading to which it is subjected, which might only occur once in say 50 or 100 years. Therefore extreme values of wave loading are clearly important and must necessarily be estimated by statistical methods, (Refs 97 to 100).

Since hydrostatic and impact pressures are generated by different, largely uncorrelated mechanisms, then each data set must be treated separately.

3.10.1 Distribution of Extreme Hydrostatic Wave Pressures

Many authors have carried out statistical analyses of wave records (Refs 101 to 104) and have found that the probability density function (p.d.f.) of wave heights is gaussian, and that the distribution of the largest wave heights from any wave record can be approximated to the Rayleigh distribution as follows;

$$P(a) = \frac{a}{\sigma_x^2} \cdot e^{-\frac{a^2}{2\sigma_x^2}} \qquad \text{.............(3.41)}$$

for the peak values of the wave height distribution at level 'a'

Simplified relationships were developed by Putz (101) based on the Rayleigh distribution, as follows;

$$H_m = 0.625\ H_s \qquad \text{..............................(3.42)}$$

$$H_{max} = 1.770\ H_s \qquad \text{..............................(3.43)}$$

$$H_{max} = 2.832\ H_m \qquad \text{..............................(3.44)}$$

From Section 3.3.1 it was found that the distribution of hydrostatic wave pressures was approximately gaussian, therefore it follows that if extreme wave heights are Rayleigh distributed then extreme hydrostatic wave pressures should also be Rayleigh distributed (being dependent solely upon wave height). In which case equations 3.42, 3.43, and 3.44 should also relate to hydrostatic wave pressures by substituting the hydrostatic wave pressure P_h for wave height H . A relationship of this type was also found by Tickell et al (105) who found that long term peak forces on offshore structures had a Rayleigh distribution if non-linear effects such as drag were not included.

Thus it seems that extreme hydrostatic wave pressures might be Rayleigh distributed, but as hydrostatic wave pressure is so easily calculated for a given wave height (by the method of Sainflou) then it is better to estimate extreme hydrostatic wave pressure from the design wave height, because there is usually a large data base of wave height data available from which to make these predictions whereas there is only one winters hydrostatic wave pressure data available.

3.10.2 Distribution of Wave Impact Pressures

There is relatively little impact pressure data available from which to make assumptions as to the parent distribution, and as this data spans only seven months, from October to early May, there will be seasonal variations introduced which will bias the distribution towards the larger values of pressure measured during the winter months. Additionally, the parent distribution must be constant, which is probably a satisfactory assumption for each individual site but does not apply to the combined data from all sites because Teignmouth and Seaford data have disproportionately larger pressure maxima than the Ilfracombe data due to the smaller percentages of entrained air. Thus the data from each site must be treated separately, but as there is a scarcity of data from Seaford and Teignmouth the analysis is concentrated on the Ilfracombe data.

The observed cumulative distribution function (c.d.f.) of the Ilfracombe data is calculated from the following;

$$F_s(x) = \frac{\text{number of observations which exceed } x}{n} \quad \ldots.(3.45)$$

where n is the total number of samples.

and is shown in Figure 3.37(a), the distribution is unimodal and skewed and shows a best fit to the Weibull distribution(99) although the Rayleigh and log-normal distributions(98) provide an almost equally good fit.

Kuznetsov et al (106) also found that the impact pressure data from their model studies had a Weibull distribution.

The effects of combining all impact pressure data can clearly be seen in Figure 3.37(b) where the main body of the distribution is very similar to Figure 3.37(a) (their modes equal 13.68 and 12.39 respectively) but there is a prounced bias towards the larger pressure in Figure 3.37(b) which demonstrates that the combined impact data distribution would cause gross over estimations of the extreme pressures if used for the Ilfracombe site.

The c.d.f. F(x) of a continuous random variable having a Weibull distribution is given by the following expression, (Ref 99);

$$F(\bar{x}) = \begin{cases} 0, & \text{if } x < v \\ 1 - \exp - \frac{(x-v)^\beta}{\alpha}, & \text{if } x \geqslant v \end{cases} \quad \ldots\ldots(3.46)$$

where v is the lowest limiting value of x, α is a scale parameter and β is a shape parameter (see Appendix A)

Equation 3.46 gives the probability that a value of X is not exceeded, the probability of the exceedence of X is of more interest, therefore equation 3.46 is written as;

$$1 - F(x) = \begin{cases} 1, & \text{if } x < v \\ \exp - \left(\frac{x-v}{\alpha}\right)^\beta, & \text{if } x \geqslant v \end{cases} \quad \ldots\ldots(3.47)$$

The exact form of the parent distribution between the log - normal, Rayleigh and Weibull is not critical because as shown below all three distributions have the same extreme value distribution.

3.10.3 Extreme Value Distribution of Wave Impact Pressure

The basis for extreme value analysis is based on work by Fisher and Tippett (100) and later expanded by Gumbel (97) originally for the estimation of extreme flood levels but now used extensively in the field of extreme wind prediction (Ref 107). The method is based on random sampling of the parent distribution (each sample to be of the same size) and selecting the maximum value from each sample. These maxima are then regarded as variates in their own right with their own distribution, Fisher and Tippett found that only three extreme value distributions were possible and hence called them Type I, Type II and Type III.

If the parent distribution is of the Weibull form (or the log-normal or Rayleigh) then the extreme value distribution will be Fisher - Tippett Type I(100) (also called Gumbel distribution). The c.d.f. of a Type I distribution is given by

$$F(x) = \exp\left[- \exp - \alpha (x - u) \right] \qquad \text{.............(3.48)}$$

where u is the mode of the distribution $= \mu_x - 0.577/\alpha$

α is the dispersion $= 1.282 / \sigma_x$

The standard method of estimating these parameters is due to Gumbel (97) and consists of ranking the maxima by magnitude and plotting these values as ordinate against a reduced variate y as abscissa, (see Table 3.13) this transforms the c.d.f. to a straight line, where y is given by

$$y = -\ln\left(-\ln \frac{m}{n+1} \right) \qquad \text{.............(3.49)}$$

where m is the rank of the ordinate

n is the number of extreme values

Gumbel suggests fitting the best straight line 'by eye' or by least squares, but both of these methods lead to biased estimates of u and α because each point is given equal weighting whereas less confidence will be attached to those points at either end of the line and clearly the largest point will have the least confidence because it is not exceeded, so no information is available on its probability of exceedence. A method has been proposed by Lieblein(108) using what he calls BLUE (best linear unbiased estimators) which gives each point the correct weighting which leads to unbiased estimates of u and α (see Appendix A).

The impact pressure data from Ilfracombe was sampled chronologically using a sample size of eight which gave fourteen extreme values, these extreme values are plotted in Figure 3.38, where they show a fairly good fit to a straight line and so suggest that extreme impact pressure has a Type I distribution as assumed from the parent distribution. The mode and dispersion were calculated after weighting the data using Liebleins BLUE, this then allows calculation of the return period (see Appendix A) which is also shown on Figure 3.38.

Projections to 50 year return periods from only seven months data are clearly not sensible as can be seen from Figure 3.38, where the largest measured extreme equals the ~~5~~20 year return value. A minimum of about three full years data would be required for predictions of return period, this would give more confidence in the values of the mode and dispersion and so allow better estimates of the 10, 20, or 50 year return impact pressures, although for reliable estimates 10 or more years data would be necessary. Thus Figure 3.38 serves only to demonstrate the method and to establish that the extreme value distribution fits the assumed Fisher - Tippett Type I distribution.

3.11 The Effects of Seawall Shape on Wave Pressures

It is difficult to determine the effects of seawall shape on the resultant wave impact pressures especially from this investigation because the seawalls at Seaford and Ilfracombe (stepped and curved walls respectively) are subjected to such different incident waves that no direct comparisons can be made. The wave impact pressures at Seaford were generally higher than those at Ilfracombe for the same size waves, but then the incident waves at Seaford were much smoother and more regular than those at Ilfracombe. So unless different shaped seawalls are constructed at the same site (so that they are subjected to identical incident waves), then it will be extremely difficult to determine the effects (if any) of seawall shape on real wave impact pressures.

During this investigation seawall shape was found to have a significant effect on the magnitude of the hydrostatic pressures which occurred immediately after a wave impact. A typical pressure history of a wave impact at Ilfracombe is shown in Figure 3.39, this figure has the familiar twin peaked trace observed by other investigators(7),(17), but a typical pressure history of a wave impact at Seaford (Figure 3.40) has only the first peak which decays in an exponential manner, the second peak is absent. The reason no well defined hydrostatic pressure peak occurs at Seaford becomes apparent when one considers the process of a wave striking a stepped wall. When a wave with a near vertical front strikes the first step, its momentum is destroyed over the height of the step giving rise to an impact pressure which developes in rise time t_1, during which time the wave above this level has passed over the first step and impacted against the second step. Thus the hydrostatic pressure measured at the first step is due to the wave above this level (which has by now expended its energy) spilling back down the wall. If the incident waves do not have a vertical face (e.g. swell) then the impact pressures do not occur and little turbulence is generated and the resulting hydrostatic pressure measured at the transducer has the familiar slow rise and fall normally associated with hydrostatic wave pressures.

3.12 Relationship Between Impact and Hydrostatic Pressures for Breaking waves

Every impact pressure history measured on the Ilfracombe seawall had two peaks, the first peak was caused by the impacting of the wave front and had a magnitude dependent upon the wave celerity, period, percentage of entrained air, etc., and the second was the hydrostatic pressure exerted by the following body of the wave. The mechanism by which these two pressures are produced is different, thus an increase in hydrostatic pressure will not necessarily imply an increase in impact pressure and vice versa although some relationship might be expected.

To investigate this relationship (if any) a frequency histogram of the ratio of impact pressure (P_i) to hydrostatic pressure (P_h), as given in Tables 3.3 to 3.12, was produced, (Figure 3.41). Data measured at the Brunel seawall is also included in Figure 3.41 and so is any data from Seaford where the hydrostatic pressure peak clearly occurs.

The histogram of P_i/P_h is seen to be excessively skewed with a long upper tail, most of the data lies between $P_i/P_h = 1$ and 2 . The data was fitted to several skew type probability distributions in order to obtain a probability description for the ratio P_i/P_h, the results are as follows;

(i) Lognormal distribution; the theoretical lognormal distribution was calculated from the following;

$$f(x) = \frac{1}{y(2\pi\,\sigma_{\ln x})^{\frac{1}{2}}} \exp\left\{-\tfrac{1}{2}\left[\frac{1}{\sigma_{\ln x}} \ln (x/m_x)\right]^{2}\right\} \ldots \quad (3.50)$$

where $\sigma_{\ln x} = \left[\ln (V_x{}^2 + 1)\right]^{\frac{1}{2}}$

$V_x = \mu_x/\sigma_x$

$m_x = \mu_x . \exp \left(-\frac{\sigma^2_{\ln x}}{2}\right)$

μ_x and σ_x are the mean and standard deviation respectively

The lognormal p.d.f. is shown in Figure 3.41, it does not fit the observed data very closely except at the upper tail and the degree of skew is insufficient.

To determine the goodness of fit of the lognormal distribution the Chi-squared test was used, (found in Refs. 98 and 99), 13 class intervals were used which gave a degree of freedom of 10. The theoretical Chi-squared (X^2) value at a level of significance of 5% was found to be;

$$X^2_{0.05,10} = 15.51$$

The actual X^2 from the data was 49.22, so as X^2_{data} is larger than $X^2_{0.05,10}$ then there is a greater than 5% chance of a measured value of P_i/P_h not fitting the lognormal distribution, so this distribution is rejected at the 5% level of significance.

(ii) Rayleigh distribution; this distribution is a particular form of

the χ^2 distribution with two degrees of freedom, and is given by the following expression;

$$f(x) = \frac{x}{\sigma_x{}^2} \exp\left[-\tfrac{1}{2}(x/\sigma_x)^2\right] \qquad \ldots\ldots\ldots\ldots\ (3.51)$$

The Rayleigh distribution (shown in Figure 3.41) has a similar degree of skew to the observed data but tends to over estimate small values of P_i/P_h and under estimate large values.

(iii) Gamma distribution; the gamma p.d.f. is a two parameter distribution given by;

$$f(x) = \frac{\lambda(\lambda x)^{K-1} \quad e^{-\lambda x}}{\Gamma(K)} \qquad \ldots\ldots\ldots\ldots\ldots\ (3.52)$$

where $\lambda = \dfrac{\mu_x}{\sigma_x{}^2}$

$K = \dfrac{\mu_x{}^2}{\sigma_x{}^2}$

$\Gamma(K)$ = the incomplete Gamma function

The Gamma distribution as shown in Figure 3.41 models the observed p.d.f. at about $P_i/P_h = 1.5$ quite closely, but greatly under estimates the density at larger values of P_i/P_h. Overall the Gamma distribution displays a poor fit to the observed data.

(iv) Gumbel distribution; the Gumbel p.d.f. is given by;

$$f(x) = \alpha \exp\left[-\alpha(x - u) - \exp -\alpha(x - u)\right] \qquad \ldots\ldots\ (3.53)$$

where μ_x = mean = $u + 0.577/\alpha$

σ_x = standard deviation = $1.28/\alpha$

The Gumbel distribution is also shown in Figure 3.41, it does not fit the observed data very closely and has a general shape very similar to the lognormal distribution.

These four theoretical p.d.f's. shown superimposed on the observed data in Figure 3.41, form a good cross-section of the available skew type distributions. None of these distributions model the observed data over the entire range of values of P_i/P_h , but most model small sections quite closely so more data is really required before these distributions can be safely rejected.

Thus from the present data there seems to be no relationship between impact pressures and hydrostatic pressures, but from the observed data the mean value of the ratio $P_i/P_h = 2.025$, therefore the average impact pressure is likely to be about twice the hydrostatic pressure, although it could be as much as seven times the hydrostatic pressure.

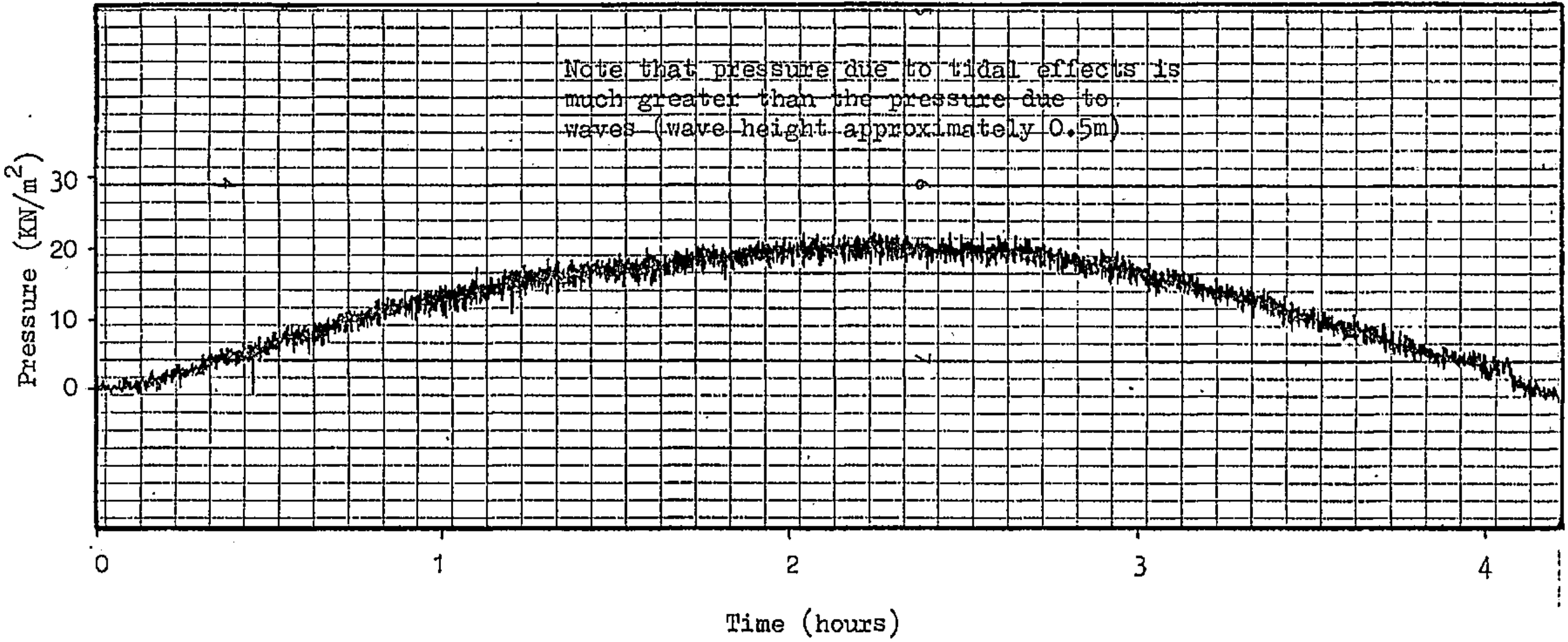

Note that pressure due to tidal effects is much greater than the pressure due to waves (wave height approximately 0.5m)

Figure 3.1 Typical condensed pressure/time history showing non-linear tidal effects (Recorded at Ilfracombe on 23.2.81)

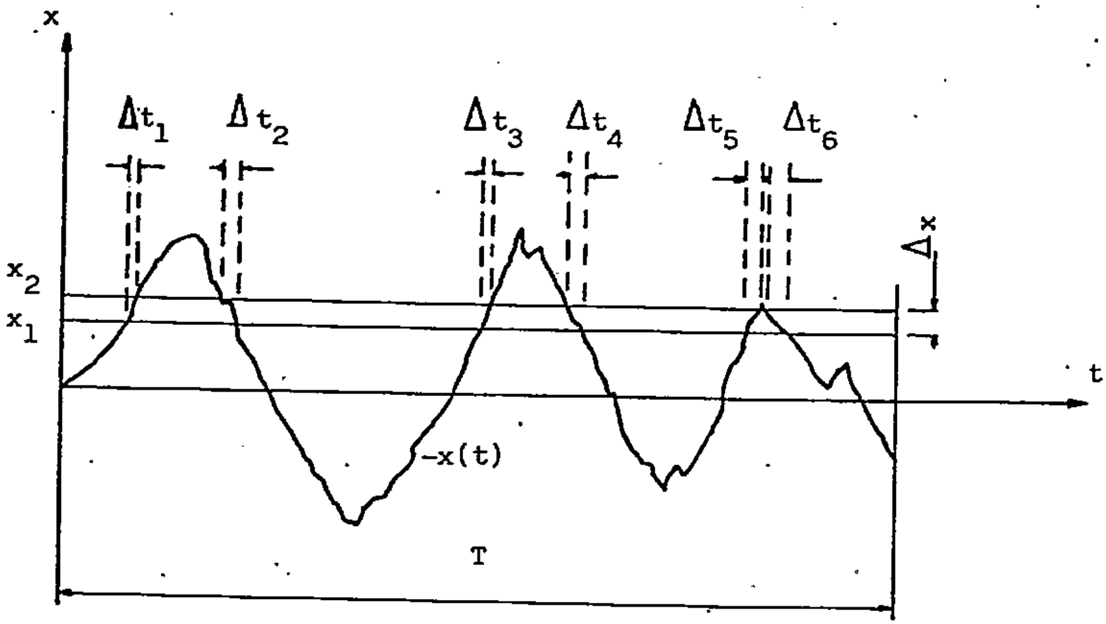
x
Δt1
Δt2
Δt3
Δt4
Δt5
Δt6
x2
x1
Δx
t
x(t)
T

Figure 3.2 Probability measurement.

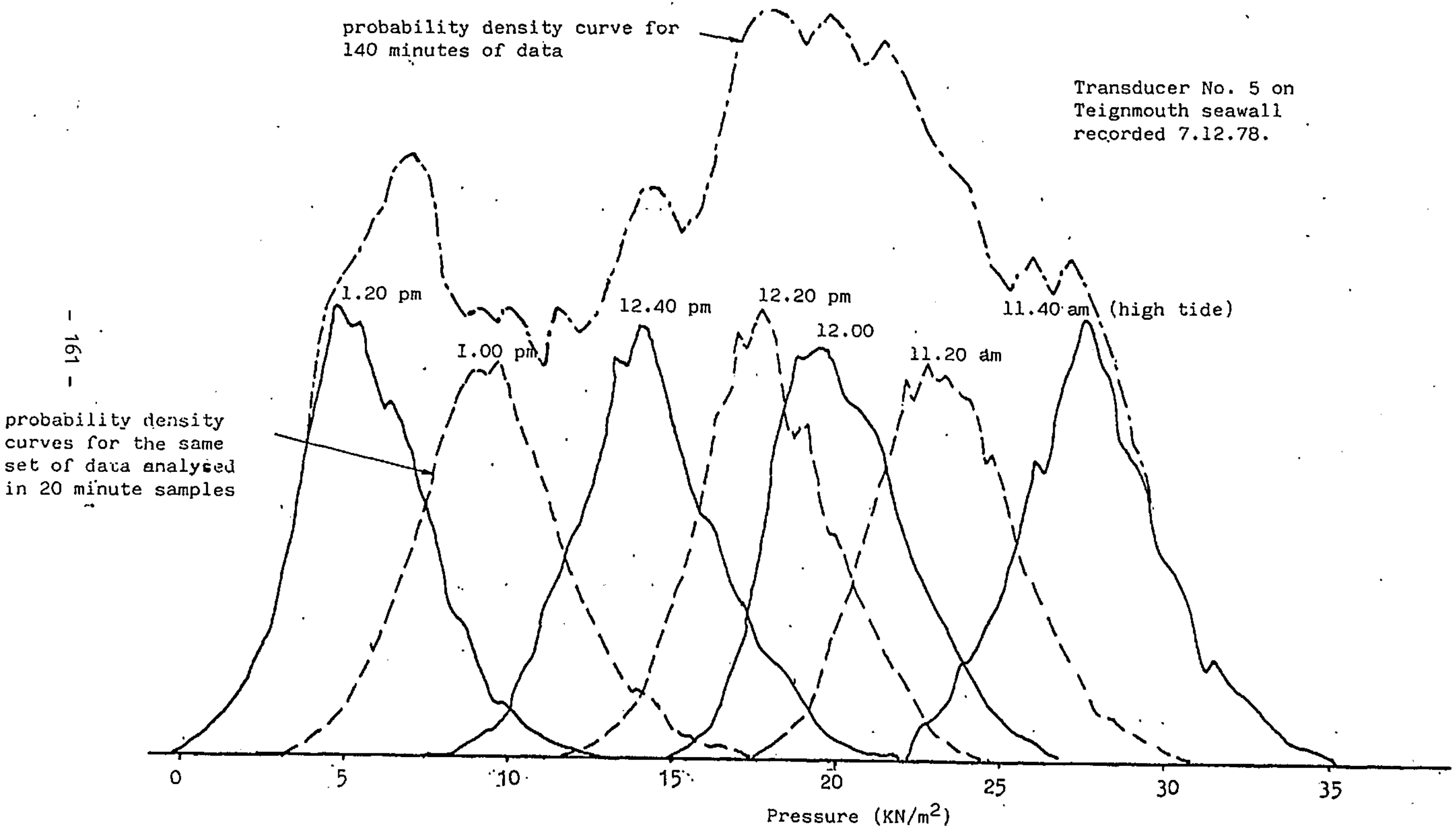

Figure 3.3 Amplitude probability density function plot showing the effect of a trend (due to tidal changes) on the pressure distribution.

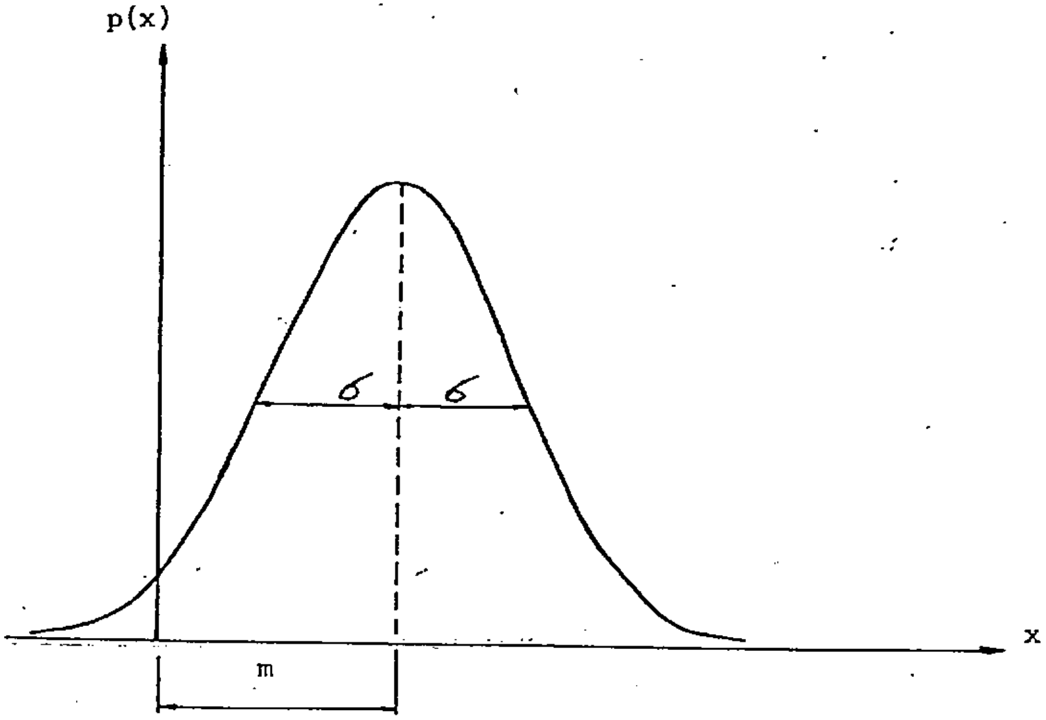

Figure 3.4 Gaussion distribution with a non-zero mean

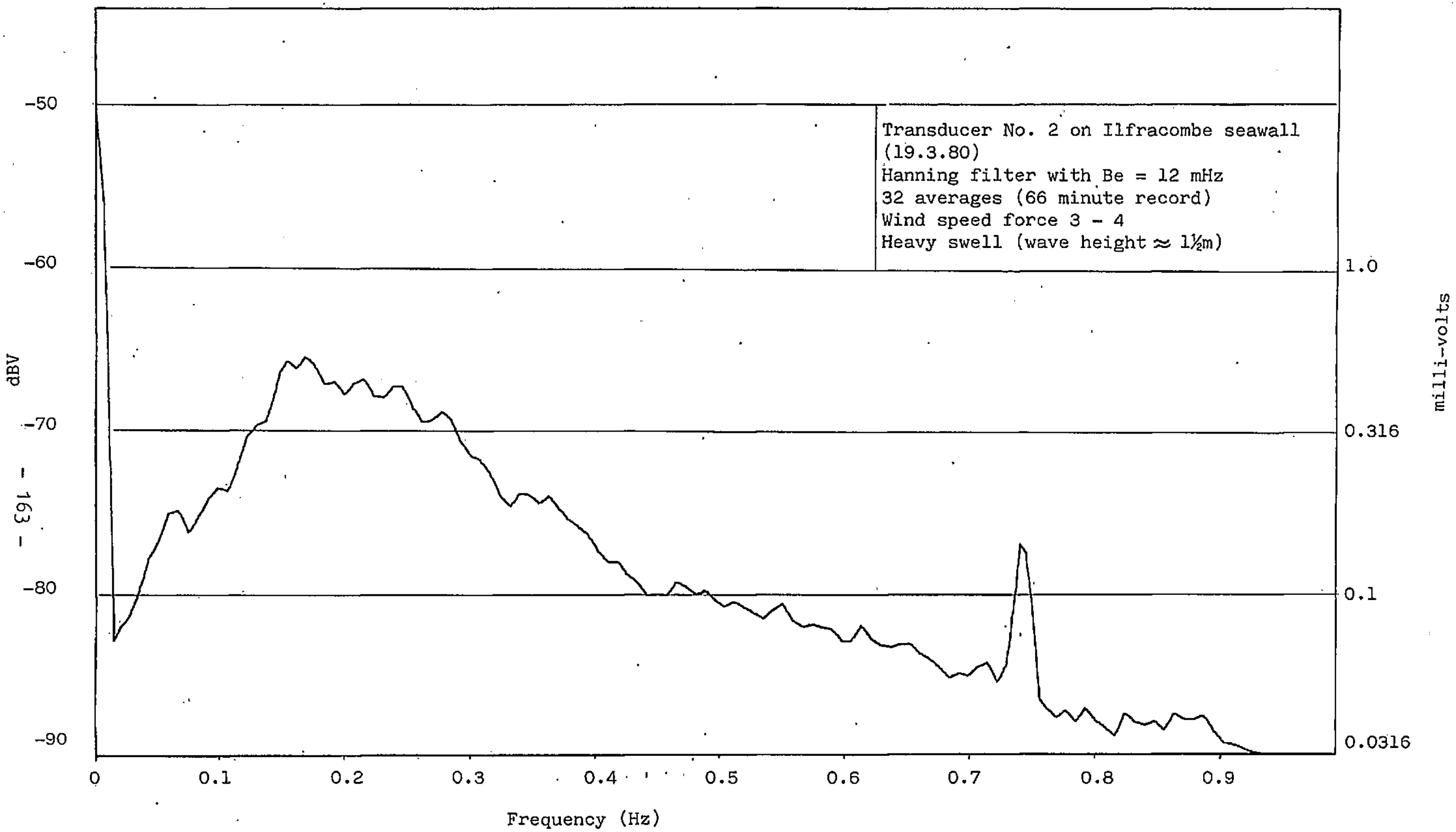

Transducer No. 2 on Ilfracombe seawall
(19.3.80)
Hanning filter with Be = 12 mHz
32 averages (66 minute record)
Wind speed force 3 - 4
Heavy swell (wave height ≈ 1½m)

Figure 3.5 Spectral density plot of swell pressure on Ilfracombe seawall.

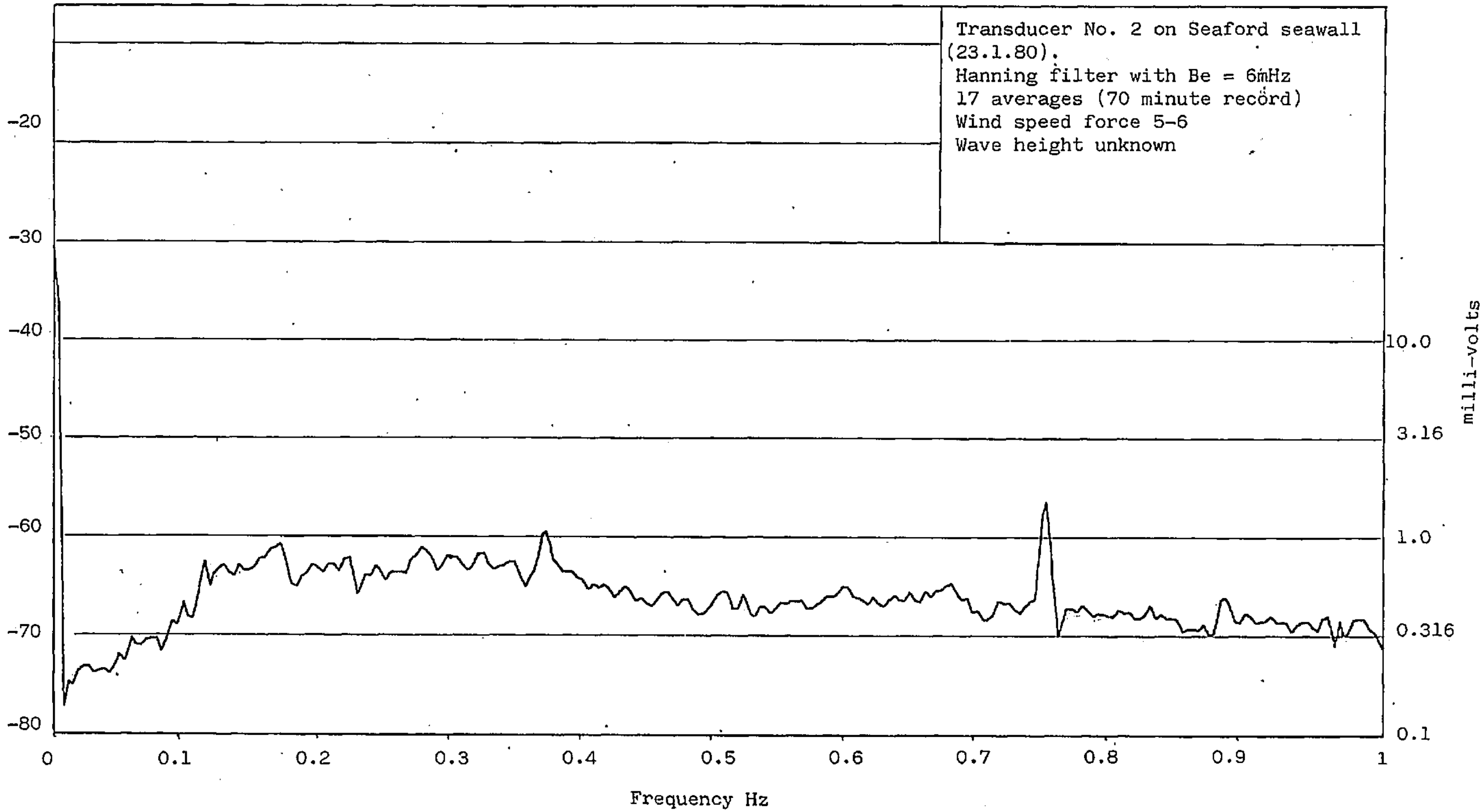

Figure 3.6 Spectral density plot of wave forces on Seaford seawall.

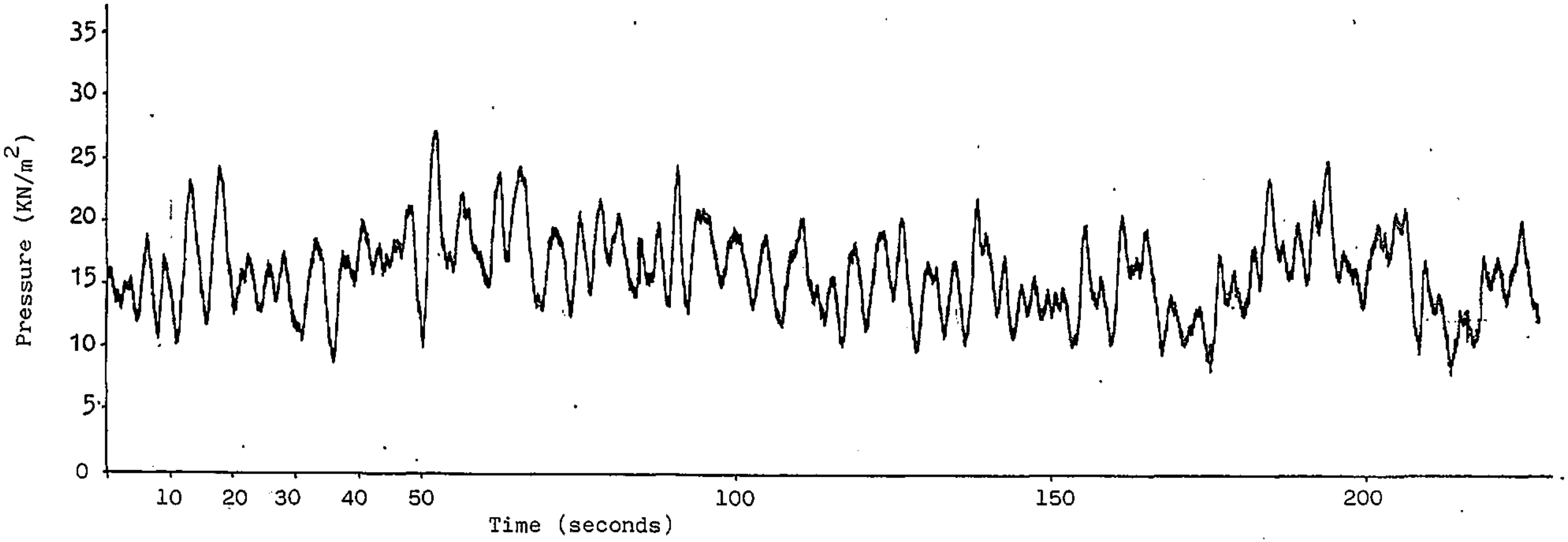

Figure 3.7 Sample pressure/time history for Ilfracombe seawall (19.3.80)
(Note, pressure transducer is completely submerged)

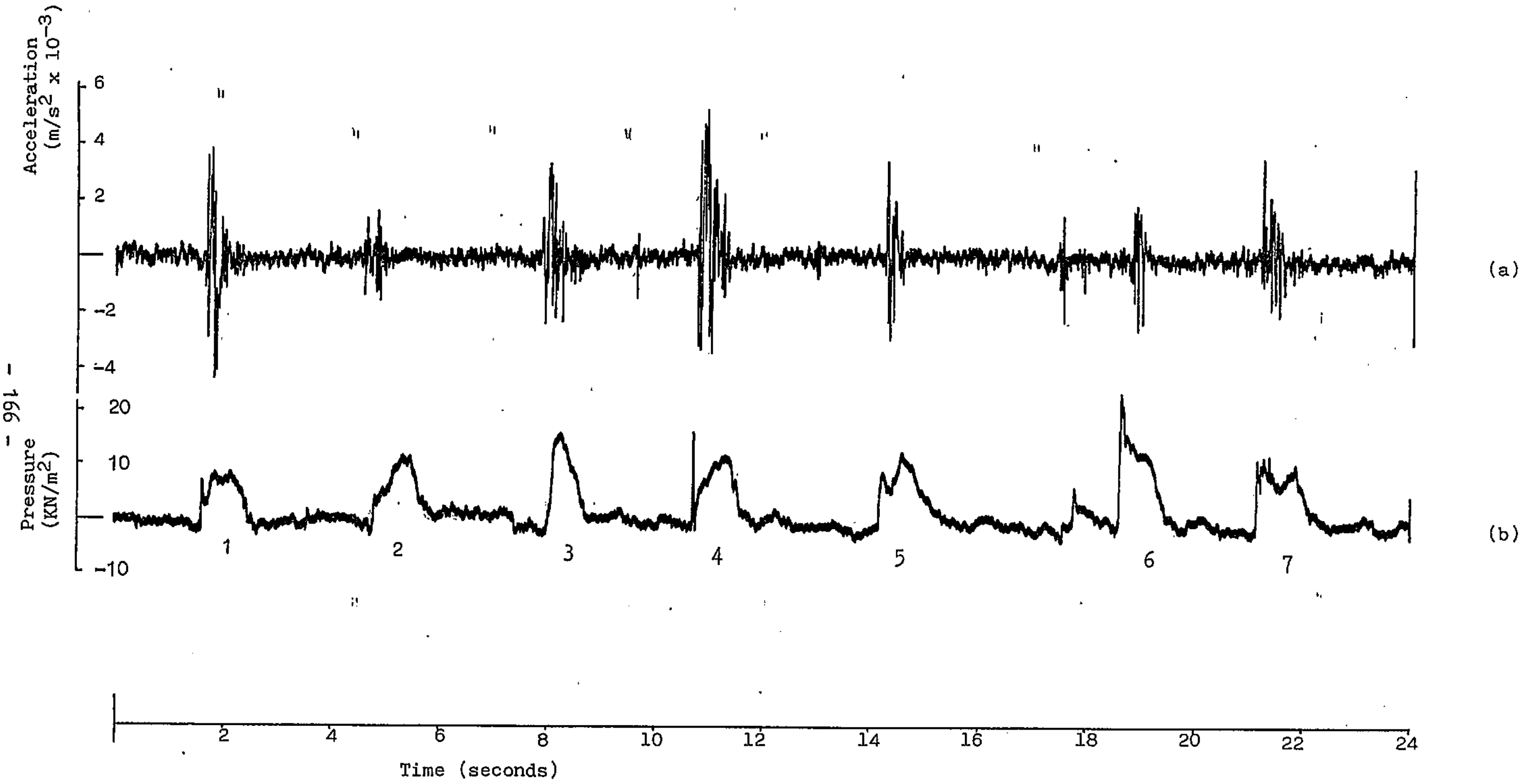

Figure 3.8 (a) Sample acceleration/time history for Seaford seawall (23.1.80) synchronised with (b) pressure/time history (note, pressure transducer located in splash zone.)

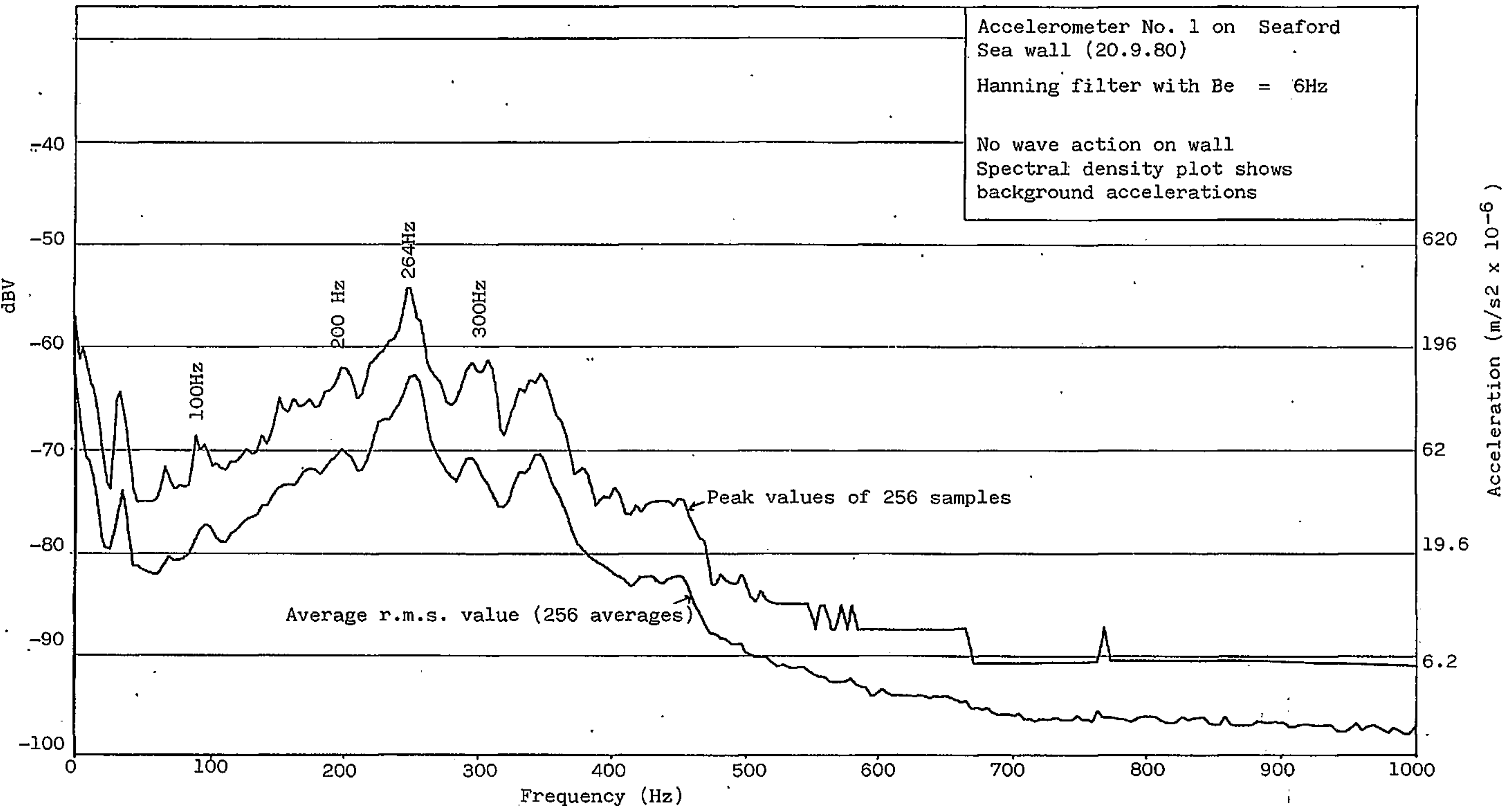

Figure 3.9 Spectral density plot of background acceleration of Seaford seawall.

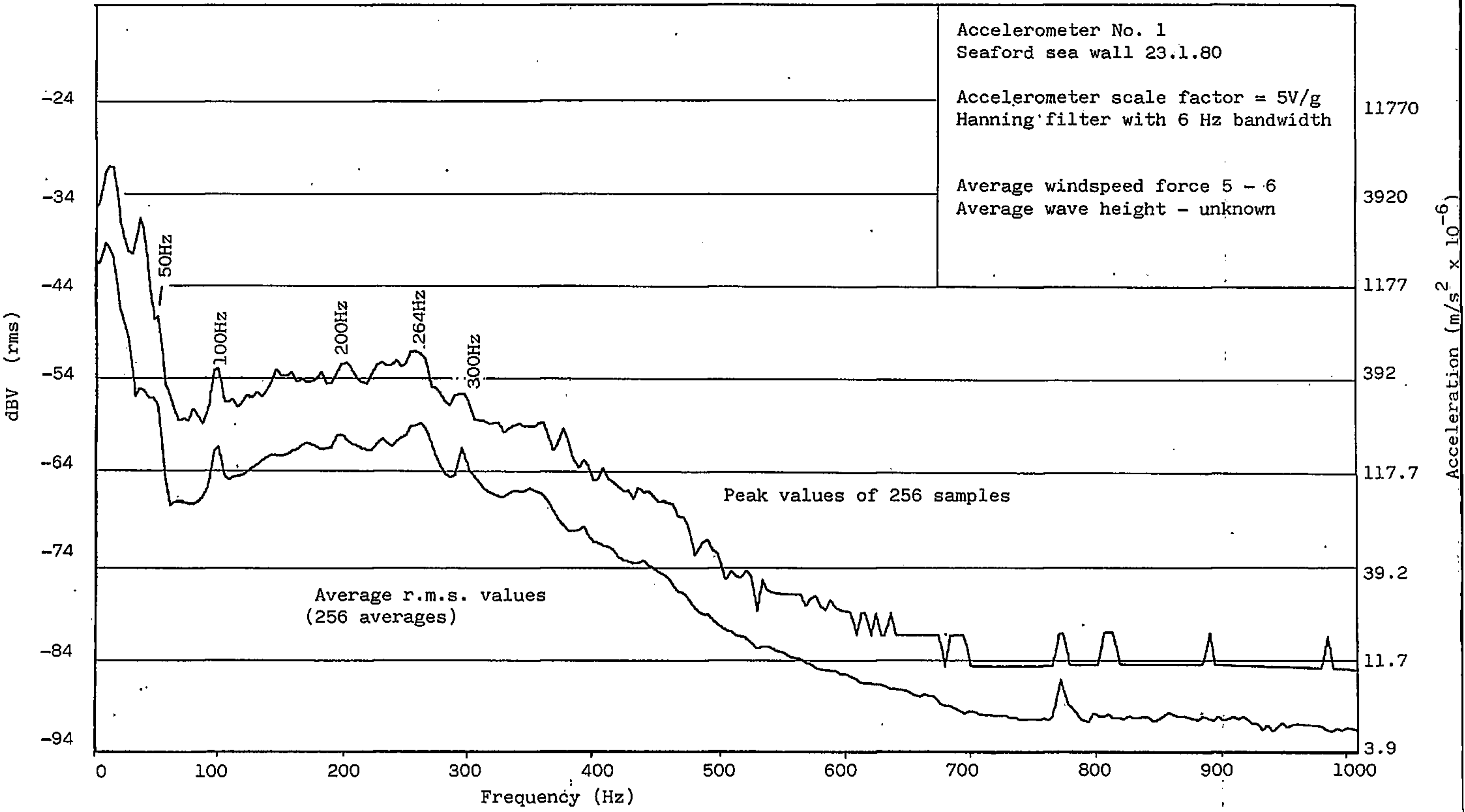

Fig. 3.10 Spectral density plots of peak and average accelerations of Seaford sea wall.

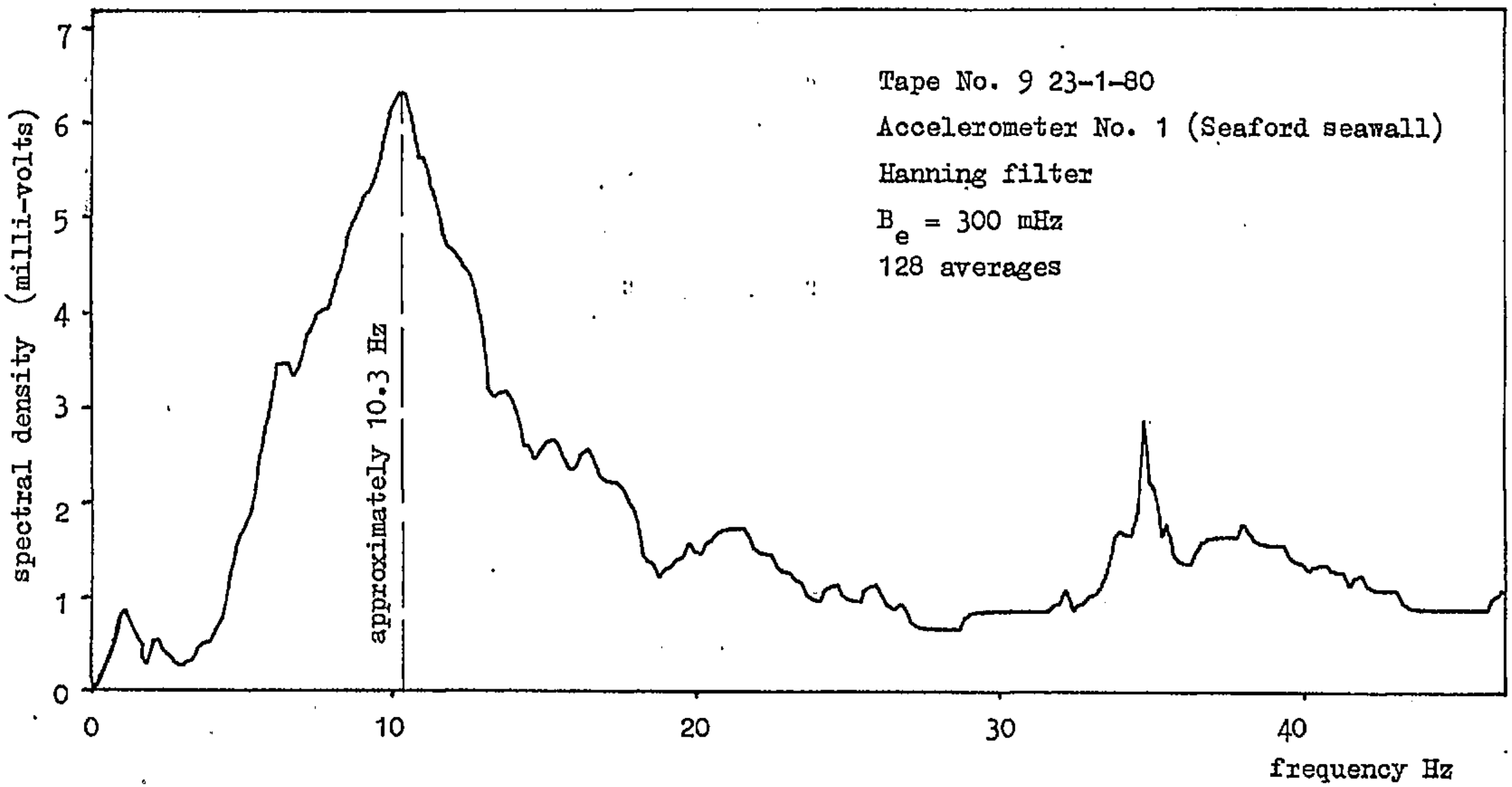

Figure 3.11 Seaford seawall response at fundamental mode of vibration.

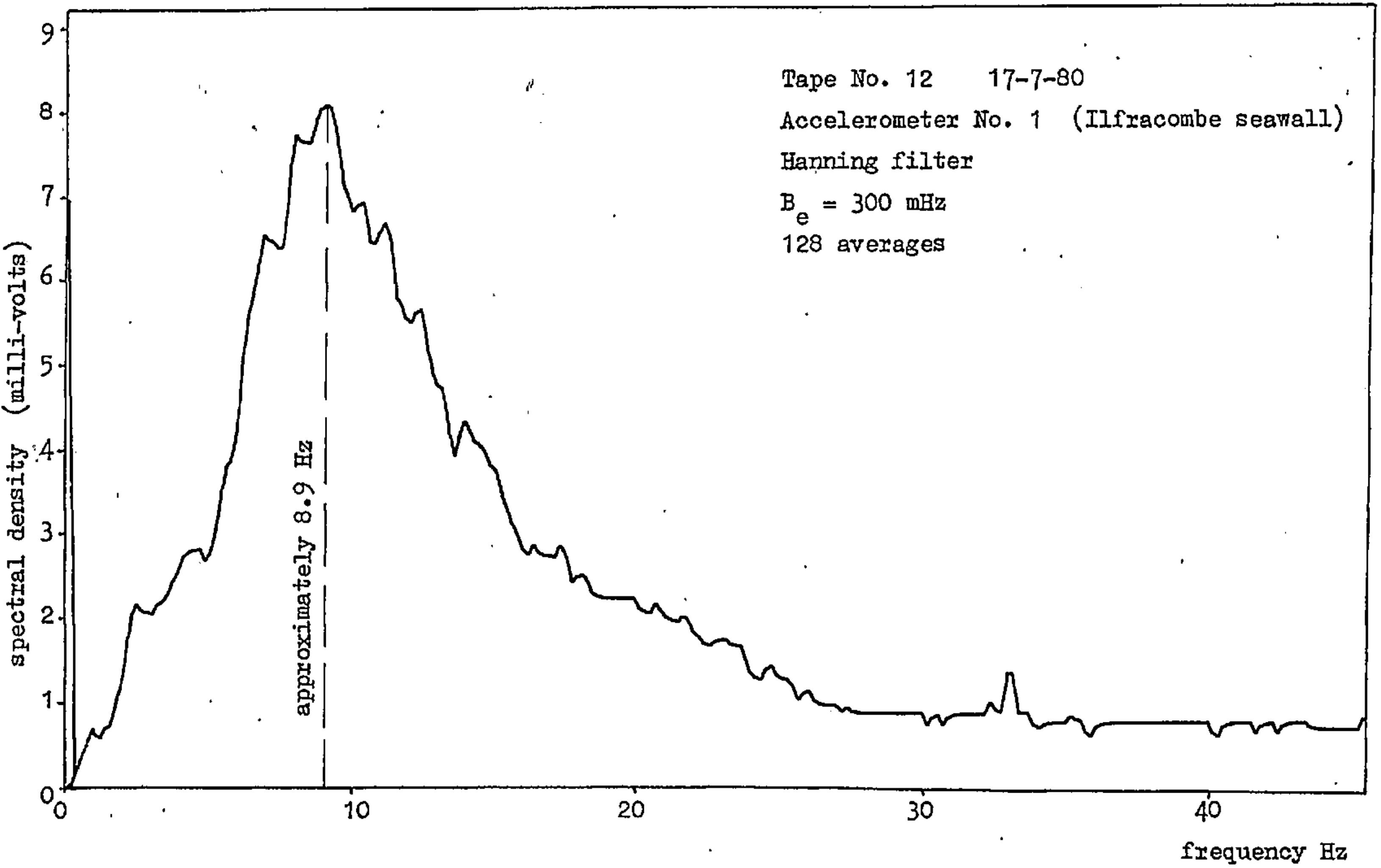

Tape No. 12 17-7-80
Accelerometer No. 1 (Ilfracombe seawall)
Hanning filter
B_e = 300 mHz
128 averages

Figure 3.12 Ilfracombe seawall response at fundamental mode of vibration.

Tape Number 14 (Ilfracombe)
No. of samples = 4096
Length of record = 22.7 mins.

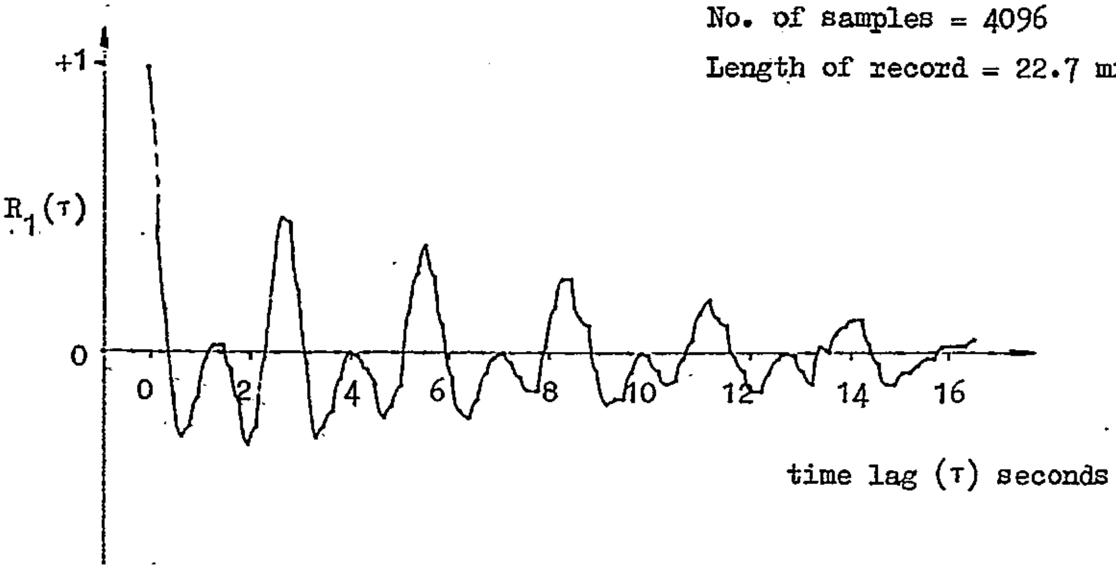

Figure 3.13(a) Correlogram of pressure measured at transducer number 1.

Tape Number 14 (Ilfracombe)
No. of samples = 16384
Length of record = 1hr 31min.

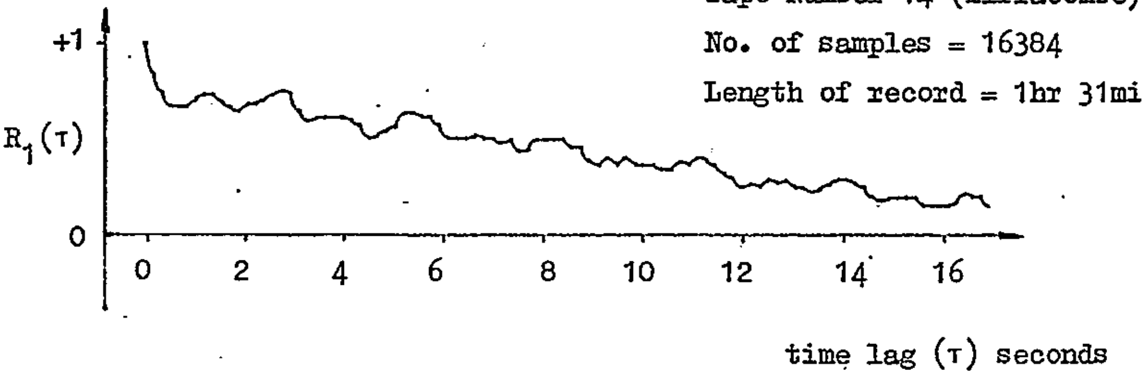

Figure 3.13(b) Correlogram of transducer No. 1 illustrating data is non-stationary over long time periods.

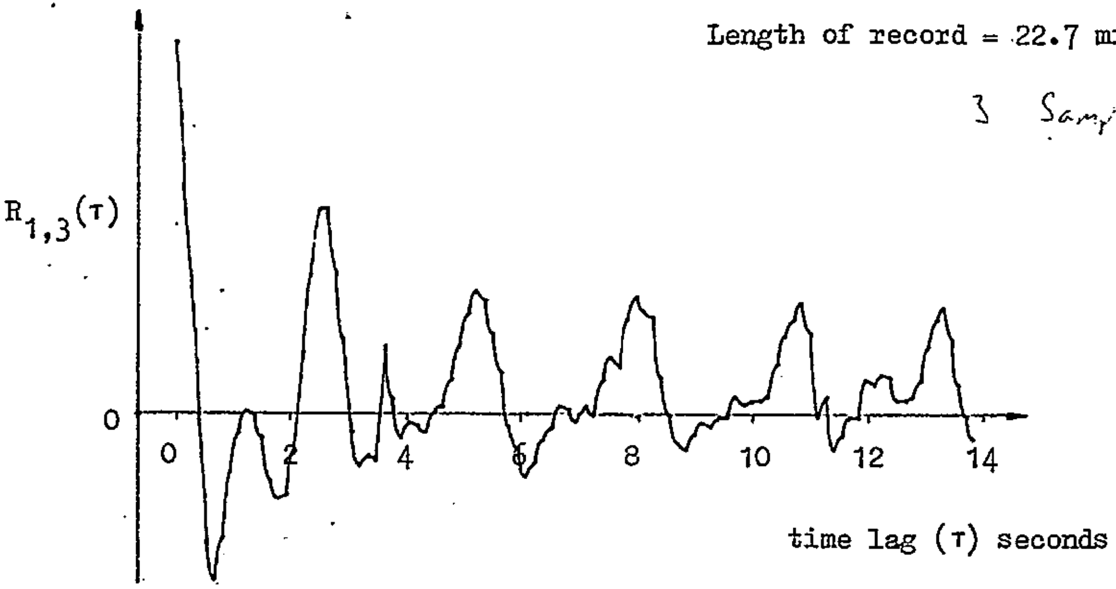

Tape Number 14 (Ilfracombe)
No. of samples = 4096
Length of record = 22.7 mins.

3 Samples/sec

Figure 3.14(a) Cross-correlogram between transducers No. 1 and No. 3, in a vertical plane.

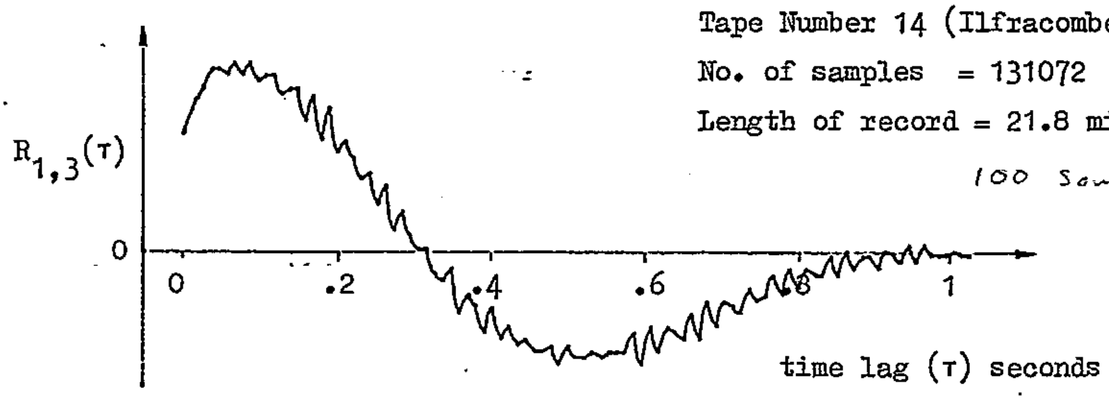

Tape Number 14 (Ilfracombe)
No. of samples = 131072
Length of record = 21.8 mins.

100 Samples/sec

Figure 3.14(b) Cross-correlogram between transducers No. 1 and No. 4, showing expanded τ scale

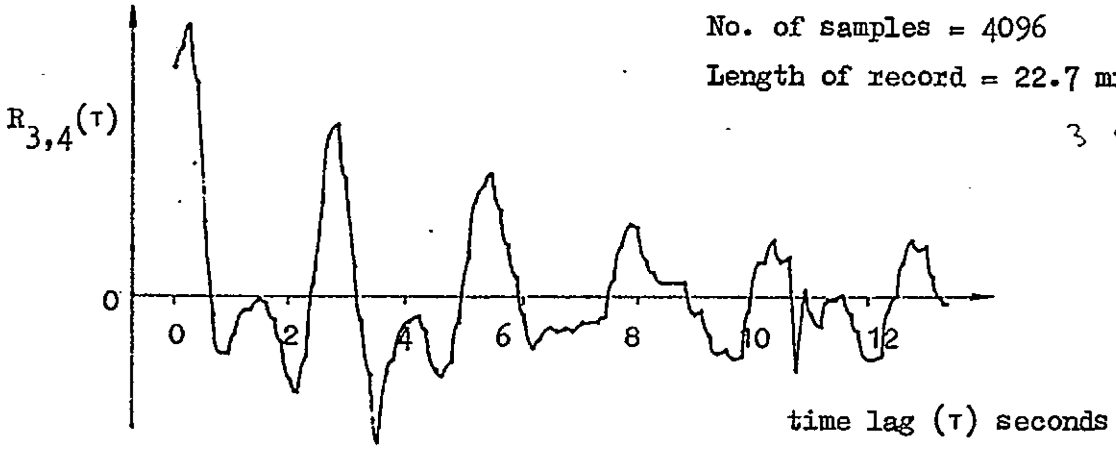

Tape Number 14 (Ilfracombe)
No. of samples = 4096
Length of record = 22.7 mins.

3 samples/sec

Figure 3.15(a) Cross-correlogram between transducers No. 3 and No. 4, in a horizontal plane.

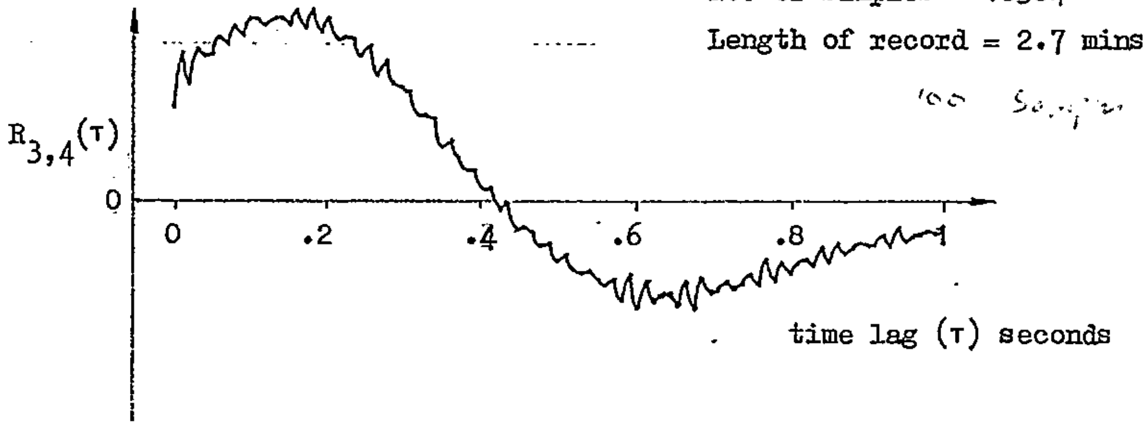

Tape Number 14 (Ilfracombe)
No. of samples = 16384
Length of record = 2.7 mins.

100 samples/sec

Figure 3.15(b) Cross-correlogram between transducers No.3 and No. 4, showing expanded τ scale.

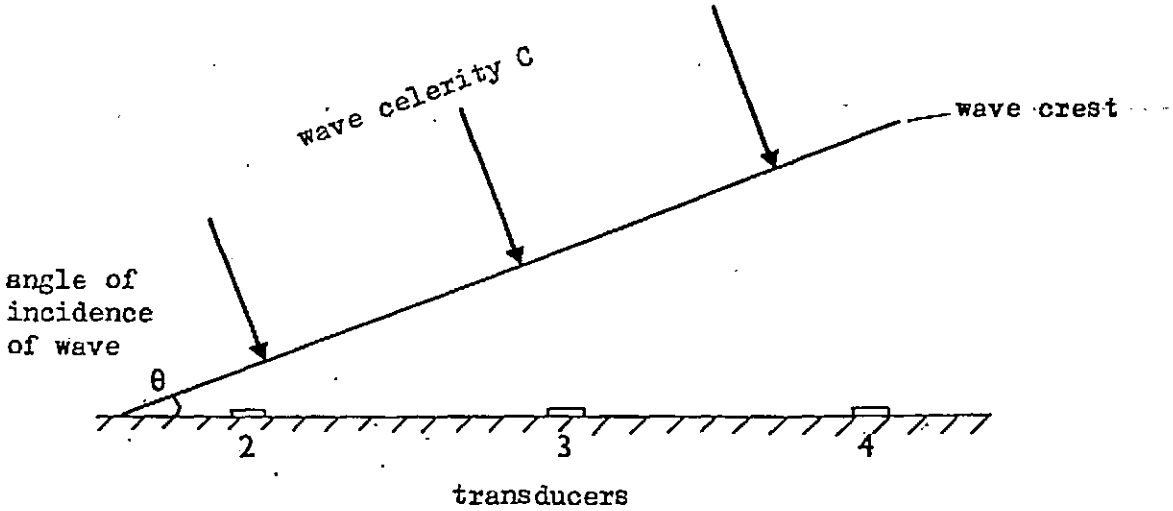
wave celerity C
wave crest
angle of
incidence
of wave
θ
2
3
4
transducers

Figure 3.17 The angle of incidence of a wave crest to the seawall

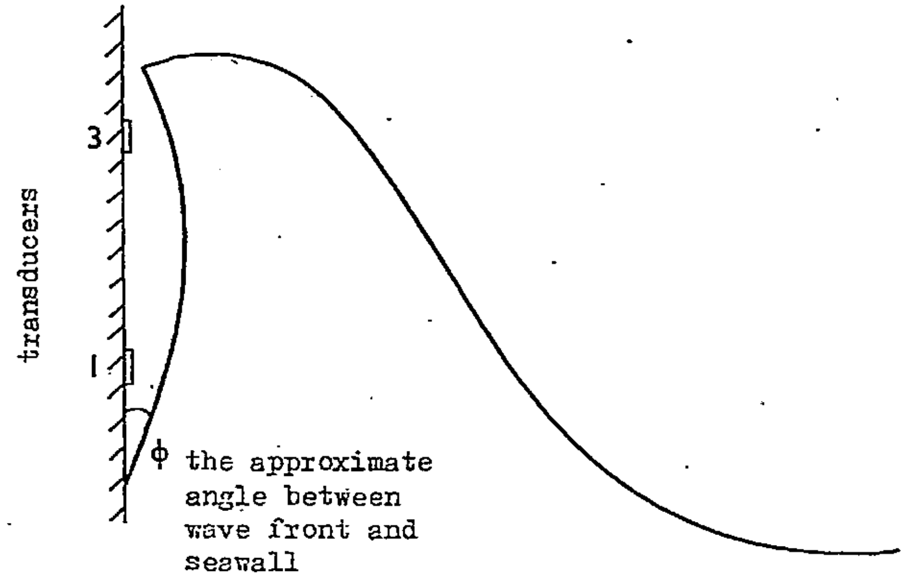
3
1
transducers
ϕ the approximate
angle between
wave front and
seawall

Figure 3.16 The approximate slope of the wave front as it strikes the seawall.

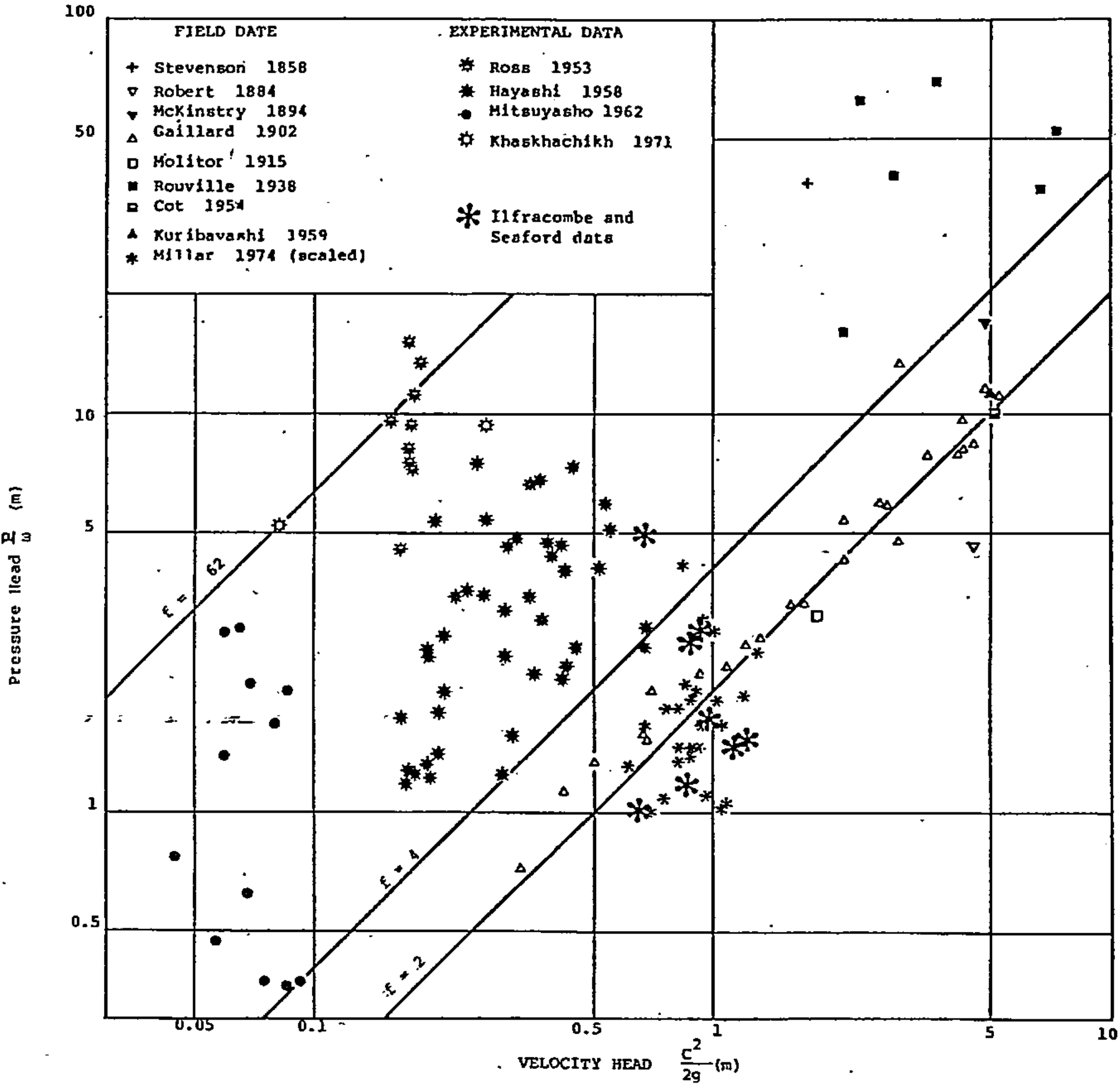

Figure 3.18 Relationship between maximum dynamic pressure and wave celerity.

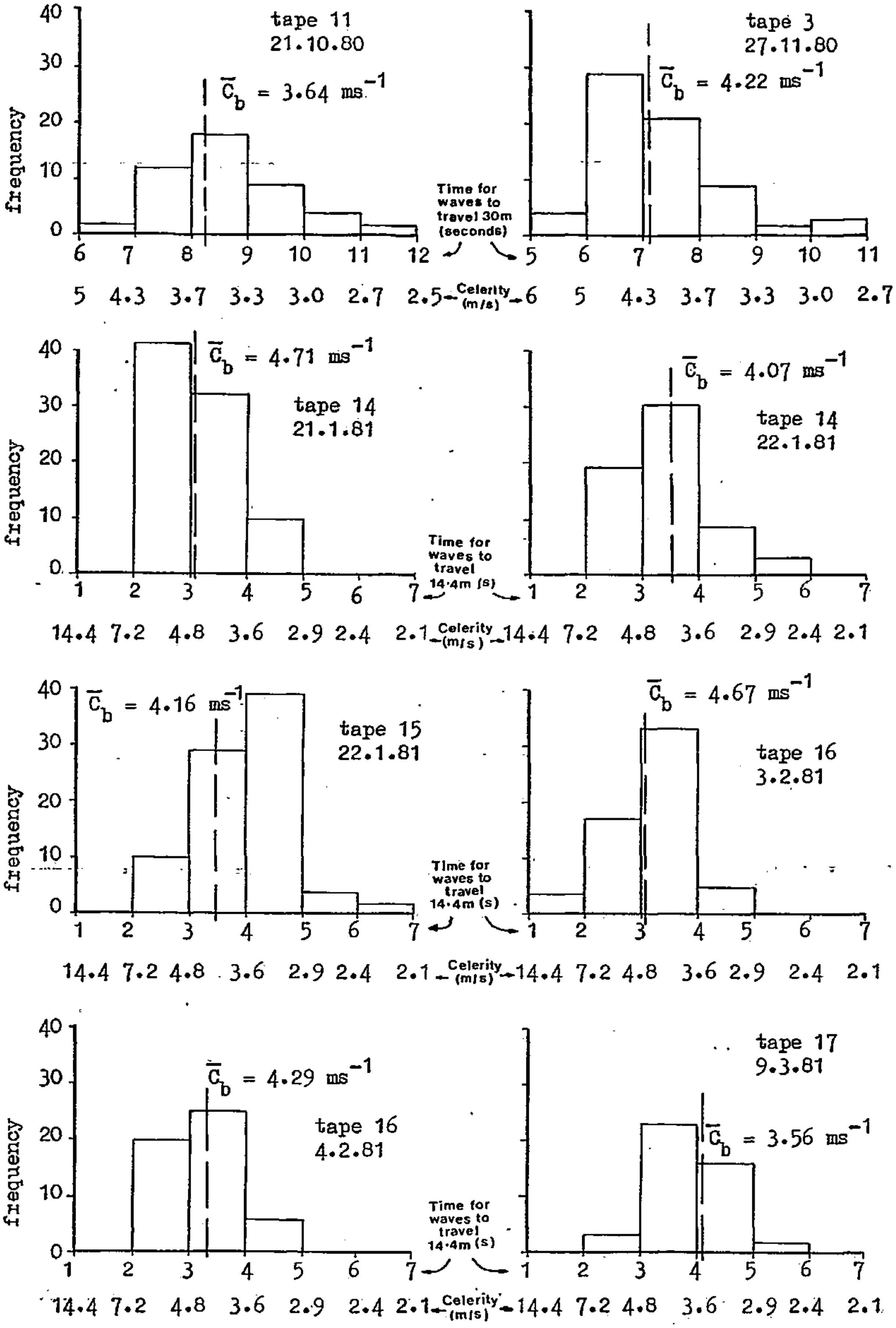

Figure 3.19 Histograms of wave celerity measured during the periods when wave impacts occurred.

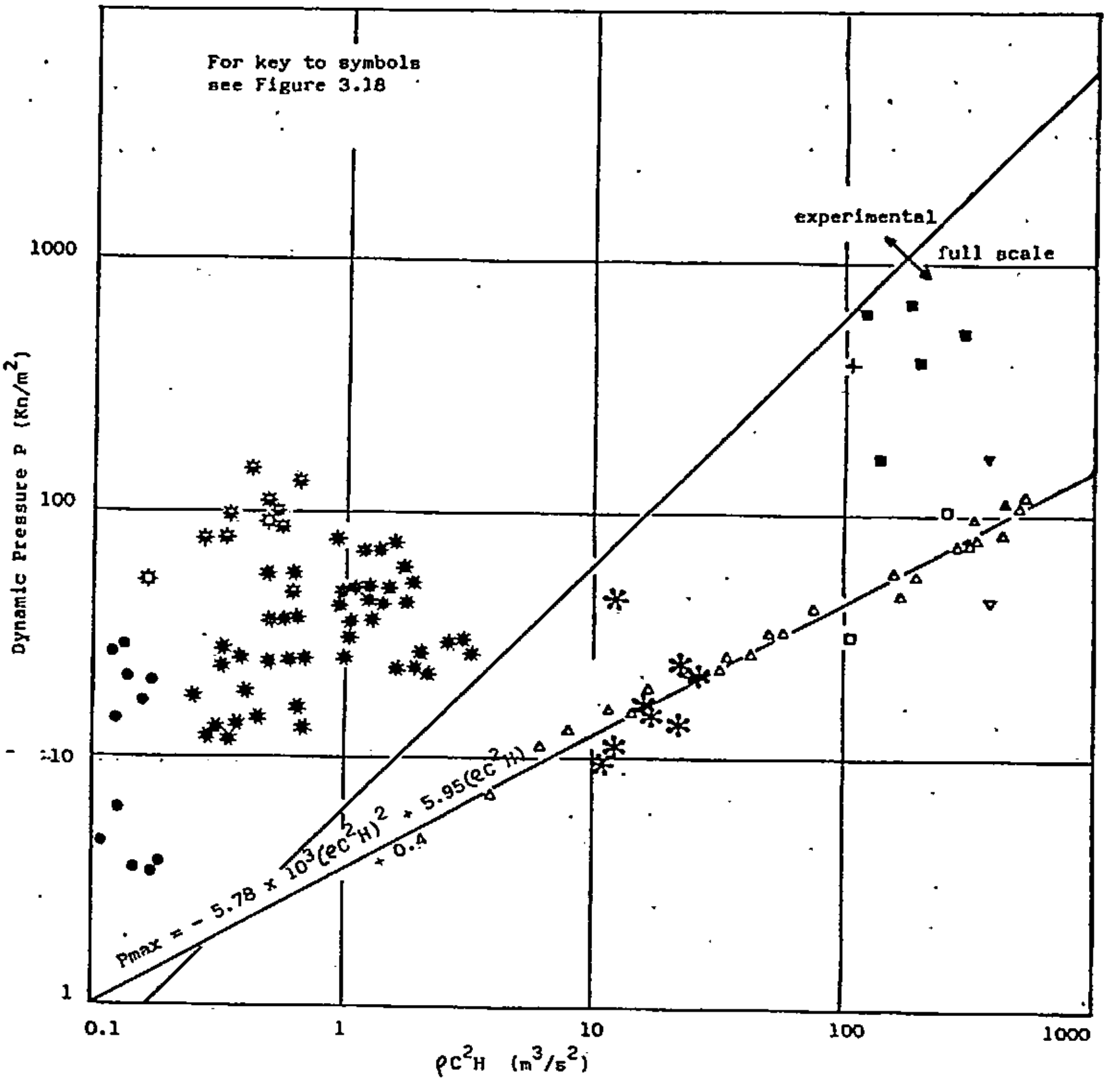

Figure 3.20 Dynamic pressure versus $C^2 \rho H$

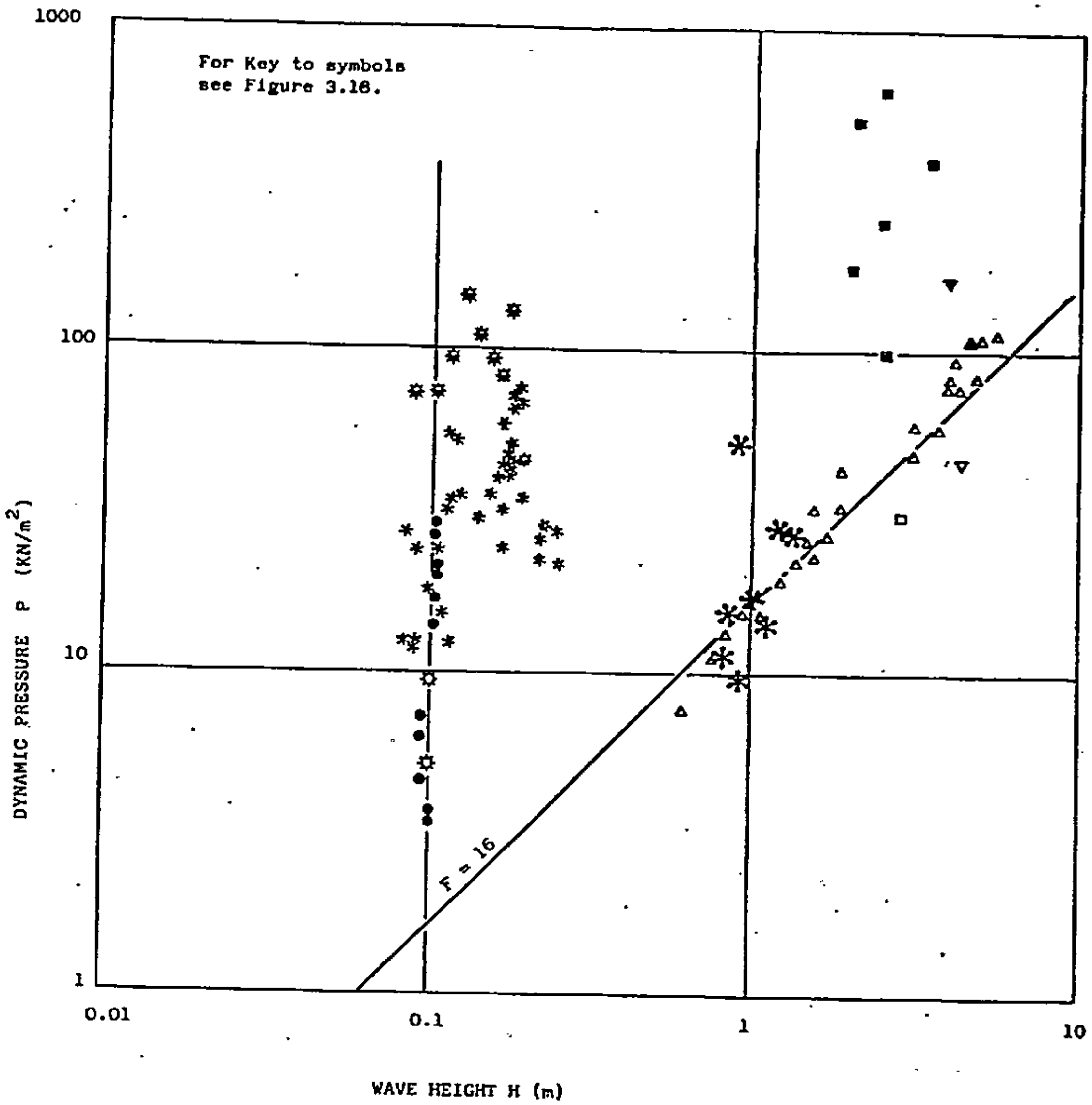

Figure 3.21 Dynamic pressure P versus wave height H

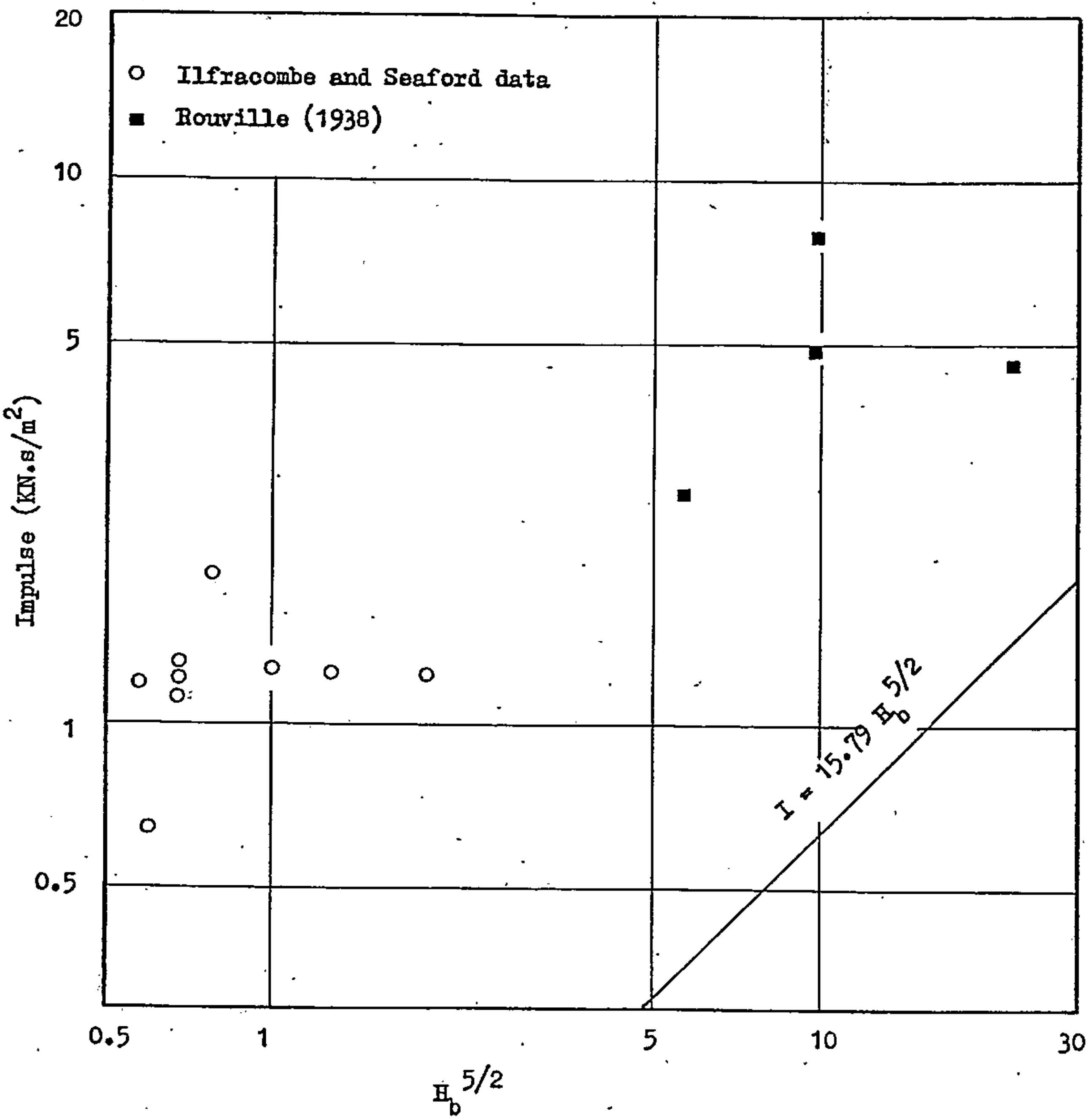

Figure 3.22 Full scale data fitted to momentum/impulse relationship based on solitary wave theory

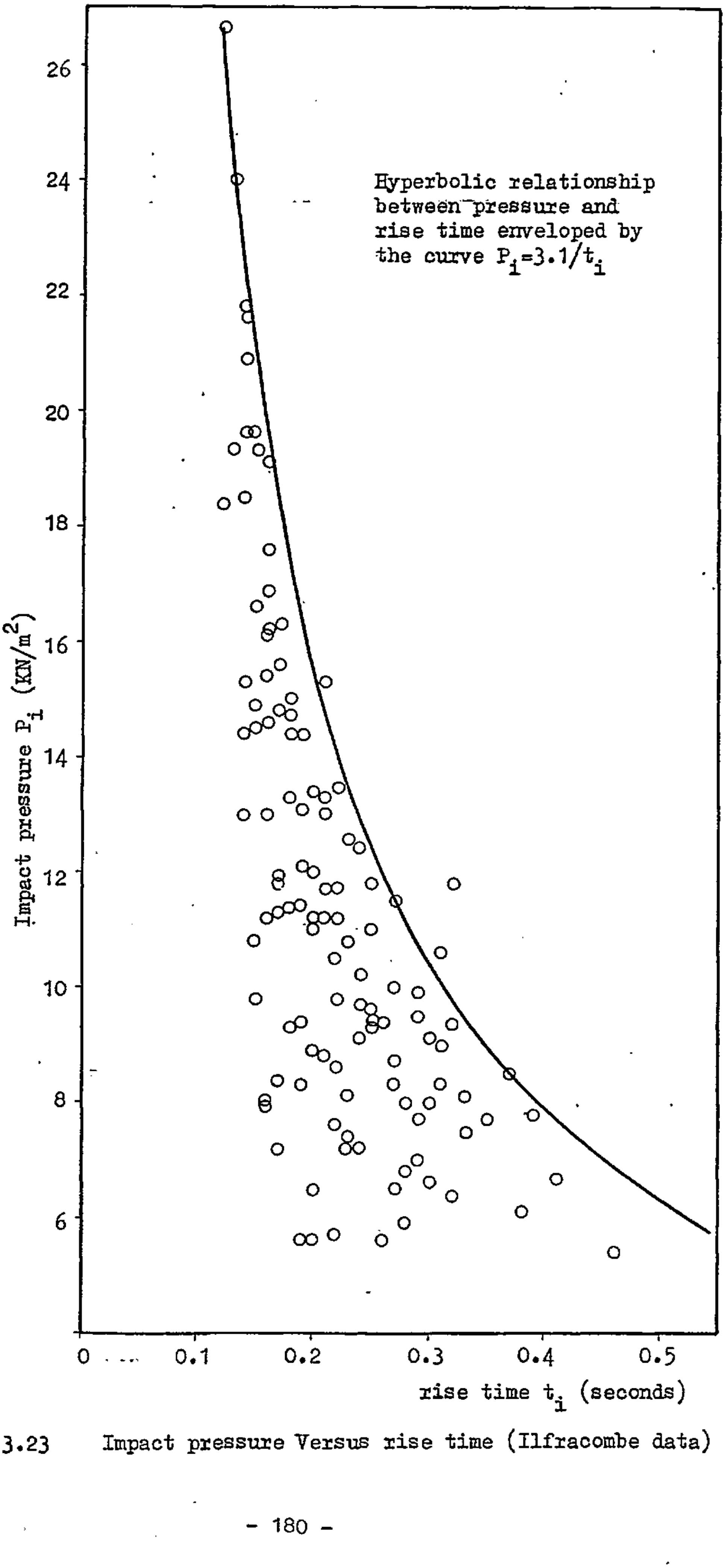

Figure 3.23 Impact pressure Versus rise time (Ilfracombe data)

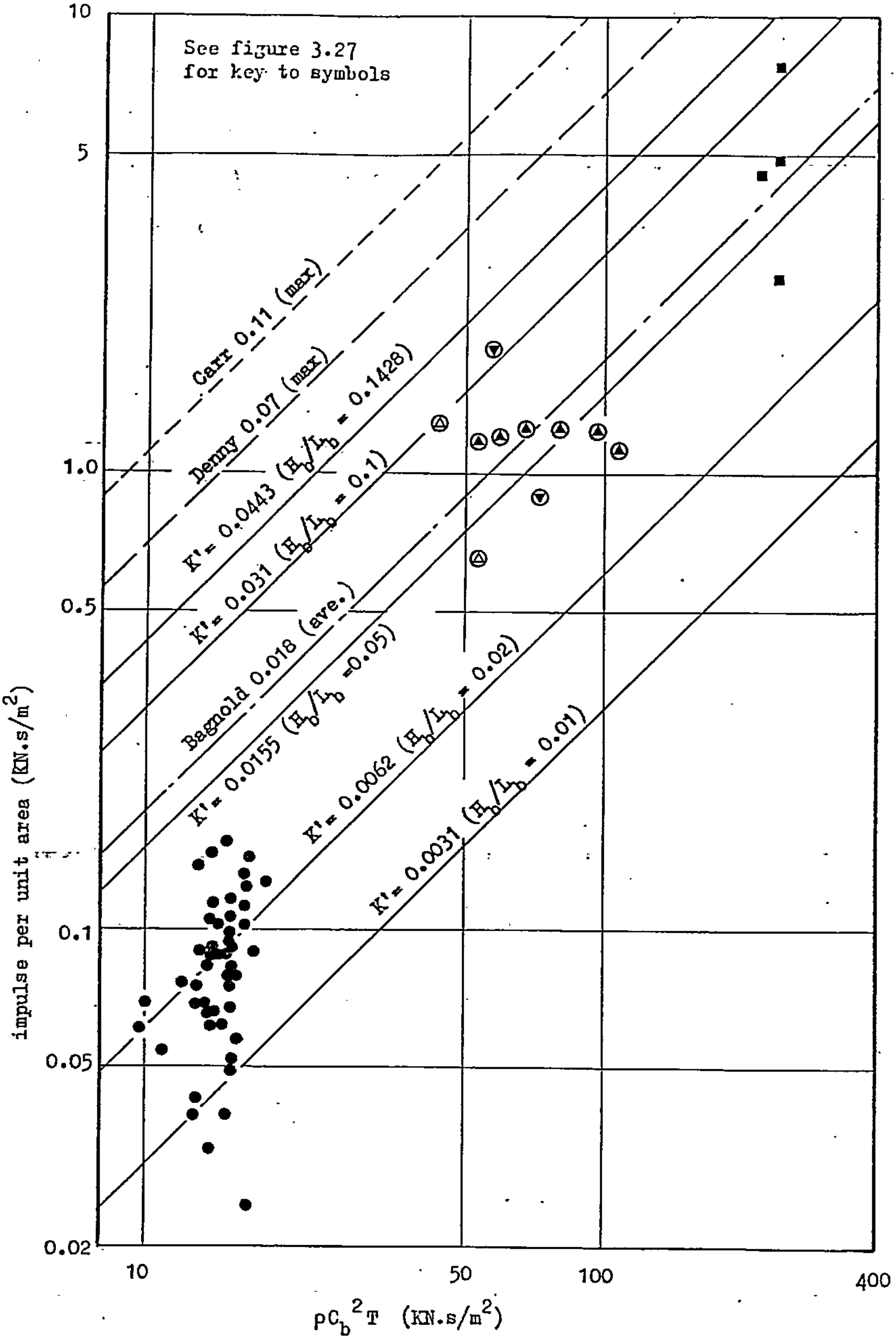

Figure 3.24 Relationship between impulse and $pC_b{}^2T$ showing dependance on H_b/L_b

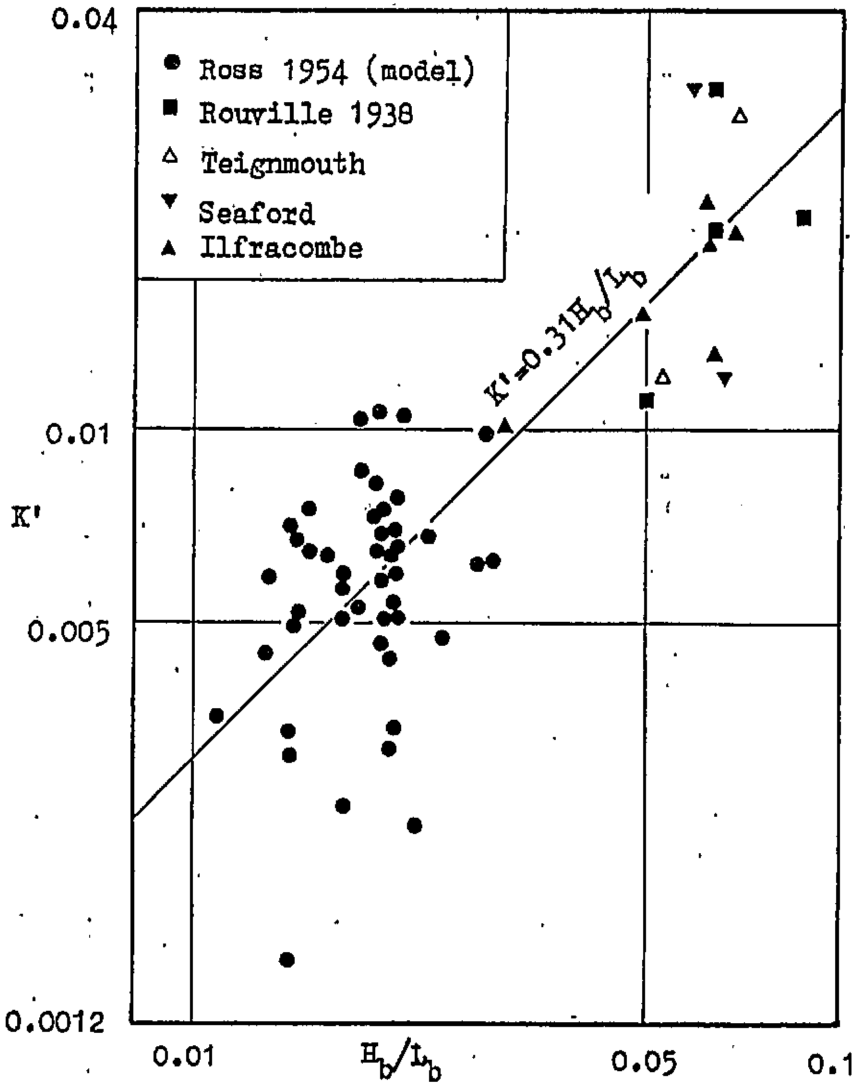

Figure 3.25 K' Versus H_b/L_b

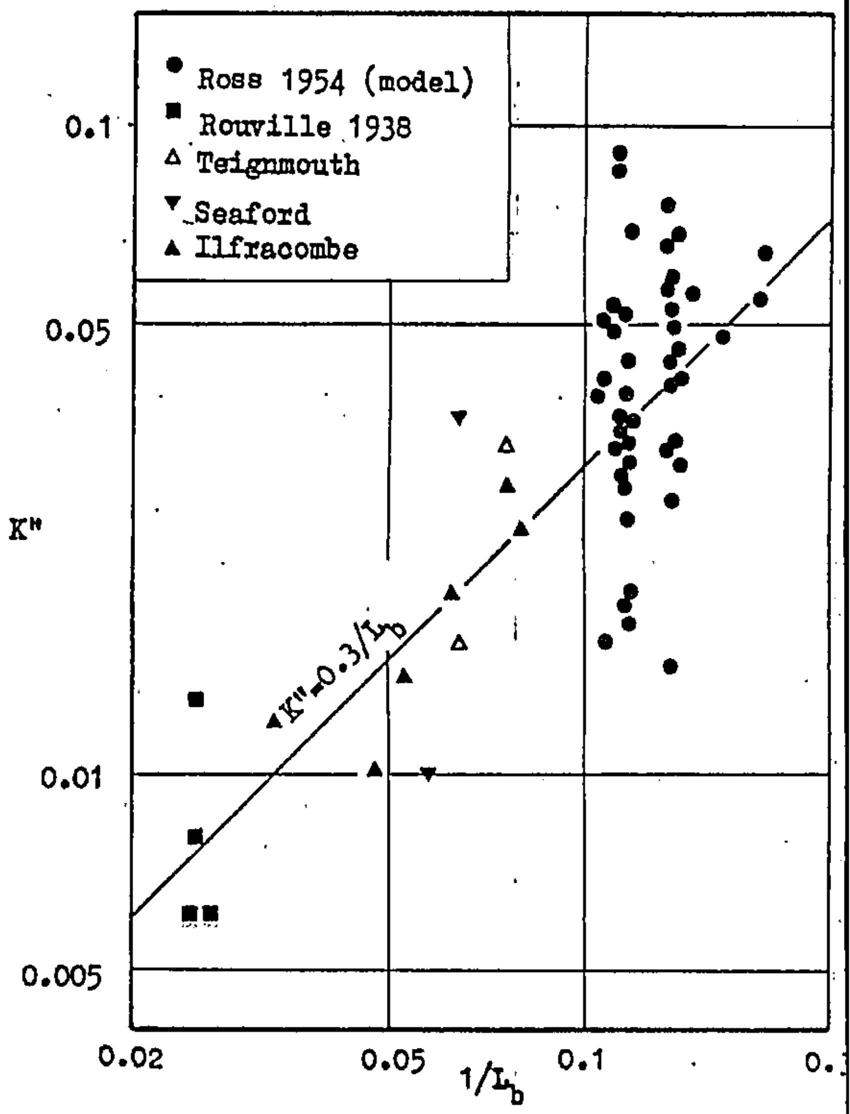

Figure 3.26 K" Versus $1/L_b$

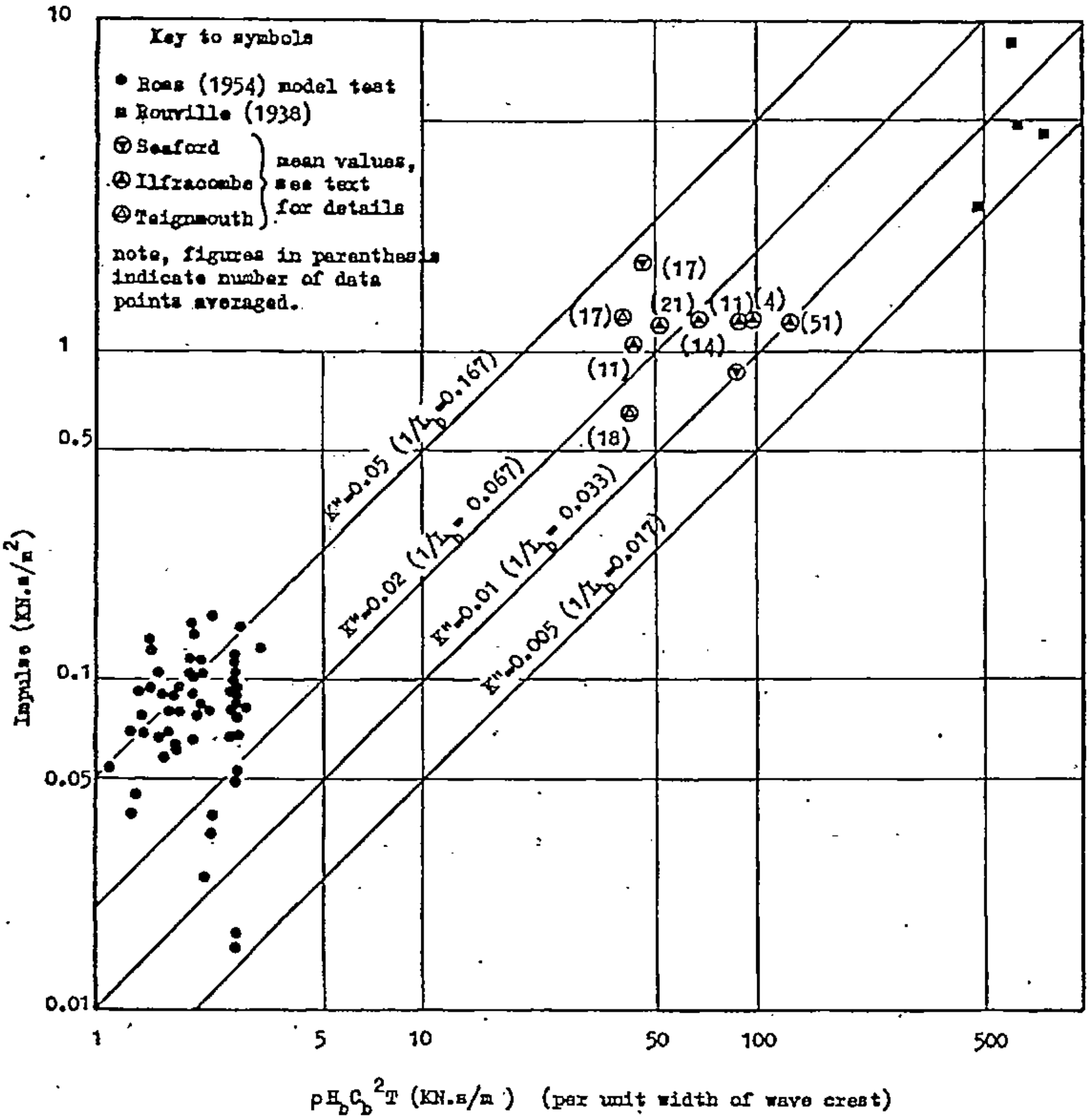

Figure 3.27 Relationship between impulse and momentum, showing the dependance upon $1/L_b$

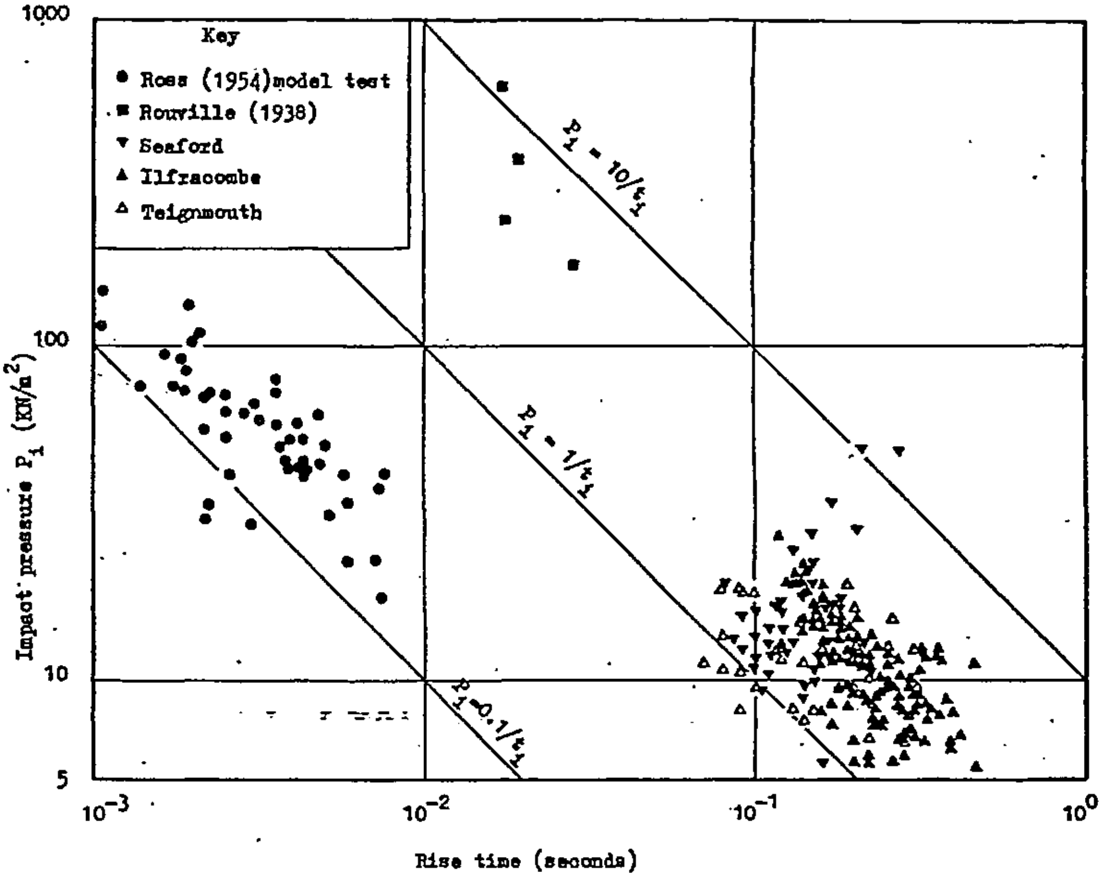

Figure 3.28 Hyperbolic relationship between rise time (t_i) and dynamic (impact) pressure (P_i).

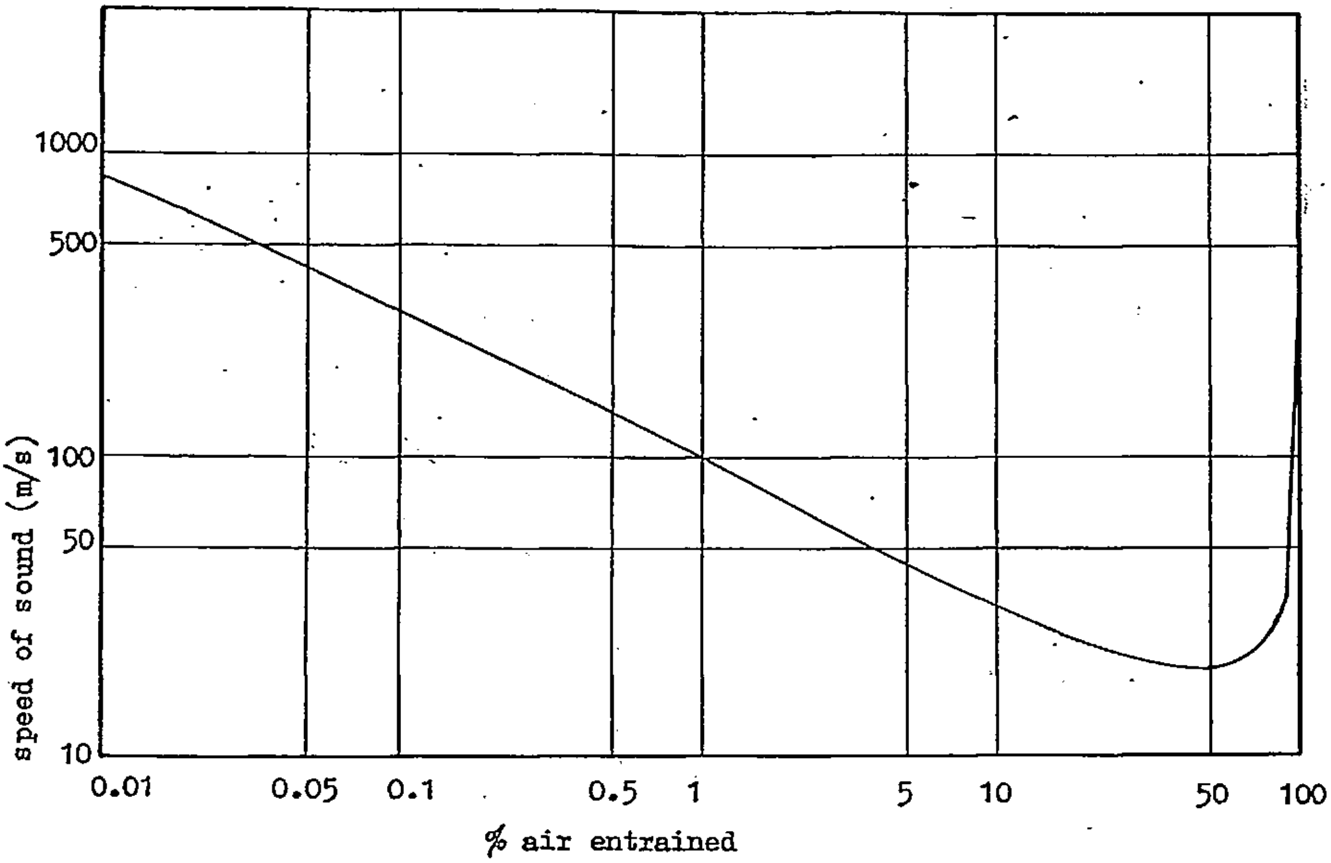

Figure 3.29 Velocity of sound in water with entrained air (after Lundgren 1969)

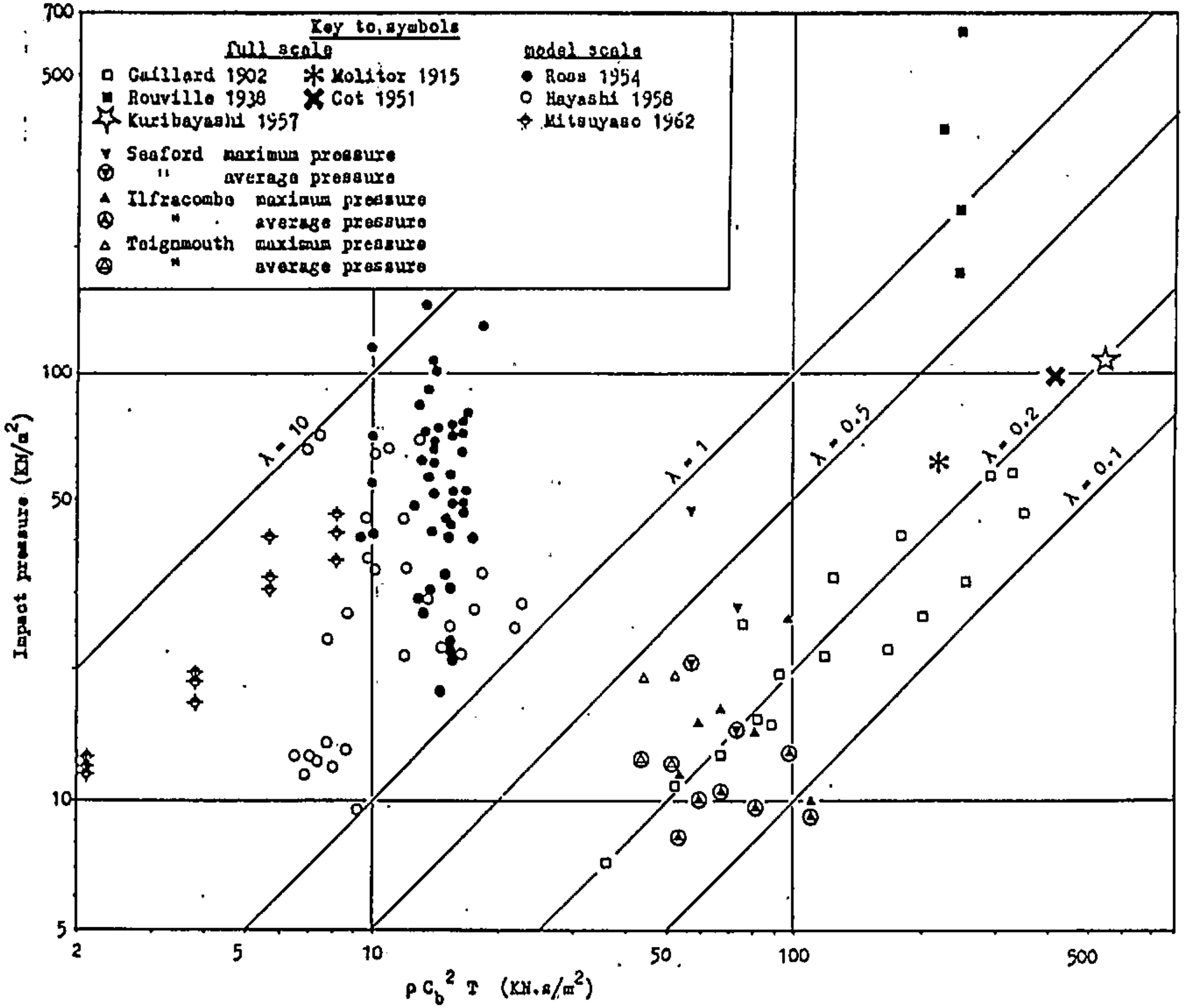

Figure 3.30 The dependence of impact pressure on the 'smoothness coefficient' (λ)

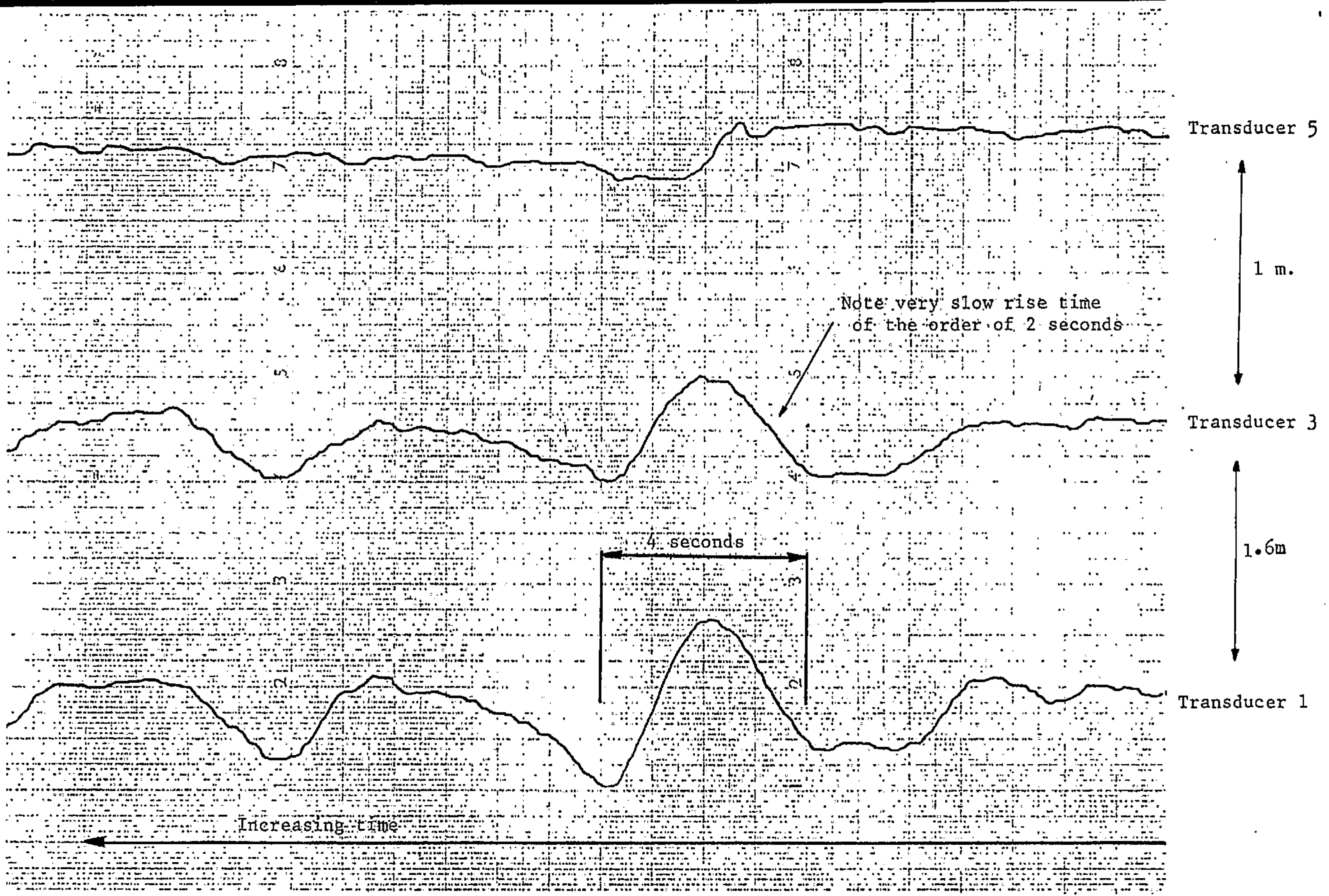

Figure 3.31 Typical pressure time history for standing waves (Recorded on Ilfracombe Seawall 25-11-80)

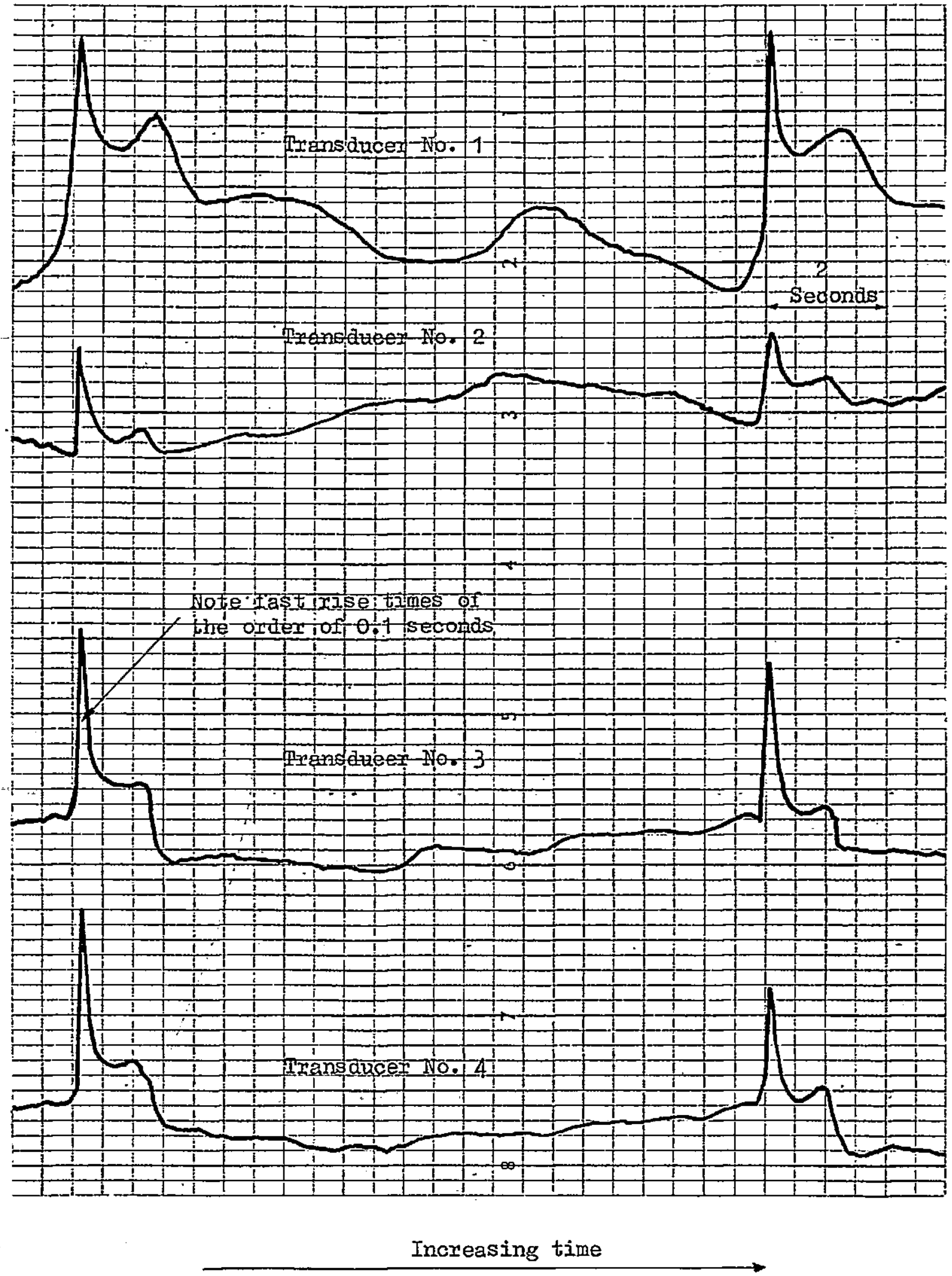

Figure 3.32 Typical pressure/time history of breaking waves (Recorded at Ilfracombe 3.2.81)

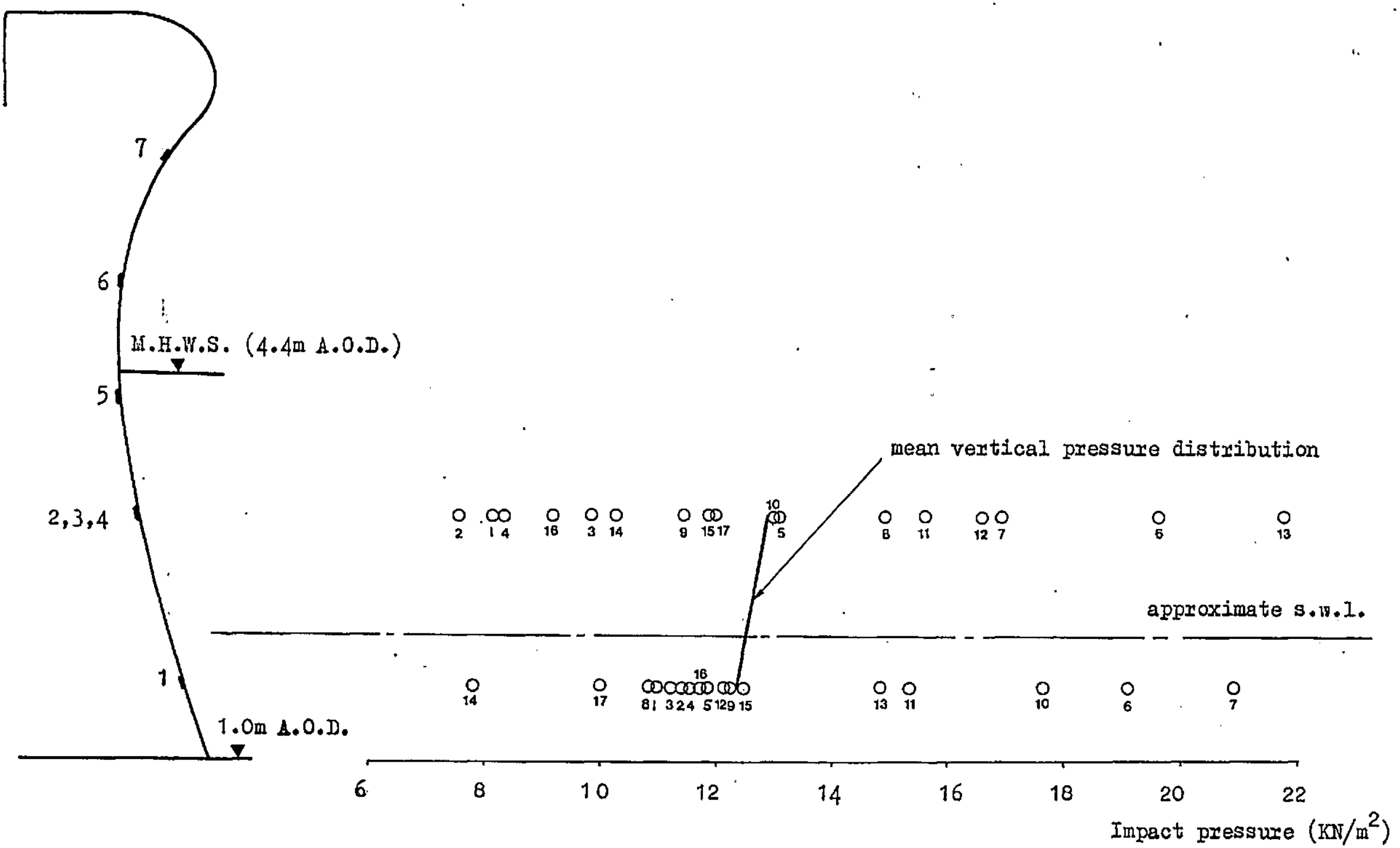

Figure 3.33 Vertical distribution of impact pressure on Ilfracombe seawall

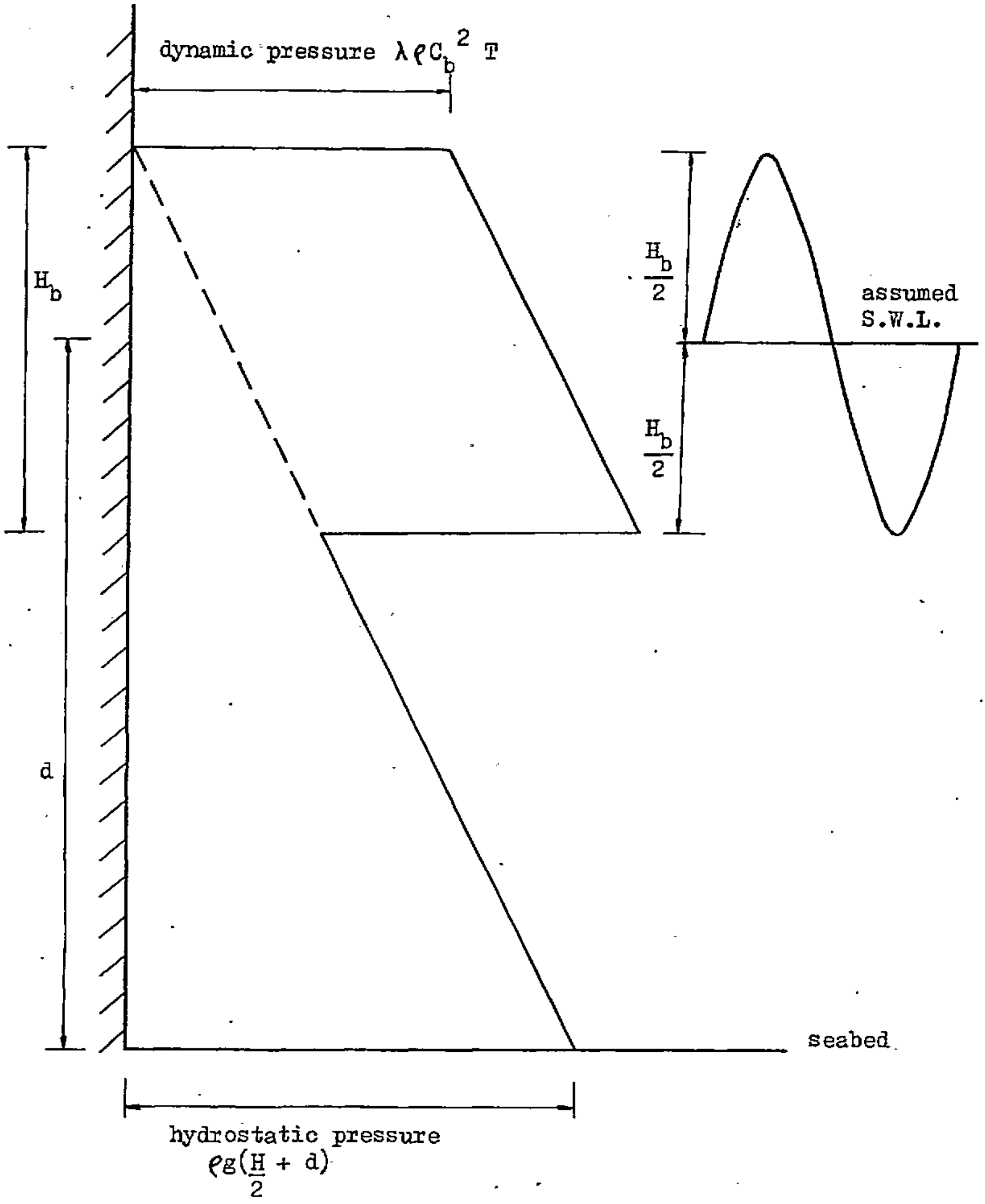
dynamic pressure $\lambda \rho C_b^2 T$
H_b
d
$\frac{H_b}{2}$
assumed S.W.L.
$\frac{H_b}{2}$
seabed
hydrostatic pressure
$\rho g(\frac{H}{2} + d)$

Figure 3.34 Proposed vertical pressure distribution for dynamic and static pressures.

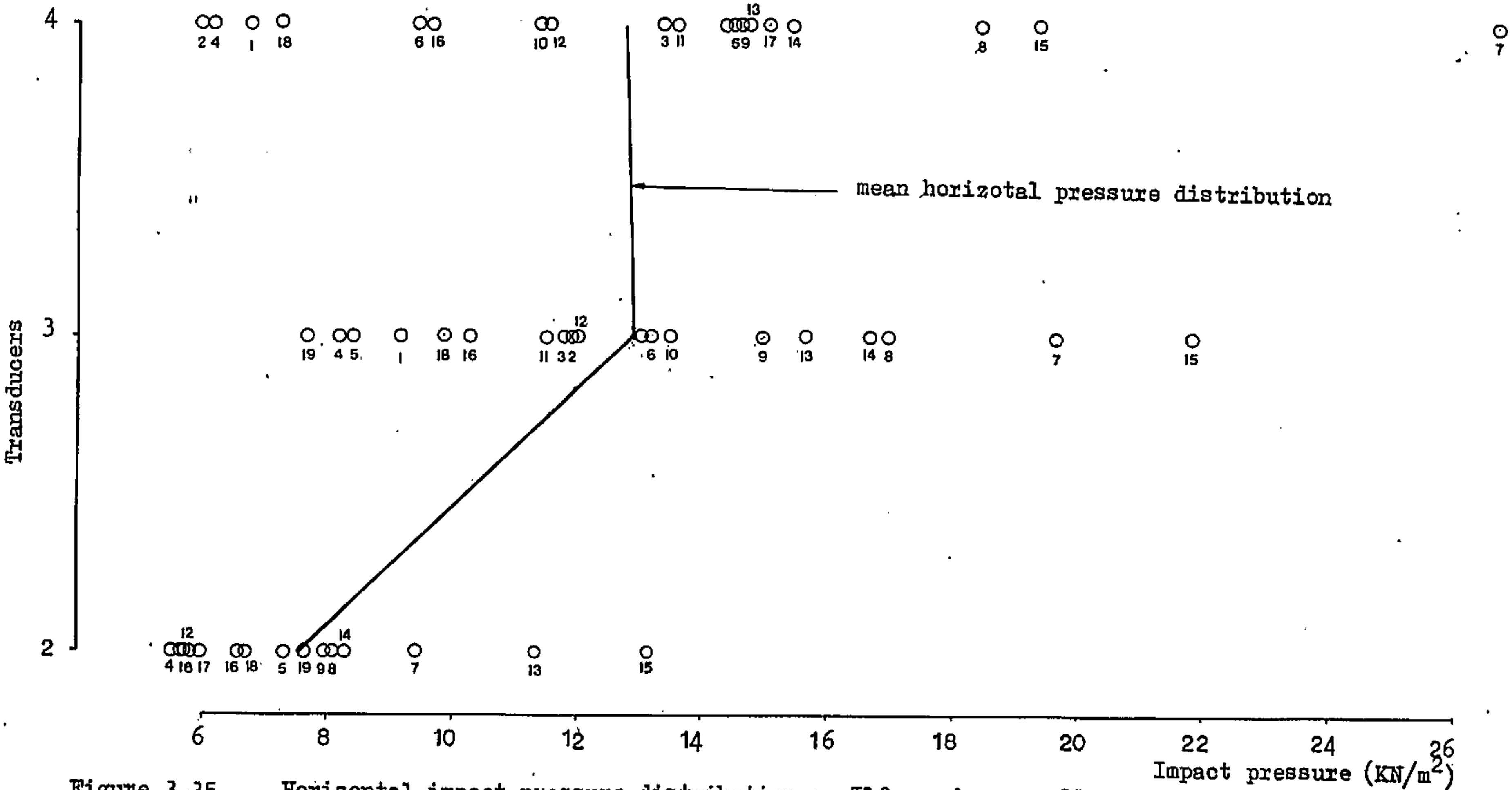

Figure 3.35 Horizontal impact pressure distribution on Ilfracombe seawall

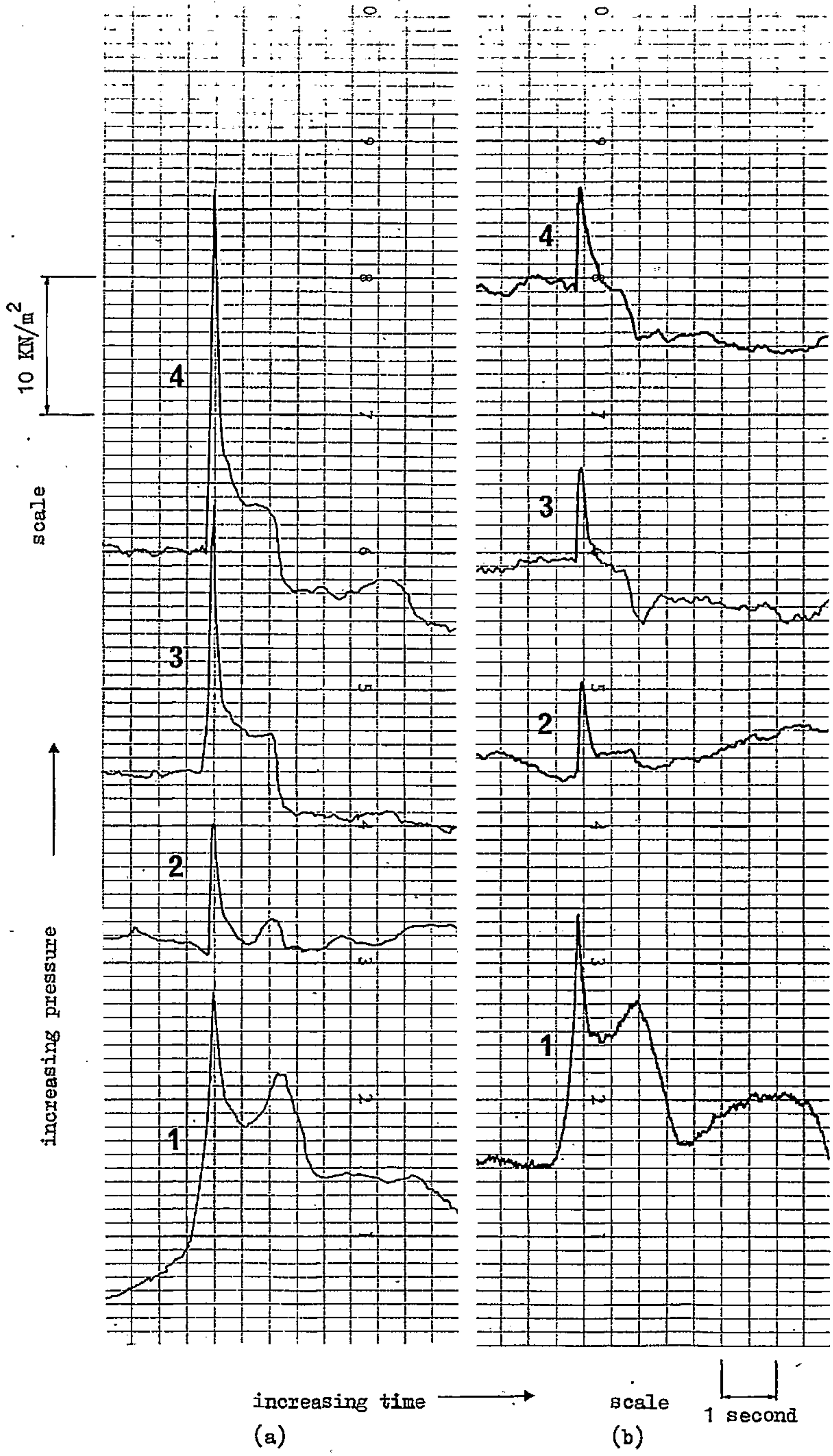

Figure 3.36 Synchronized pressure/time histories for impact on four transducers simultaneously

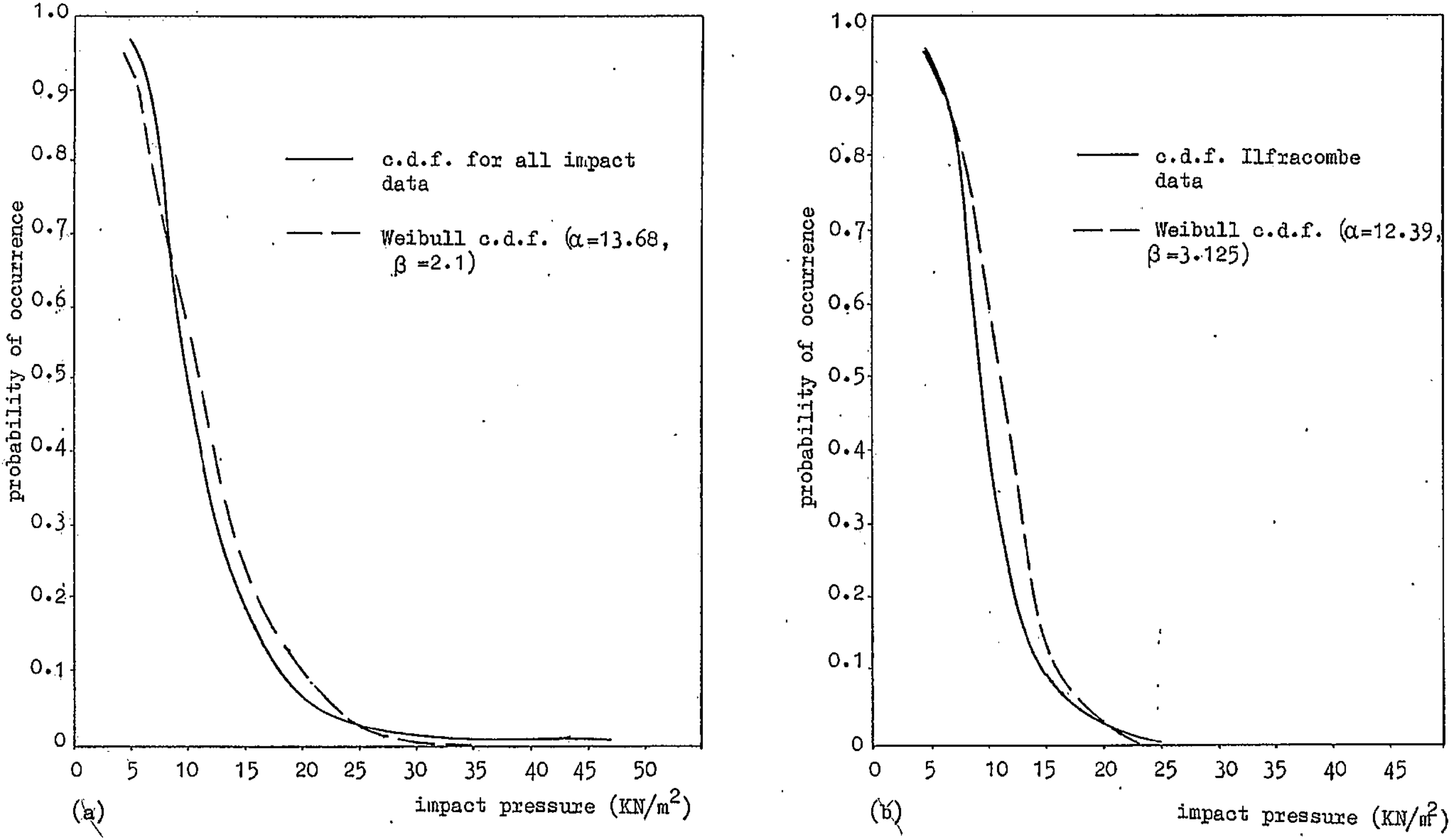

Figure 3.37 Observed and theoretical parent impact pressure distributions

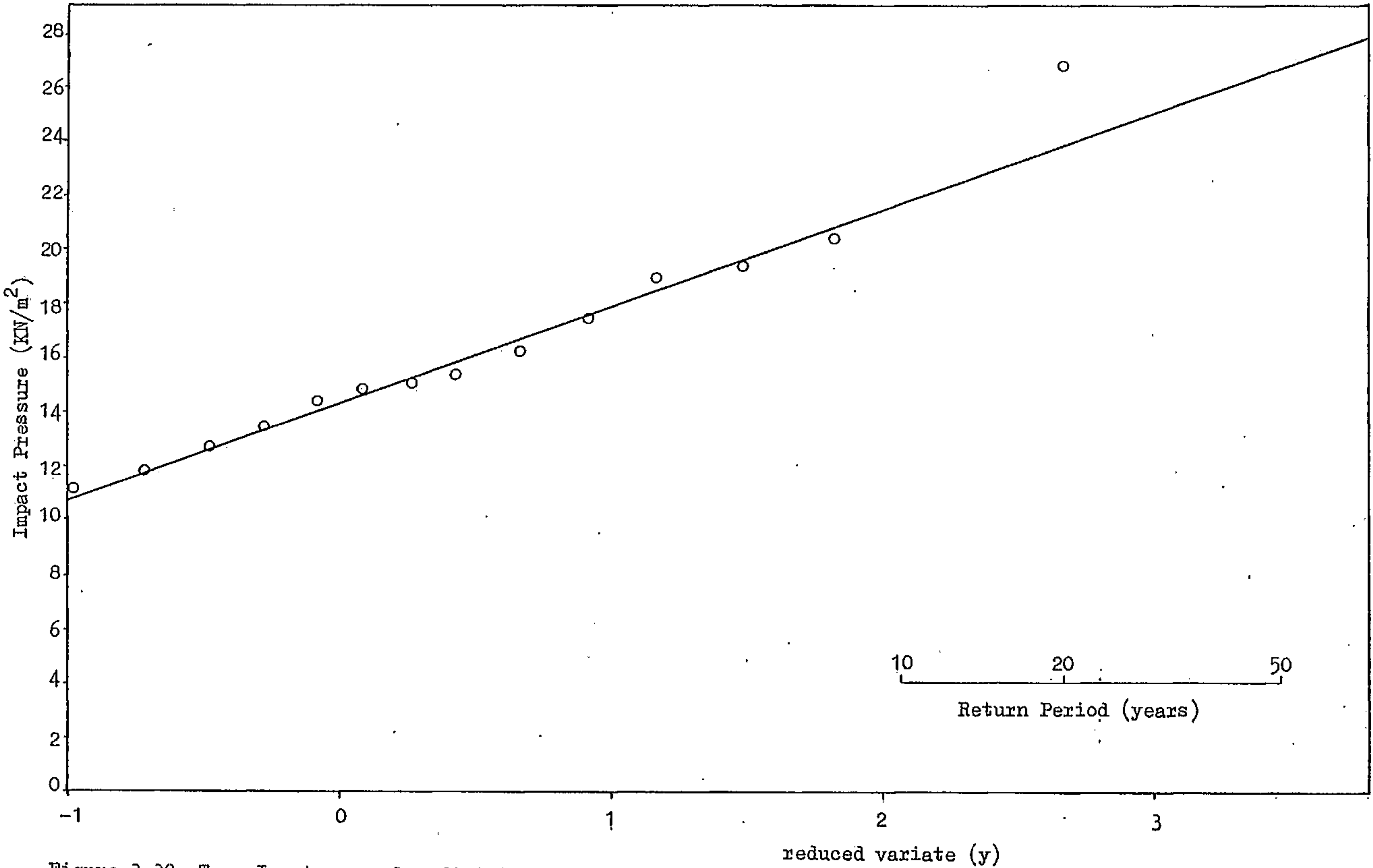

Figure 3.38 Type I extreme value distribution for wave impact pressures at Ilfracombe

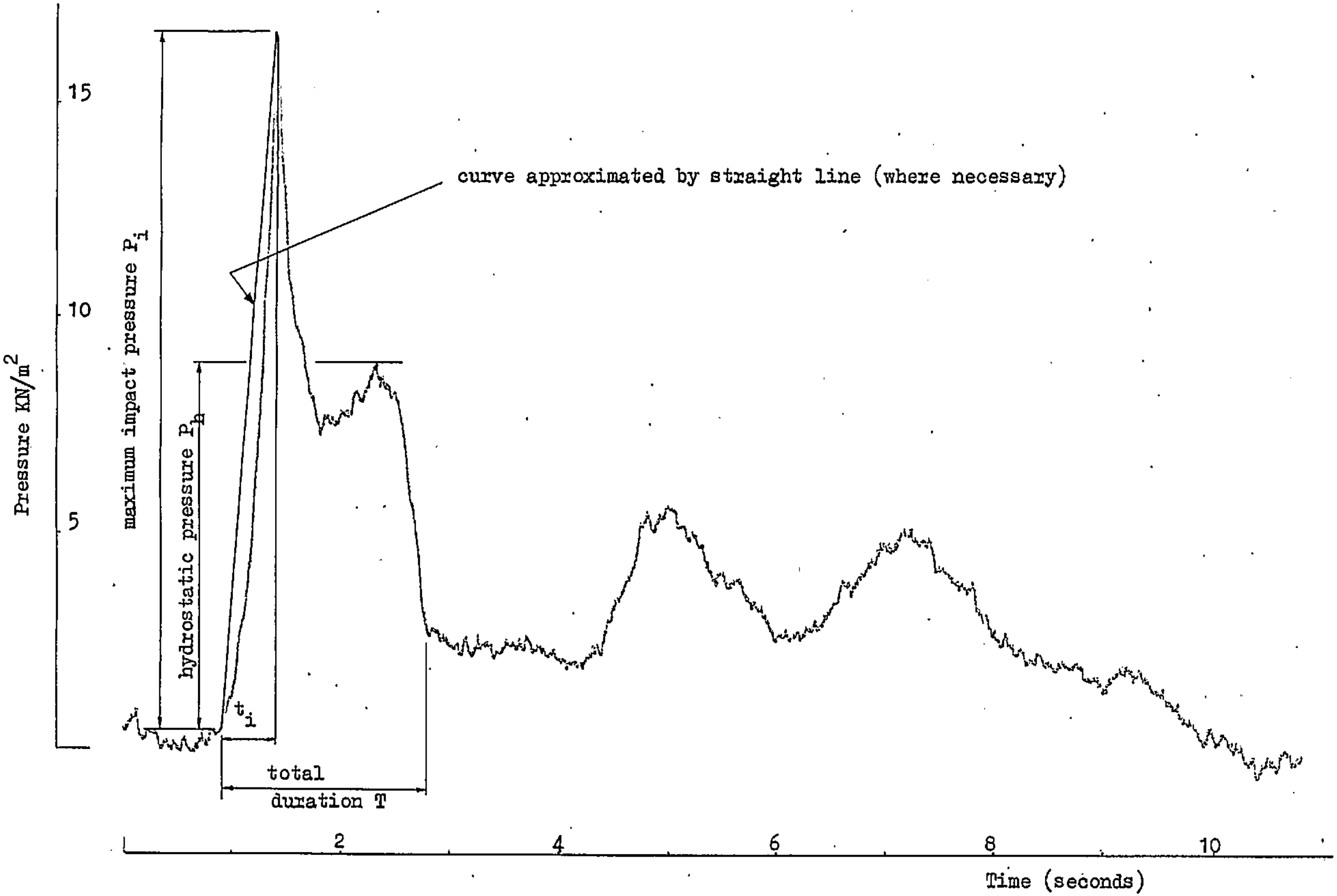

Figure 3.39 Typical pressure/time history of wave impact on Ilfracombe seawall

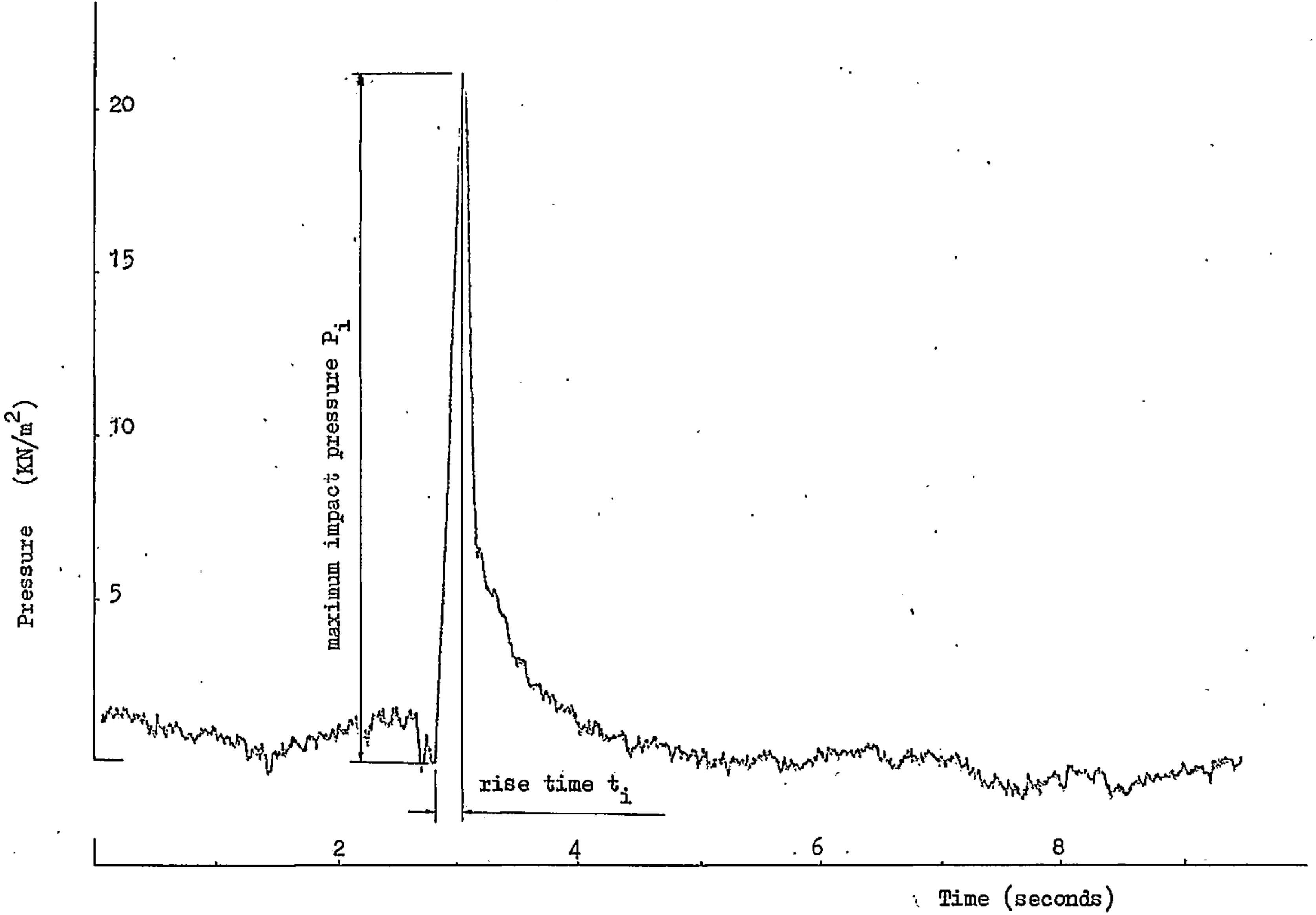

Figure 3.40 Typical pressure/time history of wave impact on Seaford seawall

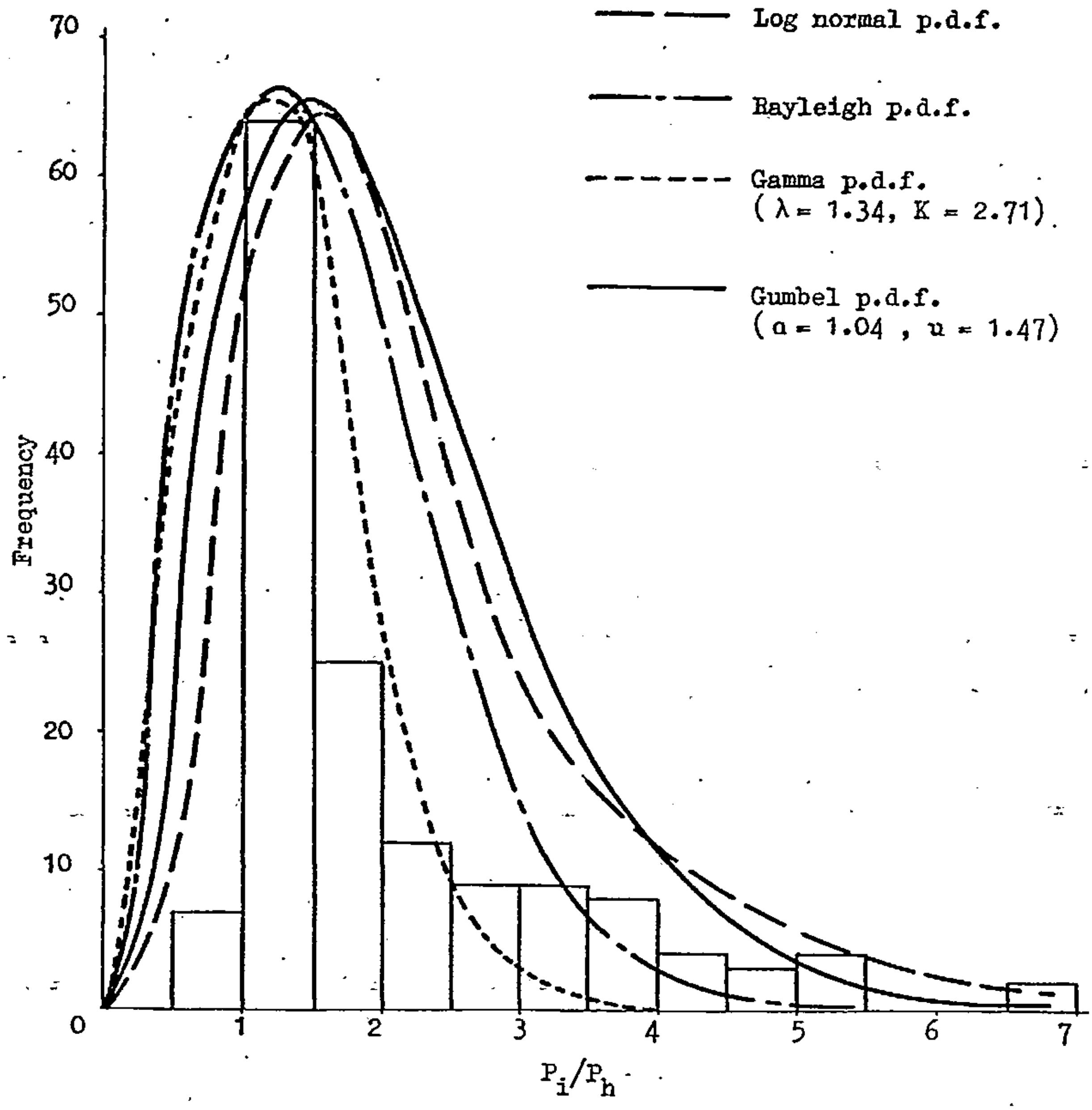

Figure 3.41: Frequency histogram of the ratio of impact pressure/hydrostatic pressure

Table 3.1 Summary of data recording sessions at Ilfracombe and Seaford

Tape Number	Site	Date	Length of Record	Channels of data	No. of impacts
2	Ilfracombe	14.3.80	1.6 hr	1	0
	"	15.3.80	1.5 hr	1	0
	"	16.3.80	1.5 hr	1	0
	"	17.3.80	1.1 hr	1	0
	"	18.3.80	1.7 hr	1	0
3	Seaford	26.11.80	1.7 hr	2	0
	"	27.11.80	3.0 hr	4	31
4	Teignmouth	7.11.78	2.1 hr	3	0
	"	6.12.78	1.1 hr	5	0
	"	7.12.78	2.8 hr	5	0
5	Ilfracombe	19.3.80	1.5 hr	3	0
	"	20.3.80	1.5 hr	3	0
	"	21.3.80	1.9 hr	3	0
6	Ilfracombe	24.11.80	4.5 hr	6	0
	"	25.11.80	3.5 hr	4	0
7	Seaford	20.9.80	1.9 hr	2	0
	Ilfracombe	24.9.80	1.0 hr	2	0
8	Seaford	18.3.80	2.0 hr	2	0
	"	19.3.80	3.1 hr	2	0
	"	20.3.80	1.7 hr	2	0
9	Seaford	23.1.80	3.9 hr	1	0
11	Seaford	20.10.80	2.0 hr	5	0
	"	21.10.80	3.2 hr	4	17
12	Ilfracombe	17.7.80	2.0 hr	3	0
	"	18.7.80	5.0 hr	4	0
13	Seaford	14.7.80	2.6 hr	1	0

Table 3.1 (cont.)

Tape Number	Site	Date	Length of Record	Channels of data	No. of impacts
14	Ilfracombe	21.1.81	3.0 hr	6	21
	"	22.1.81	3.7 hr	6	11
15	Ilfracombe	22.1.81	3.6 hr	6	14
	"	23.1.81	2.8 hr	6	0
16	Ilfracombe	3.2.81	3.5 hr	6	51
	"	4.2.81	2.9 hr	6	11
17	Ilfracombe	9.3.81	3.5 hr	7	4
	"	10.3.81	4.0 hr	7	0
19	Ilfracombe	6.4.81	3.4 hr	7	0
	"	7.4.81	3.3 hr	7	0
18	Ilfracombe	23.2.81	8.0 hr	6	0

Tape NO	Date	Site	$\bar{H}_b$ (m)	$\bar{C}_b$ (m/s)	$\bar{T}$ (sec)	$\bar{P}_i$ (KN/m^2)	$\bar{t}_i$ (sec)	$\overline{\text{Impulse}}$ (KN.s/m^2)	$\rho C_b H_b^2 T$ (KN.s/m)	No. of Impacts	$P_{i\ max}$ KN/m^2
11	21.10.80$_{pm}$	Seaford	0.90	3.64	4.3	20.44	0.16	1.89	51.28	17	48.9
14	21.01.81$_{pm}$	Ilfracombe	0.85	4.71	2.67	9.98	0.24	1.21	50.34	21	15.3
14	22.01.81$_{am}$	Ilfracombe	0.80	4.07	3.22	8.16	0.29	1.28	42.67	11	11.4
15	22.01.81$_{pm}$	Ilfracombe	1.00	4.16	3.87	10.31	0.25	1.25	66.97	14	26.7
16	03.02.81$_{pm}$	Ilfracombe	1.30	4.67	4.42	12.89	0.18	1.22	125.31	51	14.4
16	04.02.81$_{am}$	Ilfracombe	1.10	4.29	4.36	9.61	0.26	1.24	88.27	11	16.2
17	09.03.81	Ilfracombe	0.90	3.56	8.50	9.32	0.28	1.12	96.95	4	9.9
13	21.03.81	Teignmouth	0.90	3.30	4.00	12.62	0.22	1.29	39.20	17	19.1
5	07.05.81	Teignmouth	0.80	3.40	4.50	11.99	0.12	0.65	41.62	18	18.7
3	27.11.80	Seaford	1.20	4.22	4.12	14.05	0.12	0.88	88.04	31	27.7

Table No. 3.2 Summary of field data (quantities with a bar denote mean values).

Impact pressure data   Tape No. 11

Table NO. 3.3   Seaford 21.10.80

Impact Number	Transducer Number	Impact Pressure P_i (KN/m^2)	Rise Time t_i (sec)	Hydro-static Pressure P_i (KN/m^2)	Total Pressure Duration T (sec)	t_i/T $(x10^{-2})$	Impulse $P_i t_{i/2}$ $KN.s/m^2$	P_i/P_i
1	1	18.5	0.14	-	-	-	1.30	-
	2	5.5	0.16	-	-	-	0.44	-
	3	13.0	0.21	-	-	-	1.37	-
2	1	5.6	0.16	-	0.85	18.8	0.45	-
	2	9.8	0.15	-	1.05	14.3	0.74	-
	3	10.5	0.22	-	1.12	19.6	1.16	-
3	2	47.2	0.27	-	3.75	7.2	6.4	-
4	2	24.0	0.13	-	0.85	15.3	1.56	-
5	2	19.3	0.15	-	0.80	18.7	1.41	-
6	2	21.6	0.14	-	1.40	10.0	1.51	-
7	2	16.1	0.16	-	1.20	13.3	1.28	-
8	2	10.8	0.15	-	0.98	15.3	0.81	-
9	2	33.2	0.17	-	2.15	7.9	2.82	-
10	2	19.6	0.14	-	1.05	13.3	1.37	-
11	2	48.9	0.21	-	1.35	15.5	5.13	-
12	2	27.6	0.20	-	1.20	16.7	2.76	-
13	1	16.3	0.17	-	0.98	17.3	1.38	-

Impact pressure data

Tape No. 14

Table No. 3. 4

Ilfracombe 21.1.81

Impact Number	Transducer Number	Impact Pressure P_i KN/m^2	Rise Time t_i sec	Hydro-static Pressure P_h KN/m^2	Total Pressure Duration T sec	$t_{i/T}$ x10^{-2}	Impulse $P_i t_{i/2}$ KN.s/m^2	P_{i/P_h}
1	1	13.0	0.20	9.4	1.68	11.9	1.30	1.4
2	1	8.4	0.17	8.9	2.05	8.3	0.73	0.9
3	1	6.4	0.32	5.8	1.35	23.7	1.02	1.1
4	1	11.2	0.22	10.3	1.77	12.4	1.23	1.1
5	1	7.3	0.23	6.3	1.38	16.7	0.85	1.2
6	1	11.4	0.45	9.3	1.81	24.8	2.65	1.2
7	1	13.5	0.22	12.0	2.11	10.4	1.48	1.1
8	1	8.9	0.20	7.7	1.68	11.9	0.90	1.2
9	1	8.8	0.21	5.5	1.61	13.0	0.92	1.6
10	1	9.4	0.26	4.3	1.56	16.7	1.22	2.2
11	1	7.5	0.33	6.2	2.10	15.7	1.24	1.2
12	1	12.6	0.23	6.8	1.90	12.1	1.45	1.9
13	1	11.2	0.21	8.0	1.80	11.7	1.18	1.5
14	1	9.3	0.25	8.6	1.81	13.8	1.16	1.1
15	1	7.7	0.35	6.2	1.78	19.7	1.35	1.2
16	1	7.2	0.24	6.8	1.62	14.3	0.86	1.1
17	1	15.3	0.14	9.4	2.10	6.7	1.07	1.6
18	1	9.0	0.31	8.0	2.16	14.4	1.39	1.1
19	1	9.4	0.25	8.1	2.70	9.3	1.17	1.2
20	1	13.3	0.18	11.5	1.74	10.3	1.20	1.2
21	1	11.0	0.45	12.1	3.0	15.0	2.47	0.9
	2	5.4	0.46	3.9	1.95	23.6	1.24	1.4
	3	8.1	0.33	7.2	1.70	19.4	1.34	1.1
	4	6.1	0.38	7.2	1.70	19.5	1.16	0.8
22	1	11.4	0.36	12.0	2.7	13.3	2.05	1.0
	2	5.6	0.26	3.8	2.01	12.9	0.73	1.5
	3	7.6	0.22	6.1	1.60	13.8	0.84	1.2

Impact pressure data

Tape No. 14 (cont)

Table No. 3. 4

Ilfracombe 22.1.81

Impact Number	Transducer Number	Impact Pressure P_i (KN/m^2)	Rise Time t_i (sec)	Hydro-static Pressure P_j (KN/m^2)	Total Pressure Duration T (sec)	t_i/T $(x10^{-2})$	Impulse $P_i t_i/2$ $(KN.s/m^2)$	P_i/P_i
23	1	8.7	0.27	7.1	1.89	14.3	1.17	1.2
24	1	11.0	0.25	11.8	2.61	9.6	1.37	0.9
	2	6.6	0.30	4.7	2.05	14.6	0.99	1.4
	3	9.8	0.22	7.8	1.62	13.6	1.08	1.3
	4	7.2	0.23	7.8	1.71	13.5	0.83	0.9

Impact pressure data
Tape No. 15

Table No. 3.5
Ilfracombe 22.1.81

Impact Number	Transducer Number	Impact Pressure P_i KN/m^2	Rise Time t_i sec	Hydro-static Pressure P_h KN/m^2	Total Pressure Duration T sec	t_i/T x10^{-2}	Impulse $P_i t_i/2$ KN.s/m^2	P_i/P_h
1	1	11.7	0.22	8.4	1.31	16.8	1.29	1.4
2	1	8.1	0.23	6.2	1.38	16.7	0.93	1.3
3	1	8.6	0.22	8.2	1.58	13.9	0.95	1.0
4	1	9.5	0.29	9.4	1.95	14.9	1.38	1.0
5	1	8.3	0.31	6.8	1.81	17.1	1.29	1.2
6	1	8.5	0.37	8.0	1.94	19.1	1.57	1.1
7	1	12.0	0.20	10.6	2.5	8.0	1.20	1.1
8	1	8.0	0.30	7.4	2.05	14.6	1.20	1.1
9	1	9.1	0.24	7.8	1.55	15.5	1.09	1.2
10	1	14.4	0.19	8.9	2.0	9.5	1.37	1.6
11	1	11.7	0.21	9.6	1.85	11.3	1.23	1.2
12	1	16.2	0.16	8.8	1.69	9.5	1.30	1.8
13	1	7.7	0.29	8.1	1.9	15.3	1.12	1.0
14	1	10.6	0.31	9.7	2.15	14.4	1.64	1.1

Wave impact pressure data Tape No. 16

Table No. 3.6 Ilfracombe 3.2.81

Impact Number	Transducer Number	Impact Pressure P_i KN/m^2	Rise Time t_i sec	Hydro-static Pressure P_h KN/m^2	Total Pressure Duration T sec	t_i/T x10^{-2}	Impulse $P_i t_i/2$ KN.s/m^2	P_i/P_h
1	1	14.5	0.15	11.2	2.05	7.3	1.09	1.3
2	1	11.5	0.27	8.0	2.21	12.2	1.55	1.4
	2	7.2	0.17	2.3	1.35	12.6	0.62	3.1
	3	8.3	0.19	4.4	1.31	14.6	0.79	1.9
	4	14.4	0.14	4.5	1.33	8.4	1.01	3.2
3	1	11.8	0.32	9.5	2.15	14.9	1.89	1.2
	2	5.6	0.20	1.5	1.30	15.4	0.56	3.7
	3	13.1	0.19	4.0	1.31	14.5	1.24	3.3
	4	9.4	0.19	4.5	1.24	15.3	0.89	2.1
4	1	19.1	0.46	13.0	2.05	7.8	1.53	1.5
	2	9.3	0.18	2.6	1.42	12.7	0.84	3.6
	3	19.6	0.14	6.1	1.45	8.3	1.37	3.2
	4	26.7	0.12	6.5	1.35	8.9	1.60	4.1
5	1	20.9	0.14	13.7	2.25	6.2	1.46	1.5
	2	8.0	0.28	4.3	1.45	19.3	1.12	1.9
	3	16.9	0.16	4.8	1.5	10.7	1.35	3.5
	4	18.4	0.14	5.8	1.46	8.9	1.29	3.2
6	1	6.8	0.28	4.8	2.0	14.0	0.95	1.4
7	1	10.8	0.23	8.3	2.1	11.0	1.24	1.3
	2	8.0	0.16	2.1	1.5	10.7	0.64	3.8
	3	14.9	0.15	5.6	1.31	11.5	1.12	2.7
	4	14.7	0.18	5.4	1.28	7.8	1.32	2.7
8	3	13.4	0.20	3.6	1.20	16.7	1.34	3.7
	4	11.3	0.17	4.2	1.15	13.9	0.96	2.7
9	1	12.2	0.35	12.2	2.70	13.0	2.14	1.0
	3	11.4	0.18	9.8	1.60	11.3	1.03	1.2
	4	13.3	0.21	10.6	1.71	12.3	1.40	1.3

Table No. 3.6 Ilfracombe 3.2.81

Impact Number	Transducer Number	Impact Pressure P_i KN/m^2	Rise Time t_i sec	Hydro-static Pressure P_h KN/m^2	Total Pressure Duration T sec	t_i/T $x10^{-2}$	Impulse $P_i t_i/2$ $KN.s/m^2$	P_i/P_h
10	1	17.6	0.16	13.6	2.05	7.8	1.41	1.3
	2	5.6	0.19	2.1	1.65	13.3	0.53	2.7
	3	13.0	0.14	5.8	1.60	8.8	0.91	2.2
	4	11.4	0.18	5.2	1.50	12.0	1.03	2.2
11	1	15.3	0.21	10.2	2.5	8.4	1.61	1.5
	2	11.2	0.16	2.3	1.25	12.8	0.91	4.9
	3	15.6	0.17	5.0	1.27	11.8	1.33	3.1
	4	14.6	0.16	6.3	1.30	10.0	1.17	2.3
12	1	12.1	0.19	8.5	2.23	8.5	1.15	1.4
	2	7.9	0.16	2.3	1.50	10.7	0.63	3.4
	3	16.6	0.15	6.4	1.55	9.7	1.24	2.6
	4	15.4	0.16	6.3	1.52	10.5	1.23	2.4
13	1	14.8	0.17	10.7	2.05	8.3	1.26	1.4
	2	13.0	0.16	5.6	1.59	8.8	1.04	2.3
	3	21.8	0.14	6.6	1.60	8.8	1.49	3.3
	4	19.3	0.13	6.0	1.65	7.3	1.25	3.2
14	1	7.8	0.39	6.6	2.15	18.1	1.52	1.2
	2	6.5	0.20	2.9	1.35	14.8	0.65	2.2
	3	10.2	0.24	7.3	1.50	16.0	1.22	1.4
	4	9.6	0.25	7.1	1.45	17.2	1.20	1.4
15	1	12.4	0.24	13.2	2.32	10.3	1.49	0.9
	2	5.7	0.22	5.9	1.72	12.8	0.63	1.0
	3	11.8	0.17	11.4	1.80	9.4	1.01	1.0
	4	15.0	0.18	11.2	2.1	8.6	1.35	1.3

Impact pressure data Tape No. 16

Table No. 3.7 Ilfracombe 4.2.81

Impact Number	Transducer Number	Impact Pressure P_i KN/m^2	Rise Time t_i sec	Hydrostatic Pressure P_h KN/m^2	Total Pressure Duration T sec	t_i/T x10^{-2}	Impulse $P_i t_i/2$ KN.s/m^2	P_i/P_h
1	1	11.8	0.35	11.4	2.40	14.6	2.00	1.0
	3	9.1	0.30	8.9	1.7	17.6	1.36	1.0
	4	6.7	0.41	9.2	1.8	22.7	1.37	0.7
2	1	10.0	0.27	7.7	2.0	13.5	1.35	1.3
	3	11.9	0.17	4.3	1.32	12.9	1.01	2.8
	4	5.9	0.28	4.9	1.45	19.3	0.83	1.2
3	3	11.8	0.25	5.4	1.55	16.1	1.48	2.2
	4	14.4	0.18	5.6	1.45	12.4	1.30	2.6
4	1	7.0	0.29	6.5	2.0	14.5	1.02	1.1
5	1	6.5	0.27	4.4	1.6	16.9	0.88	1.5
6	1	11.2	0.20	7.3	1.88	10.6	1.12	1.5

Impact pressure data

Tape No. 17

Table No. 3.8

Ilfracombe 10.3.81

Impact Number	Transducer Number	Impact Pressure P_i KN/m^2	Rise Time t_i sec	Hydro-ststic Pressure P_h KN/m^2	Total Pressure Duration T sec	t_i/T $x10^{-2}$	Impulse $P_i t_i/2$ $KN.s/m^2$	P_i/P_h
1	1	8.3	0.27	7.8	1.65	16.4	1.12	1.1
2	1	9.7	0.24	6.6	1.64	14.6	1.16	1.5
3	1	9.4	0.32	6.5	1.88	17.0	1.50	1.4
4	1	9.9	0.29	6.5	2.1	13.8	1.43	1.5

Impact pressure data

Tape No. 5

Table No. 3.9

Teignmouth 7.5.81

Impact Number	Transdcer Number	Impact Pressure P_i KN/m^2	Rise Time t_i sec	Hydro-ststic Pressure P_h KN/m^2	Total Pressure Duration T sec	t_i/T x10^{-2}	Impulse $P_i t_i/2$ KN.s/m^2	P_i/P_h
1	1	12.1	0.12	2.4	1.3	9.23	0.73	5.0
2	1	8.0	0.13	1.7	1.05	12.38	0.52	4.7
3	1	7.5	0.14	3.3	1.1	12.73	0.53	2.3
4	1	14.5	0.14	4.0	1.1	12.73	1.02	3.5
5	1	6.6	0.24	3.3	1.4	15.7	0.73	2.0
6	1	6.4	0.18	3.2	1.2	15.0	0.58	5.3
7	1	8.0	0.09	2.8	1.1	8.18	0.36	2.9
8	1	10.7	0.08	2.9	1.2	6.67	0.43	3.7
9	1	9.5	0.10	3.3	1.35	7.41	0.48	2.9
10	1	10.4	0.09	2.6	1.2	7.5	0.47	4.0
11	1	11.5	0.12	2.8	1.35	8.89	0.69	4.1
12	1	11.3	0.07	2.2	1.25	5.6	0.40	5.1
13	1	18.7	0.09	2.8	1.2	7.5	0.84	6.7
14	1	13.5	0.08	2.9	1.2	6.67	0.54	4.7
15	1	18.3	0.10	2.8	1.35	7.41	0.92	6.5
16	1	18.6	0.08	3.5	1.25	6.40	0.74	5.3
17	1	18.1	0.09	5.2	1.45	6.21	0.81	3.5
18	1	12.1	0.16	6.0	1.5	10.67	0.97	2.0

Impact pressure data

Tape No. 13

Table No. 3.10

Teignmouth 21.3.81

impact number	transducer number	impact pressure P_i (KN/m^2)	rise time t_i (sec)	hydro-static pressure P_h (KN/m^2)	total pressure duration T (sec)	t_i/T ($x10^{-2}$)	impulse $P_i t_i/2$ (KN.s/m^2)	P_i/P_h
1	1	12.7	0.12	5.2	1.55	7.74	0.76	2.4
	2	8.4	0.22	5.3	1.5	14.7	0.92	1.6
2	1	12.6	0.25	10.3	1.9	13.16	1.57	1.2
	2	12.4	0.32	8.3	1.8	17.78	1.98	1.5
3	1	11.2	0.14	8.4	1.8	7.78	0.78	1.3
	2	9.4	0.19	5.8	1.7	11.18	0.89	1.6
4	1	9.4	0.29	8.1	2.3	12.61	1.36	1.2
	2	8.0	0.15	7.0	2.1	7.14	0.60	1.1
5	1	10.2	0.22	7.9	2.25	9.78	1.12	1.3
	2	12.3	0.31	7.6	1.85	16.76	1.91	1.6
6	2	12.5	0.12	7.3	2.2	5.45	0.75	1.7
7	1	16.5	0.20	11.0	2.2	9.10	1.65	1.5
	2	15.3	0.26	9.2	2.05	12.68	1.98	1.7
8	1	13.0	0.20	7.0	1.6	12.6	1.30	1.9
9	2	19.1	0.19	5.0	1.55	12.26	1.81	3.8
10	1	16.0	0.17	10.5	2.15	7.91	1.36	1.5
	2	15.6	0.32	10.2	2.0	16.0	2.50	1.5

Impact pressure data　　　　　　　　　　Tape No. 3

Table No. 3.11　　　　　　　　　　Seaford 27.11.80

Impact Number	Transducer Number	Impact Pressure P_i KN/m^2	Rise Time t_i sec	Hydro-static Pressure P_h KN/m^2	Total Pressure Duration T sec	t_i/T $x10^{-2}$	Impulse $P_i t_i/2$ $KN.s/m^2$	P_i/P_h
1	1	12.4	0.12	-	1.2	10.0	0.74	-
2	1	13.2	0.08	-	1.4	5.7	0.53	-
3	1	11.9	0.17	-	1.35	12.6	1.01	-
4	1	27.7	0.15	5.1	1.9	7.9	2.08	5.4
5	1	9.4	0.10	-	1.25	8.0	0.47	-
6	1	10.6	0.09	-	1.45	6.2	0.48	-
7	1	17.3	0.18	5.8	1.55	11.6	1.56	3.0
8	1	17.0	0.12	-	1.7	7.1	1.02	-
9	1	11.0	0.10	-	1.15	8.7	0.55	-
10	1	16.0	0.12	8.6	1.62	7.4	0.96	1.9
11	1	19.4	0.08	-	1.75	4.6	0.78	-
12	1	10.4	0.11	4.3	1.30	8.5	0.57	2.4
13	1	12.4	0.12	-	1.55	7.7	0.74	-
14	1	13.0	0.13	-	1.70	7.6	0.84	-
15	1	21.9	0.15	-	1.55	7.7	1.64	-
16	1	9.5	0.14	-	0.90	14.7	0.67	-
17	1	8.9	0.14	-	1.7	8.2	0.62	-
18	1	16.9	0.12	-	1.55	7.7	1.01	-
19	1	16.2	0.18	-	1.05	17.1	1.46	-
20	1	13.8	0.10	-	1.60	6.2	0.69	-
21	1	12.4	0.09	-	1.35	6.7	0.56	-
22	1	11.1	0.10	5.1	1.50	6.7	0.56	2.2
23	1	11.9	0.16	6.2	1.75	9.1	0.95	1.9
24	1	11.2	0.19	-	1.40	13.6	1.06	-

Table No. 3.11

Seaford 27.11.80

Impact Number	Transducer Number	Impact Pressure P_i KN/m^2	Rise Time t_i sec	Hydro-static Pressure P_h KN/m^2	Total Pressure Duration T sec	t_i/T $x10^{-2}$	Impulse $P_i t_i/2$ $KN.s/m^2$	P_i/P_h
25	1	13.0	0.11	-	1.35	8.1	0.71	-
26	1	13.0	0.16	8.2	1.90	8.4	1.04	1.6
27	1	14.2	0.11	-	1.31	8.4	0.79	-
28	1	15.4	0.09	-	1.40	6.4	0.69	-
29	1	15.9	0.10	-	1.70	5.9	0.79	-
30	1	12.0	0.11	5.0	1.25	8.8	0.66	2.4
31	1	14.1	0.12	6.4	1.75	6.8	0.85	2.2

Site	Date	Tape No.	Spectral density analysis		Correlation	Visual		
			range of predominant wave periods	length of sample analysed	average wave period from correlograms	min & max observed wave period	number of observations	average wave period
Seaford	21-10-80	11	10 to 2 sec	33.3 minutes	3.9 sec	2 to 8 sec	37	4.3 sec
Seaford	27-11-80	3	10 to 2 sec	33.3 minutes	3.7 sec	3 to 10 sec	61	4.2 sec
Ilfracombe	21-1-81	14	6.7 to 2.5 s	66.6 minutes	2.6 sec	2 to 6 sec	42	2.7 sec
Ilfracombe	22-1-81	14	10 to 2.5 s	66.6 minutes	2.9 sec	2 to 7 sec	92	3.2 sec
Ilfracombe	22-1-81	15	10 to 3.3 s	33.3 minutes	3.5 sec	2 to 7 sec	31	3.9 sec
Ilfracombe	3-2-81	16	-	-	-	2 to 10 sec	46	4.4 sec
Ilfracombe	4-2-81	16	-	-	-	2 to 9 sec	52	4.4 sec
Ilfracombe	9-3-81	17	13.3 to 4 s	29.2 minutes	7.7 sec	6 to 11 sec	27	8.5 sec

Table 3.12 Comparison between visual measurements of wave period and those obtained from spectral density and correlation analysis.

Sample Number	Maxima (KN/m^2)	Rank	Cumulative Prob $\frac{m}{n+1}$	Reduced Variate (y)
1	13.5	4	.267	- 0.278
2	12.6	3	.200	- 0.476
3	15.3	8	.533	0.436
4	11.4	1	.067	- 0.990
5	12.0	2	.133	- 0.700
6	16.2	9	.600	0.672
7	19.1	11	.733	1.169
8	26.7	14	.933	2.668
9	14.9	6	.400	0.087
10	17.6	10	.667	0.904
11	21.6	13	.867	1.947
12	19.3	12	.800	1.500
13	15.0	7	.467	0.273
14	14.4	5	.333	- 0.095

Table 3.13 Reduced variate y for a Fisher - Tippett type I extreme value distribution.

CHAPTER FOUR

DISCUSSION

There have been only twelve previous full scale investigations (Table 1.1) which have measured wave impact pressures on coastal structures, and of this data most is either unreliable due to crude instrumentation or inconclusive because of insufficient quantity. The difficulty in measuring real wave impact pressures led to many model studies in the laboratory, under these controlled conditions large quantities of data were generated but satisfactory scaling of this data up to full size waves was not achieved. Therefore there is an obvious need for additional reliable full scale data on the pressures produced by breaking waves in a real sea and the distribution of these pressures over the face of a structure.

This investigation has gone a long way towards fulfilling this need and has amassed more wave impact pressure data than the sum of all previous full scale investigations. The transducers developed to measure these pressures are capable of responding to wave impacts of less than one milli-second duration, are cheap to manufacture, self contained and versatile. This pressure measuring system is attached to the seawalls by a single bolt fixing and so is suitable for mounting on the face of almost any type of seawall or similar coastal structure with a minimum of expense and installation problems.

4.1 The Measurement of Wave Parameters

The local wave parameters C_b, H_b and T were measured as close to the seawalls as was possible, so for most purposes these values can be assumed to be those actually occurring at the seawalls at the moment of impact. The exact location at which these parameters were measured was a compromise between being close to the wall and being out of the region of disturbance caused by the wall, so that individual wave crests could still be picked out. By measuring wave parameters at the seawalls the total number of variables needed to define the conditions at impact were reduced to just three (C_b, H_b and T), as shown in Section 3.5. Previous equations for estimating wave impact pressures were often written in terms of parameters which were not clearly defined or else were difficult to measure, i.e. Salih-Kirgoz(36) gave an equation derived from his model studies in terms of beach slope, most beaches do not have a perfectly uniform slope and some are uneven and rocky and affected by scour which could change the slope during the course of each tide (as at Seaford), therefore beach slope is not easy to estimate for real beaches. Molitor(5) gave an impact pressure equation in terms of water particle orbital velocity, this cannot be easily measured at the instant of impact in a real sea and cannot be calculated because waves in shoaling water generally change from oscillatory to translatory as they approach the wall, so the exact orbital velocity at any point cannot be found. Minikin's equation(72) was developed for composite breakwaters in fairly deep water and so contains a parameter of water depth at the toe of the mound (D). This equation was modified in Ref.74 for use on seawalls but it still contains this deep water parameter which now becomes irrelevant and difficult to measure. Other impact pressure equations from Gaillard(3), Hiroi(4) and others contain the parameters H (wave height) and C (wave celerity), but do not specify where these parameters were measured in relation to the seawall.

Thus by specifing the measurement of C_b, H_b and T at the seawall it reduces the number of variables to three because the influence of factors such as beach slope and water depth is already included in C_b, H_b and T when measured at the seawall.

The parameters C_b, H_b and T were all measured in a number of ways by both visual and instrumental methods, as discussed in Chapter Two. At Ilfracombe, especially, the instrumental records were very difficult to interpret because individual wave crests could not often be picked out due to wave breaking in the region of the pressure transducers and because of the severe reflection and refraction induced by the rocky seabed. Wave celerity calculated from the relationship $C = (gd)^{\frac{1}{2}}$ was necessarily prone to errors because of changes in the S.W.L. caused by the tide and more importantly the level of the rocky seabed between the wave staff and the seawall was so irregular that the wave celerity did not have time to adjust to each new change in level, (d could vary by over 1m in a 20cm length of seabed at Ilfracombe, Figure 2.21). So, as the wave celerity could not respond instantly to changes in water depth then the value calculated from $C = (gd)^{\frac{1}{2}}$ could only be expected to be very approximate, hence the fairly large differences between this value and the value obtained visually.

Therefore the most reliable measures of C_b, H_b and T were regarded

as being those obtained visually. Visual measurements of wave parameters at rocky sites such as Ilfracombe have important advantages over instrumental measurements because in a confused sea state with a high degree of wave reflection it is possible to be selective with visual measurements and so obtain fair estimates of the wave parameters by ignoring reflected waves. Whereas instrumental records obtained close to the wall are likely to be contaminated by reflected waves, and so give distorted estimates of the wave parameters.

4.2 The Impulse Momentum Relationship

The impulse momentum relationship (equations 3.35 and 3.36) appears to describe the phenomenon of wave breaking quite well, as evidenced by Figure 3.24. Equations 3.35 and 3.36 are based on the gross kinematics of the wave impact and are written in terms of the local wave celerity (C_b), wave period (T) and local wave height (H_b). The equations were written in these general terms at breaking so that they would be applicable to waves of any type (i.e. oscillatory, solitary, random) assuming wave celerity can be used to represent the actual water particle velocity. Other authors (Denny(13), Carr(39)) derived equations based on the impulse momentum equation but for the particular case of a solitary wave, they reduced the equation by making various approximations so that the impact pressure was a function solely of wave height, thereby limiting the applicability of their equations to solitary waves of maximum height and steepness.

From their model studies Denny and Carr found that the fraction of wave momentum destroyed in producing the shock impulse on the wall approached a definite maximum value, given as 0.07 (Denny) and 0.11 (Carr). These values are directly equivalent to the coefficient K' in equation 3.35, the maximum value of K' possible from equation 3.35 is 0.044 (for $H_b/L_b = 1/7$), this is slightly lower than the values given by Denny and Carr. This difference in K' values was shown to be due to the approximations made by Denny and Carr (see Chapter Three Section 3.5) which tended to overestimate K' for waves of less than limiting steepness.

The relationship between wave momentum and wave impulse at breaking appears to be linear, (Figure 3.24), this means a fixed percentage of wave momentum is transformed into impulse energy, the exact percentage (given by equation 3.35) depends on the wave steepness at breaking and varies from about ½ to 4½%. Equation 3.35 applies equally well to both model and full scale breaking waves, but the exact value of the coefficient K' is open to discussion because the lack of data in Figure 3.25 allows a range of slopes to be chosen. This lack of data from other investigations is also apparent in Figure 3.24, this is because very few authors have measured the breaking wave impulse (or measured the rise time, which would allow calculation of the impulse), so their data cannot be used for comparison.

4.3 Wave impact Pressures

4.3.1 Proposed Equations

Gaillard(3), in the late Nineteenth Century was the first to

consider the phenomenon of wave breaking in any great detail. He came to the conclusion that a breaking wave impact was similar to a jet of water impacting upon a flat plate, and gave the wave impact pressure in terms of the stagnation pressure $(\frac{1}{2}\rho V^2)$, with an additional coefficient to account for non-steady flow. Most other full scale investigations adopted this equation with differing empirical coefficients. Then in the 1930's Bagnold$^{(14)}$, from his model studies, developed a theoretical model to explain the generation of wave impact pressures, he came to the conclusion that impact pressures were the result of the compression of a thin lens of air trapped between the wave front and the seawall. The thickness of this hypothetical air cushion was never actually measured by Bagnold and so his theoretical model was not validated by his experimental data. The above two theories were the most popular for explaining the generation of wave impact pressures and later investigations generally adopted either one or the other.

In this investigation, pressure transducers were mounted on the seawalls in such a way as to exclude an air cushion from between the wave front and the wall, but impact pressures still occurred. So it seems that the compression of a trapped air cushion is not the major factor governing the generation of wave impact pressures.

Gaillards equation was found to provide a poor fit to the available data, which included data from this investigation and some model scale data, as shown in Figure 3.18. This suggested that there was some additional unknown parameter influencing the generation of wave impact pressures. Upon examination of the impact pressure

histories of both real and model wave impacts there was found to be little difference in the magnitudes of the maximum impact pressures, but the rise times of real sea wave impacts were found to last 2 or 3 times longer than those of model waves, (Figure 3.28). The rise time is the time taken for the wave impact to reach its maximum value and depends on the density of the impinging air/water mixture in the wave(52). When air is entrained in the wave the speed of sound through this air/water mixture is greatly reduced (Figure 3.29), as real waves generally contain relatively large volumes of entrained air then their impact pressures will be developed much more slowly than model wave impact pressures.

A breaking wave was found to convert a fixed percentage of its momentum into impulse energy (Figure 3.24), thus as impulse $\simeq P_i t_i/2$, if the rise time increases then the impact pressure must decrease. So wave impact pressure seems to be directly proportional to the percentage of air entrained in the breaking wave. The volume of air entrained in a real sea wave cannot be measured, especially where the wave breaks and reforms as in shoaling waters. This percentage of entrained air, while not lending itself to precise measurement, must be related in shoaling water to the type of seabed (among other things). A rocky beach is likely to produce a confused sea state and a large amount of 'white water', whereas a smooth beach with uniform slope will not generally cause a wave to break until it becomes depth limited. None of the many previous empirical equations for estimating impact pressure have considered the effect of air entrainment, and the phenomenon of wave breaking is still insufficiently well understood for a rigorous mathematical approach, so equation 3.39 (as shown below) is proposed as the best rational compromise available at present, e.g.

$$P_i = \lambda \rho C_b^2 T$$

where λ is a smoothness-coefficient (from Section 3.6) related to the type of seabed in front of the seawall. For model studies with unrealistically smooth wave forms and small volumes of entrained air, λ varies between 1 and 10 and for real seawalls λ ranges from 0.1 to 0.5 (Figure 3.30). It is not possible to physically measure λ but from the data in Figure 3.30 various values of λ can be tentatively assigned to the different beach types as follows; for smooth beaches with uniform slopes a λ value of 0.5 is suggested and for rocky beaches values of λ from 0.1 to 0.2 appear to be more suitable. This manner of classification is very much over simplified because wave breaking and air entrainment is not solely dependent upon the beach type, but is also affected by wind speed and direction, beach slope, water depth and wave reflection. But, because there is limited data available it is more convenient to include all of these variables into a single quantity (λ), the value of which will remain largely subjective until more well documented data becomes available.

In Chapter Three, equation 3.39 was compared with the equations for breaking and broken wave pressures given in the Shore Protection Manual(74). The pressures calculated from equation 3.39 using λ = 0.5 were significantly lower than those given by the Shore Protection Manual equation for breaking waves, but equation 3.39 fits the data measured during this investigation (as shown in Figure 3.30) and so appears to be more applicable than the Shore Protection Manual equation, (which was based on model data). Using λ = 0.1 in equation

3.39 gave pressures similar to those given by the Shore Protection Manual for broken waves. So equation 3.39 seems to apply to both breaking and broken waves. This implies that breaking and broken waves both convert a similar percentage of their momentum into impulse energy, but as broken waves contain a very large volume of entrained air then their momentum is transformed more slowly resulting in lower impact pressures.

4.3.2 Comparison of Measured Wave Impact Pressures

The impact pressures measured during this investigation were of a similar order of magnitude to those measured by Millar et al(11), the most recent investigation, but considerably lower than those measured by other full scale investigations. The reasons for this can be found by examining the different sites used, Rouville et al(7), Cot(8) and Kuribayashi et al(9) all used harbour walls where there was deep water, whereas this investigation and that of Millar were conducted in shoaling water. The deep water sites have the potential for large waves with high celerity, but in shoaling water both wave height and celerity are restricted by water depth thereby limiting the wave momentum and consequently the impact pressures. If Millar's data is compared with that from Ilfracombe and Seaford (as shown on page 224), it can be seen that the Seaford data has impact pressures quite similar to those measured by Millar, this is to be expected because both sites have unobstructed foreshores with fairly regular slopes and both sites experienced similar waves. The beach at Seaford is steeper than at Cape Cod hence the higher maximum impact pressure which probably occurred because higher waves with greater celerity can approach closer to the Seaford wall before breaking.

The impact pressures measured at Ilfracombe are significantly lower than those at either Seaford or Cape Cod. This is because the foreshore at Ilfracombe is very rocky which creates a confused sea state and generally causes waves to at least partially break before reaching the wall, thereby entraining large volumes of air. Thus even though the majority of impact pressure data was measured at Ilfracombe (112 impacts in six recording sessions compared with 48 impacts in two sessions at Seaford), the maximum impact pressure is relatively low when compared with the Seaford data. This is because the comparatively large volume of air entrained in a breaking wave at Ilfracombe means it will have a smaller λ value and consequently will produce smaller impact pressures, (as deduced from Section 3.6)..

	Average Pressure	Maximum Pressure	Average Wave Height
Ilfracombe	10.1 KN/m^2	26.7 KN/m^2	0.99 m
Seaford	17.2 KN/m^2	48.9 KN/m^2	1.05 m
Cape Cod (Millar et al)	19.0 KN/m^2	41.4 KN/m^2	0.90 m

4.4 Vertical Impact Pressure Distribution

From previous investigations, both model and full scale, there has been disagreement as to the location of the maximum impact pressure in the vertical plane. Many investigators measured the maximum impact pressure at still water level (S.W.L.), i.e. Hiroi(4), Luiggi(6) and Gaillard(3), this led Minikin(72) to produce his well known vertical impact pressure distribution (Figure 1.8) with its maximum at S.W.L., reducing parabolically to zero at both the wave crest and trough. Other investigators measured the maximum impact pressure near the wave crest (Bagnold(14)) or near the wave trough (Rundgren(43)). During this investigation, at Ilfracombe, the location of the maximum impact pressure was found to vary between the top and bottom of the wave, although the average impact pressure distribution appeared to be uniform over the height of the breaking wave.

The extent of the wave impact during breaking has generally been paid less attention than the location of the maximum pressure. However, Bagnold considered impact pressures could only occur over the height of a compressed air cushion which extended from the wave crest to a level $0.4H_b$ below the crest, Ross(35) found impact pressures occurred from near the crest to some distance below S.W.L., and Larras(40) found impact pressures occurred over a large zone near S.W.L.

Thus there seems to be a considerable amount of disagreement as to the extent of the wave impact pressure over the face of the wall, as well as to the location of the maximum impact pressure. Even where two investigations use waves of similar characteristics, there is still no guarantee of similar results. This is due, in part, to the various types of breaking waves encountered, Millar et al(11) found a plunging wave generated a maximum pressure near the base of the wave yet a bore generated a maximum near the wave crest, these two extremes of breaking wave types were both encountered at the same site. Therefore it would seem that the maximum impact pressure and the vertical pressure distribution are governed by the type of breaking wave. The wave type is very difficult to characterise in a real sea at the instant of impact, and as the designer is only generally interested in the maximum possible impact pressure then it is not practical (or possible) to produce vertical impact pressure distributions for each breaking wave type.

Most seawalls will be subjected to all conditions of breaking waves during their lifetimes, therefore it would be unwise to design a seawall using a vertical pressure distribution for a specific type of breaking wave, (unless it was the worst case). Hence the vertical impact pressure distributions of Molitor(5), Luiggi(6), Minikin(72), etc., which have a maximum value at S.W.L. with a triangular type distribution above and below this level do not generally represent the worst case of loading (for overturning). The worst case would probably occur for a maximum pressure at or near the wave crest. At Ilfracombe the maximum impact pressure was measured at the wave crest for approximately 50% of all recorded vertical pressure distributions. So in the light of current data, these triangular type distributions appear suspect. Therefore a uniform vertical impact pressure distribution, which probably represents the worst case for sliding and overturning, is proposed. The impact pressure calculated from equation 3.39 is applied uniformly over the height of the breaking wave as shown in Figure 3.34. There is some evidence to support this proposed impact pressure distribution, the Shore Protection Manual gives the same vertical pressure distribution but for broken waves only and Muir-Wood(95) also gives the same distribution, for breaking waves, but extending only over height $0.75H_b$ (measured down from the wave crest).

CHAPTER FIVE

CONCLUSIONS AND SUGGESTIONS FOR FURTHER RESEARCH

Conclusions

(1) The high pressure transient wave impacts appear to be caused by the wave front striking the seawall and not by the compression of an air cushion.

(2) Wave impact pressures of up to seven times the hydrostatic pressure were measured, although very high pressure impacts (as measured by Rouville et al(7) were absent, probably due to the high percentage of air entrained in the breaking wave.

(3) Von Karman's(52) water hammer expression ($\rho V_s U_i$) does not seem to apply to wave impact pressures, even allowing for the reduction in V_s due to air entrainment.

(4) None of the many previous empirical or semi-empirical equations used to estimate wave impact pressures apply throughout the range of model and full scale impacts. Each equation seems only to fit a particular set of circumstances.

(5) Wave impact pressures were found to last appreciably longer than previously thought, of the order of 100 to 200 milli-seconds. This is about 100 times longer than most model scale impacts and from 4 to 10 times longer than those measured by Rouville et al.

(6) No explicit mathematical relationship was found to relate the wave impact pressure to measured wave parameters, although impact

pressure was found to be a function of wave celerity (C_b) and wave period (T) in the following form (equation 3.39),

$$\text{e.g.} \qquad P_i = \lambda \rho C_b^2 T$$

where the coefficient λ is essentially dependent upon the percentage of air entrained in the wave at breaking. Recommended values for λ are given in Chapter Three.

(7) Wave impact pressures cannot be scaled from model to full size waves with any degree of certainty because the major factor in the generation of impact pressures is the percentage of air entrained in the breaking wave. This percentage of entrained air cannot be calculated or scaled and will always be disproportionately lower in model scale waves because of surface tension effects.

(8) The largest impact pressures occurred when the wave front was vertical or nearly vertical.

(9) Wave impact pressures were measured, on occasion, simultaneously by up to four pressure transducers, of these four transducers, two were located 1.6m apart vertically (approximately at the wave crest and trough) and two were spaced 1.5m apart horizontally. Therefore it seems that wave impact pressures can occur simultaneously over large areas (covering the height of the breaking wave) and are not just isolated, localised events as previously thought.

(10) The vertical impact pressure distribution appears, from the limited data available, to be substantially uniform over the

height of the breaking wave, any localised high pressures are probably due to an uneven dispersion of the entrained air over the height of the wave.

(11) The wave impulse measured on the seawalls was found to be a fixed percentage of the wave momentum dependent only upon the local wave steepness (H_b/L_b), this percentage increased as H_b/L_b increased.

(12) The impulse momentum relationship (equation 3.35) applies to all cases of breaking waves examined including, model scale waves, data from this investigation and data from Rouville et al. The scaling law for the impulse between model and full scale waves appear to be linear.

Suggestions For Further Reasearch

(i) More data is required on the vertical distribution of real wave impact pressures, this could be obtained by increasing the number of pressure transducers over the height of the breaking wave from the two in use at present to say five. This would enable the assumption of a linear distribution to be assessed.

(ii) Wave height, celerity and period were not measured for every individual wave that produced an impact pressure, only average values were estimated for each recording session. This has meant that over 150 individual wave impacts have had to be reduced to just 8 average values so that they could be plotted in Figures 3.24 to 3.27. These average values are sufficient for an initial appraisal but because the exact position of each data point is unknown then the degree of error in any relationship found from this data can not be assessed. So ideally the wave height, celerity and period need to be measured for every incident wave, this will allow better estimates of the relationships in Figures 3.24 to 3.27 and give some indication of their accuracy.

(iii) This investigation needs to be extended to include other seawalls with a range of incident wave characteristics different to those encountered at either Ilfracombe or Seaford. This will give an indication of the applicability of equations 3.39 and 3.35 to waves outside of the particular range for which these equations were developed. Also, it is worth investigating further, the effects of wall profile on the wave impact pressure. This would be best carried out at two sites with very similar beaches and prevailing incident waves, so that any differences in pressure would be due mainly to the differences in wall profile and not confused by differences in the incident waves, as at Ilfracombe and Seaford.

PART B

ANALYTICAL SEAWALL MODELLING

INTRODUCTION TO PART B

When waves break on a seawall there is a possiblity that transient impact pressures many times the hydrostatic pressure will occur. Methods of estimating the magnitude of these impact pressures are available (see Part A of this thesis), but very little is known of the response of the seawalls when subjected to these pressures. Some authors (Ross(35) and Hayashi et al(17)) assumed that these short duration transient pressures had no structural significance on full size seawalls, (these conclusions were drawn from model experiments). Yet the majority of the empirical and semi-empirical equations used by seawall designers are based on the magnitude of the impact pressure. Therefore if impact pressures have no structural significance then seawalls designed to withstand the impact pressure will be very conservative structures.

Thus there is a need for prototype data on the structural behaviour of real seawalls subjected to wave impact pressures. The only previous investigation to attempt to measure the structural response of a coastal structure subjected to wave loading was that of Kuribayashi et al(9), although they limited the scope of their investigation to measuring the period of vibration of the breakwater.

The first prototype data on the response of real seawalls was measured during this investigation by using accelerometers mounted on top of the seawalls, (the data is presented in Part A). This data seemed to indicate that seawalls did respond to the transient wave impact pressures, as shown in Figure 3.8, although this could not be determined conclusively because it was not possible to isolate the seawall response to a single wave impact. Therefore it is necessary to produce analytical models of the seawalls based on the prototype data available in Part A of this thesis. These analytical models will then be subjected to various wave impact loads, covering the whole range of model and full scale wave impacts as measured during this investigation and by other authors. This should then lead to a good understanding of the dynamic and static behaviour of real seawalls under all types of wave loading.

CHAPTER SIX

DYNAMIC SEAWALL ANALYSIS

6.1 Introduction

Seawall design is generally treated as a static problem, with the real seawaves being replaced by a maximum or design wave for a given return period. This is probably sufficient for most components of wave loading which have a fairly low frequency and so generate small inertial forces in the structure which can be neglected. But in a real sea there are likely to be waves with a range of frequencies, some of which might induce a dynamic response in the structure. There is also the occasional transient wave impact load which is definitely of a dynamic nature, but because of its very short duration it is unclear whether it has any structural significance. Therefore the dynamic analysis must be considered from two different approaches;

(1) A statistical analysis will be required to evaluate the seawall response to the random hydrostatic wave loading.

(2) A deterministic analysis will be required to evaluate the seawall response to the impulsive wave impact load.

In any dynamic problem the main parameters needed to fully define the structural response and behaviour of the system are the mass, stiffness and damping, and in marine structures there are the additional effects of scour, changes in pore water pressure in the foundations and the added mass of water constrained to move with the structure. The structural response is also closely related to the loading conditions, i.e. a periodic load will produce a harmonic response, although not necessarily in phase. In the case of seawalls in the breaker zone the wave loading will be of a random dynamic nature for which the resulting structural response (deflection, stress) will also be random and dynamic. As a first order of approximation the seawalls can be assumed to be simple single degree of freedom systems, higher order models can then be produced at a later stage if and when required.

6.2 Single Degree of Freedom (SDOF) Seawall Models

The idealisation of a structure as a SDOF system may seem to be too crude to be worthwhile, but in most cases it will provide an insight into the behaviour of the structure and will give a fair indication of the magnitude of the natural frequency at the fundamental mode of vibration.

The basic dynamic equation for the natural frequency, with no damping and free vibration is;

$$\omega_1 = \sqrt{\frac{K}{M}} \qquad \ldots\ldots\ldots\ldots\ldots\ldots\ldots\ldots\ldots\ldots \quad (6.1)$$

where ω_1 = angular natural frequency (rads/sec)

K = stiffness (KN/m)

M = mass (KN)

The simplest representation of a seawall is a cantilever of height h and uniform cross section, as shown over page.

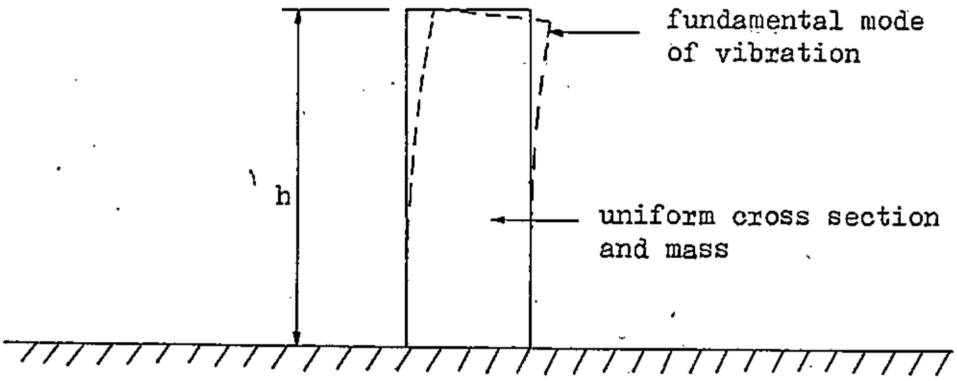

The mass of the cantilever is made the same as the mass of the real seawall, the second moment of area (I) of the real seawall changes with height h therefore I in the model is taken to be the average second moment of area of the real seawall. Thus if both the height and second moment of area of the cantilever model are similar to those of the real seawall then the model stiffness will also be similar.

The undamped natural frequency of this model can be found from the following equation (Harris and Crede(76)) for free vibration;

$$f_1 = \frac{1}{2\pi} X_i \sqrt{\frac{E\,I\,g}{\mu\, h^4}} \quad \text{Hz} \quad \ldots\ldots\ldots\ldots (6.2)$$

where f_1 = natural frequency

E = modulus of elasticity (KN/m^2)

μ = mass per unit height of seawall (kg/m)

h = height of seawall (m)

I = second moment of area (m^4)

g = acceleration due to gravity (m/s^2)

X_i = a coefficient = 3.52 for fundamental mode
22.40 for second mode
61.70 for third mode

from equations 6.1 and 6.2 the stiffness (K) approximates to;

$$K = X_i \frac{E\,I}{h^3} \qquad \ldots\ldots\ldots\ldots\ldots\ldots\ldots\ldots\ldots\ldots\ldots\ldots(6.3)$$

The frequencies of the first three modes of vibration and the approximate stiffness for both the Seaford and Ilfracombe seawalls are given below;

Mode of vibration	Seaford	Ilfracombe
Fundamental mode	34.0 Hz	18.4 Hz
Second mode	216.7 Hz	117.1 Hz
Third mode	597.0 Hz	322.5 Hz
Seawall stiffness MN/m	637×10^3	204×10^3

From this idealized model it is seen that the Seaford seawall is stiffer and so its natural frequencies of vibration are comparatively higher than those of the Ilfracombe seawall.

The E value (modulus of elasticity) used in the above calculations was taken as 30.10^9 KN/m^2, but for dynamic loading E is not a constant but increases with increasing frequency of load. For full details see Refs. 109, 110 and 111.

The frequencies given above are likely to be over estimates of the natural frequencies because in practise a proportion of the foundations, backfill and sea water will be constrained to move with the seawalls, thereby increasing the overall effective mass of the structure which in turn leads to a lowering of the natural frequencies of vibration, (natural frequency is proportional to 1/mass).

In Chapter Three the fundamental mode of vibration for the Ilfracombe and Seaford seawalls was found to be 8.9 Hz and 10.3 Hz respectively. These values are significantly lower than those obtained above, this indicates that the seawalls cannot be analysed in isolation from the surrounding foundations and backfill because their mass contributes significantly to the response of the structure. So any seawall model must allow for the effects of the foundations.

6.3 Structural Damping

The degree of damping in a structure can not be calculated at the design stage, so values are usually obtained by examining the response of similar completed structures. Damping can increase for modes of vibration higher than the first, this increase is approximately proportional to the amount of strain energy in each mode(82).

Damping may be estimated from either a correlogram or spectral density plot of structural vibration, measured during this investigation by accelerometers. For a correlogram to be useful, a single natural frequency must be isolated by filtering, auto-correlation analysis will then result in a correlogram which decays in a logrithmic manner, (as for a lightly damped single degree of freedom structure subjected to an impulse). The logrithmic decrement (δ) can be estimated from the following equation;

$$\delta = \frac{1}{n} \log_e \frac{a_o}{a_n} \qquad \text{.........................} \quad (6.4)$$

where n = the number of cycles between the peaks a_o and a_n

a_o = the amplitude of the initial peak

a_n = the amplitude after n cycles

$\delta = 2\pi\xi$

ξ = proportion of critical damping (damping ratio)

Damping values were not estimated from auto-correlation analysis for this investigation because suitable bandpass filters were not available.

The other method of estimating structural damping via spectral density analysis is based on the width of the peak at the fundamental (bending) natural frequency of vibration.

The damping ratio (ξ) is estimated from the following;

$$\xi = \frac{\Delta\omega}{2\,\omega_1} \qquad \text{............................} \quad (6.5)$$

where $\Delta\omega$ = the width of the spectral density curve at ω_1

ω_1 = the resonant natural frequency

The width of the spectral density curve at the structures natural frequency (ω_1) is measured at an amplitude of $D_{max}/2$, this level is referred to as the half power point, and D_{max} is the maximum amplitude of the peak ω_1. If the spectral density axis is in db's then the half power point becomes the level 3 db down from D_{max}.

If the spectral density curves (of response) for the Ilfracombe and Seaford seawalls are examined, (Figures 3.11 and 3.12 respectively) the percentage critical damping from equation 6.5 is;

Seawall	% critical damping
Ilfracombe	27.6
Seaford	19.8

These values are extremely high for the type of structure(102) and taken at face value would probably mean the seawalls were excessively cracked. The highest value was measured at Ilfracombe and could indicate that the precast blocks were not fixed securely enough and so the wall was not behaving as a monolithic structure, (there is evidence at Ilfracombe that some blocks are free to move relative to each other because the edges between some ajoining blocks are broken away, particularly between the top two rows of blocks). But the most likely explanation for these large values is the effect of the hydrodynamic damping and the added mass of water. The hydrodynamic damping will vary for the seawalls from a value of zero when there is no water at the wall, to a maximum value at high tide. Therefore the hydrodynamic damping will be constantly varying, which in turn means the natural frequencies of the structure will be affected. The added mass of water constrained to move with the seawalls is also changing in the same way as the hydrodynamic damping, and will therefore also cause fluctuations in the resonant natural frequency. So because the

the natural frequencies are continuously varying (although only slightly), then spectral density plots such as Figures 3.11 and 3.12, which were necessarily produced from long samples of data, will show wide peaks at about the natural frequency. A better estimate of the structural damping could be obtained by exciting the seawall at low water with a rotating mass vibrator (or similar means of excitation), the structural damping could then be found by the methods previously discussed, but now the effects of hydrodynamic damping and added mass would be absent thus allowing better estimates to be made.

The value of the added mass of water is generally calculated from potential flow theory (for offshore structures) by assuming the structure is small in relation to the wave length and so does not disturb the flow. But seawalls are large in relation to the wave length and there is generally no flow past them, so potential flow theory can not be used to calculate the added mass. Therefore this added mass of water constrained to move with the seawalls can not be quantified and would need to be determined experimentally.

6.4 Multi-Degree of Freedom Systems (MDOF)

Whilst the idealised single degree of freedom system may be suitable for the initial appraisal of the dynamics of a structure, it is often insufficiently accurate for a more detailed study. Hence the need to model the structure allowing a suitable number of degrees of freedom to fully define the response at the frequencies of interest. In a dynamic analysis the loading causes an acceleration of the mass which is resisted by the inertia forces, because in most real structures the mass is distributed continuously then the accelerations and displacements

must be defined at all points to completely define the inertia forces. Therefore some form of discretisation of the mass would greatly simplify the analysis. The two most common methods are by lumping the mass at discrete nodal points and assuming inertia forces are only developed at these points, or by using a finite element analysis where the structure is divided into a number of elements connected by nodes at their edges, (this method is discussed in more detail in Chapter Seven).

Each node in the idealised structure is then allowed a specified number of degrees of freedom. Generally the more degrees of freedom a structure is allowed the more accurate will be the resulting analysis (a point will obviously be reached where it becomes uneconomic to extend the number of degrees of freedom any further). Damping forces will almost certainly be included in a more rigorous analysis. Damping can be included in structures such as seawalls by considering the damping force to be represented by a force proportional to the velocity of the structure but with opposite sign, this is known as viscous damping.

The general dynamic equation of motion for a SDOF system with damping is;

$$M \ddot{x} + C \dot{x} + K x = F(t) \qquad \ldots\ldots\ldots\ldots\ldots\ldots (6.6)$$

where $M \ddot{x}$ is the inertia term, $C \dot{x}$ is the damping term, $K x$ is the stiffness term and $F(t)$ the applied force.

To solve equation 6.6 for the case of a MDOF system, first consider the particular case when applied force and damping terms equal zero (i.e. free vibration).

The equation of motion can be written in matrix form as;

$$\left[M\right] \ddot{x} + \left[K\right] x = 0 \quad \ldots\ldots\ldots\ldots\ldots\ldots\ldots\ldots (6.7)$$

this expands, for n degrees of freedom, to equation 6.8;

$$\begin{bmatrix} M_1 & 0 & - & - & - & 0 \\ 0 & M_2 & & & & \\ | & & \diagdown & & & \\ | & & & \diagdown & & \\ | & & & & \diagdown & \\ 0 & \cdot & & & & M_n \end{bmatrix} \begin{bmatrix} \ddot{x}_1 \\ \ddot{x}_2 \\ \\ \\ \\ \ddot{x}_n \end{bmatrix} + \begin{bmatrix} K_{11} & K_{12} & - & - & - & K_{1n} \\ K_{21} & K_{22} & & & & \\ | & & \diagdown & & & \\ | & & & \diagdown & & \\ | & & & & \diagdown & \\ K_{n1} & & & & & K_{nn} \end{bmatrix} \begin{bmatrix} x_1 \\ x_2 \\ \\ \\ \\ x_n \end{bmatrix} \quad \ldots\ldots (6.8)$$

mass matrix   stiffness matrix

acceleration   displacements

In dynamics problems the mass and stiffness matrices are always symmetrical about the leading diagonal, assuming the response is harmonic then the solution becomes;

$$\left.\begin{aligned} x &= X_0 \cos(\omega t - \varphi) \\ \dot{x} &= -X_0 \sin(\omega t - \varphi)\omega \\ \ddot{x} &= -X_0 \cos(\omega t - \varphi)\omega^2 = -\omega^2 x \end{aligned}\right\} \quad \ldots\ldots\ldots\ldots (6.9)$$

thus equation 6.7 can be written as ;

$$(-[M]\,\omega^2 + [K])\, x = 0 \qquad \ldots\ldots\ldots\ldots\ldots\ldots\ldots (6.10)$$

The non-trivial solution is found from the determinant of the terms in in brackets, i.e.

$$\left| -[M]\,\omega^2 + [K] \right| = 0 \qquad \ldots\ldots\ldots\ldots\ldots\ldots\ldots (6.11)$$

the solution of which will yield n natural frequencies corresponding to the n degrees of freedom of the system.

This method of solving equation 6.7 has its limitations, it becomes very unwieldy to use by hand with all but the simplest of structures, and it proves difficult to work with on the computer. Therefore for hand calculations this method is best employed with structures with relatively few degrees of freedom, which usually means lattice or frame type structures for which it is convenient to lump the mass of the structure at a few discrete points, usually taken as the joints. Generally three dimensional solids such as seawalls are analysed using the finite element method, as each three dimensional finite element will have a minimum of eight corner nodes this means this technique generates large volumes of data best tackled on a computer. The most widely used method to overcome these difficulties is to treat the problem as an eigen value problem and reduce equation 6.7 to the standard eigen value form, found in most dynamics books (Refs. 82 and 112 to 114).

$$\text{i.e.} \quad \left\{ [L]^{-1}\,[K]\,[L]^{T} \right\} y - \lambda y = 0 \qquad \ldots\ldots\ldots\ldots (6.12)$$

where $[L]^{-1}$ = upper triangular matrix of decomposed $[M]$

$[L]^T$ = transpose of $[L]^{-1}$.

y = eigenvectors

$\lambda = \omega^2$ = eigen values

In this form equation 6.12 can be solved using the many available computer programs written for this purpose.

6.4.1 The Transfer Function (Receptance) Method

Another powerful method of analysing MDOF systems is to use the transfer function or receptance method. This technique relates the response of a system to the input (excitation) force via a transfer function. Taking the simple case of a damped SDOF system subjected to a sinusoidal force, the dynamic equation of motion may be written as;

$$M\ddot{x} + C\dot{x} + Kx = F e^{j\omega t} \quad \ldots\ldots\ldots\ldots\ldots (6.13)$$

disregarding the imaginary terms, the solution becomes;

$$\left.\begin{aligned} x &= X_o \exp j(\omega t - \phi) \\ \dot{x} &= j\omega X_o \exp j(\omega t - \phi) = j\omega x \\ \ddot{x} &= -\omega^2 X_o \exp j(\omega t - \phi) = -\omega^2 x \end{aligned}\right\} \quad \ldots\ldots\ldots\ldots\ldots (6.14)$$

substituting equation 6.14 into 6.13 gives

$$x = \left[\frac{1}{-M\omega^2 + K + j(C\omega)}\right] \cdot F \exp j\omega t \quad \ldots\ldots\ldots\ldots (6.15)$$

The transfer function relating input force F to output displacement x is contained within the brackets, i.e.

$$\text{Transfer function } H(j\omega) = \frac{1}{-M\omega^2 + K + j(C\omega)} \quad \ldots\ldots (6.16)$$

replacing ω by $2\pi f$, equation 6.16 becomes

$$H(jf) = \frac{1}{-M\,(2\pi f)^2 + K + Cj(2\pi f)} \quad \ldots. (6.17)$$

The input and output do not need to be restricted to force and displacement as any system with a linear input/output relationship will theoretically be linked by a transfer function of the type shown in equation 6.16.

For a MDOF system equation 6.13 becomes;

$$\left\{-[M]\,\omega^2 + j[C]\omega + [K]\right\} x(t) = F(t) \quad \ldots\ldots\ldots. (6.18)$$

and the transfer function, equation 6.16, becomes;

$$\frac{1}{-[M]\,\omega^2 + j[C]\omega + [K]} \quad \ldots\ldots\ldots\ldots\ldots\ldots (6.19)$$

These preceeding methods of dynamic analysis assume the time variation of the loading is fully known, so the analysis is deterministic. Therefore the seawall response to a measured wave impact can be found using these methods, but not seawall response to random wave loading, (random loading is discussed further in Section 6.6).

6.5 Response to Impact Loading

An approximation of the seawall response to a wave impact can be obtained by considering the seawall as a SDOF system with no damping, as follows;

Assuming the wave impact can be represented by a traingular impulse as shown below, (ignoring the slowly varying hydrostatic pressure which can be treated as a static load).

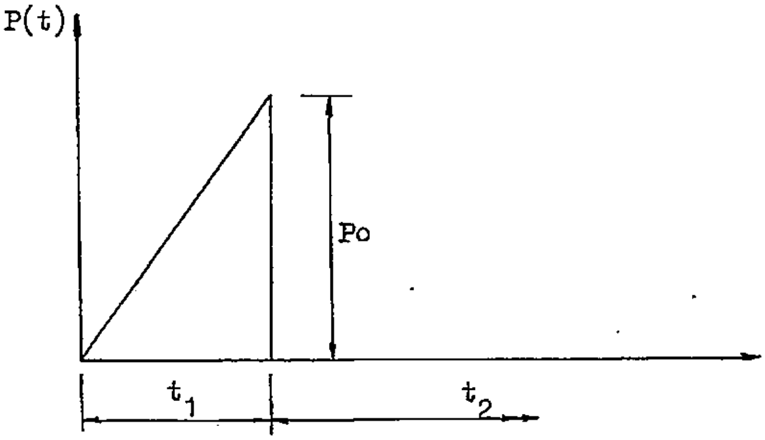

the magnitude of this applied force, in equation form, is

$$Po\ (\frac{t}{t1}) \qquad 0 \leqslant t \leqslant t_1$$

thus equation 6.6 becomes

$$M\ddot{x} + Kx = Po\ (\frac{t}{t_1}) \quad 0 \leqslant t \leqslant t_1 \qquad \ldots\ldots\ldots\ldots \text{(6.20)}$$

The seawalls response will be divided into two distinct phases, (1) the loading phase and (2) the free vibration phase. The wall response during the free vibration phase is important because for very short duration impacts when $t_1 < T$ (where T is the period of vibration of the structure), the maximum displacement occurs after the load has been

withdrawn.

The response during phase 1 is due to a combination of free vibration and the loading condition. If the load is of short duration then the maximum displacement is dependent mainly upon the magnitude of the applied impulse and is not much affected by the form of the loading(115). Thus an approximate method may be used to evaluate the maximum response (displacement) to a short duration impulsive loading as follows;

from the impulse momentum relationship

$$M \Delta \dot{x} = \int_0^{t_1} P(t)\, dt \qquad \ldots\ldots\ldots\ldots\ldots\ldots\ldots\ldots\ldots (6.21)$$

or

$$\Delta \dot{x} = \frac{1}{M} \int_0^{t_1} P(t)\, dt \qquad \ldots\ldots\ldots\ldots\ldots\ldots\ldots\ldots\ldots (6.22)$$

where $\Delta \dot{x}$ is the change in velocity produced by the applied load.

In phase 2 the free vibration can be represented by simple harmonic motion (SHM), given by(115)

$$x(t_2) = \dot{x}(t_1) \sin \frac{\omega t_2}{\omega} + x(t_1) \cos \omega t_2 \qquad \ldots\ldots\ldots (6.23)$$

$$\text{for} \quad t_2 = t - t_1 \geqslant 0$$

The displacement at the end of phase 1 ($x(t_1)$) is small and so can be neglected. The velocity at the start of phase 2 ($\dot{x}(t_1)$) is

approximately equal to $\Delta \dot{x}$, so substituting equation 6.22 into equation 6.23 gives;

$$x(t_2) \quad \frac{1}{M\omega}\left[\int_{0}^{t_1} P(t)\,dt\right] \sin \omega t_2 \qquad \text{..........} \; (6.24)$$

Equation 6.24 can only be used to estimate the displacement for short duration loads where the maximum displacement can be assumed to occur in phase 2.

e.g. applying the following impulsive load to the idealised model of the Ilfracombe seawall from Section 6.2,

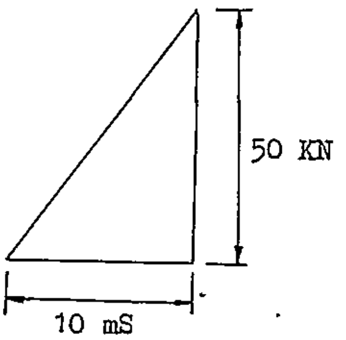

$$\int_{0}^{t_1} P(t)\,dt \quad = 0.5 \text{ KN.s}$$

The fundamental natural frequency of the Ilfracombe seawall model in Section 6.2 was found to be 18.4 Hz,

$$\text{therefore } \omega = 2\pi f = 115.6 \text{ rads/sec}$$

and from Eq. 6.24 ($M = 370.10^3$ kg)

$$x = \frac{9.81 \;\; 0.5}{370.10^3 \;\; 115.6} \sin \omega t$$

x_{max} will occur when $\sin\omega t = 1$

so $x_{max} = 1.1 \cdot 10^{-4}$ mm

This method is only suitable for SDOF systems subjected to short duration impacts, but it does provide a quick and simple first order approximation of the structural deflection.

When the duration of the impact is of the same order or greater than the natural period of the structure, then equation 6.20 will have to be solved from first principles by finding the particular and complementary solutions to the dynamic equation of motion and adding them to give the equation for the structural response. Also, in general the loading will not be integrable so will need to be evaluated by numerical integration, and damping will also probably need to be considered. Thus real structural dynamics problems are often solved using one of the many finite element packages available. The finite element method is used in Chapter Seven to analyse a MDOF model of the Ilfracombe seawall subjected to impulsive loading.

6.6 Response to Random Wave Loading

The wave loading on seawalls in shoaling water is generally random, thus the analysis must be statistical because of the lack of precise information on the forcing function. It is convenient to perform this analysis in the frequency domain since spectral density information on the forcing function is readily available.

By assuming the forcing function is stationary and periodic of time T $(= 2\pi/\omega)$, it may be represented by the following Fourier series;

$$F(t) = \frac{1}{T}\int_{-T/2}^{T/2} F(t)\,dt + \sum_{r=1}^{\infty}\left\{\left(\frac{2}{T}\int_{-T/2}^{T/2} F(t)\cos r\omega t\,dt\right)\right.$$

$$\left.\cos r\omega t + \left(\frac{2}{T}\int_{-T/2}^{T/2} F(t)\sin r\omega t\,dt\right)\sin r\omega t\right\} \quad \ldots (6.25)$$

which in complex form is;

$$F(t) = \sum_{r=-\infty}^{\infty}\left(\frac{1}{T}\int_{-T/2}^{T/2} F(t)\exp -j\omega t\,dt\right)\exp j\omega t\,d\omega \quad \ldots (6.26)$$

If the period T is extended to infinity then $\Delta\omega$ tends to zero, and in the limit equation 6.26 becomes the following Fourier integral;

$$F(t) = \frac{1}{2\pi}\int_{-\infty}^{\infty}\left(\int_{-\infty}^{\infty} F(t)\exp -j\omega t\,dt\right)\exp j\omega t\;d\omega \quad \ldots\ldots (6.27)$$

where

$$\int_{-\infty}^{\infty} F(t)\exp -j\omega t\,dt = F(j\omega) \quad \ldots\ldots\ldots\ldots\ldots\ldots (6.28)$$

$F(t)$ is in the time domain and $F(j\omega)$ is in the frequency domain, replacing ω by $2\pi f$, equation 6.27 becomes;

$$F(t) = \int_{-\infty}^{\infty} F(jf) \exp j2\pi ft \; df \qquad \text{...............} \; (6.29)$$

and equation 6.28 becomes

$$F(jf) = \int_{-\infty}^{\infty} F(t) \exp -j2\pi ft \; dt \qquad \text{...............} \; (6.30)$$

Equations 6.29 and 6.30 are almost symmetrical apart from the negative sign in the exponential term of equation 6.30 and are known as the Fourier transform pair, they allow a quantity F to be expressed in terms of either the time or frequency domain.

From equation 6.29 it can be shown that(82);

$$\int_{-\infty}^{\infty} F^2(t) \; dt = \int_{-\infty}^{\infty} \left| F(jf) \right|^2 \; df \qquad \text{.................} \; (6.31)$$

changing the limits to consider only the single sided (positive) spectral density,

$$\int_{-\infty}^{\infty} F^2(t) \; dt = 2 \int_{0}^{\infty} \left| F(jf) \right|^2 \; df \qquad \text{................} \; (6.32)$$

to allow the Fourier integral to converge, only a finite time record of length $-T/2 < t < T/2$ is considered, this results in a mean square time averaged value of $F(t)$ of ;

$$< F^2(t) > = \frac{1}{T}\int_{-T/2}^{T/2} F^2(t)\, dt \qquad \ldots\ldots\ldots\ldots\ldots (6.33)$$

combining equations 6.33 and 6.32;

$$< F^2(t) > = \frac{2}{T}\int_{0}^{\infty} \left| F(jf) \right|^2 df \qquad \ldots\ldots\ldots\ldots (6.34)$$

where $\frac{2}{T}\left| F(jf) \right|^2 = S_{FF}(f)$ which is the single sided spectral density, in this case it is the force spectral density as a function of frequency. The mean square value of the forcing function (pressure in this case) is related to the force spectral density as follows;

$$< F^2(t) > = \int_{0}^{\infty} S_{FF}(f)\, df \qquad \ldots\ldots\ldots\ldots\ldots\ldots (6.35)$$

This equation unlike the Fourier integrals, will converge to a steady value which is represented by the area under the force spectral density versus frequency curve. Similarly the mean square value of the response is given by the area under the response spectral density versus frequency curve, given in equation form as;

$$< X^2(t) > \; = \int_0^\infty S_{XX}(f)\; df \qquad \ldots\ldots\ldots\ldots\ldots\ldots \quad (6.36)$$

It can be shown by use of the Duhamel integral (Refs. 115 to 118) that

$$S_{XX}(f) \; = \; \left| H(jf) \right|^2 \; S_{FF}(f) \qquad \ldots\ldots\ldots\ldots\ldots\ldots \quad (6.37)$$

Equation 6.37 is shown graphically in Figure 6.1

For MDOF systems equation 6.37 becomes;(82)

$$S_{X_i X_i}(f) \; = \sum_{r=1}^{\infty} \sum_{s=1}^{\infty} \bar{H}_{ir} H_{is} \; S_{F_r F_s}(f) \qquad \ldots\ldots \quad (6.38)$$

The transfer function now becomes a complex n by n matrix and the output spectral density terms contain cross spectral density components. An equation of the form of Eq. 6.38 will be required for the response in each degree of freedom from i = 1 to n.

Therefore for most structures this method will be very lengthy unless there are few degrees of freedom, or if the cross spectral densities are not required or can be assumed to be zero.

An alternative approach which gives essentially the same results as the above method but avoids the need to consider cross spectral density terms uses a time domain analysis to build up a transfer function.

This is achieved by applying a sinusoidal force of unit amplitude to the structure, the resulting displacement is found at that frequency and gives a single point on the frequency domain transfer function. This process is repeated using sinusoidal forces of varying frequencies until a transfer function covering the range of frequencies required is set up. This transfer function can then be used with the force spectral density as for a SDOF system, (equation 6.37 and Figure 6.1).

This alternative method is used in Chapter Seven to set up a transfer function for a MDOF model of the Ilfracombe seawall, over the frequency range zero to 20 Hz, (the fundamental mode of vibration occurs at 8.9 Hz).

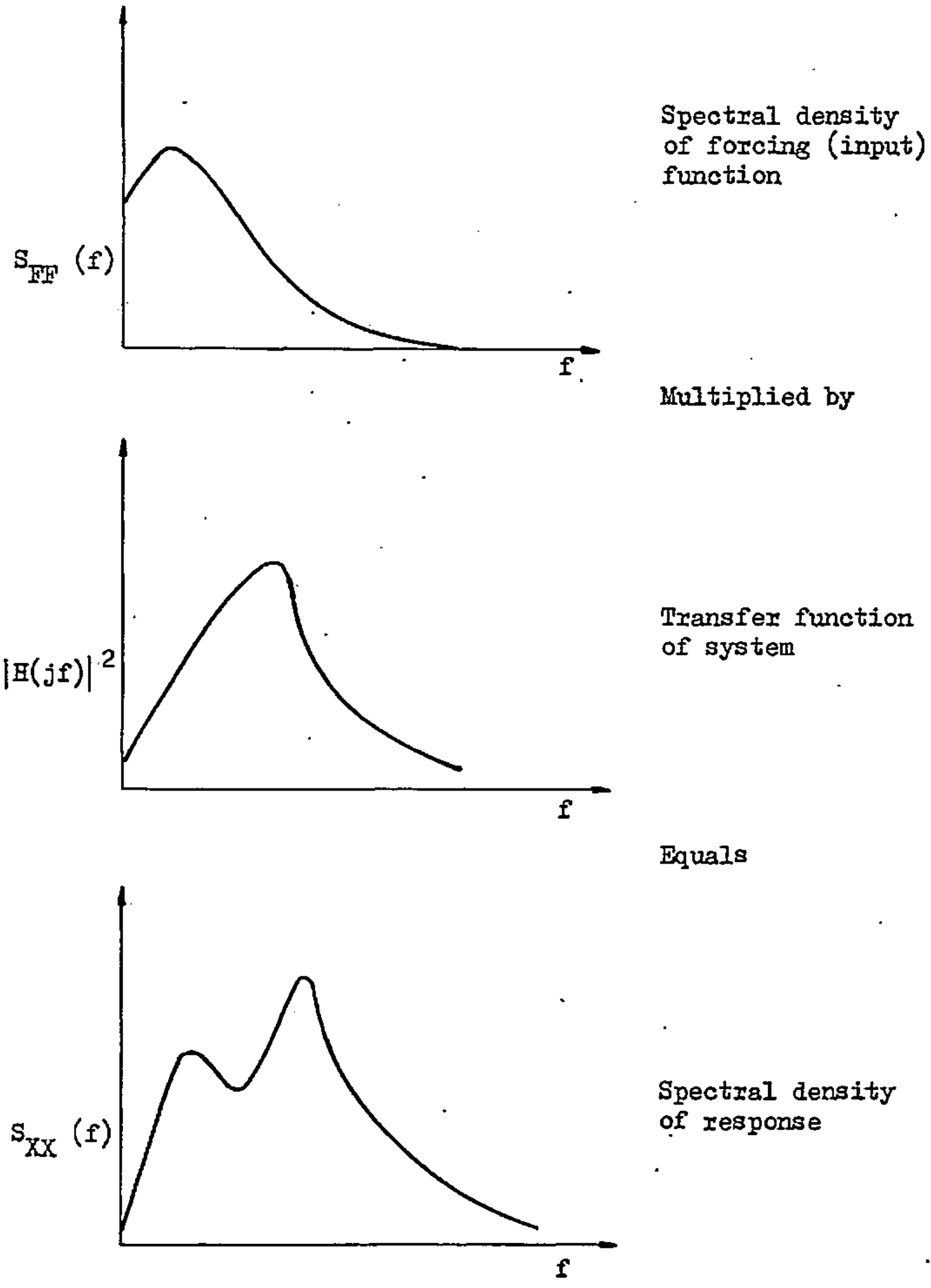
$S_{FF}(f)$
f
Spectral density of forcing (input) function
Multiplied by
$|H(jf)|^2$
f
Transfer function of system
Equals
$S_{XX}(f)$
f
Spectral density of response

Figure 6.1 Input-output spectral relationship for a linear system.

CHAPTER SEVEN

SEAWALL MODELLING BY FINITE ELEMENTS

7.1 Introduction

The seawalls analysed during this investigation may be considered as continuous systems because being monolithic, there is no obvious way in which they can be divided into discrete mass/spring systems. As continuous systems they theoretically have an infinite number of natural frequencies because of their infinite degrees of freedom, and so lend themselves to finite element analysis.

The finite element concept is essentially a method by which a continuous system may be approximated to, by its subdivison into discrete regions (finite elements) interconnected through nodal points on each region(119). Each individual element has its material properties specified and is allowed a finite number of degrees of freedom, the finite element approach is particularly useful for irregular shaped structures or anisotropic materials. The degree of accuracy of the analysis is proportional to the number of degrees of freedom and number of elements used.

The particular finite element package used for this analysis was developed at Nottingham University and is known as PAFEC 75 (Program for Automatic Finite Element Calculations). The PAFEC package, whilst being able to calculate the usual stresses, deflections, mode shapes and natural frequencies, can also be used for non-linear problems such as creep, large displacements and plasticity and for dynamic problems with either sinusoidal or transient forces. The ability to carry out a plastic analysis is made use of in Section 7.10, where the forces necessary to plastically deform the transduer diaphragm are calculated. In Sections 7.6 and 7.7 it is the ability to calculate the structural response to sinusoidal and transient forces that is made particular use of.

7.2 The Need for a Finite Element Analysis

In the previous chapters the confusion over the structural significance of impact pressures has been made apparent. The majority of proposed equations for estimating the maximum (design) wave pressure (including those developed from this investigation, and those actually used by many seawall designers) are based upon the infrequently occurring impact pressure. Yet some authors (Ross(35), Hayashi et al(17)) have suggested these impact pressures have no structural significance and hence should not be the basis for the design pressure.

It has already been shown that impact pressures occasionally act over large areas and have a significant duration, (Chapter Three) but the only evidence so far that impact pressures have any effect other than localised is found when wave pressure histories on the seawalls are compared with corresponding wall accelerations. Figure 3.9 is an example, here it can be seen that when an impact pressure spike occurs superimposed upon the hydrostatic pressure (impacts 1 and 4), the resulting wall accelerations, and hence displacements, are generally larger than for the hydrostatic pressures alone. This indicates that impact pressures are having a gross effect on wall response not just a localised effect, this is not conclusive and needs corroborating by means of a mathematical model which accurately describes the dynamic and static characteristics of the real seawalls.

The finite element models were developed for the Ilfracombe and Seaford seawalls using the main frame computer at Plymouth Polytechnic (a Prime dual 550) at level 3.4 in the PAFEC suite.

7.3 Modelling Techniques

The accuracy of the solutions obtained by finite element modelling is dependent upon the number of degrees of freedom allowed, which is in turn dependent upon the number of finite elements used. The more complicated the structure the more degrees of freedom are required to acheive a desired accuracy, but in most cases 60 degrees of freedom will result in accuracies of the order of 95% (this refers to the fundamental natural frequency), when using the PAFEC suite of programs.

The rate of erosion at Seaford (35mm/year) was such that it was decided to model the wall both before and after refacing to determine the changes in deflections, natural frequencies, etc. brought about by erosion. These two Seaford seawalls were modelled using eight noded quadrilateral isoparametric and six noded triangular isoparametric plate elements. Each plate element was allowed two degrees of freedom at each node in the x (U_x) and y (U_y) directions, unless otherwise restrained. The elements (of unit width) could only be subjected to inplane forces, resulting in inplane stresses and deflections, all longitudinal bending and twisting effects were ignored.

The Ilfracombe seawall was constructed from precast concrete blocks slotted onto dowel bars, these dowel bars were continuous over the height of the wall, so were included in the finite element model. The wall was modelled using six and eight noded elements as for Seaford, but in addition beam elements were used to represent the dowel bars. These beam elements were allowed only two degrees of freedom at each node (i.e. U_x and U_y), freedoms U_z, φ_x, φ_y and φ_z were all clamped.

The Seaford seawall model without erosion had 125 plate elements, 438 nodes and 810 degrees of freedom, the Seaford model with erosion had 117 plate elements, 415 nodes and 734 degrees of freedom. The Ilfracombe seawall model had, 175 plate elements, 65 beam elements, 559 nodes and 1294 degrees of freedom, see Figures 7.1, 7.2 and 7.3 respectively.

7.3.1 Model Constraints

As a first step the models were assumed fully fixed at all interfaces between the structure and surrounding soil, this assumption, as expected, resulted in unrealistic deflections and natural frequencies because ground/structure interaction was not taken into account. Although the models did serve as a useful proving ground to allow the correction of numerous minor problems associated with the running of the PAFEC package.

The seawall models were accurately constructed to the same physical shape and density as the real seawalls, but this meant that natural frequencies and deflections of the models could only be corrected by modifing the properties or physical shape of the model, both of which were unacceptable. Therefore improved models were developed to incorporate strips of foundation and backfill around the wall, the properties of which could be changed until the desired frequencies, deflections, etc. were acheived, this enabled the seawall properties and shape to remain true. The width of this strip of foundation and backfill had to be a compromise between including sufficient area to allow local distortions around the structure to dissipate and keeping the size of the model within the limits of the computer core space available. By including a large amount of surrounding soil in the model the number of degrees of freedom, and hence the cost of the analysis, were considerably increased. The width of the strip of foundation and backfill was limited to about 1m by the amount of computer core available, this was insufficient to allow local distortions and stress concentrations to dissipate. Also the boundary conditions imposed on this strip were not representative of the actual boundary conditions existing at the real structures. These problems were partially solved by including very rigid, dense elements in the foundations and backfill at strategic points around the structure, this was not a mathematically rigorous solution but it did produce satisfactory results. (Figures 7.4, 7.5 and 7.6).

7.4 Modelling Seawall Response

The seawalls can be assumed to be subjected to both dynamic and static forces, where the dynamic component is due to breaking waves, and the static component is due to the head of water at the wall, including the contribution from the wave height. The (hydro)static pressure at the wall is a combination of the height of S.W.L. above the toe and the wave height H, the pressure exerted by the height of the wave is actually of a dynamic nature but of such low frequency (of the order of 0.2 Hz) that it may be considered as static, provided impact pressures do not occur.

7.4.1 Static Modelling Considerations

A static analysis of the Seaford and Ilfracombe seawalls was carried out to help provide a complete picture of the structural behaviour of the seawalls, and as a check on the continuity between finite elements provided by the stress contours.

The modelling for a static analysis is fairly simple provided the exact physical shape and properties of the structure are known. In the case of the Ilfracombe and Seaford seawalls good estimations of the modulus of elasticity E and density ρ of the walls, foundations and backfill were obtained from the construction documents and drawings, as were the dimensions of the seawalls.

In a static analysis the only structural parameters normally of interest are the stress and deflection, the accuracy of model deflections could be assessed against deflections measured on the real seawalls. No stress measurements were made on the real seawalls, therefore the accuracy of the stress contours could only be assessed by engineering judgement, i.e. checking that stress concentrations were occurring near the point of application of the loads, etc. The stress contours provided a useful check on the accuracy of the model because the degree of accuracy was proportional to the amount of mis-match in the continuity of stresses at element boundaries.

Seawall deflections were measured using linear drive servo accelerometers which could respond to low frequency vibrations, but not static loads. Therefore the only wall movements measured were those caused by the fluctuations in the wave height at the wall, the contribution of the static head of water at the wall could not be measured directly. The accelerometers were suitable for either horizontal or vertical operation, by rotating the unit through 90° from the horizontal to the vertical an output of +5 volts was produced, at any other angle of rotation between 0° and 90° a voltage of $V = \sin\varphi \times 5$ volts was produced, (where φ = the angle through which the accelerometer is rotated). Therefore an estimate of the wall deflection caused by static loading can be made at any state of the tide by measuring the d.c. offset in the accelerometer output. This voltage is proportional to the angle of wall rotation, from which an estimate of horizontal wall deflection can be calculated, (the accelerometer must be zeroed with no water at the wall for the estimate to be valid, amplifier drift must also be avoided).

The only wall deflection which can be equated to the forces producing it with any degree of certainty is that caused by the hydrostatic wave pressure, therefore only the hydrostatic pressure exerted by the wave height is applied to the finite element models, this pressure is calculated by assuming the waves to be fully reflected from the seawall (i.e. standing waves), as shown in Figure 7.7. The theory of Miche was used to calculate the standing wave pressure because Wiegel(83) considers this theory to be better than that of Sainflou(71), the

contribution of the static head of water at the wall was not included.

e.g. from Miche(83), the pressure at the base of the wall due to the wave height is;

$$P_b = \left(d + \frac{\overline{H}}{\cosh 2\pi d/L} \right) \rho g \quad \dots\dots\dots\dots\dots\dots \text{(7.1)}$$

and $\delta h = \frac{\pi \overline{H}^2}{L} \left(1 + \frac{3}{4 \sinh^2 (2\pi d/L)} - \frac{1}{4 \cosh^2 (2\pi d/L)}\right) \coth 2\pi d/L$

where $\overline{H}$ is the wave height that would exist at the wall were the wall not there.

δh is the mean level of the standing wave above S.W.L.

The characteristics of the waves used are given below, these waves were used because corresponding accelerometer measurements were available thus allowing the wall deflections to be calculated.

	$\overline{H}$ (m)	L (m)	d (m)	h (m)	$\frac{\overline{H}}{\cosh 2\pi d/L}$	wall deflection from accelerometer
Ilfracombe	0.85	12.6	1.5	0.56	0.658 m	0.0308 mm
Seaford no erosion	0.90	15.6	2.0	0.49	0.669 m	0.0258 mm

These pressures were applied to the Ilfracombe model at a S.W.L. of

2.5m (A.O.D.) and to the Seaford models at a S.W.L. of 2.0m (A.O.D.), because wall deflections were available at these states of the tide. The accelerometer on top of the Ilfracombe seawall (corresponding to node 193 in the model) indicated a mean wall deflection of 0.031mm and at Seaford a deflection of 0.026mm was indicated at node 139, for the above wave action. The properties of the foundations and backfill in the models were then modified so that the models gave the same static deflections as measured on the real seawalls. Deflections were only measured at one point on the real seawalls and the models were then modified so that they gave a corresponding deflection at that point in the model, but there was no way of knowing if the overall deflected shapes were the same.

Stress contours were also plotted for the above loading conditions and checked for continuity especially at areas of high stress concentrations, if the mis-match was greater than 5% of the magnitude of the stress then the elements at that point were re-meshed. Sample stress contour plots are shown in Figures 7.8, 7.9 and 7.10.

7.4.2 Dynamic Modelling Considerations

The relevant structural parameters necessary for a dynamic analysis are difficult to quantify because in many cases they cannot be measured. Two of the most important parameters affecting a dynamic analysis are the stiffness and the damping, neither of which could be measured directly during this investigation but had to be obtained by trial and error. Additional problems also occur due to the added mass of water constrained to move with the structure, this, and the structures natural frequencies change as the tidel level rises and falls. Then

there is the soil/structure interaction and the hydrodynamic damping both of which are largely indeterminable. One further problem which might affect seawalls is the change in poor water pressure in the foundations due to the varying heads of water at the wall, this could introduce uplift and/or back pressures, this problem does not occur at Ilfracombe or Seaford as both walls are founded upon rock.

The basic dynamic equation governing the natural frequencies of a structure is;

$$\omega_n = \sqrt{\frac{K}{M}(1 - 2\xi^2)} \quad \text{..................} \quad (7.2)$$

where ξ is the damping ratio = $C/2(MK)^{\frac{1}{2}}$

ω_n is the angular natural frequency

and K, M and C are the stiffness, mass and damping terms.

The natural frequency of a structure may therefore be increased by increasing the stiffness, or reducing the mass or damping. For many civil engineering structures the damping term is so small that it has very little effect upon the natural frequency and can be neglected for most applications, thus equation 7.2 reduces to;

$$\omega_n = \sqrt{\frac{K}{M}} \quad \text{..........................} \quad (7.3)$$

The mass term is a function of volume V and density ρ ;

$$M = \rho V$$

and the stiffness term K is a function of modulus of elasticity E, second moment of area I and length L;

$$K = A \frac{E I}{L^3} \quad \text{-- where A is some coefficient}$$

To maintain the same physical shape in the model as in the real structure, then V, I and L must remain unchanged leaving only ρ and E as the variable parameters with which to alter the natural frequency of the model. Thus to increase ω_n, E must be increased and ρ decreased. To decide whether it is more appropriate to modify the stiffness or mass terms it is necessary to know the approximate values of the forcing and natural frequencies and whether the structural response is governed primarily by the stiffness or mass terms, as shown in Figure 7.11.

From Figure 7.11 the structural response is governed by the following;

$\omega_n > \omega$ response is controlled by stiffness

$\omega_n \simeq \omega$ response is controlled by damping

$\omega_n < \omega$ response is controlled by mass

The frequency of gravity waves is in the range 0.05 to 1.0 Hz (20 to 1 second period), whilst the natural frequencies of the seawalls are of the order of 8 to 10 Hz (fundamental natural frequency), thus $\omega/\omega_n < 1$ and the structural response is controlled by the stiffness term. When

impact pressures are considered (Section 7.5) the forcing frequency is of a similar order to the fundamental frequency and the response is governed mainly by the damping.

In the PAFEC system structural damping is catered for by either including damping as a percentage of critical damping in the damping ratio (= ξ x 100%), this percentage of critical damping is then specified for each mode of vibration. Or alternatively, damping can be included as a proportion of the stiffness and/or mass matrices as a damping matrix, e.g. returning to equation 6.6;

$$[M]\{\ddot{x}\} + [C]\{\dot{x}\} + [K]\{x\} = [F]$$

where $[C] = \eta[K] + \gamma[M]$ .... (7.4)

η = proportion of stiffness matrix used in damping matrix

γ = proportion of mass matrix used in damping matrix

As response to wave loading is largely controlled by stiffness, equation 7.4 can be reduced to;

$$[C] = \eta[K] \qquad \text{.............................. (7.5)}$$

η can be related to the damping ratio ξ by introducing ;

$[U]$ which is a matrix of the normalised modes of vibration

and $\left[U^T\right]$ which is the transpose of $\left[U\right]$

resulting in;

$$\left[U^T\right]\left[K\right]\left[U\right] = \left[\lambda\right] \qquad \ldots\ldots\ldots\ldots\ldots\ldots\ldots\ldots (7.6)$$

and

$$\left[U^T\right]\left[C\right]\left[U\right] = \left[\lambda'\right] \qquad \ldots\ldots\ldots\ldots\ldots\ldots\ldots\ldots (7.7)$$

where $\left[\lambda\right]$ is a diagonal matrix with terms ${\omega_k}^2$

$\left[\lambda'\right]$ is a diagonal matrix with terms $2\xi\omega_k$

ω_k is the kth natural frequency

combining equations 7.5, 7.6 and 7.7

gives

$$\left[U^T\right]\left[C\right]\left[U\right] = \eta\left[U^T\right]\left[K\right]\left[U\right] \qquad \ldots\ldots\ldots\ldots\ldots\ldots\ldots\ldots (7.8)$$

or

$$\left[\lambda'\right] = \eta\left[\lambda\right] \qquad \ldots\ldots\ldots\ldots\ldots\ldots\ldots\ldots (7.9)$$

Equation 7.9 can also be written as

$$2\xi\left[\omega_k\right] = \eta\left[{\omega_k}^2\right] \qquad \ldots\ldots\ldots\ldots\ldots\ldots\ldots\ldots (7.10)$$

thus the damping ratio $(\xi) = \frac{1}{2}\eta\,\omega_k \qquad \ldots\ldots\ldots\ldots\ldots\ldots\ldots\ldots (7.11)$

Therefore the proportion of the stiffness matrix used as a damping matrix is approximately half of the damping ratio. A typical value of the damping ratio for civil engineering structures of this type is 0.02 (Ref.83), the very large values of ξ found in Chapter Six (i.e. 27.6 and 19.8% for Ilfracombe and Seaford respectively) are not used because they are unrealistically high as explained in Chapter Six.

When modelling the seawalls, the natural frequency of the fundamental bending model can be modelled exactly, but all higher modes of vibration will be subject to slight errors because the model boundary conditions are not exactly representative of the real structures. This does not introduce large inaccuracies into the models because the higher modes of vibration are not greatly excited so the majority of the energy is contained in the fundamental mode of vibration.

The fundamental modes of vibration for the Ilfracombe and Seaford (no erosion) seawalls are 8.9 and 10.3 Hz respectively, these values were obtained from the spectral density plots of seawall accelerations (see Section 3.2.3). The properties of the foundation and backfill in the models were altered (by trial and error) until both static deflections and fundamental natural frequencies were the same as those of the real structures. When these conditions were acheived it could confidently be assumed that the models closely reproduced both the static and dynamic response of the real seawalls to the degree necessary for further analysis.

7.5 Seawalls Subjected to Transient Excitation

As already mentioned, many authors are of the opinion that transient impact pressures have no structural significance, i.e. Ross(35) states "the larger pressures are of too short duration for a structure of much weight to be moved appreciably", he concludes "usually the high pressures will not be important". Hayashi and Hattori(17) conclude "when the duration (of the impact pressure) is very small, the wave pressure, even if its intensity is very large, may not have the effect of a force". These comments resulted from model experiments in wave tanks where the transients lasted in the order of one milli-second, whilst full scale transients generally have a duration of 0.1 to 0.2 seconds, (see Chapter Three).

In this section the effects of real transient pressures on seawalls are investigated, with particular regard to the resulting structural response.

7.5.1 Transient Response Analysis by PAFEC

Because of the random nature of the transient wave forces, they can not be represented by an excitation force derived by the superposition of a number of sinusoids. Therefore an analytical solution is not possible, hence a deterministic method must be used, enabling the solution to proceed by a stepwise or numerical intergration technique, (the forcing function must be known at all points in time before this technique can be used, statistical data alone is not sufficient).

The most inherently stable of the commonly used numerical methods is the Newmark-Beta method, hence this method is used for the transient analysis.

In a numerical approach the displacements at time $t + \delta t$ are needed, they can be found by introducing the Newmark-Beta parameter (β) as follows;

$$\{x\}_{t+\delta t} = \{x\}_t + \delta t\{\dot{x}\}_t + (\tfrac{1}{2} - \beta)\cdot \delta t^2 \{\ddot{x}\}_t + \beta \delta t^2 \{\ddot{x}\}_{t+\delta t} \quad \cdots (7.12)$$

when combined with equation 6.6 i.e $[M]\{\ddot{x}\} + [C]\{\dot{x}\} + [K]\{x\} = \{F\}$

this leads to the recurrence relationship (120);

$$\begin{aligned}\{x\}_{t+\delta t} = [R_3]\{x\}_t - [R_2]\{x\}_{t-\delta t} + \beta \delta t^2 [R_1] \cdot \Big[&\{F\}_{t+\delta t} \\ &+ (1/\beta - 2)\{F\}_t + \{F\}_{t+\delta t} \Big] \quad \cdots\cdots\cdots\cdots (7.13)\end{aligned}$$

the matrices $[R_1]$, $[R_2]$ and $[R_3]$ above , are given by;

$$[R_1] = ([M] + \delta t/2[C] + \beta \delta t^2/2)^{-1}$$

$$[R_2] = [R_1]\,([M] - \delta t/2[C] + \beta \delta t^2[K])$$

$$[R_3] = [R_1]\,(2\,[M] - (1 - 2\beta)\cdot \delta t^2[K])$$

The $\{F\}$ terms in equation 7.13 are the lists of the values of the forces at the times indicated by the subscript.

This process uses the displacements vector $\{x\}$ at times $t - \delta t$ and t in order to find $\{x\}$ at times $t + \delta t$, therefore at time $t = 0$ a starting algorithim is required, as follows;

$$\{x\}_{\delta t} = \frac{([M] + (\delta t[C])/2 + \delta t^2(\beta - \tfrac{1}{2})[K])\,\{x\}_o - \delta t[M]\{\dot{x}\}_o}{([M] + (\delta t[C])/2 + \delta t^2\beta\,[K])} \quad \ldots (7.14)$$

this equation assumes the initial displacements $\{x\}_o$ and velocities $\{\dot{x}\}_o$ are known.

The value of β chosen refers to the way in which the accelerations $\{\ddot{x}\}$ vary through each time step, as shown below;

value	Remarks
0	Acceleration constant over each time step, equal to start value
$\frac{1}{8}$	Acceleration has a time step change at times $t + \delta t/2$, $t + 3\delta t/2$, etc.
$\frac{1}{6}$	Linear variation of acceleration over each time step.
$\frac{1}{4}$	Acceleration constant over each time step, equal to mid-step value

values of 1/6 or 1/4 will be suitable for most applications, $\beta = 1/4$ gives unconditional numerical stability but may distort vibratory period, $\beta = 1/6$ gives less numerical stability but more stability of vibratory period, $\beta = 1/6$ was used in this analysis.

7.5.2 Response to Wave Impact Pressure

Seawall response to real wave impact pressures was only investigated with the Ilfracombe seawall model because this was the only site at which any simultaneous vertical impact pressure distributions were measured. Because the method of analysis is deterministic, the time history of the wave impact must be known for all time, so a vertical pressure distribution (containing both impact and hydrostatic components) as actually measured, was applied to the Ilfracombe model as shown in Figure 7.12.

Impact pressures were only measured at transducers number 1 and 3 (nodes 115 and 77 in the model) a distance of 1.6m apart, pressures were assumed to act over the whole area between these two transducers with the pressures at the intermediate nodes (nodes 104 and 91) found by linear interpolation. The maximum impact pressure at transducer No. 1 occurs fractionally before that on transducer No. 3, this delay appears to be about 0.005 seconds, therefore the time step δt in the Newmark-Beta analysis was taken as 0.005 seconds and the percentage critical damping was taken as 0.02 . The resulting structural response (deflection) is shown in Figure 7.13. This figure shows a large dynamic deflection due to the impact pressure followed by a lower almost static deflection caused by the second (hydrostatic) peak in the pressure history. The magnitude of this dynamic deflection is about four times the static deflection, although the dynamic (impact) pressure is only two to three times larger than the static pressure. Therefore this large dynamic deflection must be the result of dynamic amplification caused by the impact pressure, (this is investigated in more detail in Section 7.7).

Thus it seems likely that impact pressures occuring in real seas, with rise times of the order of 0.1 seconds, cause significant structural response.

The magnitude of this impact generated response is 0.115mm (at node 193) and occurs after 0.50 seconds. The applied impact pressure reached its maximum after 0.47 seconds, thus the response of the seawall is lagging behind the applied force by about 30 milli-seconds. This shows that a large structure, such as a seawall, cannot respond instantly to changes in the loading conditions.

The actual seawall deflection was not measured for this individual impact, but the average deflection for this period of impacts was about 0.035mm, so it seems that the predicted maximum deflection of 0.115mm is of the correct order of magnitude. This also indicates that the percentage of critical damping used for this analysis (0.02%) is of the right order.

7.6 The Effects of Damping on Structural Response

Seawalls are generally constructed from natural stone, mass or reinforced concrete, initially these structures will have a damping ratio of about 0.02(83), but during their lifetime they are liable to cracking, either through shrinkage, subsidence, harsh service conditions etc., also erosion is likely in some cases. Both erosion and cracking will cause the structral damping to vary during the lifetime of the structure. The effects, on damping, of changes in mass of a structure (due to erosion) can be calculated from equation 6.6, but the effects of

cracking can not be quantified.

The degree of cracking in concrete structures is important because cracking increases the damping ratio (ξ), even if the cracks are not discernable by eye they can still increase ξ, and as cracking continues ξ can be increased two or three fold$^{(83)}$. Therefore as the degree of seawall damping is likely to change during its lifetime, it is useful to investigate the effects of changes in damping on structural response. The damping ratio of the Ilfracombe seawall model was varied from 0.005 to 0.08 in increments of 0.015 to cover the expected range of values for seawalls. The model was subjected to the vertical pressure history shown in Figure 7.12, the resulting wall displacement is plotted against the damping ratio, as in Figure 7.14.

In Figure 7.14 wall displacement is seen to decrease with increasing damping ratio, this was the expected outcome as indicated by Figure 7.11. The reduction in displacement is not linear with increasing damping ratio, probably due to rounding errors and the relatively large time step used in the Newmark-Beta analysis, but there is a definite downwards trend.

The undamped wall response gives a maximum displacement of 0.120mm, whilst the displacement at the damping ratio assumed for the Ilfracombe seawall ($\xi = 0.02$) is 0.115mm, a difference of less than 5%. Even the displacement for a damping ratio of 0.08 is only 19% less than the undamped displacement. Therefore it appears that small changes in damping caused by cracking or erosion of seawalls will have little effect on the response, although, of course, cracking will effect the integrity of the structure and could lead to failure.

So if the structure can be assumed to be lightly damped then only a small error is introduced by taking it to be undamped, but a large saving is made in computations. Thus seawalls similar to that at Ilfracombe can probably be assumed to be undamped for most purposes with only a small loss of accuracy.

7.7 The Effects of Rise Time on Structural Response

Impact pressures have been measured in the laboratory with minimum rise times of the order of 0.5 milli-seconds(14), it was on the basis of this sort of data that authors suggested that impact pressures have no structural significance. Yet full scale impacts in a real sea can have rise times of the order of 100 to 200 milli-seconds, as measured during this investigation. Impact pressures with these longer durations have been shown in Section 7.5.2 to cause appreciable deflections in a real seawall.

In Chapter Three, Section 3.4, it was seen that rise time was largely dependent upon the percentage of air entrained in the breaking wave, generally in a real sea there will be considerable air entrainment, but because millions of waves impinge on a seawall during its lifetime there is a possibility that a perfect breaking wave with very little entrained air will strike the wall. If this happens then an extreme shock pressure with short duration will occur, Rouville et al(7) measured just such a pressure of 690 KN/m^2 with a rise time of about 25 milli-seconds. Therefore it would be useful to know if these short duration impacts generate a response in a real seawall. This would determine whether the high pressures, with short rise times, measured in model studies are a suitable basis on which to design real seawalls. So with this in mind, an arbitary impact pressure was applied to the Ilfracombe seawall model (ξ =0.02) at nodes 115, 104, 91 and 77. The total impulse of this arbitary impact was fixed at 1.22 KN.s/m^2 (this was the average impact impulse measured on the Ilfracombe seawall), and the rise time was varied between 1 and 200 milli-seconds to cover the range of both model and full scale wave impacts.

The six cases of loading chosen are shown below;

load case	rise time (t)	impact pressure (P)	impulse = Pt/2
1	1 mS	2440 KN/m^2	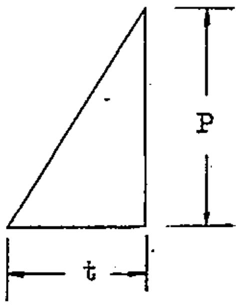
2	10 mS	244 KN/m^2	
3	50 mS	48.8 KN/m^2	
4	100 mS	24.4 KN/m^2	
5	150 mS	16.3 KN/m^2	The impulse is constant at 1.22 KN.s/m^2
6	200 mS	12.2 KN/m^2	

In this table load cases 4 to 6 correspond to the type of rise times and impact pressures measured during this investigation, and load cases 1 and 2 show the very high pressures possible (for the same impulse) but for very short rise times. The resulting dynamic deflections of the Ilfracombe seawall model for the above six loading cases are compared in Figure 7.15 with the deflections produced by the static application of the same loads.

From Figure 7.15 it is seen that the ratio dynamic deflection/ static deflection reaches a maximum value at a rise time of about 40 mS. This represents a static deflection of 12.2% and remains constant at this value for all rise times greater than 40 mS, but for rise times less than 40 mS this percentage falls very rapidly to a value of 0.02% at a rise time of 1 mS. This indicates that the seawall cannot respond fully to forces of less than about 40 mS duration, as was found in Section 7.5.2.

The maximum dynamic deflection does not approach the value of the equivalent static deflection because the applied load is not stationary and only reaches its maximum value for an instant (e.g. a cusp), hence the load has dissipated before the structure has had time to respond fully.

Figure 7.15 was produced assuming a damping ratio of 2%, the dynamic deflection is likely to be reduced for larger values of the damping ratio, as demonstrated by Figures 7.11 and 7.14.

For a wave impact lasting 7 milli-seconds the Ilfracombe seawall model has a dynamic deflection which is only 1% of that produced by the static application of the same load, so it seems unlikely that impacts of this duration, or less, will have any significant gross effect on the deflection of the real seawall, although the high pressures associated with these impacts might have a localised effect. As most model investigations measured rise times less than 7 milli-seconds then it would appear that the model test data is not suitable for the basis of full scale seawall design and if used, would produce highly conservative structures.

Figure 7.15 is shown in non-dimensionalised form in Figure 7.16, by plotting the ratio t_i/T against dynamic amplification, (where t_i is the rise time and T is the natural period of vibration of the seawall). From this figure it can be seen that the maximum dynamic amplification occurs at a value of t_i/T of approximately 0.5, thus it seems that the seawall cannot respond fully to impacts with durations less than about half the natural period of vibration of the structure. The dynamic amplification for impacts lasting longer T/2 seconds seems to be governed by the magnitude of the impulse, as is seen from load cases 3, 4, 5 and 6 which all have rise times $\gg T/2$ seconds with the same value impulse and so have the same dynamic amplifications. Whilst the dynamic amplification for impacts lasting less than T/2 seconds is governed by the rise time t_i as can be seen from load cases 1 and 2 where the dynamic amplification increases as the rise time increases for impacts with $t_i \ll T/2$ seconds, even though the impulse remains constant.

7.7.1 The Effects of Multiple Impacts on Structural Response

In Figure 7.15 it was seen that a triangular impulse generated a maximum dynamic deflection which was only about 12% of that produced by the static application of the same load. This idealized triangular impulse represents the case where a single (vertical) wave front impinges against a seawall reaching its maximum value simultaneously over the whole wave front. In a real sea it is possible that two or more waves could impinge on a wall in quick succession perhaps due to wave reflection (which is a distinct possibility at Ilfracombe due to rocky foreshore). Thus if two or more impacts occur in quick succession then the wall will still be responding to the first impact when the second impact occurs in which case the dynamic deflection is likely to be greater than that shown in Figure 7.15.

As already seen the seawall cannot respond instantly to wave impact loading (maximum response generally occurs about 30 milli-seconds after the impulse has reached its maximum value, see Figure 7.17), therefore the maximum seawall deflection occurs after the impulse on the wall has finished. Thus when the wave impulse has finished the seawall is still accelerating in the direction of the wave impact (Figure 7.17), so if a second impulse occurs soon after the first then the wall will already be moving in the direction of the impact so there will be less resistence to overcome, so large deflections might be expected. If the second impulse occurs more than about $\frac{T}{4}$ milli-seconds after the first then the seawall will have started to return to its equilibrium position, so the second impulse will have to overcome the opposing seawall inertia, thus the cumulative deflection will probably be smaller than if the impacts occur within $\frac{T}{4}$ milli-seconds of each other.

To examine the effects on seawall response of two successive wave impacts, each of the six triangular impulsive load cases from Section 7.7 were applied twice in quick succession to the Ilfracombe seawall model. The time delay between these successive impacts was made $\frac{T}{8}$ milli-seconds for the first case and then increased to $\frac{3T}{8}$ milli-seconds for the second case, the resulting structural response is shown in Figure 7.18.

In this figure it is seen that the greatest dynamic amplification occurs when the time delay between impacts is $\frac{T}{8}$ milli-seconds, when the time delay is increased to $\frac{3T}{8}$ milli-seconds then the dynamic amplification is only slightly greater than that for an individual impact. The maximum dynamic amplification caused by two successive impulses $\frac{T}{8}$ milli-seconds apart reaches a value of 1.07, whilst the same two impulses applied $\frac{3T}{8}$ milli-seconds apart produce a maximum dynamic amplification of 0.17 and the same impulse applied once only produces a maximum dynamic amplification of 0.12. Therefore it seems that if a second impulse occurs whilst the seawall is still responding to the first impulse then the cumulative structural response can be much greater than that caused by two individual impacts, i.e. the deflection produced by an individual impact was 12% of the equivalent static displacement, but the deflection produced by the same impact applied twice with a $\frac{T}{8}$ milli-second time delay was 107% of the static deflection, an increase in deflection of over 800%.

7.7.2 Resonant Amplification

The natural frequency of the Ilfracombe seawall is 8.9 Hz, thus load case number 4 (from Section 7.7), with a rise time of 0.1 seconds, has a frequency of the same order as the natural frequency of the wall. No resonant amplification is apparent at this, or any other frequency, in Figure 7.15, the reason for this is that it takes a number of loading cycles to build up resonance in a structure (from rest), as shown below(115);

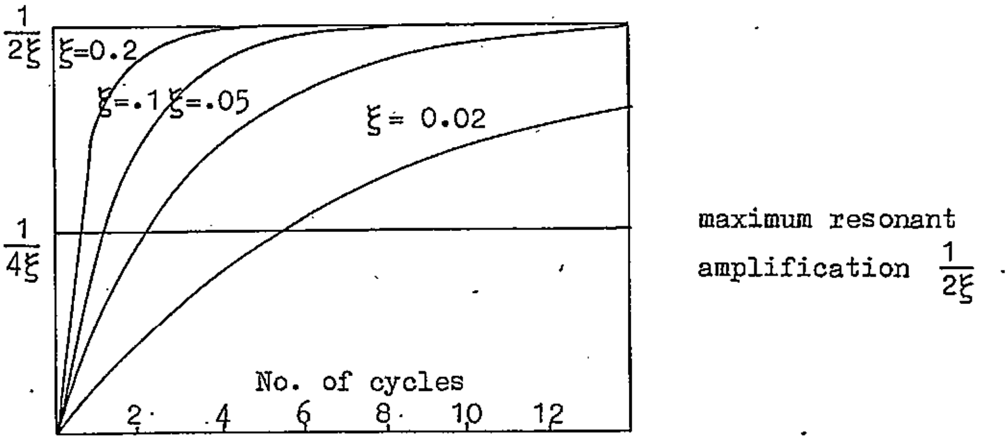

Rate of build up of resonant response from rest

Therefore a single impact, even if its frequency is the same as the structures natural frequency, will cause an insignificant amount of resonant amplification. Thus in a real sea where impacts occur only during the impinging of the wave front, about every four seconds (at Ilfracombe), no resonant amplification will occur because the effects of the first impact will have died away in the four seconds before the next impact occurs.

7.8 The Transfer Function Between Wave Pressure and Seawall Response

The transfer function concept was introduced in Chapter Six, where it was shown that the input or excitation spectral density was related to the output or response spectral density by means of a frequency domain transfer function , (Eq. 6.37). To solve equation 6.37 for a MDOF system would probably involve the computation of cross spectral density components, as shown in equation 6.38, therefore the alternative method given in Section 6.6 is used. This method sets up a frequency domain transfer function by applying a number of sinusoidal forces of single frequency and unit amplitude to the structure and finding the displacement for each frequency sinusoid used.

For this investigation a transfer function was only constructed for the Ilfracombe seawall over the frequency range 0 Hz to 20 Hz. This transfer function, Figure 7.19, was set up by applying single frequency sinusoidal forces of unit amplitude in 0.5 Hz increments from 0 to 20 Hz, the seawall displacement was found for each incremental force and plotted against the frequency of that force to form the transfer function. The vertical axis of Figure 7.19 was normalised by dividing through by the displacement at 0 Hz, this then gives a non-dimensionalised plot of the system gain. This transfer function can now be multiplied by the spectral density of the excitation force on the seawall to give the spectral density of the seawall response. The spectral density of the excitation force is shown in Figure 7.20 and has a peak at about 0 Hz and then flattens off to a fairly steady level between 2 and 20 Hz. The product of Figures 7.19 and 7.20 is shown in Figure 7.21, where the predicted spectral density of seawall response is shown along with the measured spectral density of seawall response. The measured spectral density plot shown in Figure 7.21 is an expansion of Figure 3.12 plotted on a log scale.

The measured and predicted plots of seawall response show good correlation of spectral densities from 0 to 1 Hz and again at the fundamental natural frequency (8.9 Hz), but at all other frequencies the measured spectral density greatly exceeds the predicted values. There are a number of factors which could account for this and one of the most likely is that the excitation spectral density (Figure 7.20) was only measured at one transducer and is assumed to be the only excitation force on the wall, but the excitation force varies with elevation because the pressure varies with elevation. Thus the measured seawall response (Figure 7.21) is not due solely to the excitation force shown in Figure 7.20. Also the finite element model takes no account of the constantly varying natural frequency brought about by continuous changes in the hydrodynamic damping, which if included in the model would cause the peak in the transfer function (Figure 7.19) to be much broader and more representative of the actual structural response.

7.9 The Effects of Erosion at Seaford

The Seaford finite element model without erosion was modelled to give similar deflections and natural frequencies to the real seawall, the Seaford model with erosion was then given the same material properties for the wall, foundations and backfill as the model without erosion. As both models had exactly the same constraints and material properties then any changes in response would be due solely to the erosion of the wall.

The following table summarises the changes in static and dynamic response of the models when subjected to the wave pressure shown in Figure 7.4

Model	Deflection at node 139 due to pressure shown in Figure 7.4	Fundamental natural frequency
Seaford without erosion	0.026 mm	10.3 Hz
Seaford with erosion	0.004 mm	10.47 Hz

The model with erosion has a smaller deflection at node 139 than the model without erosion, this is because it is tending to rotate rather than move horizontally, as shown in Figures 7.22 and 7.23. This rotation occurs because the resultant force on the wall with erosion has a greater vertical component than that on the wall without erosion. This difference in angle of the resultant force occurs because

the hydrostatic pressure acts normal to the face of the wall, so the wall without erosion will have a larger horizontal pressure component because it has a greater surface area which is predominately vertical due to the vertical fronted steps.

The natural frequency increases by about 1½% for the wall with erosion, this increase is proportional to the reduction in mass of the wall due to the erosion.

The stresses generated in the wall without erosion are seen to be highly concentrated on the face, in the region of the steps (Figure 7.8), these stress concentrations are induced by the sharp angles of the steps. Thus, as expected, the wall with erosion has none of these stress concentrations on the wall face (Figure 7.9). The stress concentrations around the perimeter of the two models are caused by approximations in the modelling, in the real seawall these stresses would be dissipated throughout the foundations and backfill.

Thus it seems that the erosion of the wall at Seaford has very little effect on its dynamic response, or static response as the deflections at the base of the wall are of the same order for both models. The main effect of the erosion seems to be in relieving the stress concentrations in the face of the wall, and in changing the angle of the resultant hydrostatic force. In some circumstances this latter point might have an effect on the stability of the wall when considering the overturning moments.

7.10 Finite Element Analysis of a Pressure Transducer Diaphragm

The pressure transducers built into the seawall at Seaford quickly became so severely damaged by the shingle in the impinging waves that they were rendered useless and so had to be replaced, (this damage is discussed in more detail in Chapter Two). The transducer diaphragms (26mm dia. x 1mm thick stainless steel) generally all had a permanent deformation of 3mm at their centres, this was the limit of travel, as shown in Plate 2.16.

An approximation of the force necessary to cause this damage was sought in order to allow comparison with the wave impact pressures actually measured by the transducers (whilst they were still functioning correctly). The analysis was carried out using the PAFEC package, as the deformations were permanent, a plastic rather than elastic analysis was used, (plastic analysis is catered for by PAFEC). The 26mm diameter diaphragm was the only part of the transducer to be modelled, (to save on computer time), so in order to represent the constraints applied to the diaphragm by the transducer body the edges of the diaphragm were assumed fully fixed. The diaphragm was divided into 48 elements, being a combination of 3 and 4 sided two dimensional thin plate elements with a total of 49 nodes, as shown in Figure 7.24.

The actual loading condition occurring in the field due to the combined wave and shingle impact could not be determined, but was probably a combination of a uniformly distributed load due to the wave impact and a point load due to the shingle impact. From inspection of the damaged transducers small indentations could be seen on the

deformed diaphragm. Thus the main damage was probably caused by the impact of shingle, the area over which these impacts occurred would depend on the size and shape of the individual pieces of shingle, which again could not be determined. Hence two load cases were chosen for the plastic analysis; (i) a central point load and (ii) a uniformly distributed load, these two load cases represent the two possible extremes of loading, (the loading was assumed as static, whereas in practice it would be dynamic).

The PAFEC point load analysis (load case (i)) estimated an 18 KN load (Figure 7.25), and the uniformly distributed load analysis (load case (ii)) estimated a pressure of 125 x 10^3 KN/m^2 (Figure 7.26), both to produce a 3mm plastic deformation at the centre of the diaphragm. Therefore it is possible to say that the transducer diaphragm was not deformed solely by a uniformly distributed hydrostatic pressure because this would require a pressure of 125 MN/m^2 when the maximum wave pressure measured at Seaford was only 48 KN/m^2. The point load assumption requires a force of 18 KN to cause a 3mm deformation, this is perhaps conceivable if a very angular piece of shingle struck the centre of the diaphragm. But more likely the deformation was caused in small stages by shingle impact over a matter of days, culminating in the deformation shown in Plate 2.16.

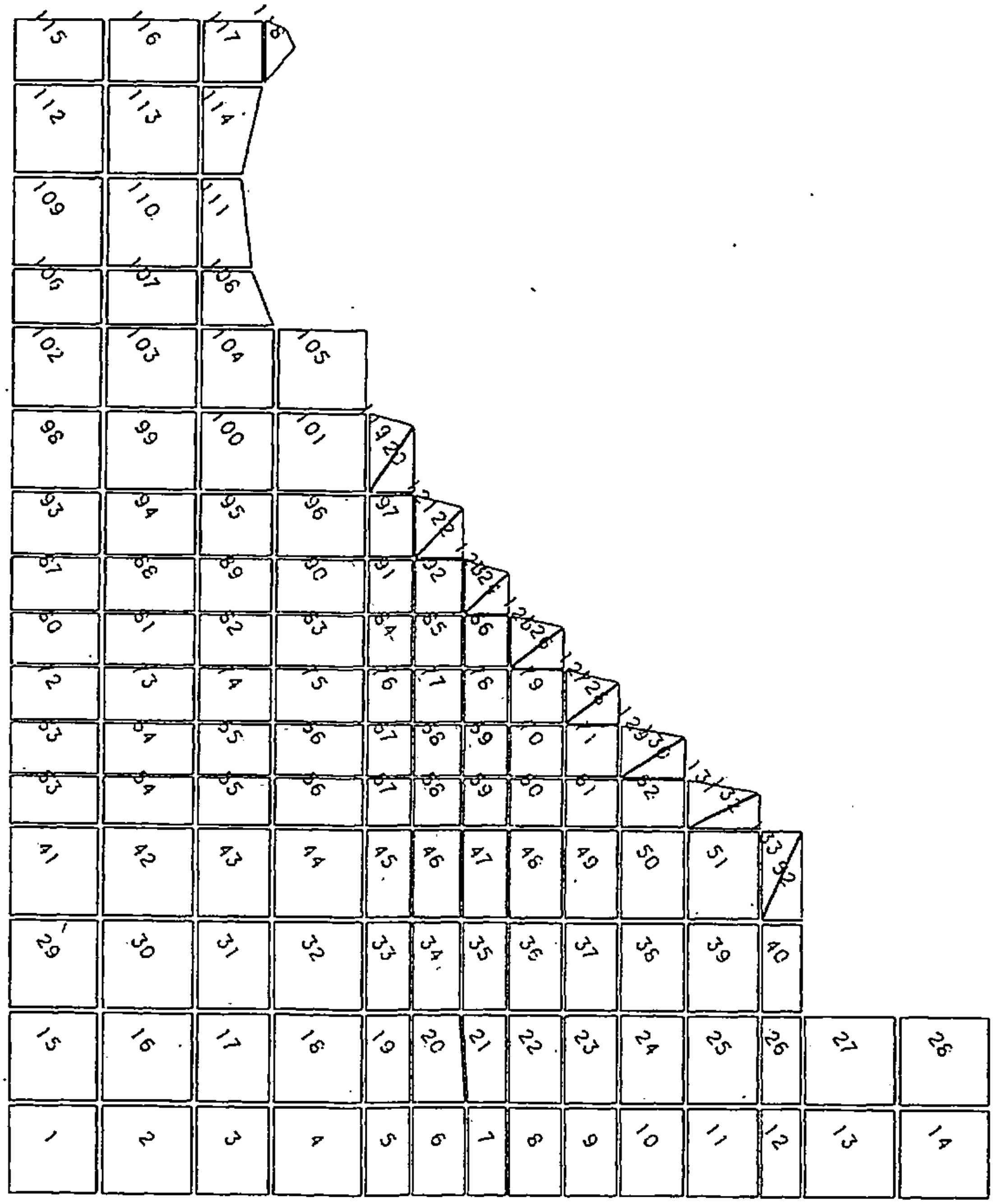
115
116
117
118
112
113
114
109
110
111
102
103
104
105
98
99
100
101
93
94
95
96
97
41
42
43
44
45
46
47
48
49
50
51
29
30
31
32
33
34
35
36
37
38
39
40
15
16
17
18
19
20
21
22
23
24
25
26
27
28
1
2
3
4
5
6
7
8
9
10
11
12
13
14

Figure 7.1 Finite element model of the Seaford seawall without erosion (element numbers shown)

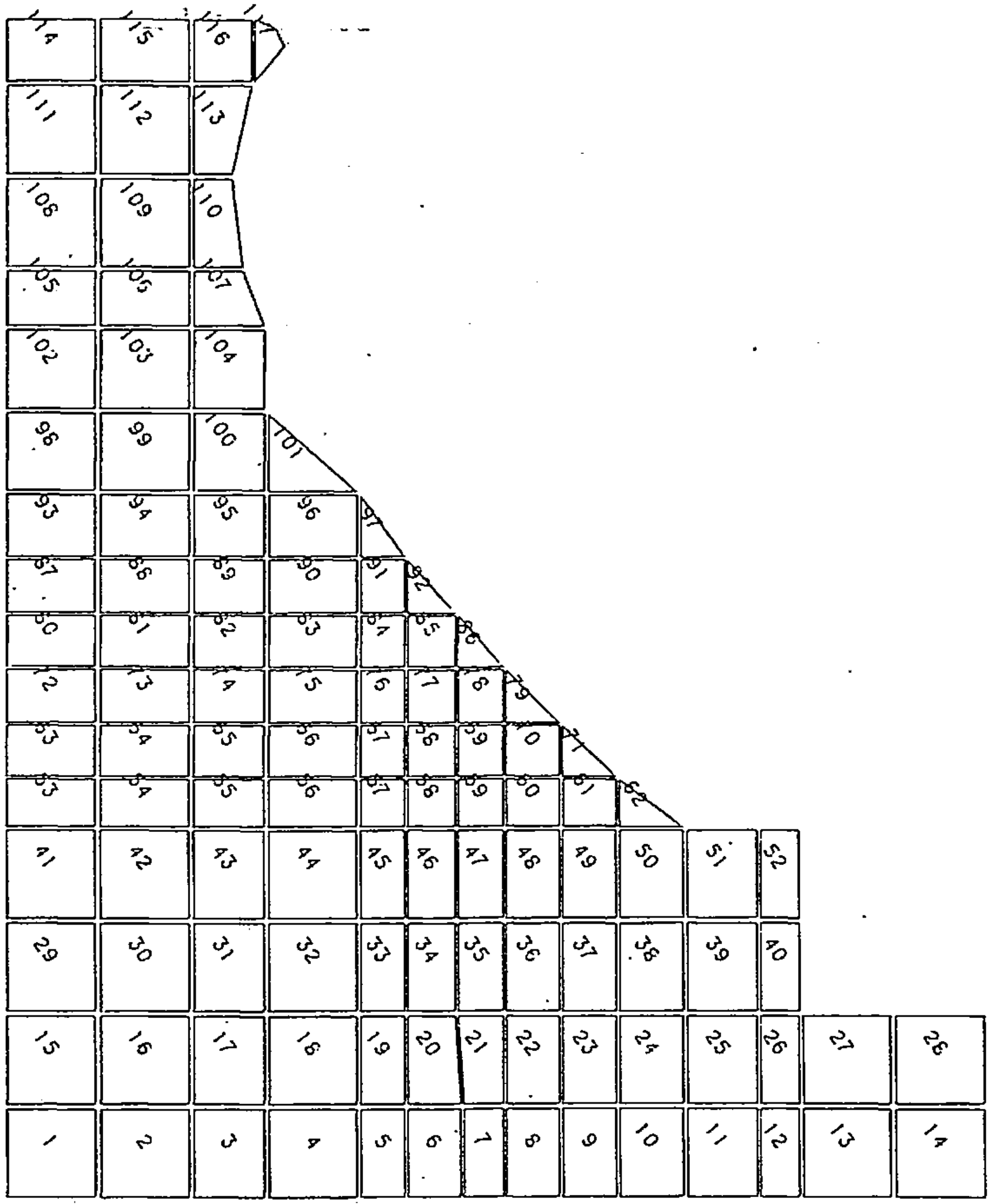

Figure 7.2 Finite element model of the Seaford seawall with erosion (element numbers shown)

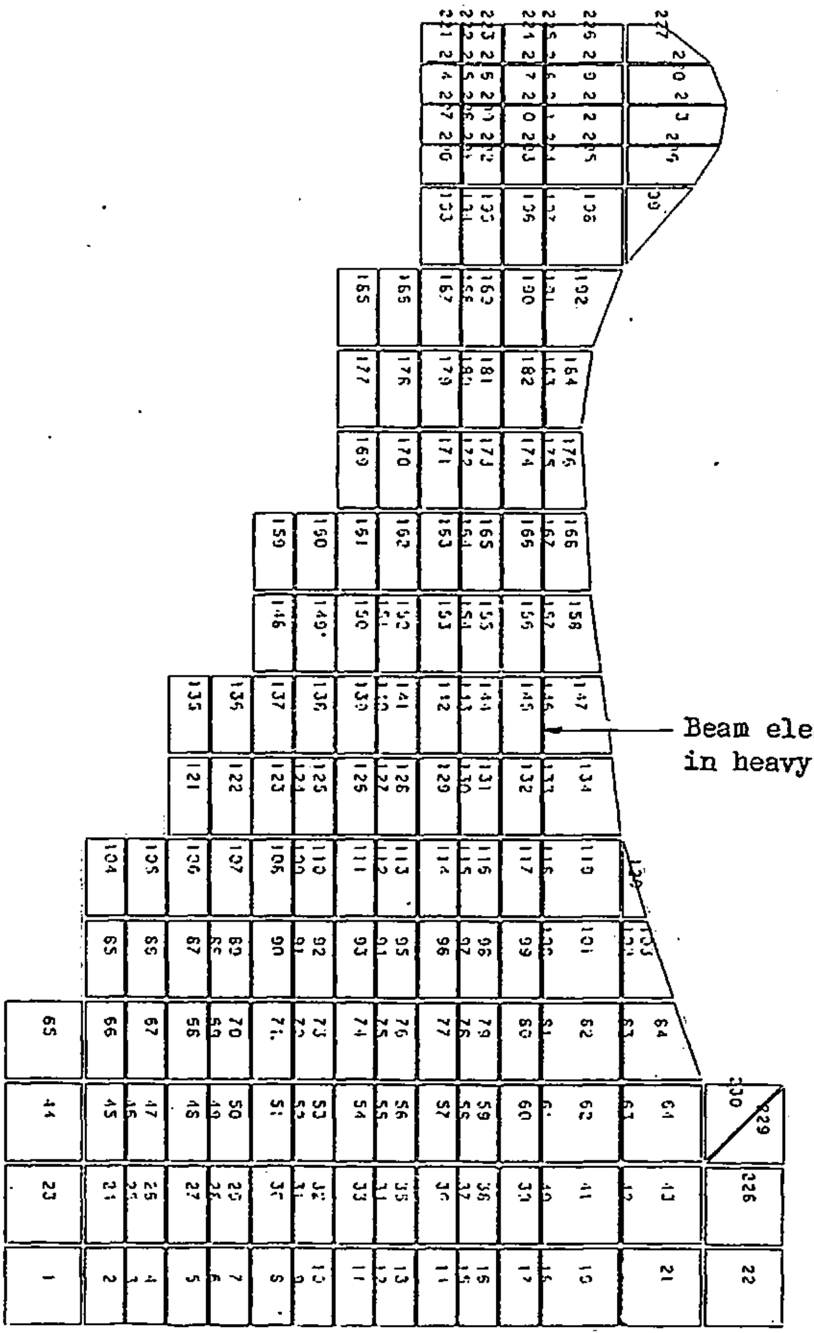

Beam elements shown in heavy lines

Figure 7.3 Finite element model of the Ilfracombe seawall (element numbers shown)

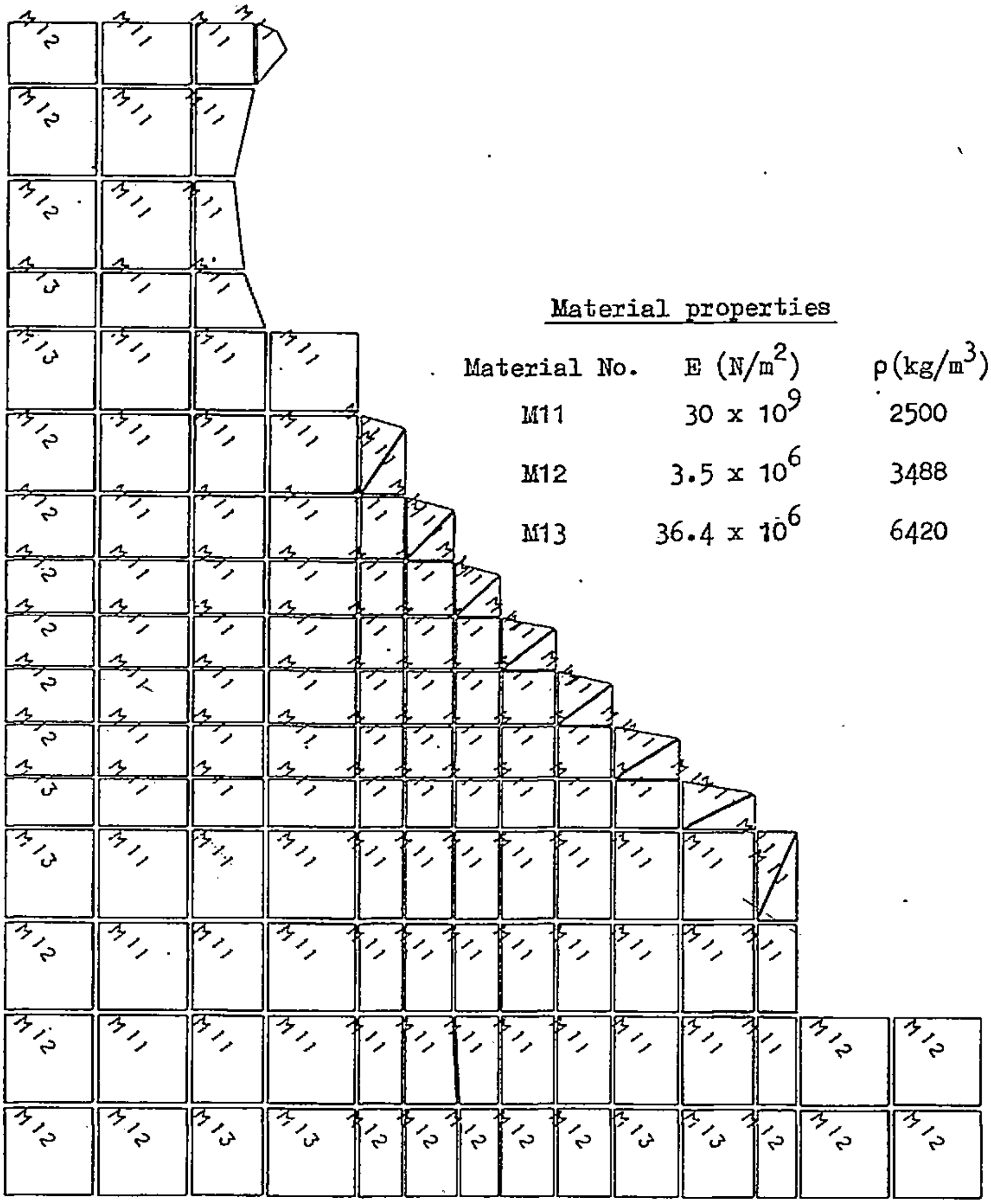

Material properties

Material No.	E (N/m^2)	ρ(kg/m^3)
M11	30×10^9	2500
M12	3.5×10^6	3488
M13	36.4×10^6	6420

Figure 7.4 Finite element model of the Seaford seawall (without erosion) showing the material properties of the foundation and backfill necessary to ensure a model response similar to the real wall response.

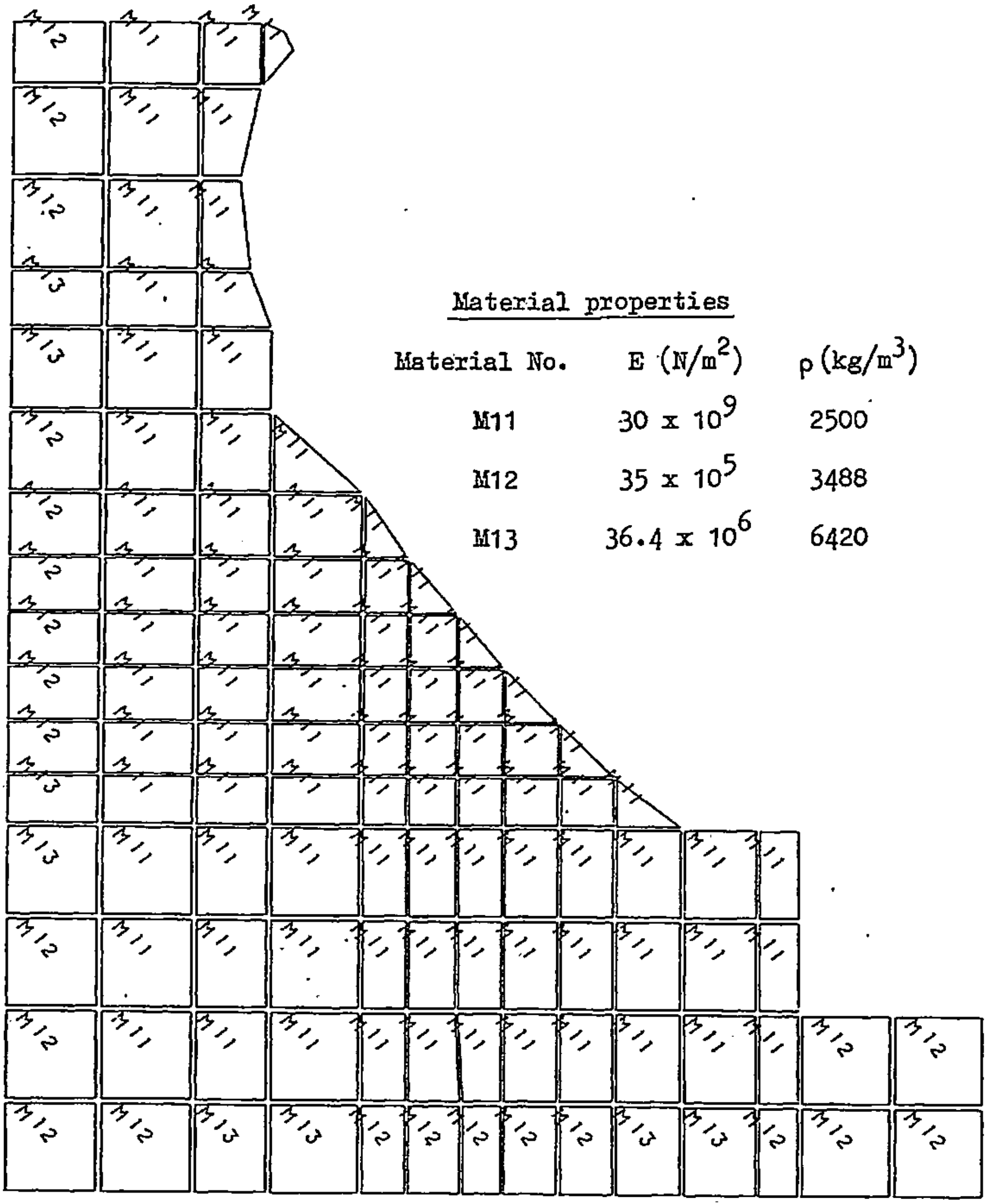

Material properties

Material No.	E (N/m^2)	ρ (kg/m^3)
M11	30×10^9	2500
M12	35×10^5	3488
M13	36.4×10^6	6420

Figure 7.5 Finite element model of the Seaford seawall (with erosion) showing the material properties of the foundation and backfill necessary to ensure a model response similar to the real wall response.

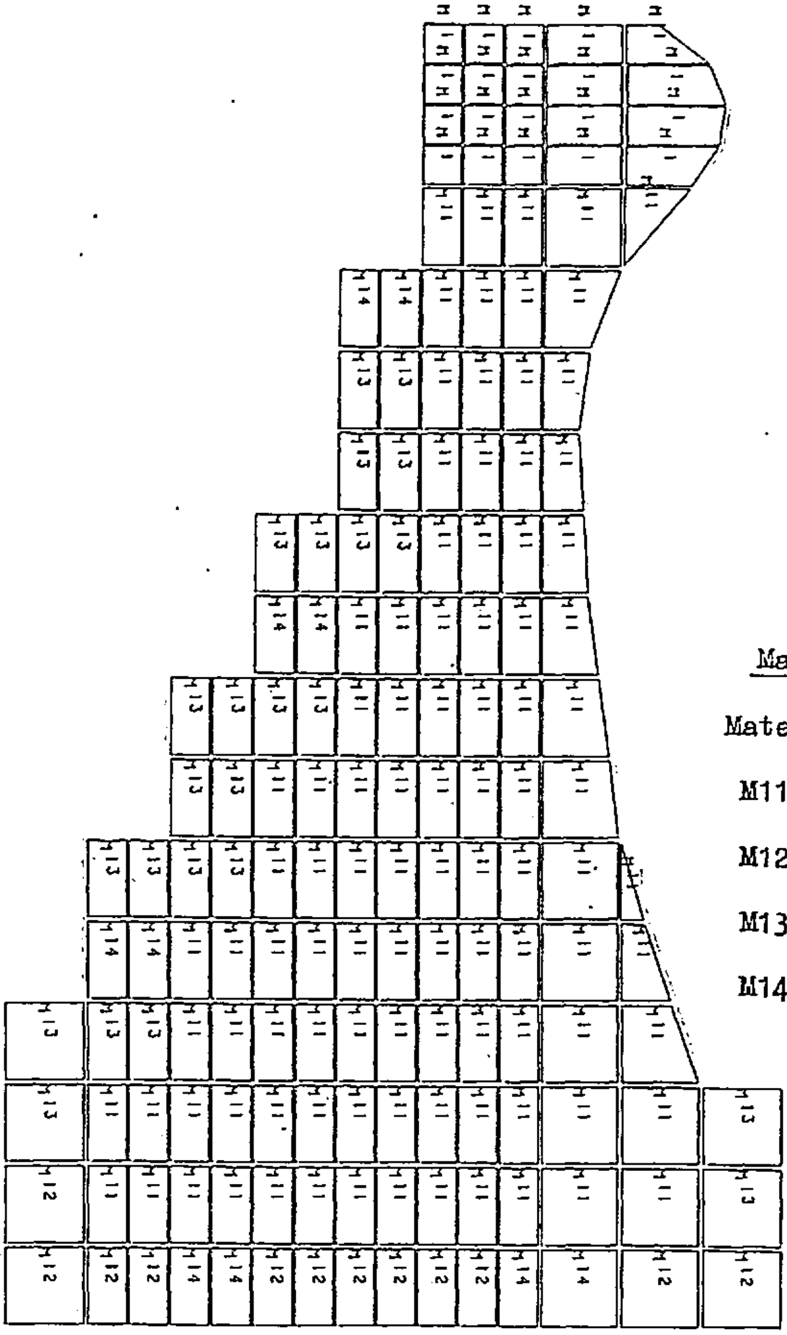

Material properties

Material No.	E (N/m^2)	$\rho(kg/m^3)$
M11	30×10^9	3000
M12	3.67×10^6	2352
M13	3.95×10^6	2996
M14	1.42×10^7	8230

Figure 7.6 Finite element model of the Ilfracombe seawall showing the material properties of the foundation and backfill necessary to ensure a model response similar to the actual wall response.

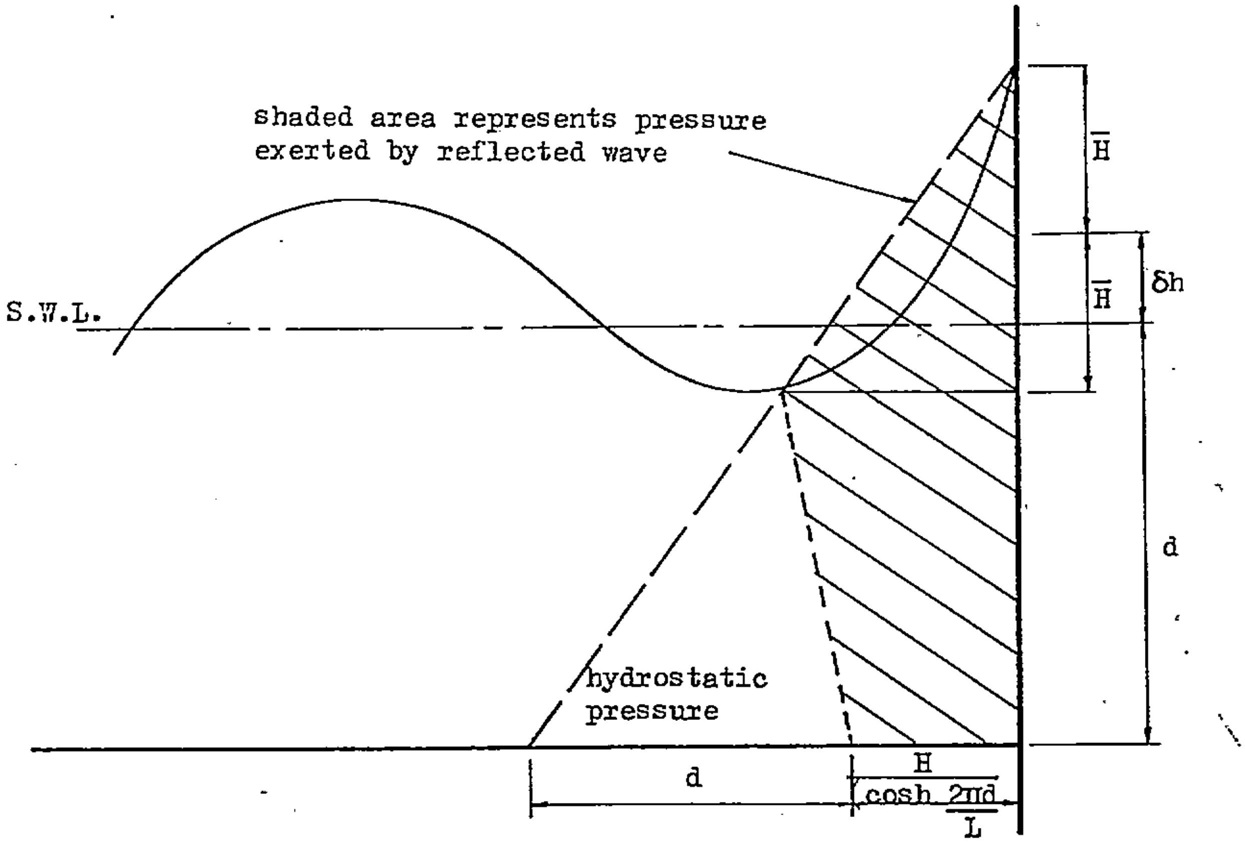
shaded area represents pressure exerted by reflected wave
S.W.L.
$\overline{H}$
$\overline{H}$
δh
d
hydrostatic pressure
d
$\frac{H}{\cosh \frac{2\pi d}{L}}$

Figure 7. 7 Hydrostatic wave pressure for fully reflected waves (not to scale)

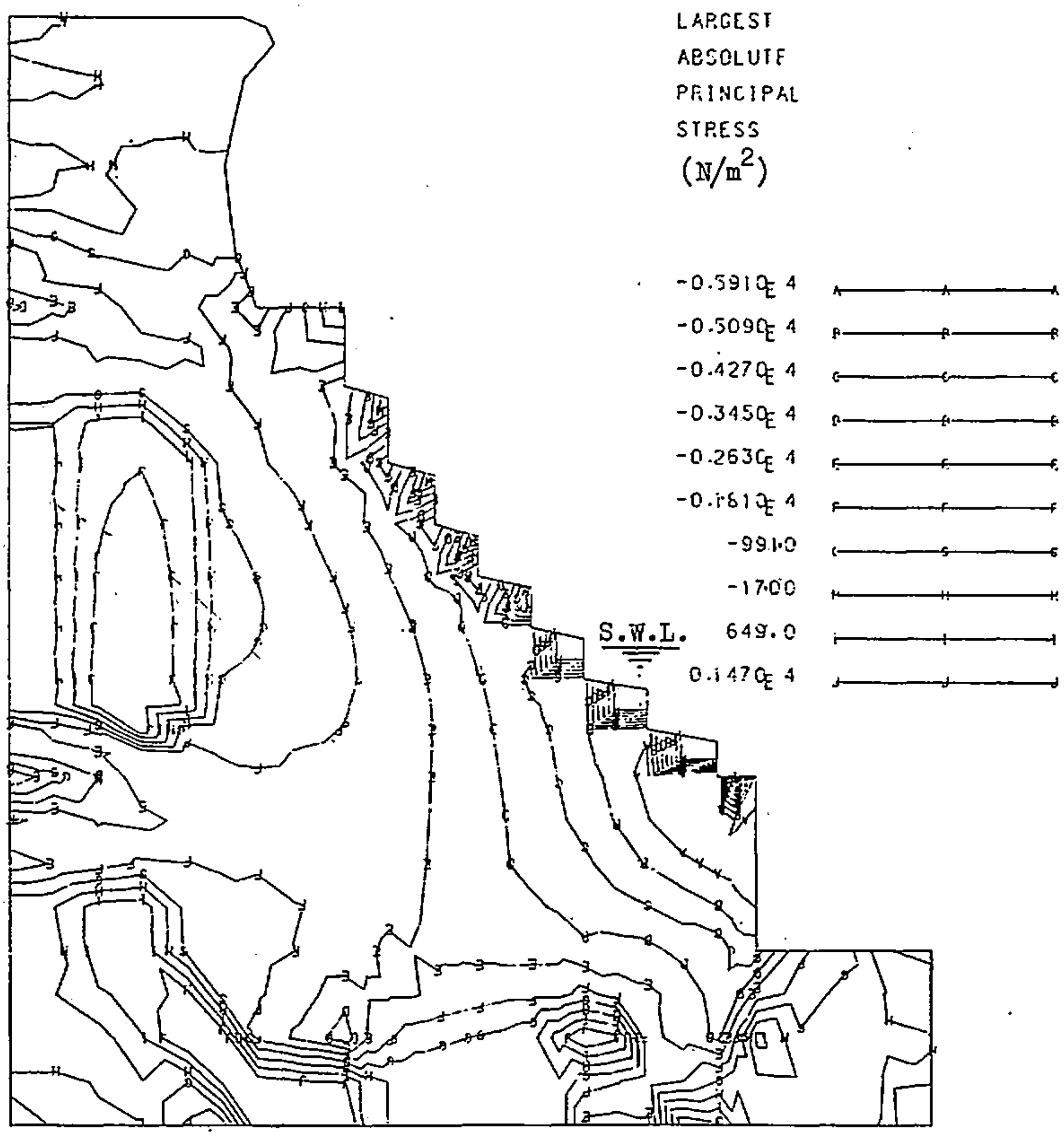

Figure 7.8 Stress contours on the Seaford seawall (no erosion) due to the pressure in figure 5.7 being applied at a S.W.L. of 2.0m A.O.D.

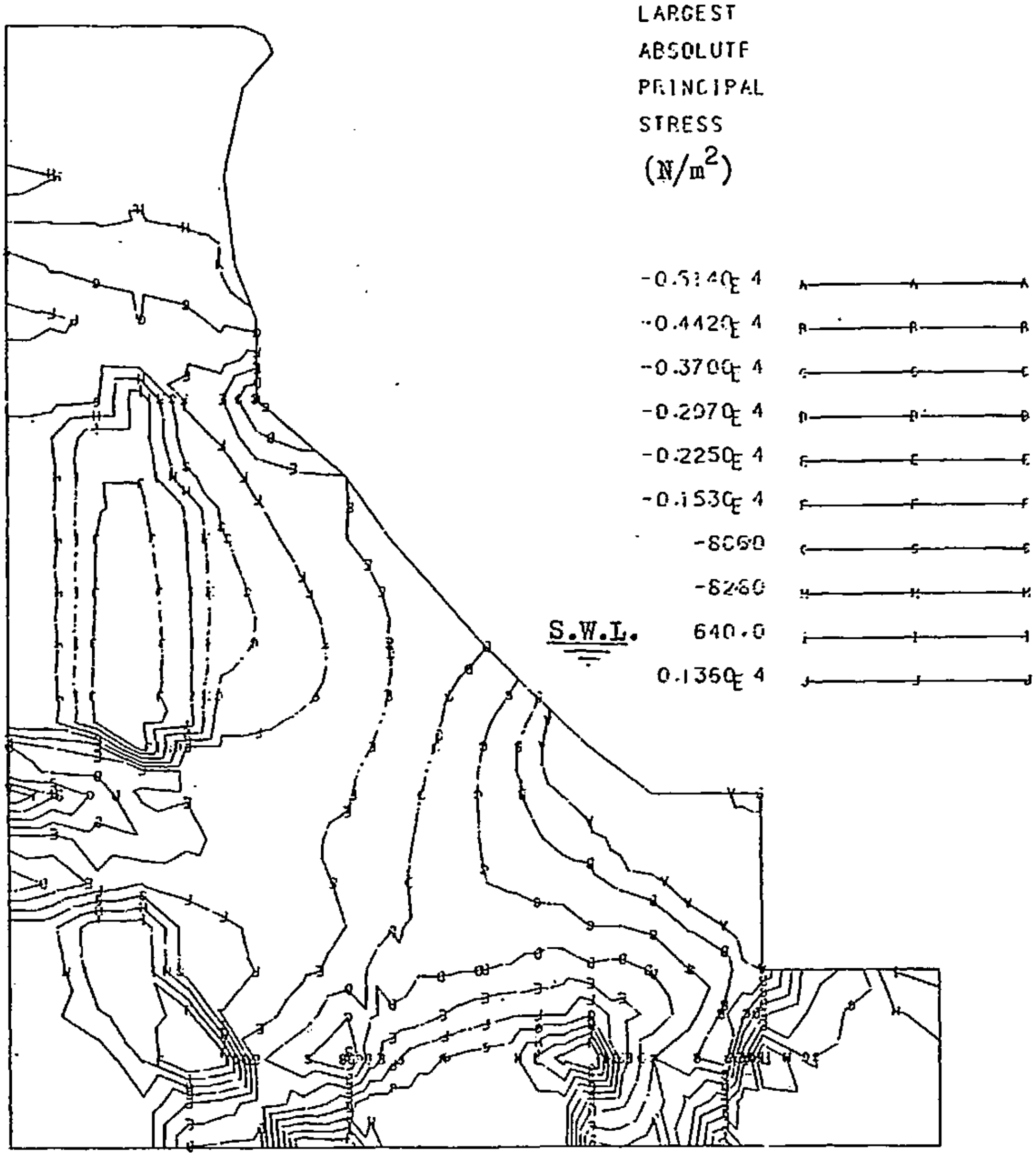

Figure 7.9 Stress contours on the Seaford seawall (with erosion) due to the pressure in figure 5.7 being applied at a S.W.L. of 2.0m A.O.D.

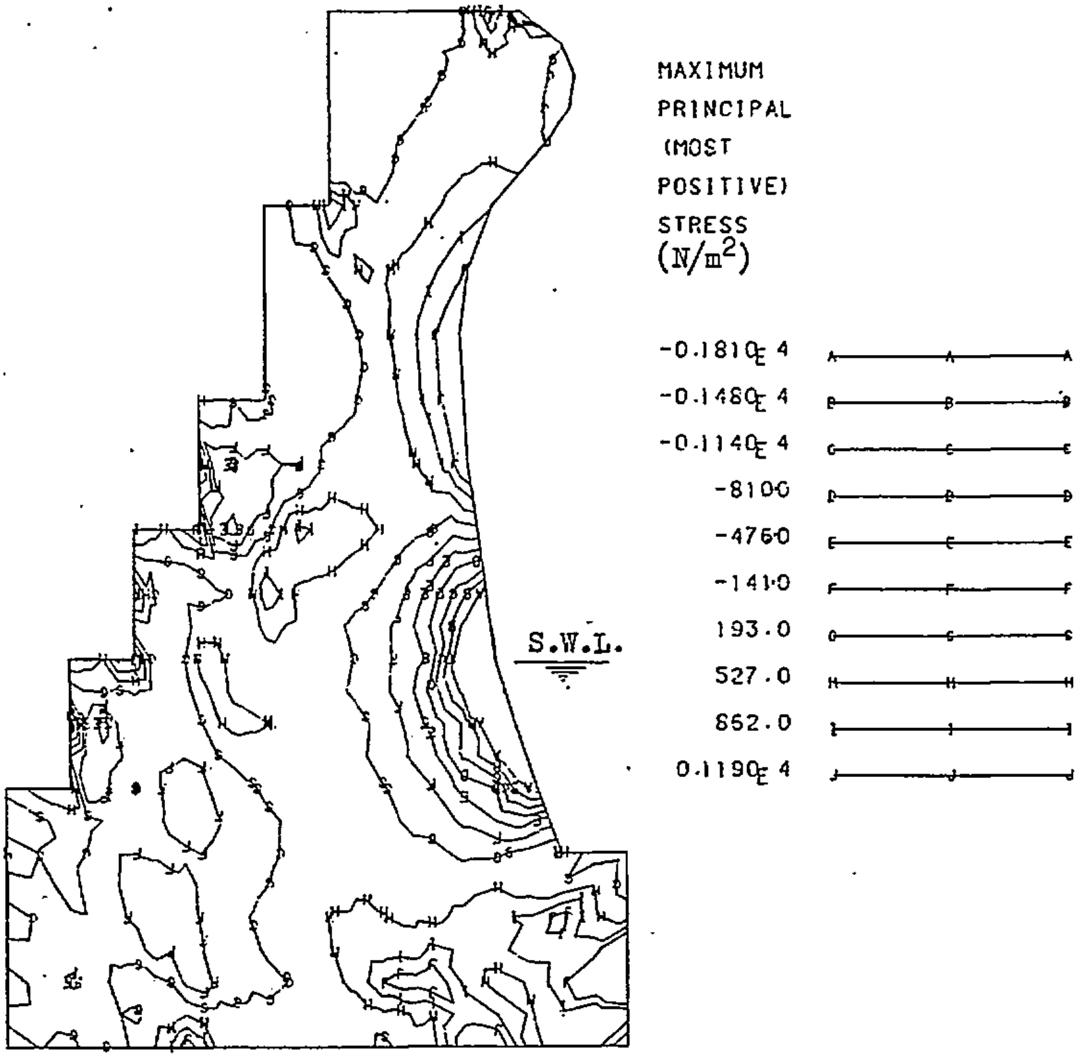

Figure 7.10 Stress contours due to the pressure in figure 5.7 being applied at a S.W.L. of 2.5m A.O.D. on the Ilfracombe seawall.

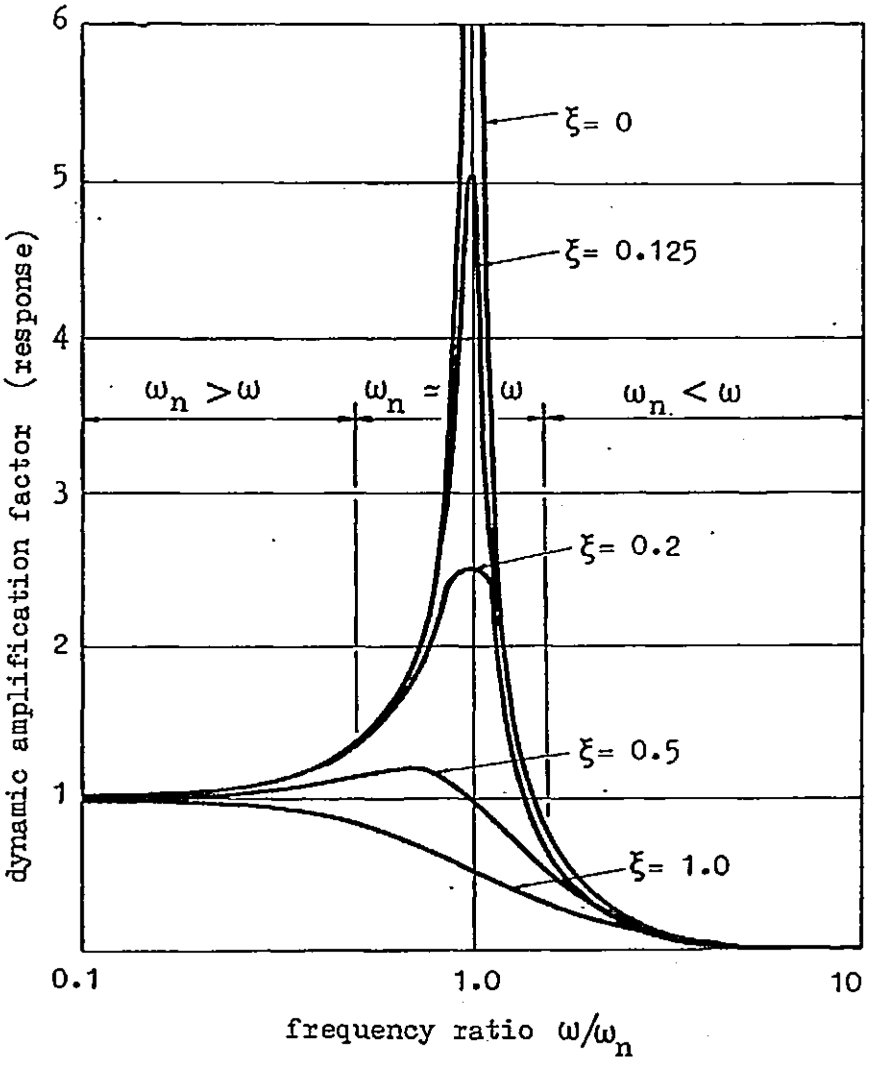

Figure 7.11 Relationship between structural response and frequency ratio.

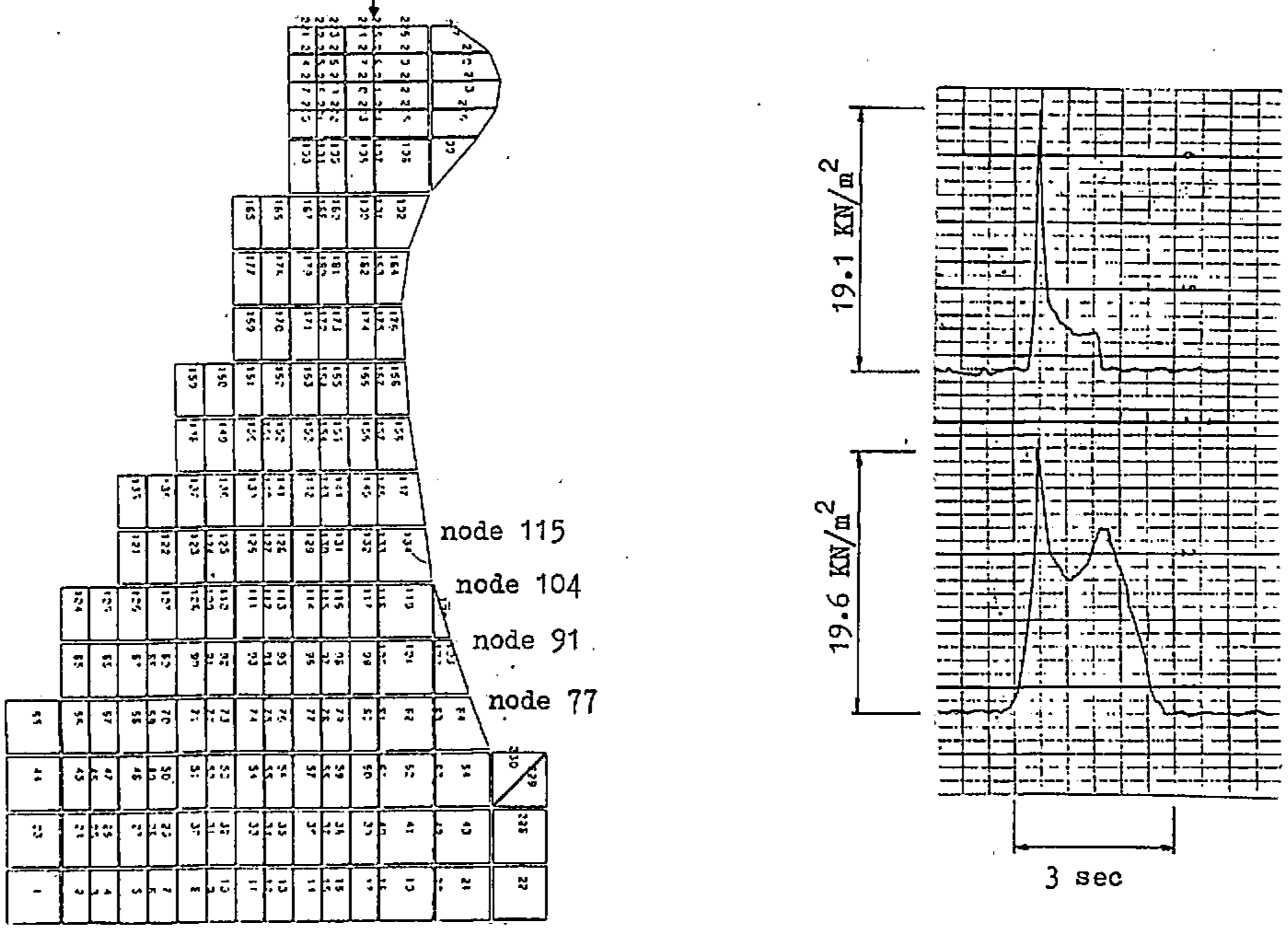

Both real and model seawall response measured at node 193

impact pressure measured at transducer No. 3 and applied to node 115 in the model.

the pressure applied to nodes 104 and 91 was obtained by linear interpolation between the pressures at nodes 115 & 77

impact pressure measured at transducer No. 1 and applied to node 77 in the model.

Figure 7.12 The impact pressure history as actually measured on the Ilfracombe seawall and as applied to the finite element model of this seawall.

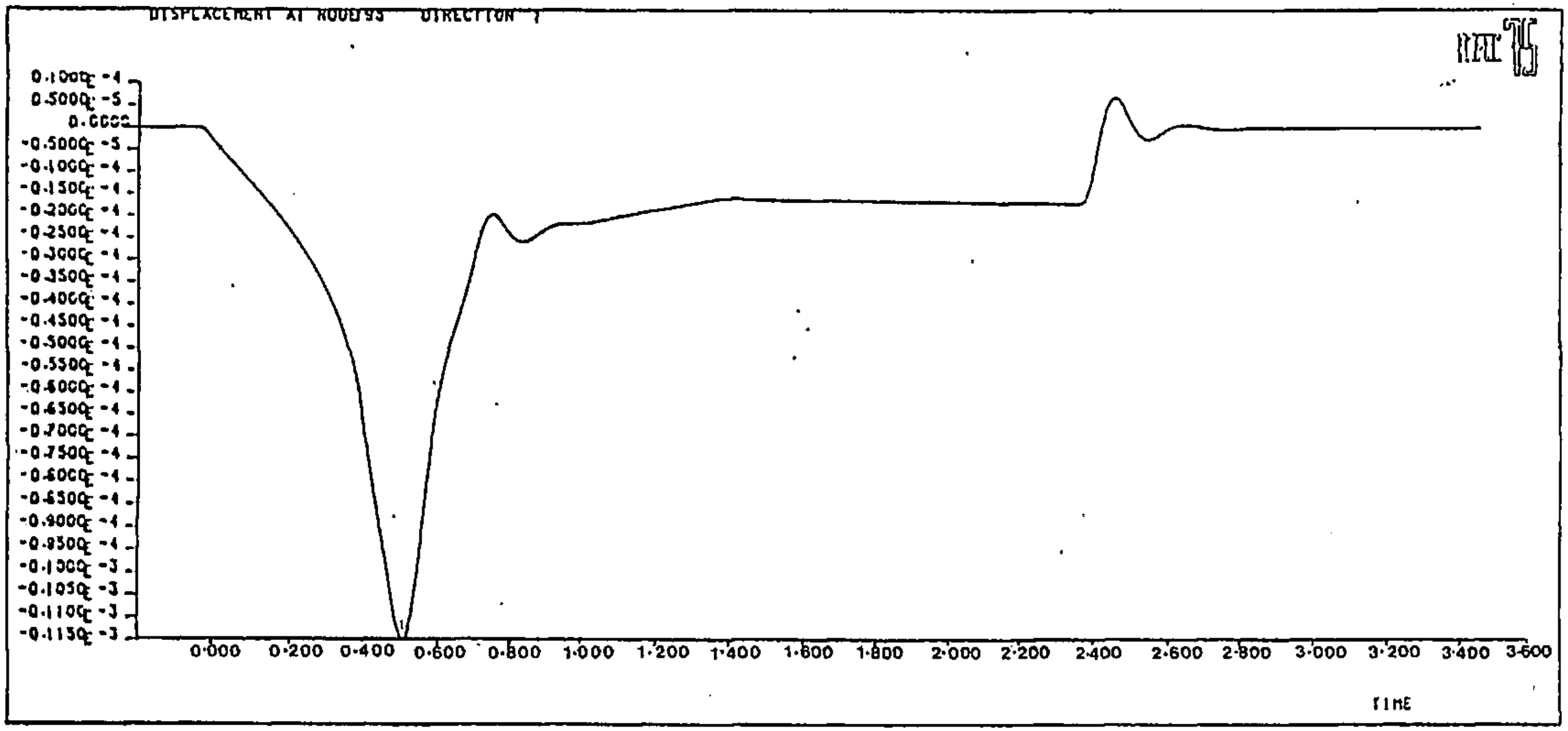

Figure 7.13 Ilfracombe (model) seawall displacement at node 193 for the impact pressure history shown in figure 7.12.

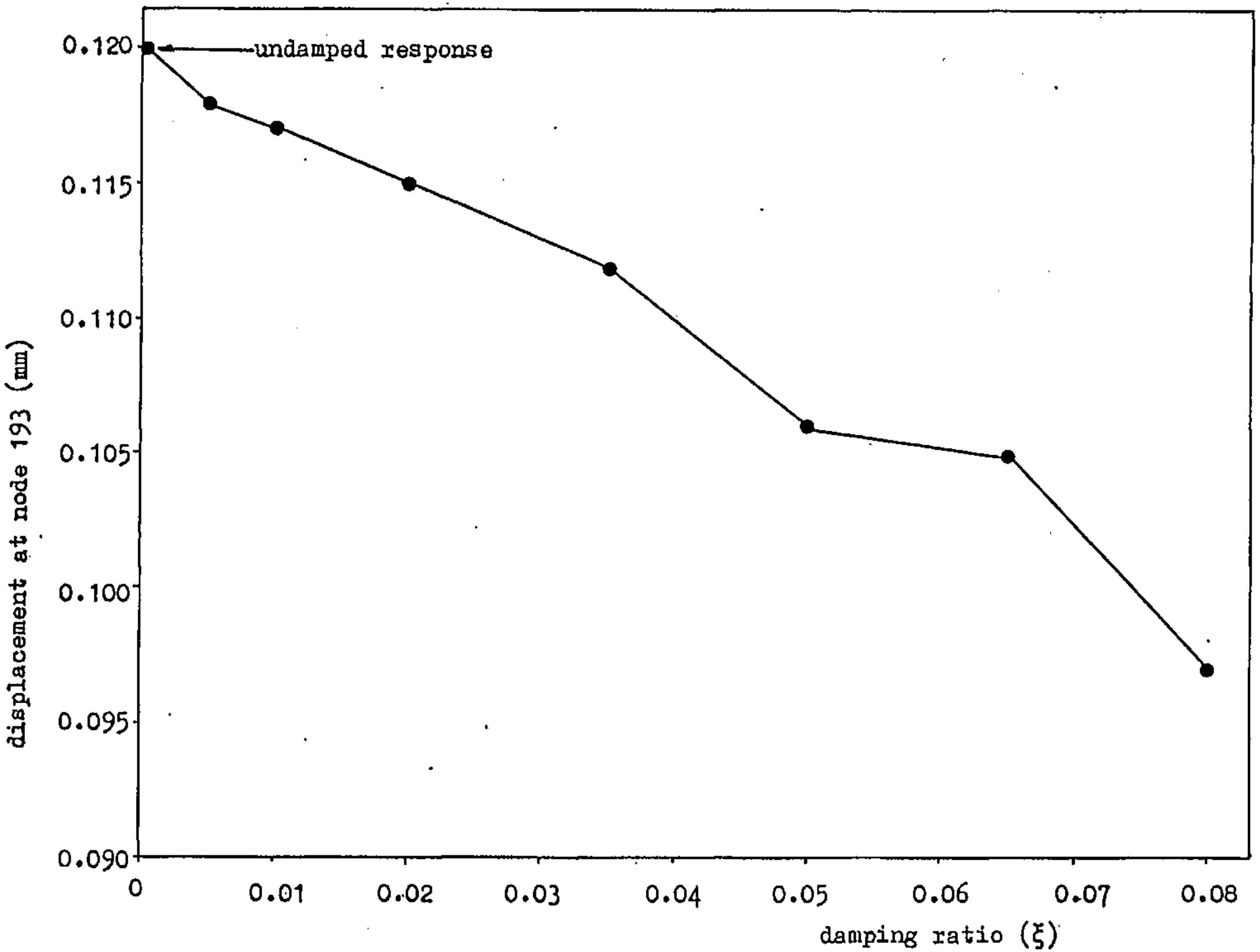

Figure 7.14 The effects of changes in damping ratio on structural response

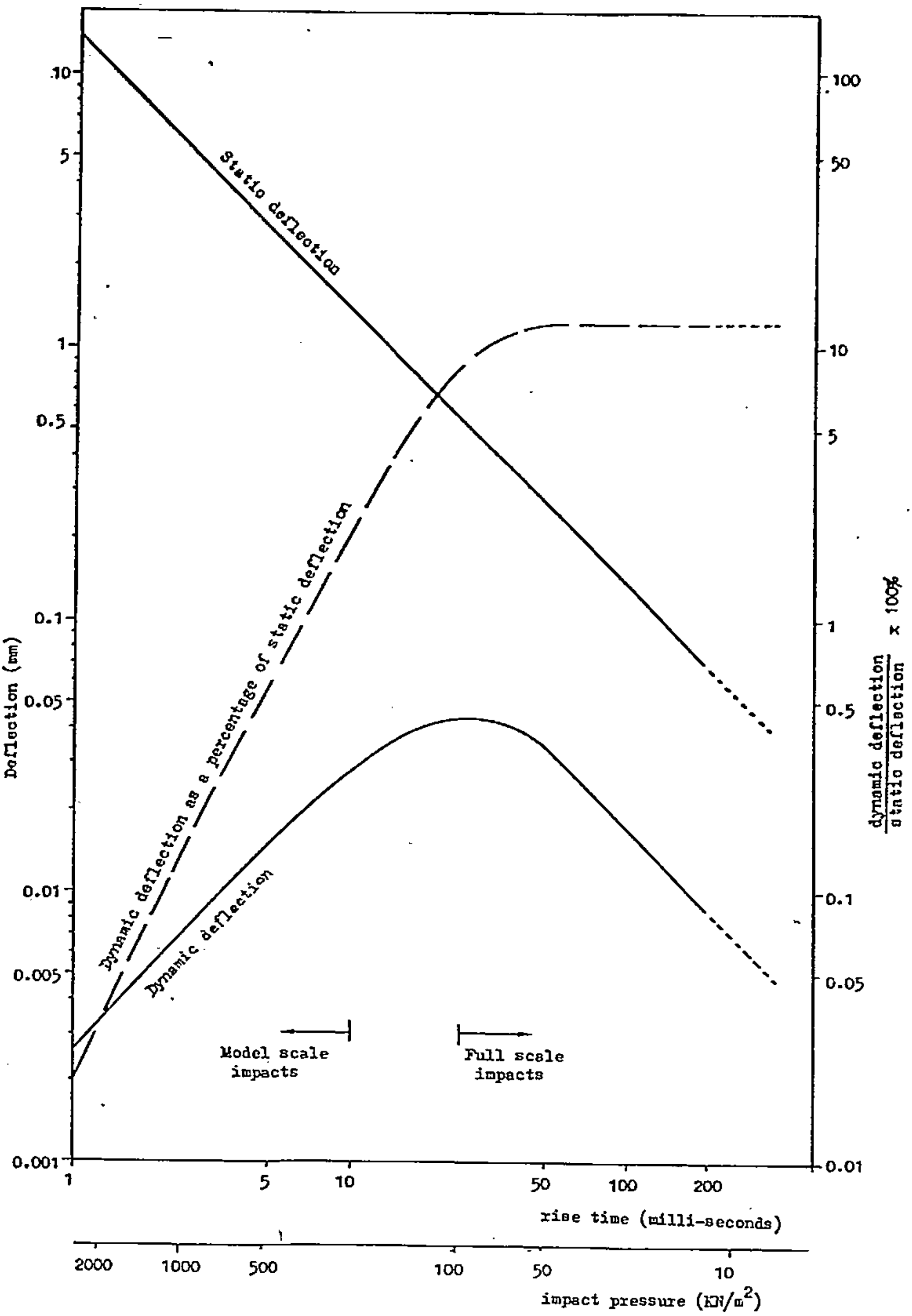

Figure 7.15 The effect of rise time and impact pressure on seawall response (deflection).

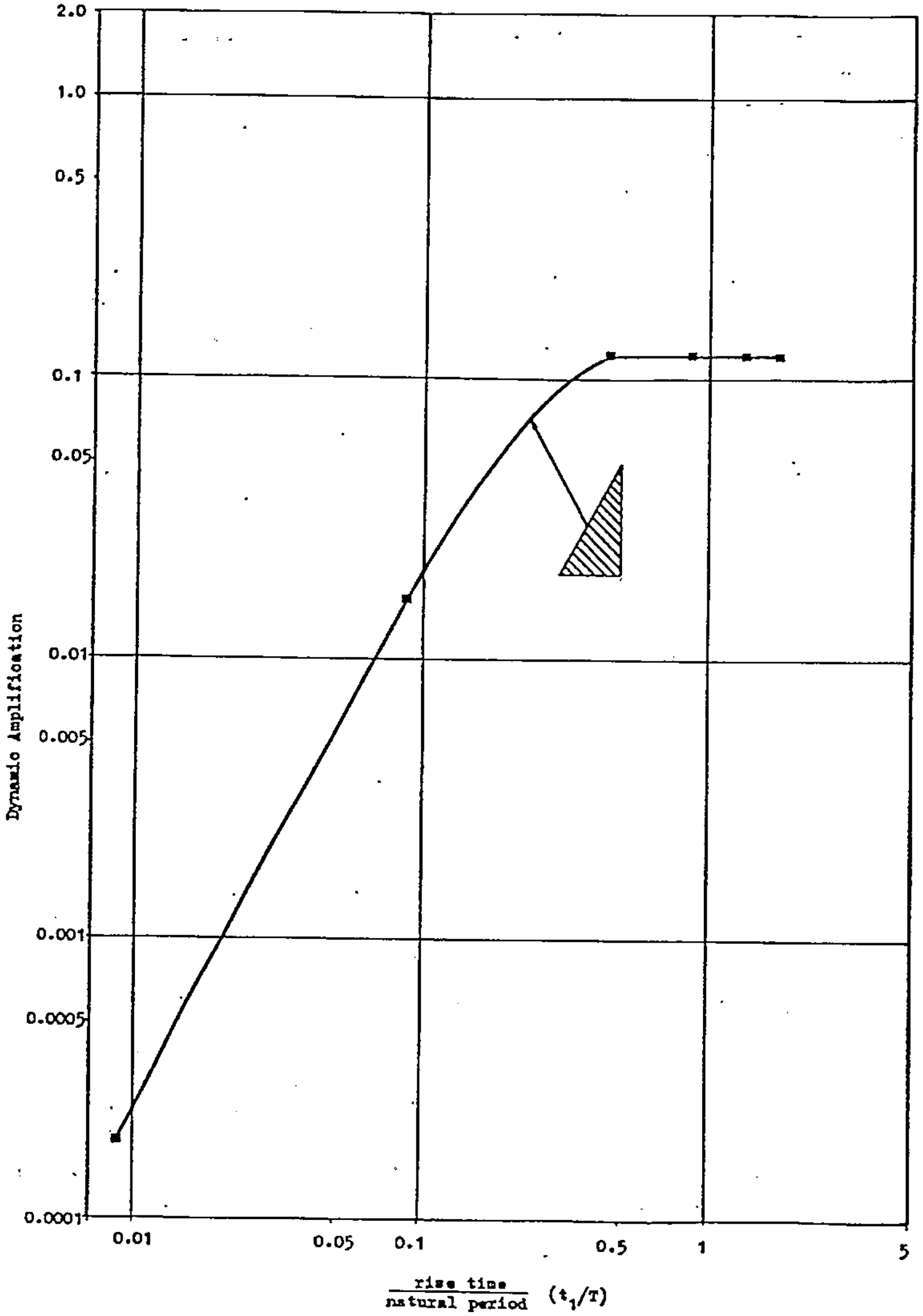

Figure 7.16 Non-dimensionalised response of the Ilfracombe seawall model when subjected to impacts with varying rise times

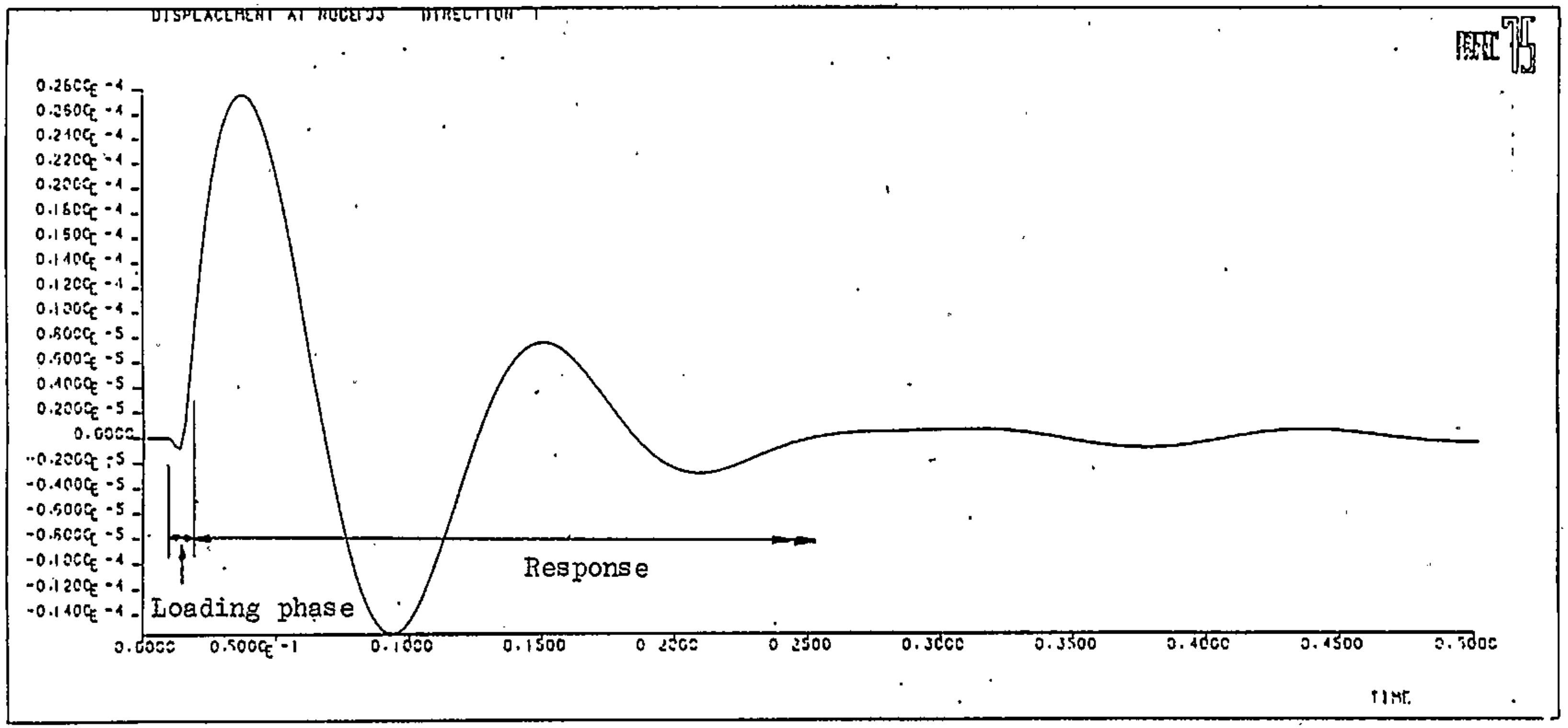

Figure 7.17 The displacement of the Ilfracombe seawall model at node 193 when subjected to a triangular impulse (load case number 2)

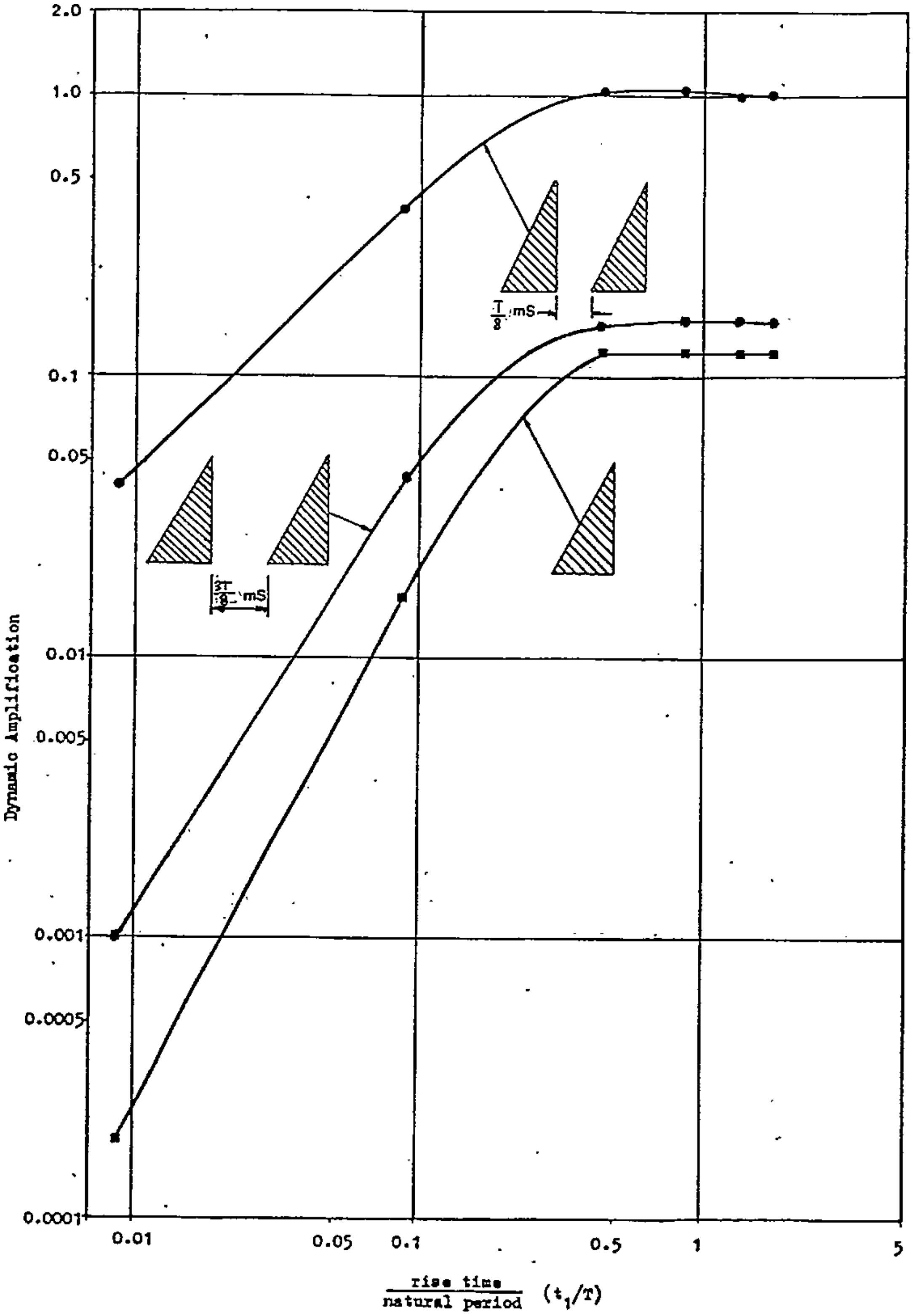

Figure 7.18 The effects of multiple impacts on wall response

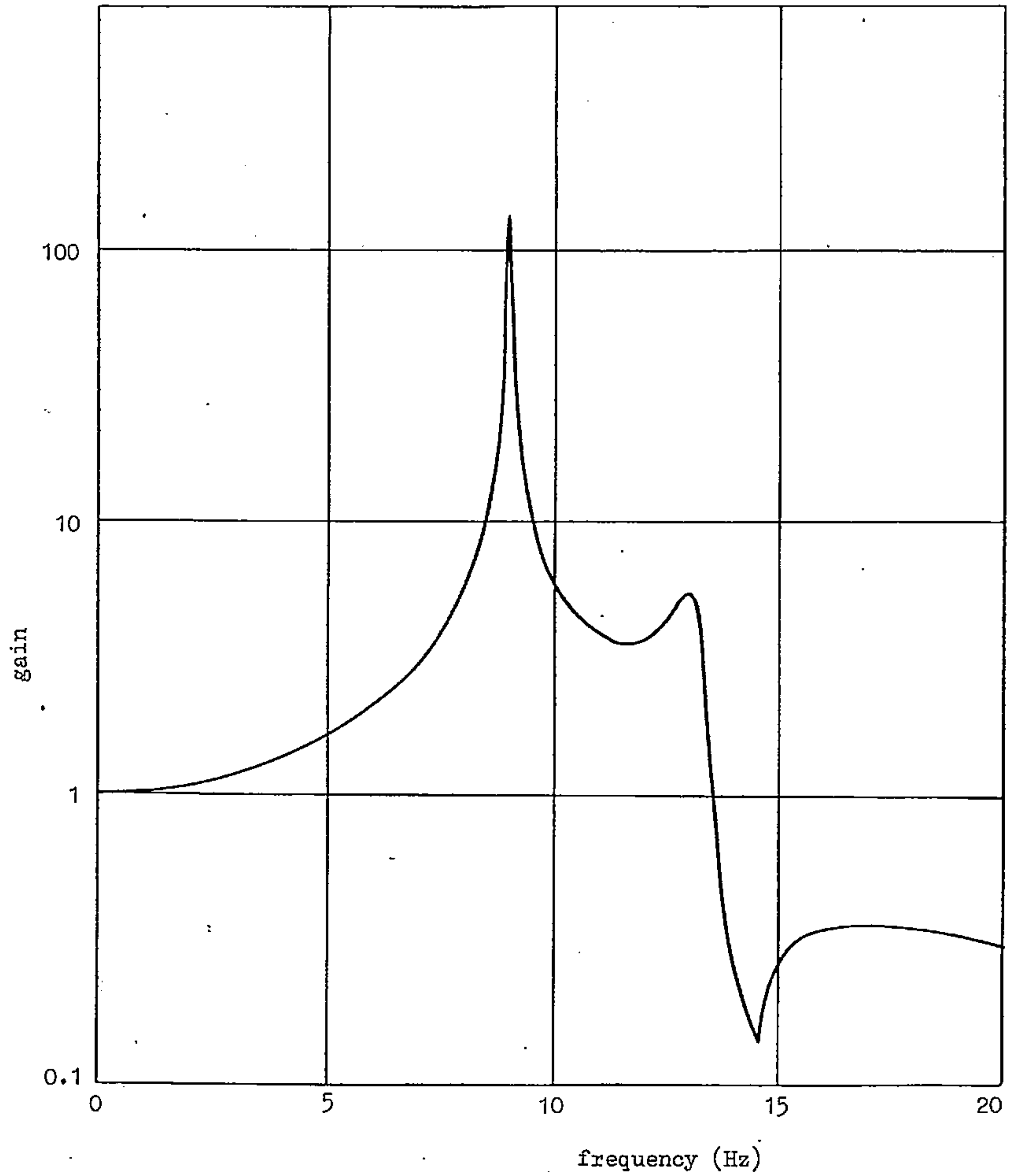

Figure 7.19 Transfer function between wave pressure and response for the Ilfracombe seawall

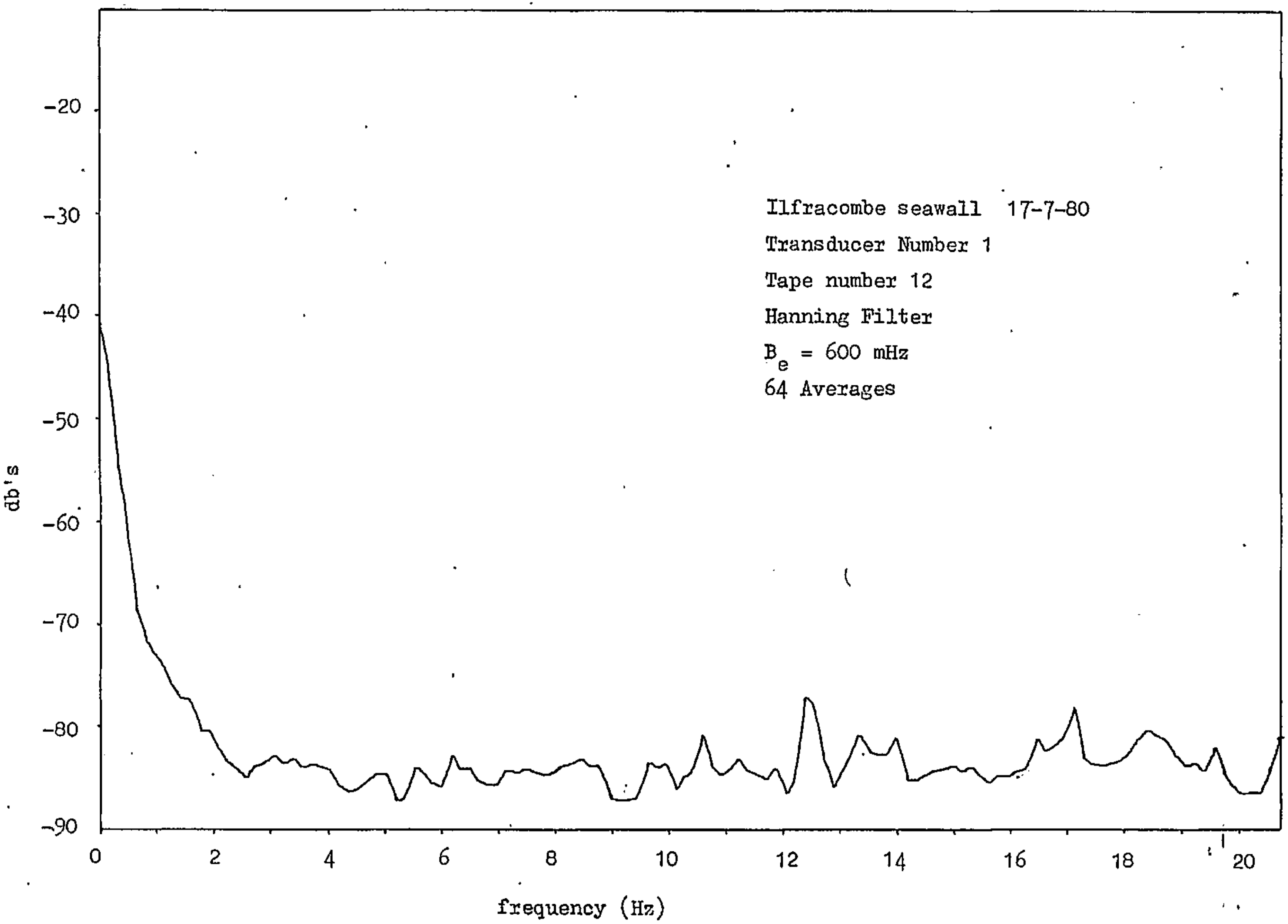

Ilfracombe seawall 17-7-80

Transducer Number 1

Tape number 12

Hanning Filter

B_e = 600 mHz

64 Averages

Figure 7.20 Excitation spectral density measured on the Ilfracombe seawall

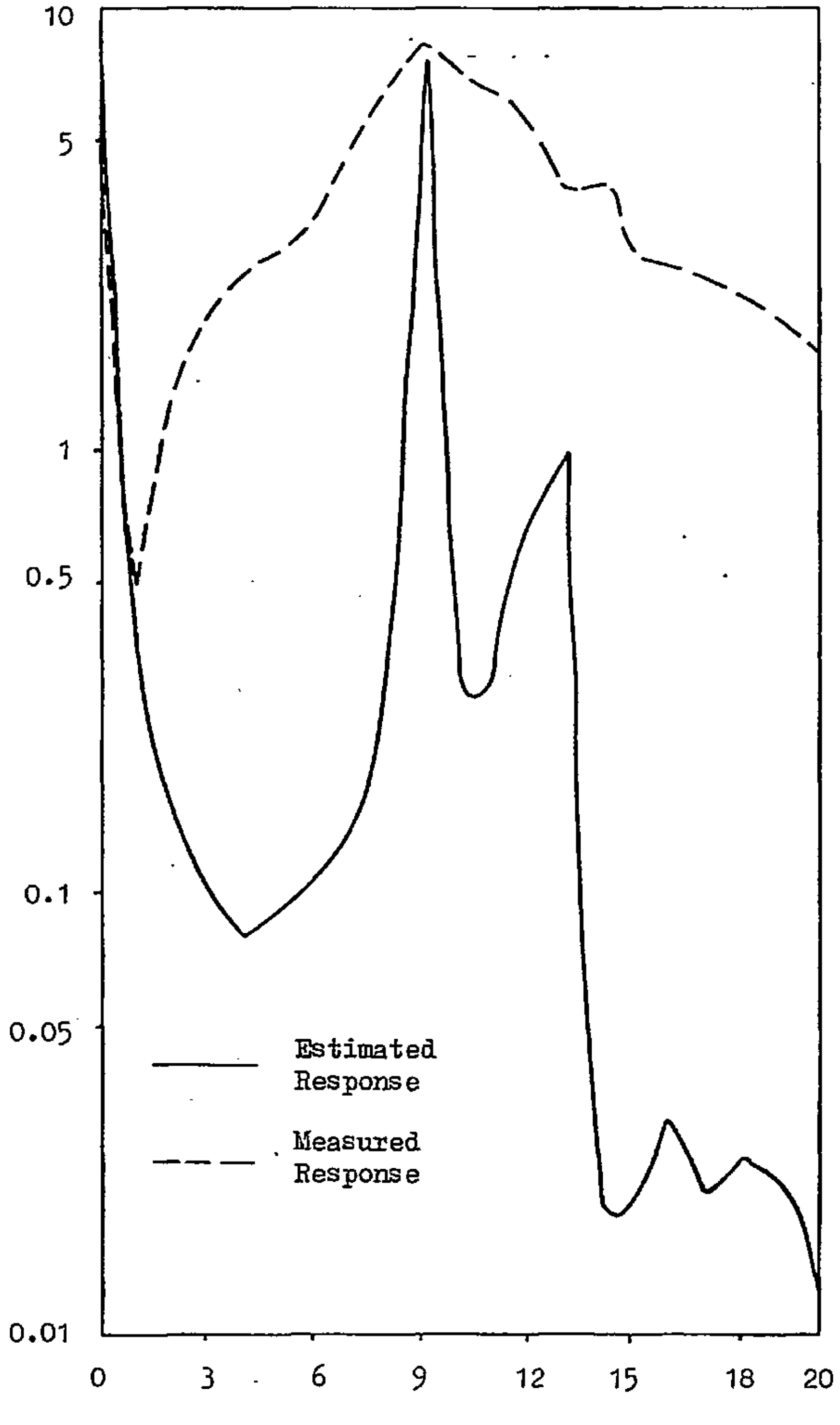

Figure 7.21 Comparison between measured and estimated spectral density of response for the Ilfracombe seawall

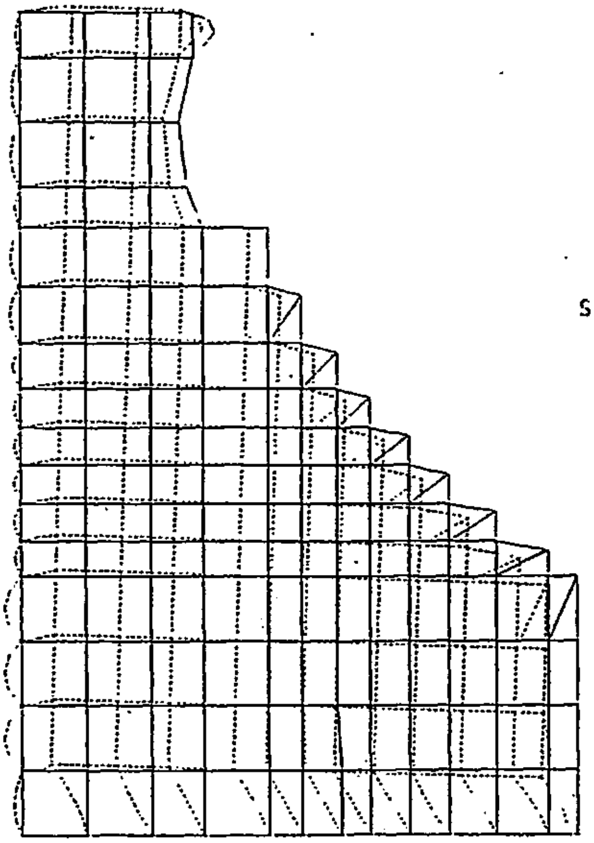

SCALE = 0.1667E-1 mm :1 mm

Figure 7.22 Deflection of the Seaford seawall (without erosion)

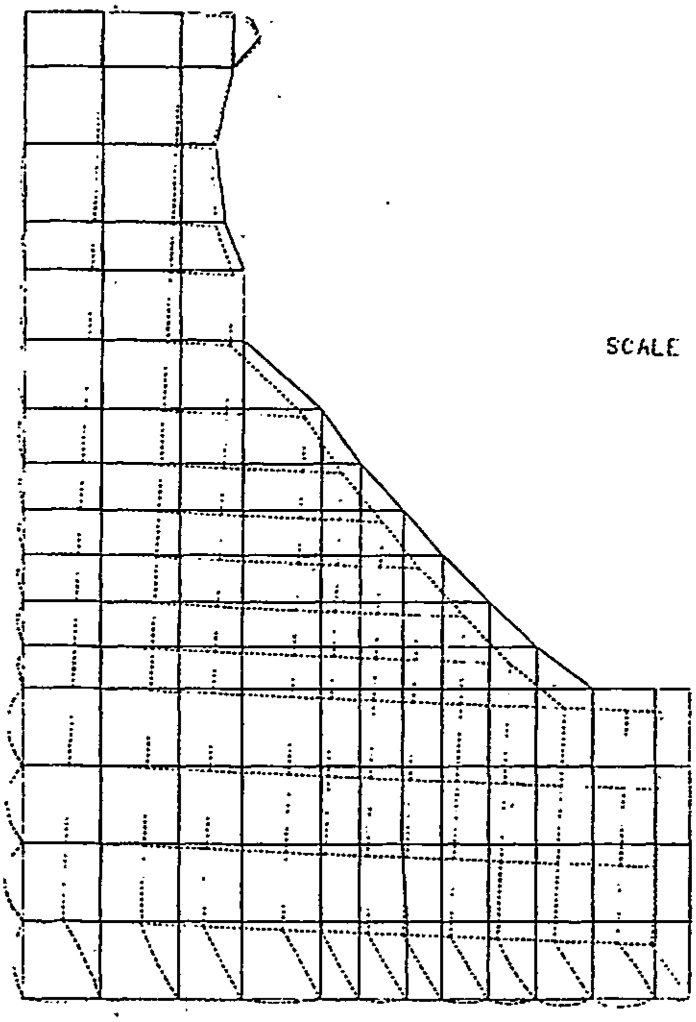

SCALE = 0.2000E-1 mm : 1 mm

Figure 7.23 Deflection of the Seaford seawall (with erosion)

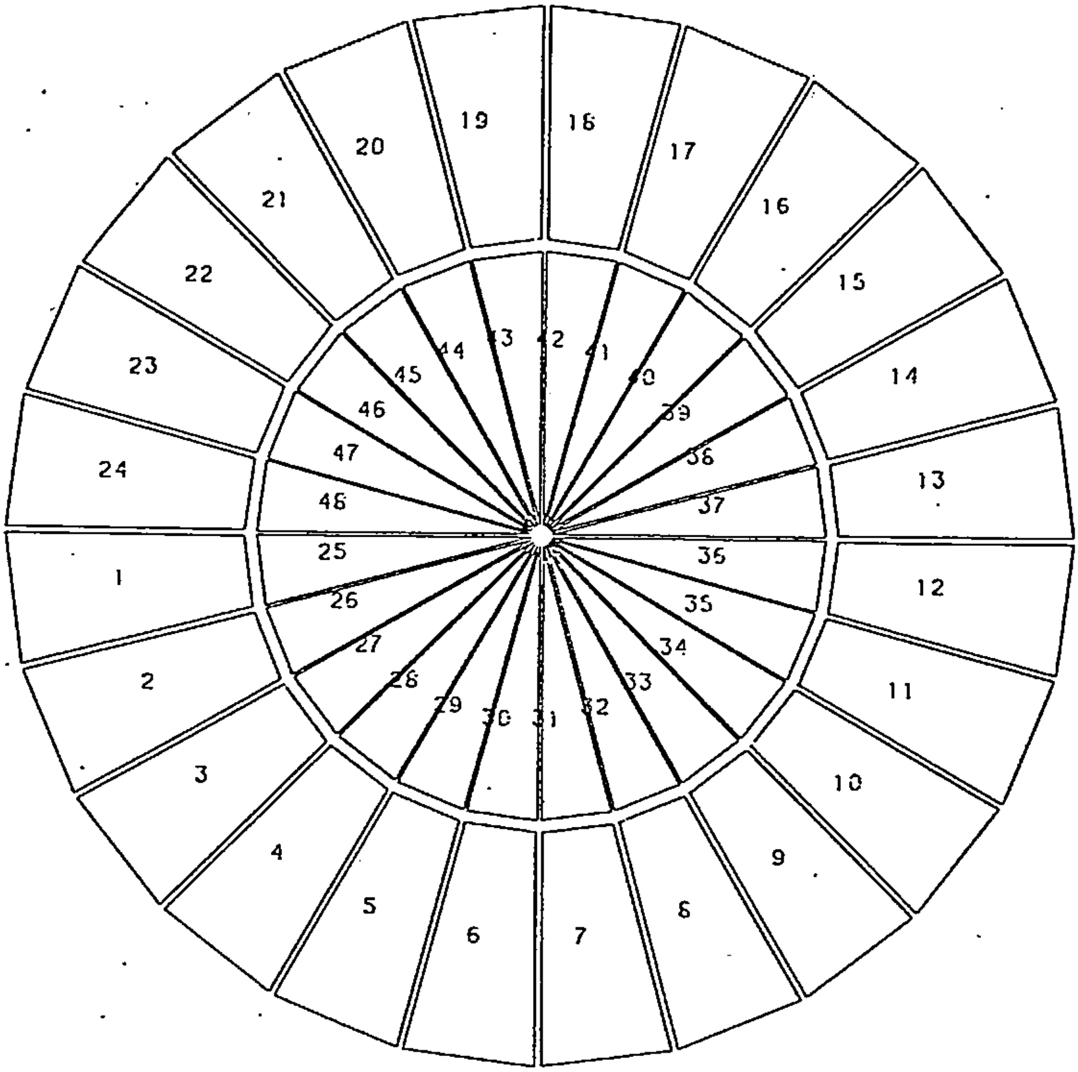
1
2
3
4
5
6
7
8
9
10
11
12
13
14
15
16
17
18
19
20
21
22
23
24
25
26
27
28
29
30
31
32
33
34
35
36
37
38
39
40
41
42
43
44
45
46
47
48

Figure 7.24 Finite element model of transducer diaphragm.

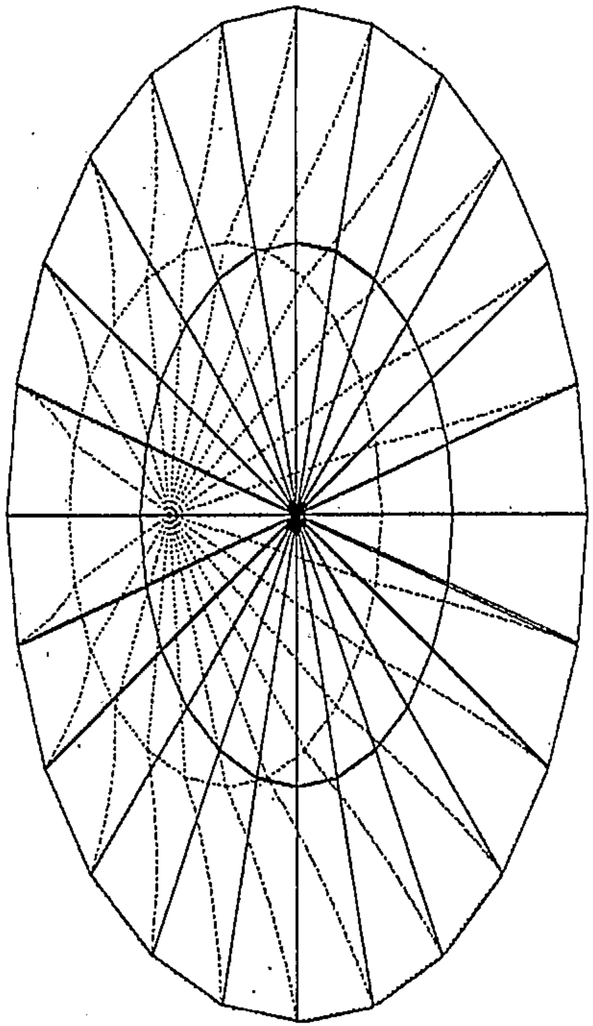

Figure 7.25 Deflected shape of transducer due to a u.d.l.

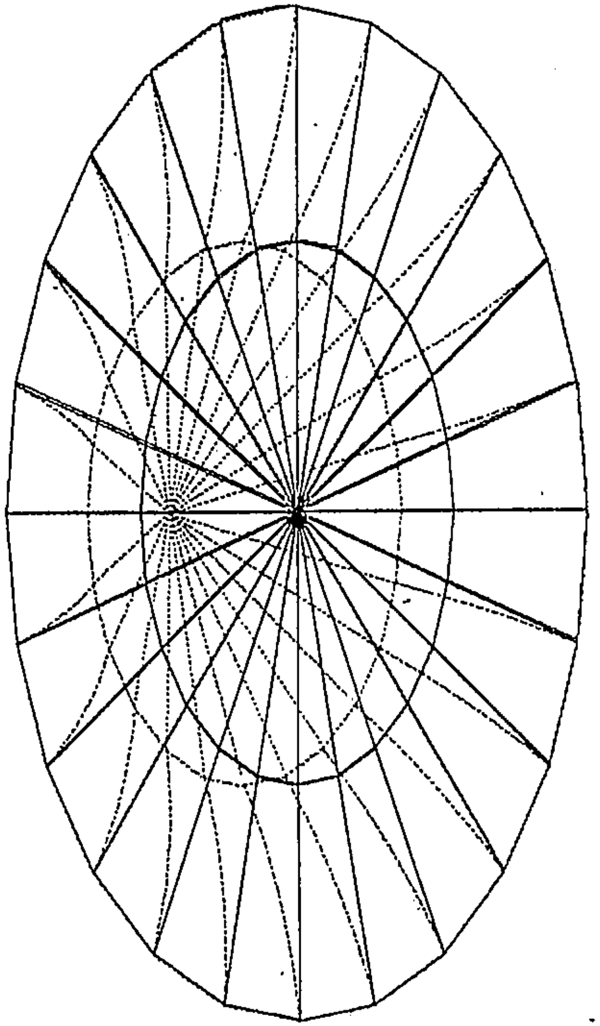

Figure 7.26 Deflected shape of transducer due to a point load.

CHAPTER EIGHT

DISCUSSION

8.1 Modelling Difficulties

The idealised SDOF models of the Ilfracombe and Seaford seawalls used in Chapter Six gave poor estimates of the natural frequencies when compared with the actual values measured on the walls. These SDOF models over estimated the Seaford natural frequency by three times and the Ilfracombe natural frequency by more than twice. The reason for these poor estimates is that the models were based only on the seawalls themselves, no allowance was made for soil structure interaction from the backfill and foundations which act with the seawalls.

It is not possible to calculate the mass of the rock and soil etc. which acts with the seawall for a general case because it depends on the material properties of the foundation and backfill and on the degree to which the seawall is tied into its surroundings, (i.e. piled foundations will transmit the forces on the wall to a larger mass of soil and so will involve more material than a flat footing). The natural frequency of the Ilfracombe seawall alone (from the SDOF model), is 18.4 Hz, the measured value for the combined wall and surrounding is 8.9 Hz, therefore using the relationship $\omega_n = (K/M)^{\frac{1}{2}}$ the approximate mass of the surroundings moving with the seawall can be found, (assuming the stiffness term remains the same).

e.g. for the wall alone $\omega = 2\pi 18.4 = \sqrt{\frac{K}{Mw}}$ .... (1)

for the wall and surroundings $$2\pi 8.9 = \sqrt{\frac{K}{Mw + Ms}} \quad \ldots\ldots\ldots\ldots (2)$$

rearranging (1) $$18.4^2 \cdot Mw = K \quad \ldots\ldots\ldots\ldots (3)$$

rearranging (2) $$8.9^2\ (Mw + Ms) = K \quad \ldots\ldots\ldots\ldots (4)$$

combining equations (3) and (4) gives;

$$Ms = \left(\frac{18.4}{8.9}\right)^2 Mw - Mw$$

$$Ms = 3.2\ Mw$$

Therefore the mass of the surroundings moving with the Ilfracombe seawall is approximately 3 times the mass of the wall, similarly for Seaford the mass of the surroundings moving with the wall is approximately 9 times the mass of the wall. This large difference is partly accounted for because the backfill at Ilfracombe does not reach the top of the wall, so there is no backfill constrained to move with the wall at this level. Thus it seems there is little point in considering the seawalls in isolation from their surroundings because of the large inaccuracies introduced.

Therefore it is not worth embarking on a MDOF analysis until the mass of the surroundings acting with the wall, and the distribution of this mass around the wall, have been determined. It is not possible to calculate the value and distribution of this mass except by trial and error, this can be a lengthy and tedious job best tackled using a computer. For this investigation MDOF models were developed for the Ilfracombe and Seaford seawalls using the PAFEC finite element package and a Prime 550 computer. The final distribution and properties of the foundations and backfill necessary to give the correct static and dynamic response are shown in Figures 7.4 and 7.6. The fundamental natural frequencies of these models were made the same as those of the real seawalls, as were the static deflections. But because an insufficient width of foundations and backfill were included in the models (due to lack of computer core space), the stresses in the structure could not dissipate fully, so in Figures 7.8 and 7.10 stress concentrations can be seen along the back edges of the foundations and backfill, where in the real structure these stresses would be absent. But the effects of these modelling approximations are slight and mainly affect the dynamic response of the models at the higher modes of vibration.

8.2 Seawall Response to Transient Wave Impacts

Six cases of impact, all with the same total impulse but with varying combinations of rise time and impact pressure were applied to the model of the Ilfracombe seawall. The optimum rise time to produce the maximum seawall deflection was approximately T/2 seconds. Impacts with rise times greater or less than T/2 seconds produced smaller deflections, as seen in Figure 7.15. As all six load cases had the same impulse, then it can be seen that for impacts lasting less than T/2 seconds, the value of the impulse is not of primary importance in determining the resulting deflection, the deflection in this region is controlled by the rise time and increases as the rise time increases.

But for impacts lasting longer than T/2 seconds the rise time no longer becomes important and the deflection is now governed by the value of the impulse. For the Ilfracombe and Seaford seawalls this optimum rise time is of the order of 100 milli-seconds. Therefore the high impact pressures measured in model studies will have a negligible effect on full size seawalls because of their very short rise times (of the order of 1 milli-second), so the equations for estimating the wave impact pressure which are based on model scale data, such as Minikin's(72), are not applicable to full scale structures.

In Section 7.7 it was seen that a single triangular impulse had little effect on seawall response, producing a maximum dynamic amplification of 0.12 (Figure 7.16). But when the same impulse was applied twice in quick succession then the resulting dynamic amplification was much larger and in some cases (when the time delay between impacts was $\frac{T}{8}$ milli-seconds), the dynamic deflection could be even greater than the static deflection (Figure 7.18).

These impulses were applied to the Ilfracombe seawall model assuming it to be initially stationary, but in a real sea this is unlikely because the wave pressure (including the hydrostatic pressure) is dynamic so the total force on the wall is never stationary (static) thus wave impacts will probably never be acting on a stationary seawall. Therefore a single wave impact could produce a much larger deflection than that shown in Figure 7.15 if the seawall happens to be moving in the same direction as the wave impulse at the moment of impact, and conversely if the seawall is moving in the opposite direction to the wave impulse then very small deflections would be expected. As millions of waves will impinge on a seawall during its lifetime then it is possible that the conditions will be such that very large dynamic deflections will be produced by a wave impact, which could mean the stresses in the wall will exceed the ultimate tensile or compressive stresses of the material thus causing a localised failure.

8.3 The Frequency Domain Transfer Function

In Section 7.8 a frequency domain transfer function was set up to relate the spectral density of wave pressure to the spectral density of seawall response, this transfer function was built up by applying a number of sinusoidal forces to the seawall model in order to represent a random sea. The seawall response estimated by use of this transfer function bore little resemblance to the measured response (Figure 7.21) and tended to under estimate the spectral densities at most frequencies above 1 Hz. This poor correlation is caused by either the measured excitation spectral density not being representative of the general excitation forces, or the transfer function being inaccurate, or a combination of both.

The seawall response at any point is due to the direct wave action plus the stresses and vibrations transmitted along the wall from other sections, thus the excitation force measured at the pressure transducer (Figure 2.20) is only part of the total excitation force acting on that section of seawall, (the additional component of the excitation force cannot be measured). Therefore the estimated response spectral density can not be expected to be the same as the measured value (even if a more accurate transfer function could be set up), but nevertheless the estimated response spectral density in Figure 7.21 does provide a good approximation of the spectral density at the fundamental natural frequency.

CHAPTER NINE

CONCLUSIONS AND SUGGESTIONS FOR FURTHER RESEARCH

Conclusions

(1) The finite element modelling suggests that the impact pressures measured during this investigation are of sufficient duration to generate a significant dynamic response in the seawalls, and as these impacts occasionally act simultaneously over large areas (as seen in Chapter Three) then the total dynamic deflection can be substantial and of the same order, or greater, than the static deflection.

(2) The very high pressure, short duration wave impacts measured in model scale laboratory studies will have a negligible effect on the response of full size seawalls.

(3) For a given impulse, a wave impact on the Ilfracombe seawall will produce a maximum dynamic displacement when the rise time approximately equals half of the natural period of vibration of the structure.

(4) Dynamic seawall deflection for wave impacts with rise times greater than T/2 seconds is proportional to the wave impulse, and for impacts with rise times less than T/2 seconds the deflection is governed by the magnitude of the rise time (the magnitude of the impulse is of secondary importance within the range $0 < t_i < T/2$).

(5) The cumulative effect on structural response of two or more

wave impacts occurring in quick succession can greatly exceed the response caused by the individual impacts. The magnitude of this increase in deflection is dependent upon the time delay between impacts, i.e. a single wave impact approximated by a triangular impulse, produced a maximum dynamic amplification in the Ilfracombe seawall model of 0.12, when the same impact was applied twice in succession with a time delay between impacts of $\frac{3T}{8}$ milli-seconds the maximum dynamic amplification was 0.17 (a 40% increase in deflection for a 100% increase in impulse), but when the time delay was reduced to milli-seconds the dynamic amplification increased to 1.07 (an increase of over 800% for a 100% increase in impulse).

SUGGESTIONS FOR FURTHER RESEARCH

(i) It would be useful to produce analytical models of other seawalls to investigate the effects on structural response, of impulses with varying rise times. Thus it could be seen if the optimum rise time of T/2 seconds was a response particular to the Ilfracombe seawall or whether it is a general result applicable to any seawall.

References

1. GODA, Y. New wave pressure formulae for composite breakwaters. Proc. Conf. Coastal Eng. Vol. 3, 1974, pp 1702-1720.

2. STEVENSON, T. The design and construction of harbours second Ed, 1874, Edinburgh.

3. GAILLARD, D.D. Wave action in relation to engineering structures. U.S.Army Corps of Engrs. 1904. (reprinted 1935).

4. HIROI, I. The force and power of waves. The Engineer. 1920, pp 184-185.

5. MOLITOR, D.A. Wave pressures on seawalls and breakwaters. Trans. A.S.C.E. Vol. 100, 1935, pp 984-1002.

6. LUIGGI, Dr.L. Correspondence on improvement of the Port of Valparaiso. Proc. I.C.E. Vol 214, 1922, pp 40-45.

7. ROUVILLE, M. BESSON, P. & PETRY, P. Etat actual des etudes internationales sur les efforts dus aux lambs. Annales de Ponts et Chaussees. 108 (2), 1938, pp 5-113.

8. COT, P.D. Le laboratoire du Harve pour la measuer des efforts dus aux lambs. Proc. 5th Conf. Coastal Eng. Sept. 1954.

9. KURIBAYASHI, T. MURAKI, Y. & UDAI, G. Field investigation of waves forces on breakwaters. Coastal Eng. in Japan, Vol. 2 1959, pp 17-27.

10. MURAKI, Y. Field observations of wave pressures, wave run up and oscillation of breakwater. Proc. 10th Conf. Coastal Eng. Vol. 1, 1966, pp 302 - 321.

11. MILLER, R.L. LEVERETTE, S. O'SULLIVAN, J. & TOCHKO, J. Field measurements of impact pressures in surf. Proc. 14th Conf. Coastal Eng. Vol. 3, 1974, pp 1761-1777.

12. MARCHI, E. RAITERI, E. SCARSI, G. & STURA, S. Storm wave pressures on the breakwater of Genoa Harbour. 16th Int. Assn. for Hydraulic Research, Vol. 1, 1975, pp 246-253.

13. DENNY, D.F. Further experiments on wave pressures. I.C.E. Feb. 1951, pp 330-345.

14. BAGNOLD, R.A. Interim report on wave pressure research. J. Instn. Civil Engrs. 1939, pp 202-226.

15. GODA, Y. Experiments on the transition from non-breaking to post breaking wave pressures. Coastal Eng. in Japan, Vol. 15, 1972, pp 81-92.

16. HOMMA, M. & HORIKAWA, K. Experimental study on total wave force against seawall. Coastal Eng. in Japan, Vol. 8, 1965, pp 119-129.

17. HAYASHI, T. & HATTORI, M. Pressure of the breaker against a vertical wall. Coastal Eng. in Japan, Vol. 1, 1958, pp 25-37.

18. HAYASHI, T. & HATTORI, M. Thrusts exerted upon composite-type breakwaters by the action of breaking waves. Coastal Eng. in Japan, Vol. 7, 1964, pp 65-84.

19. HUDSON, R.Y. Wave forces on breakwaters. Trans. A.S.C.E. 118, 1953, pp 653-674.

20. KAMEL, A.M. Shock pressures on coastal structures. A.S.C.E. Waterways Div. WW2, Aug. 1970 pp 689-700.

21.	LUNGREN, H.	Wave shock forces; an analysis of deformations and forces in the wave and in the foundation. Proc. Symp. Res. on Wave Action, Hydro Delft, paper No. 4, Vol. 2, 1969.
22.	MITSUYASU, H.	Experimental study on wave force against a wall. Coastal Eng. in Japan, Vol. 5, 1962, pp 23-47.
23.	MITSUYASU, H.	Shock pressures of breaking waves. Proc. 10th Conf. Coastal Eng. Vol.1, 1966, pp 268-283.
24.	MOSHAGEN, H. TOERUM, A.	Wave induced pressures in permeable seabeds. A.S.C.E. Waterways Div. Vol. 101, WW1, Feb. 1975, pp 49-57.
25.	NAGAI, S.	Perforated wall breakwater. Dock & Harbour Authority, Oct. 1976, pp 194-198.
26.	NAGAI, S.	Pressures of breaking waves on composite type breakwaters. Advances in Hydroscience. Vol. 9, 1973, pp 296-324.
27.	NAGAI, S.	Wave forces on structures. Advances in Hydroscience, 1967.
28.	NAGAI, S.	Pressures of standing waves on vertical wall. A.S.C.E. Waterways Div. WW1, Vol. 95, 1969, pp 53-76.
29.	NAGAI, S.	Pressures of partial waves.A.S.C.E. Waterways Div. August 1968.
30.	NAGAI, S.	Shock pressures exerted by breaking waves on breakwaters. Trans. A.S.C.E. paper No.3261, 1960, pp 772-809.
31.	NAGAI, S.	Investigation of wave pressure formulae due to damage of breakwaters. Proc. 14th Conf. Coastal Eng. Vol. 3, 1974, pp 1721-1740.

32. PLAKIDA, M.E. Pressure of waves against vertical walls. Proc. 12th Conf. Coastal Eng. Vol. 3, Sept. 1970, pp 1451-1468.

33. REPORT - Peterhead Bay Harbour - model studies on overtopping of the South breakwater. H.R.S. Jan. 1975.

34. RICHERT, G. Model law for shock pressures against breakwaters. Coastal Eng. Conf. London, 1968.

35. ROSS, C.W. Shock pressures of breaking waves. Proc. 4th Conf. Coastal Eng. 1954, pp 323-332.

36. SALIH-KIRKGOZ, M.S. Breaking waves: their impact on vertical walls and action on slopes. Ph.D. Thesis, Univ. Liverpool, 1978.

37. WEGGEL, J.R. The impact pressure of breaking waves. Ph.D. Thesis, Univ. Illinois, 1968.

38. WIEGEL, R.L. & SKJEI, R.E. Breaking wave force predictions. A.S.C.E. Waterways Div. WW2, 1958.

39. CARR, J.H. Breaking wave forces on plane barriers. Calif. Inst. Tech. Report No. E-11.2, Oct. 1951.

40. LARRAS, J. Le deferlment des lambs sur les Jetees verticales. Annales des Ponts et Chaussees. Vol. 107, 1937, pp 643-680.

41. FUHRBOTER, A. Laboratory investigation of impact forces. Mitt. Franzius - Institut Heft 28, 1966.

42. MUNK, W.H. Wave action on structures. American Inst. Minning and Metallurgical Eng. Tech. Pub. No. 2322, March 1948.

43. RUNGREN, L. Water wave forces. Bulletin No. 54, Inst. Tech. Inst. of Hydraulics, Stockholm, 1958.

44. WEGGEL, J.R. & MAXWELL, W.H. Experimental study of breaking wave pressures. Offshore Tech. Conf. Texas, 1970.

45. STICKLAND, I.W. Hydraulics Reaseach Group, I. of W. Dock and Harbour Authority, April 1976, pp 368-69

46. BENASSAI, E. The stability against sliding of breakwaters under the action of breaking waves. Bulletin Permanent Int. Assn. Navigation Congress, No. 21, 1975.

47. DELMONTE, R.C. Forces exerted by waves breaking seaward of a vertical seawall. University Berkeley California, June 1972.

48. CAMFIELD, F.E. & STREET, R.L. Shoaling of solitary waves on small slopes. A.S.C.E. Waterways and Harbours Div. Vol. 95, WW1, 1969, pp 1-22.

49. GODEAU, A.J. DELEVIL, G.E. DORIS, C.G. & HEAS, J.Y. Statistical analysis of non-linear dynamic response of fixed structures to random waves, fatigue evaluation. Offshore Tech. Conf. Vol. 4, 1977, pp 493-502.

50. ACKERMANN, N.L. & CHEN, P.H. Impact pressures produced by breaking waves. Proc. 14th Conf. Coastal Eng. 1974, Vol. 3 pp 1778-1788.

51. KAMEL, A.M. Water wave pressures on seawalls and breakwaters. Army Eng. Waterways Exp. Station, Vicksburg, Feb. 1952, 52p.

52. Von KARMAN, T. The impact of seaplane floats during landing. Tech. Note No. 321, National Advisory Comm. for Aeronautics, Washington, U.S.A. 1929.

53. KEULEGAN, G.H. & CARPENTER, L.H. Forces on cylinders and plates in an oscillating fluid. J. Res. Nat. Bur. Stds. 60, No. 5, May 1958, pp 423-440.

54. RAMKAMA, A. A model law for wave impacts on coastal structures, 16th Conf. Coastal Eng. Vol. 3, 1978, pp 2308-2327.

55. GARRISON, C.J. TORUM, A. IVERSON, C. & PERKINSON, B.T. Wave forces on large volume structures, a comparison between theory and model tests. A.S.C.E. Waterways Div. Vol. 95, WW4, 1969.

56, GARRISON, C.J. GERMAN, F.H. & PERKINSON, B.T. Wave forces on bottom mounted large diameter cylinders. A.S.C.E. Waterways Div. Vol. 101, WW4, Nov. 1975, pp 345-356.

57. KHASKHACHIKH, G. & VANCHAGOV, O. Regular wave effects on walls made of cylinders. A.S.C.E. Waterways Div. WW4, Nov. 1971, pp 735-754.

58. WEGGEL, J.R. HALL, W. & MAXWELL, C. Numerical model for wave pressure distributions. A.S.C.E. Waterways Div. WW3 Vol. 96, 1970, pp 623-642.

59. MARSH, F.D. & WIEGEL, R.L. Cnodial waves: tables of functions. Council on wave reseach, the Engineering Foundation, 1961.

60. DEAN, R.G. Hybrid methods of computing wave loading. Offshore Tech. Conf. Vol. 4, 1977, pp 483-92.

61. DEAN, R.G. Relative validities of water wave theories. A.S.C.E. Conf. Civil Eng. in the Oceans, 1967, pp 1-31.

62. HUDSON, R.Y. DALRYMPLE, R.A. & DEAN, R.G. Comparison of wave forces computed by linear and stream function methods. Offshore Tech. Conf. Vol. 2, 1974, pp 17-25.

63. LAITONE, E.V. Higher approximations to non-linear water waves. Ph.D. Thesis, Stanford Univ. 1962.

64. LAMBRAKOS, K.F. & BRANNON, H.R. Wave force calculations for stokes and non-stokes waves. 6th Offshore Tech. Conf. Vol. 2, 1974, pp 47-60.

65. Le MEHAUTE, B. DIVOKY, D. & LIN, A. A comparison of theories and experiments. Proc. 11th Conf. Coastal Eng. Vol. 1, 1968, pp 86-107.

66. MORGAN, G.W. Time-saver method for wave force analysis. Offshore Tech. Conf. Vol. 2, 1974, pp 33-46.

67. SARGINSON, E.J. Empirical relations for shallow water waves. Proc. I.C.E. Dec. 1980, Part 2, pp 1025-1027.

68. SKJELBREIA, L. & HENDRICKSON, J. Fifth order gravity wave theory. Proc. 7th Conf. Coastal Eng. Vol. 1, 1960, pp 184-196.

69. STOKER, J.J. The breaking of waves in shallow water. Annals New York Academy of Sciences. Vol. 51, 1949.

70. SUENDSEN, I.A. & BRINK-KJAER, O. Shoaling of Cnoidal waves. Proc. Conf. Coastal Eng. Vol. 1, 1972, pp 365-383.

71. SAINFLOU, E.J. Treatise on vertical breakwaters. Annales des Ponts et Chaussees, No. 4, 1928.

72. MINIKIN, R.R. Wind, waves and maritime structures. Charles Griffin and Co. 1963.

73. MINIKIN, R.R. Breakwaters. Engineering, June 1943, pp 441-443.

74. REPORT - Shore Protection Manual. U.S. Army Coastal Eng. Res. Centre. 1973.

75. ROWE, R.P. The Port of Teignmouth. Dock and Harbour Authority, March 1976, pp 337-338.

76. HARRIS, C.M. Shock and vibration handbook, Vols. 2 and 3. McGraw-Hill, 1961.

77. CATALOGUE - Welwyn workshop notes. Welwyn strain measurement Ltd. Basingstoke.

78. CATALOGUE - Schaeitz servo-accelerometers. Tech. Report No. 4501A, Slough, Berkshire.

79. REPORT - A study of servo accelerometer design for low frequency vibration measurement. Inst. Sound and Vibration Res. Report No. 85, Sept. 1975.

80. MITCHELL, W.S. Shock and vibration instrumentation: accelerometers. The Shock and Vibration Digest, Vol. 19, No. 1 Jan. 1977.

81. SILVESTER, R. Coastal engineering, 1 generation, propagation and influence of waves. Elsevier, 1974.

82. REPORT - Dynamics of marine structures. Report UR8, Ciria Underwater Engineering Group, 1978.

83. WIEGEL, R.L. Oceanographical Engineering. Prentice-Hall Int. 1964.

84. Le MEHAUTE, B. An introduction to hydrodynamics and water waves. Springer- Verlag, 1976.

85. BENDAT, J.S. & PIERSOL, A.G. Random data; analysis and measurement procedures. Wiley, 1971.

86. BEVINGTON, P.R. Data reduction and error analysis for the physical sciences. McGraw-Hill, 1969.

87. CHATFIELD, C. The analysis of time series; theory and practice. Chapman and Hall, 1975.

88. ANDERSON, O.D. Time series analysis and forecasting. Butterworths, London, 1976.

89. COOLEY, J.W. & TUKEY, J.W. An algorithim for the machine calculation of complex fourier series. Math. Comp. No. 19, April, 1965.

90. KINSMAN, B. Wind waves; their generation and propagation on the ocean surface. Prentice-Hall, 1965.

91. BERKELEY-THORN, R. & SIMMONS, J.C.F. Sea defence works, design, construction and emergency works. (2nd Ed) Butterworths, 1971.

92. Le BLOND, P.H. & MYSAK, L.A. Waves in the ocean. Elsevier Scientific Pub. Co. 1978.

93. IPPEN, A.T. Estuary and coastline hydrodynamics. McGraw-Hill, 1966.

94. LITTLE, D.H. Harbours and Docks, Civil Eng. Ref. Book. Butterworths Scientific Pub. Ltd.

95(a). MUIR-WOOD, A.M. Coastal hydraulics. MacMillan, 1969

95(b). MUIR-WOOD, A.M. & FLEMING, C.A. Coastal hydraulics (2nd Ed). MacMillan Press Ltd. 1981.

96. QUINN, A.D. Design and construction of Ports and marine structures. McGraw-Hill, 1974.

97. GUMBEL, E.J. Statistics of extremes. Columbia Univ. Press, 1958.

98. BENJAMIN, J.R. Probability, statistics and decision for Civil engineers. McGraw-Hill, 1970.

99. DERMAN, C. GLESER, L.S. & OLKIN, L. A guide to probability theory and application. Holt, Rinehart and Winston Inc. 1973.

100. FISHER, R.A. & TIPPETT, L.H.C. Limiting forms of the frequency distribution of the largest or smallest member of a sample. Proc. Cambridge Philosophical Society, Vol 24, 1928, pp 180 - 190

101. PUTZ, R.L. Statistical analysis of wave records. Proc 4th Conf. Coastal Eng. 1954, pp 13 - 24.

102. NATH, J.H. Probability distributions of breaking wave heights. Proc. Int. Symp. Ocean Wave Measurement and Analysis, Vol. 1, 1974, pp 379-395.

103. DRAPER, L. Derivation of a design wave from instrumental records of sea waves. I.C.E. Proc. Part 3, 1963 pp 291 - 304.

104. TUCKER, M.J. Analysis of records of sea waves. I.C.E. Proc. Part 3, 1963, pp 305 - 316.

105.	TICKELL, R.G. BURROWS, R. & HOLMES, P.	Long term loading on offshore structures. Proc. I.C.E. Part 2, 1976, pp 145 - 162.
106.	KUZNETSOV, A.I. & KHASKHATCHIKV, G.	Load analysis from wave groups. 16th Conf. Coastal Eng. Vol. 3, 1978, pp 2328 - 2359.
107.	MAYNE, J.R. & COOK, N.J.	Extreme Wind analysis Proc. Conf. 'Wind engineering in the eighties'. CIRIA, London, 1980.
108.	LIEBLEIN, J.	Efficient methods of extreme-value methodology. Nat. Bureau standards, Washington D.C. Rept No. NBSIR 74-602, Oct. 1974.
109.	CODE OF PRACTICE	C.P.110, Part 1, Appendix D.
110.	Proceedings -	The structure of concrete. C. & C.A. 1965.
111.	REPORT -	Recommendations for the design and construction of concrete sea structures. F.I.P. 3rd Ed.
112.	MUGA, B.J. & WILSON, J.F.	Dynamic analysis of ocean structures. Plenum Press, 1970.
113.	HOUSNER, G.W. & HUDSON, D.E.	Applied mechanics; dynamics, 2nd Ed. Van Nostrand, 1959.
114.	CRANDELL, S.H. & MARK, W.D.	Random vibrations in mechanical systems. Academic Press, 1963.
115.	CLOUGH, R.W. & PENZIEN, J.	Dynamics of structures. McGraw-Hill, 1975.
116.	BOX, G.E.P. & JENKINS, G.M.	Time series analysis forecasting and control. Holden-Day, 1971.

117. BRILLNGER, D.R. Time series - data analysis and theory. Holt, Rinehart and Winston Inc. 1975.

118. JENKINS, G.M. & WATTS, D.G. Spectral analysis and its applications. Holden-Day, San Francisco, 1968.

119. ZIENKIEWICZ, O.C. The finite element method in engineering science. McGraw-Hill, 1971.

120. PAFEC 75 MANUALS Data preparation and theory and results manuals. PAFEC Ltd. Nottingham.

APPENDIX A

A.1 Calculation of the parameters of the Weibull distribution

If a random variable X has a Weibull distribution then the p.d.f. f(x) of X has the form;

$$f(x) = \begin{cases} \frac{\beta}{\alpha} \left(\frac{x - \nu}{\alpha} \right)^{\beta - 1} \exp - \left(\frac{x - \nu}{\alpha} \right)^{\beta}, & \text{if } x \geqslant \nu \\ 0, & \text{if } x < \nu \end{cases} \qquad \ldots (A.1)$$

where α and β are positive constants and ν is non-negative, if α, β and ν are known then the distribution whose p.d.f. is given by Eq. A.1 is completely determined. It can be shown(98) that if X has a Weibull distribution with parameters α, β and ν then the c.d.f. F(x) of X is given by;

$$F(x) = \begin{cases} 0, & \text{if } x < \nu \\ 1 - \exp - \left(\frac{x - \nu}{\alpha} \right)^{\beta}, & \text{if } x \geqslant \nu \end{cases} \qquad \ldots\ldots\ldots\ldots\ldots (A.2)$$

The parameter ν is the smallest possible (non-negative) value of the observations of a random variable X, in the case of impact pressures the smallest possible value of X must be zero, (although the smallest value measured was 5.4 KN/m^2) therefore ν is set to zero.

From Ref.. 99

$$\mu_x - \nu = \alpha \Gamma (1 + 1/\beta) \qquad \ldots\ldots\ldots\ldots\ldots\ldots (A.3)$$

or $$\alpha = \frac{\mu_x - \nu}{\Gamma(1 + 1/\beta)} \quad \text{.....................(A.4)}$$

also from Ref. 99, β can be found from;

$$\frac{(\mu_x - \nu)^2}{\sigma_x^2 + (\mu_x - \nu)^2} = \frac{\Gamma(1 + 1/\beta)\ \Gamma(1 + 1/\beta)}{\Gamma(1 + 2/\beta)} \quad \text{....... (A.5)}$$

where $\Gamma(\ )$ is a Gamma function and μ_x and σ_x are the mean and standard deviation of process X. Using the estimated value of ν (i.e. $\nu = 0$) and tables of the Gamma function $\Gamma(\ )$, values of the parameters α and β can be found using equations A.4 and A.5.

For all impact data the following parameters are obtained;

$\sigma_x = 6.125$ KN/m^2 , $\mu_x = 12.12$ KN/m^2 , $\beta = 2.1$, $\alpha = 13.68$

and for the Ilfracombe data separately;

$\sigma_x = 3.92$ KN/m^2 , $\mu_x = 11.10$ KN/m^2 , $\beta = 3.125$, $\alpha = 12.39$

Equation A.2 can now be solved for F(x) after rewriting as;

$$1 - F(x) = \exp - \tau \quad \text{........................ (A.6)}$$

where $$\tau = \left(\frac{x - \nu}{\alpha}\right)^{\beta}$$

A value of τ can now be calculated for each value of x, then by using tables of exp $-\tau$ (i.e. table T.8 in Ref. 98), a value of $1 - F(x)$ for each value of x is obtained.

Graphs of the function $1 - F(x)$ versus impact pressure are shown in Figures 3.37(a) and 3.37(b). The values of τ, $1-F(x)$ (theoretical) and $1 - F(x)$ (observed) are given in Table A.1.

Class	Class Mid-point	Frequency		τ		$1 - F(x)$		Observed c.d.f.	
		All	Ilf.	All data	Ilf. data	All data	Ilf. data	All data	Ilf. data
4 - 6	5	8	6	0.12	0.06	0.887	0.942	0.951	0.946
6 - 8	7	21	18	0.25	0.17	0.779	0.844	0.823	0.786
8 - 10	9	39	28	0.42	0.37	0.657	0.691	0.604	0.536
10 - 12	11	38	23	0.64	0.69	0.527	0.502	0.415	0.330
12 - 14	13	32	13	0.91	1.16	0.402	0.301	0.274	0.214
14 - 16	15	20	13	1.23	1.82	0.301	0.165	0.177	0.098
16 - 18	17	13	4	1.60	2.68	0.202	0.067	0.128	0.063
18 - 20	19	13	4	2.02	3.80	0.135	0.022	0.055	0.027
20 -22	21	5	2	2.50	5.20	0.082	0.006	0.037	0.009
24 - 26	25	1	0	3.60	8.97	0.027	0	0.030	0.009
26 - 28	27	2	1	4.23	11.41	0.015	0	0.018	0
32 - 34	33	1	0	6.45		0.001		0.012	
46 - 48	47	1	0	13.56		0		0.006	
48 - 50	49	1	0	14.80		0		0	

Table A.1 Theoretical impact values for a Weibull c.d.f.

A2. Estimating The Parameters Of A Type I Extreme Value Distribution Via Liebleins BLUE

In reference 108 Lieblein sets out a method for estimating the mode (u) and dispersion ($1/\alpha$) of a Fisher - Tippett Type I distribution using a weighting factor Lieblein calls the 'Best Linear Unbiased Estimator' (BLUE).

Lieblein's method requires that the extreme value data be ordered (as in Table A.2), the data is then multiplied by the weighting coefficients a_i and b_i (given in Ref 108).

The resulting numerical estimates of the mode and dispersion are given by the following;

$$\text{mode} = \sum_{i=1}^{n} a_i \; x \qquad \text{.............(A. 7)}$$

$$\text{dispersion} = \sum_{i=1}^{n} b_i \; x \qquad \text{.............(A. 8)}$$

These values are then inserted into equation 3.48 which gives the extreme value distribution of the data.

i.e. using the mode and dispersion obtained from Table A.2 the extreme value distribution for the Ilfracombe data becomes

$$F(P_i) = \exp \left[- \exp - 3.13 \; (P_i - 14.5) \right] \qquad \text{...(A. 9)}$$

This equation then allows estimates to be made of the probability of occurence (or exceedence) of a given impact pressure.

Sample Number	Ordered Maxima P ord	BLUE Coefficient a_i	BLUE Coefficient b_i
4	11.4	.163309	-.0285316
5	12.0	.125966	-.098775
2	12.6	.108230	-.045120
1	13.5	.095223	-.013039
14	14.4	.084619	.008690
9	14.9	.075484	.024282
13	15.0	.067331	.035768
3	15.3	.059866	.044262
6	16.2	.052891	.050418
10	17.6	.046260	.054624
7	19.1	.039847	.057083
12	19.3	.033526	.057829
11	21.6	.027131	.056652
8	26.7	.020317	.052646

$$\text{mode} = \sum_{1}^{14} a_i P_{ord} = 14.499, \quad \text{disp} = \sum_{1}^{14} b_i P_{ord} = 3.132$$

Table A.2 Using Liebleins BLUE to estimate the mode and dispersion of a Fisher - Tippett Type I extreme value distribution.

A.3 Calculation of Return period

The cumulative distribution function (c.d.f.) of the Fisher - Tippett Type I distribution is given by equation 3.48,

i.e

$$F(x) = \exp\left[- \exp - \alpha(x - u)\right]$$

where F(x) is the probability that the maximum impact pressure is less than u.

Equation 3.48 can be written in terms of impact pressure as follows;

$$F(P_i) = \exp\left[- \exp - \alpha\,(P_i - u)\right] \quad \text{......(A.10)}$$

If the return period associated with the given impact pressure P_i is T years, then the probability of exceedence in any one year will be 1/T, therefore;

$$F(P_i) = 1 - \frac{1}{T} \quad \text{...............(A.11)}$$

substituting A.11 into A.10 gives

$$1 - \frac{1}{T} = \exp\left[- \exp - \alpha(P_i - u)\right] \quad \text{......(A.12)}$$

taking logarithms of Eq A.12, twice, gives

$$P_i = u - \frac{1}{\alpha}\left\{\ln\left[- \ln\ (1 - \frac{1}{T})\right]\right\} \quad \text{......(A.13)}$$

when the return period T is large then equation A.13 can be approximated to;

$$P_i = u - \frac{1}{\alpha} \left[\ln \frac{1}{T} \right] \quad \text{............(A.14)}$$

or

$$P_i = u + \frac{1}{\alpha} \ln T \quad \text{............(A.15)}$$

Having calculated the mode (u) and dispersion ($\frac{1}{\alpha}$) from Appendix A.2, the impact pressure P_i is found by substituting values of return period T into Equation A.15, as shown below;

Impact pressure	Return period
21.7 KN/m^2	10 years
23.9 KN/m^2	20 years
26.7 KN/m^2	50 years

These values of return period can then be superimposed on the extreme value distribution plot, as in Figure 3.38.